

CONTENTS

Reviews

Meningeal lymphatic vessels: their morphology, location, and clinical implications 109

Adil Asghar, Ravi K. Narayan, Ashutosh Kumar

Morphometrics of the stapedius muscle: A systematic review of cadaveric studies 117

Bhagath Kumar Potu, Soubhagya R. Nayak, Ahmed A. Jaradat

Original Articles

Morphometry of abductor pollicis longus relevant to surgical reconstruction of hand 125

Dhivyalakshmi Gnanasekaran, Raveendranath Veeramani, Aravindhan Karuppusamy, Grace Suganya

Evaluation of the effect of n-hexane extract of *Leptadenia hastata* on the histomorphology of the liver in streptozotocin induced diabetic Wistar rat 135

Martha O.O. Attah, Tamunotonye W. Jacks, Sani H. Garba

The effect of corn silk, as a hypoglycemic, on the congenital malformations caused by diabetes in mice: A morphological study 145

Dema Alsudairi, Fatma Al-Qudsi

Histological evaluation of L-arginine-mediated exocrine pancreatic injury in rats and the potential implication of the probiotic (*Lactobacillus Acidophilus*) 159

Dalia A. Mandour, Asmaa M. Tolba

Ponticulus Posticus prevalence in Uruguayan population: dry bone and cervical CT imaging 179

Fernando Martínez, Juan Del Castillo, Santiago Hermosilla, Juan Kenny, Nicolás Sgarbi, Juan Emmerich

Origin and branching pattern of external carotid artery - a cadaveric study 187

Aby S. Charles, Suganthy Rabi, Anjali Jain, Parminder K. Rana

Influence of each hesperidin and insulin on diabetes-induced testicular alterations in adult albino rats 197

Maha S. Abd Elsamie, Mona H. Mohammed Ali, Omayma M. Mahmoud, Eman M. Kamel

Anatomical study of the external pudendal artery at the anatomy laboratory of Bamako 211

Tata Touré, Babou Ba, Abdoulaye Kanté, Moumouna Koné, Gaoussou Simpara, Ousmane I. Touré, Mahamadou Daou, Falé Traoré, Demba Yatera, Nouhoum Ongoïba

Evaluation of the therapeutic role of stem cells in experimental acetaminophen induced hepatotoxicity in adult male albino rat 223

Lamya A. Abd Elsalam, Shereen E. Tawfeek, Eman H. Nadwa, Bahaa Eldin A. Khaled

The anatomic study of extracranial structures related to tuberculum pharyngeum 241

Nazli G. Ceri, Ayse G. Sahmelikoglu, Fulden Cantas, Gizem Sakalli

Case Report

Rare variant of hepatic arterial supply: a cadaveric case report with a literature review 247

Domagoj Ivanković, Andrea Blažević, Dominik Vicković, Danko Mikulić

Letter to the Editor

In regard to “Unusual case of absence of suprascapular notch and foramen” 253

Azzat Al-Redouan, David Kachlik

Meningeal lymphatic vessels: their morphology, location, and clinical implications

Adil Asghar, Ravi K. Narayan, Ashutosh Kumar

Department of Anatomy, AIIMS Patna, India

SUMMARY

For long the CNS had been considered to lack lymphatics. The last few years have been spotted with works conflicting the immune-privilege status of CNS. Experimental evidence has assured the presence of lymphatics in the meninges, the meningeal lymphatic vessels (mLVs), along the venous sinuses carrying the immune cells along with drainage of cerebrospinal fluid (CSF). This article aims to explain the findings of multiple studies indicating the existence and clinical importance of the mLVs along with the controversies that refute the concept. A total of 30 studies were included after the search for literature was conducted in three major databases: PubMed, Scopus and Google scholar till through May 2020, with appropriate MESH terms like CNS, lymphatics, meninges, drainage, and glymphatics. Despite evidence supporting the existence of functional lymphatics in CNS, there has been conflict in opinion about the clearance by glymphatic system. Few have countered the CSF clearance mechanism, stating that those experiments showing such finding were performed on post-mortem tissue. The discovery of mLVs emphasizes a re-evaluation of fundamental neuroimmunology theory while enlightening a shift in the aetiology of neuro-inflammatory and neurodegenerative disorders accompanying the dysfunctional immune system.

Key words: CNS – Lymphatics – Meninges – CSF drainage – Glymphatics

INTRODUCTION

The lymphatic system implements protein homeostasis and immune surveillance. The classical dogma of the immune-privileged status of the central nervous system (CNS) is gradually diminishing with the discovery and evidence-based explanation of drainage routes for meningeal lymphatics. The previous texts and literature considered the central nervous system devoid of lymphatics and hence no connections to the tonsils, adenoids, and deep cervical lymph nodes (cLNs) were to be considered. This conventional wisdom is now being challenged on the basis of new experimental findings (Louveau et al., 2015; 2017; 2018; Aspelund et al., 2015; Dissing-Olesen et al., 2015; Da Mesquita et al., 2018; Ahn et al., 2019; Chen and Wang, 2020).

Louveau et al. (2015) showed presence of lymphatic channels using immunohistochemical markers in the whole-mount meninges of mouse brain. They observed vessel-like patterns in the endothelial distribution along the sinuses, in which immune cells (T-cell) were linearly aligned and the endothelial linings were positive for the vascular endothelial marker CD31 and classic lymphatic endothelial cell (LEC) markers such as Lyve-1, Prox1, vascular endothelial growth

Corresponding author:

Dr. Ravi Kant Narayan, Senior Resident, Department of Anatomy, AIIMS Patna, India. E-mail: narayanintouch@gmail.com

Submitted: July 3, 2020. Accepted: November 8, 2020

factor receptor 3 (VEGFR3), and the podoplanin. They also provided preliminary data for the presence of Lyve-1 and podoplanin expression in the meningeal coronal sections around the superior sagittal sinus in humans (Louveau et al., 2015; 2017; 2018). Later, Absinta et al. (2017), detected the presence of meningeal lymphatic vessels (mLVs) along the venous sinuses present in the dura, particularly along the straight and superior sagittal sinuses, also along the branches of the middle meningeal artery, in five human volunteers and three marmoset monkeys using image contrast (gadolinium) MRI. These preliminary experiments suggested that meningeal lymphatics exist in humans, which were perhaps unnoticed by earlier studies due to their peculiar anatomical localization. Now accumulative evidence corroborates that these mLVs express the molecular characteristics of LECs and transports the immune cells and fluid from the cerebrospinal fluid (CSF) to the deep cervical lymph nodes (cLNs) (Louveau et al., 2015; 2017; 2018; Aspelund et al., 2015; Ahn et al., 2019; Raper et al., 2016; Absinta et al., 2017).

The search strategy was performed to identify recent information about the localization and function of glymphatics and meningeal lymphatic vessels, as well as novel findings surrounding their role in the pathophysiology of neurodegenerative disease. The search was conducted in three major databases: PubMed, Scopus and Google scholar till through May 2020. The literature was searched after collecting the appropriate MESH terms for meningeal lymphatic vessels and glymphatics. The search strategy used was: ((Glymphatic) AND (cytoplasmic transport) OR (axonal flow)) AND ((efflux) OR lymph flow) OR perineural flow)) AND ((nervous system) OR brain OR cerebrum OR Cerebral OR meningeal fold) AND (((Human) OR mammal)) AND (meningeal [All Fields] OR dural [All Fields]) AND (“lymphatic vessels”[MeSH Terms] OR (“lymphatic”[All Fields] AND “vessels”[All Fields]) OR “lymphatic vessels”[All Fields] OR “lymphatics”[All Fields] OR “lymphatic system”[MeSH Terms] OR (“lymphatic”[All Fields] AND “system”[All Fields]) OR “lymphatic system” [All Fields])). A total of 30 studies were collected after removing the duplicates from all three major

databases. The articles dealing with the human or rodents or other mammalian brain lymphatics or glymphatics were included in the study, whereas the studies on non-mammalian species were excluded.

ANATOMICAL LOCATION AND MORPHOLOGY OF MENINGEAL LYMPHATICS VESSELS

Louveau et al. (2015) showed that the meningeal lymphatic vessels (mLVs) are localised mostly in the dorsal skull, along the transverse sinus (TS) and superior sagittal sinus (SSS). Ahn et al. (2019) reported mLVs in lateral or basal parts of the skull (basal mLVs) too. They noted that the basal mLVs directed by the side of the sigmoid sinus and petro-squamosal sinus (PSS) were wider and had branch-like, protruding capillaries in abundance (Fig. 2). The characteristic features of blunt-ended capillaries, typical oak-leaf-shaped lymphatic valves, and LECs advocated their similarity to the typical LVs (Fig. 1c). However, the mLVs of the dorsal skull were observed to be inappropriate for carrying and draining the macromolecules of the CSF because of the continuous sealed zipper-like junctional pattern of LECs with underdeveloped morphology (Fig. 1a). Conversely, the branched capillary basal mLVs presented mostly with pre-eminent, sporadically secured loose button-like coupling motif of LECs (Fig. 1c). Around the foramina of the skull, the basal mLVs had more zipper-type couplings with lymphatic valves (Ahn et al., 2019; Papadopoulos et al., 2020).

The peripheral lymphatic vessels (LVs) are categorized into two types: collecting and capillary lymphatic vessels. Dorsal mLVs falls in the category of capillary LVs, which are specialized for the carrying macromolecules and fluid because of characteristics like the lack of the smooth muscle cells (SMCs) and loose button-like LEC junctions. Basal mLVs present with amalgamated attributes of both collecting and capillary LVs, marked by diversity in the junctional/ coupling patterns and by the absence of SMCs (Ahn et al., 2019). Due to the presence of valves, basal mLVs are considered as ‘pre-collecting mLVs’ instead of ‘collecting mLVs’ (which possess compact zipper-like LEC junctions along with SMCs and a lymphatic valve

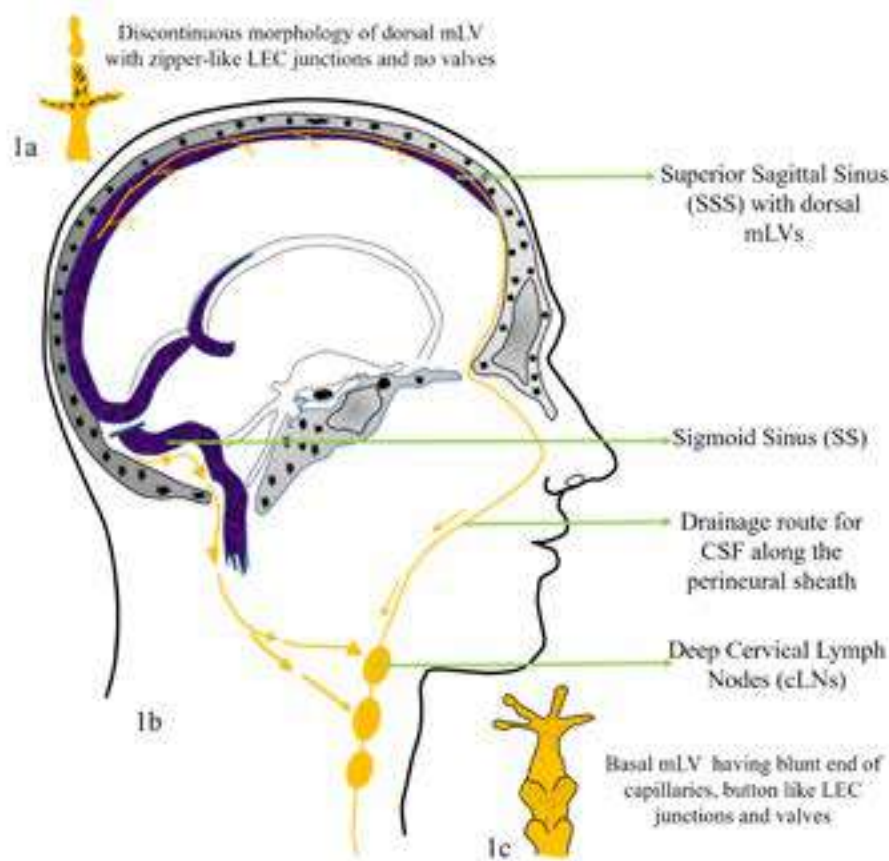


Fig. 1.- a – showing dorsal mLVs, which are thin, discontinuous, valve less and have zipper-like LEC junctions; b – mid-sagittal section of the cranium with a green line in between the dural sinuses representing mLVs. Dorsal mLVs run along either sides of the superior sagittal sinus (SSS) and drain to the deep cLNs via perineural sheath across the cribriform plate, while the basal mLVs runs along the sigmoid sinus (SS) and also drain to the deep cLNs after exiting the cranial cavity via jugular foramen; c – morphology of basal mLVs, which have larger diameter with valves, blunt end capillaries and button like LEC junctions.

per lymphangion segment). The characteristic features of basal mLVs enables them to commit for the dual role of uptake and transport of CSF (Da Mesquita et al., 2018; Chen and Wang, 2020).

DRAINING CSF THROUGH THE BASAL OUTFLOW

In many different species, Schwalbe (1869) stipulated a part for the LVs in drainage of CSF in the regions of both cranium and spinal cord (Yang et al., 2013). Boulton et al. (1998) injected a radiolabel tracer in CSF and tried to quantify extracranial drainage of the CSF by cannulating lymphatic vessels of the deep cervical region in sheep. Similar evidence was earlier presented by Bradbury and Westrop (1983) in rabbits. These studies suggested that approximately 30-50% of the CSF outflow occurs via LVs along the sheaths of cranial nerves and the cribriform plate (nasal mucosa & olfactory nerve; Fig. 1b), while the rest is presumed to have drained via arachnoid villi. Ma et al. (2017) showed in mice that the LVs

were the most significant pathway for drainage of both small molecule tracers from the CSF and macromolecules.¹⁷

The mLVs present a draining channel for the interstitial fluid (ISF) and CSF into the cervical lymph nodes (cLNs) (Absinta et al., 2017; Antila et al., 2017; Dupont et al., 2020). Aspelund et al. (2015) and Louveau et al. (2015) illustrated in mice models that mLVs exhibits a significant part in clearing the solute of ISF and CSF (Louveau et al., 2018; Absinta et al., 2017). Both of them have given stress on dorsal mLVs, but were silent on the basal mLVs. Ahn et al. (2019) showed in mice that drainage of CSF is primarily done by mLVs present at the cranial base. After injecting the contrast into the lateral ventricle of mice brain with stable vital signs, a swift escalation in contrast enhancement was observed initially in the lateral ventricle on the right, and then in basal outflow near the skull foramina, especially the jugular foramen, and finally the contrast reached the deep cervical LNs (Louveau et al., 2018). They explained that, as

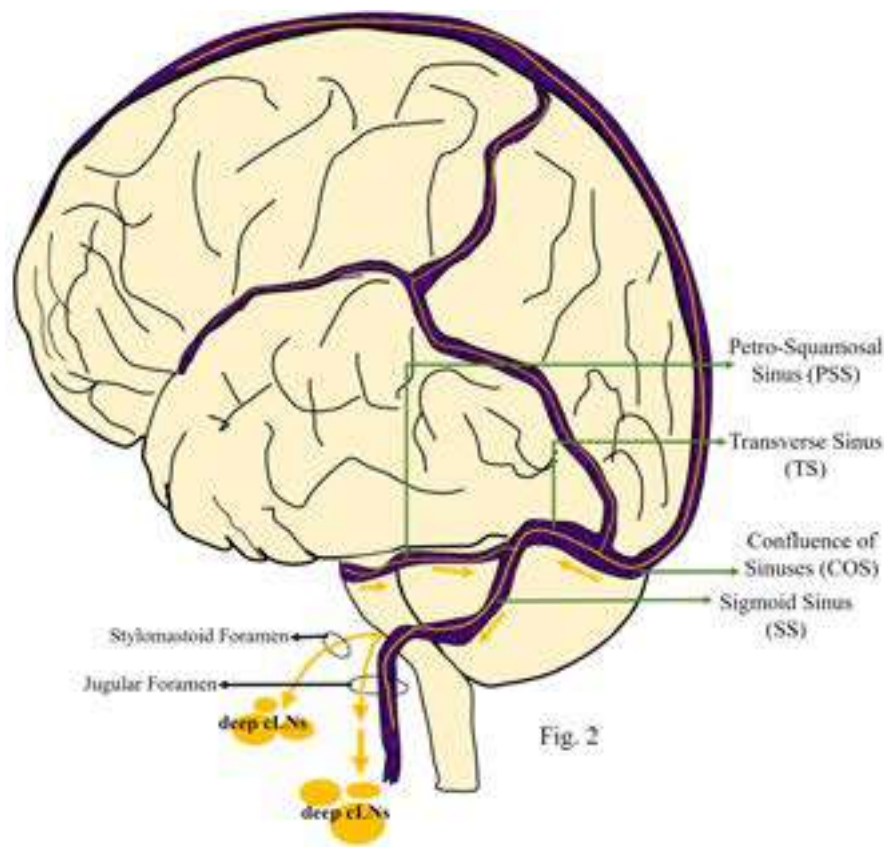


Fig. 2.- Dural venous sinuses in relation to the brain with a green line running between the dural sinuses, representing mLVs. Green arrows are representing flow of the fluid along the basal mLVs which are running along, transverse sinus (TS), petro-squamosal sinus (PSS) and sigmoid sinus (SS). Some of the basal mLVs exit the cranial cavity via stylomastoid foramen, while others exit via jugular foramen and drain into deep cervical lymph nodes (cLNs).

the branched capillary basal mLVs are detected within a much thinner layer of the dura near the subarachnoid space, and separated from that by a loose arachnoid barrier as compared to the dorsal mLVs, so basal mLVs were more likely to be facilitating the carriage and transport of CSF than dorsal mLVs.

Although these animal studies strongly suggest for similar scenarios in humans, a direct evidence in humans is still lacking. Besides, none of the studies have yet commented on the role of physiological and diurnal variations in mLVs-mediated clearance of CSF.

THE LINK BETWEEN THE MENINGEAL LYMPHATIC VESSELS AND 'GLYMPHATIC SYSTEM'

The 'glymphatic system' can be explained as a CSF/lymphatic system dependent on glial cells present all over the brain, comprising of a meshwork of para-vascular spaces that permits the systematic disposal of wastes and interstitial

solutes. Well-described Virchow-Robin spaces (VRS) are being appraised to be the initiation point for the glymphatic system (Ilyff et al., 2013; Louveau et al., 2017). The clearance of CSF by the glymphatic system implies a unique mechanism. From the subarachnoid spaces the CSF is first pushed into the para-arterial spaces (via trans-parenchymal swapping in extracellular tissue), thereafter portals out via para-venous spaces to get back in subarachnoid compartments. Evidently, coupling of para-arterial CSF influx to para-venous ISF clearance within the brain by Aquaporin-4-dependent astroglial water fluxes suggests that the glymphatic pathway interact with the mLVs along the perivascular spaces (Ilyff et al., 2012).

There is a conflict in opinion about the clearance by glymphatic system. Few have countered the CSF clearance mechanism stating that those experiments showing such finding were performed on post-mortem tissue. Some of them claimed that minute openings were present

in pia mater covering the arteries, which provided an anatomical route for macromolecules and CSF to be taken into the para-vascular space via the basal cistern. Nedergaard and colleagues explained the route in which AQP4-dependent convection in brain parenchyma is required for transferring of solutes from CSF to ISF. The consistent evidence explains parenchymal diffusion in the paravascular spaces via either dispersive or convective flow. It is sufficient to explain movement of solutes in the brain (Asgari et al., 2016; Jin et al., 2016). The authors who oppose the glymphatic mechanism claimed that CSF circulation is upregulated in awake state and downregulated in sleep. They argued for re-evaluation of Aquaporin-4-dependent parenchymal and para-vascular waste clearance and asked to study the redistribution of solute in para-vascular space after deletion of Aquaporin-4 channel from astrocyte foot process (Smith et al., 2017). CSF circulation may be decreased in sleep state but no study refutes the claim of high glymphatic efflux in sleep state and anesthetized rodents.

ROLE OF MLVS IN NEURO-IMMUNOLOGY AND DISEASES

The discovery of mLVs emphasizes a re-evaluation of fundamental theory in neuroimmunology while enlightening a shift in the aetiology of neuro-inflammatory and neurodegenerative disorders accompanying the dysfunctional immune system. The meningeal lymphatics are now thought to be the major route for clearance of macromolecules such as alpha-synuclein in Parkinson's disease, amyloid body in Alzheimer's disease, multisystem atrophy, Lewy body disease, and all prion-like proteinopathies, and demyelinating disease like multiple sclerosis (Iliff et al., 2012; Jaffe et al., 2019; Song et al., 2020; Pal et al., 2020; Balint et al., 2020; Frederick and Louveau, 2020).

The distension of the dural mLVs and the accumulation of T lymphocytes in mice occurs when collecting vessels draining to the deep cervical lymph nodes are ligated. This indicates that these vessels play a part in presentation of antigen and immune surveillance of the CNS

(Louveau et al., 2015). This decoding of the mechanism by which T cells may participate in immuno-surveillance of the CNS might be of much help in therapeutically altering the susceptibility of the brain to viral infections in immunocompromised individuals (HIV+ patients and transplant recipients) (Iliff et al., 2012).

Apart from the above-mentioned entities, the mLVs may also be involved in abnormal protein drainage from the brain tumours into the lymph nodes, thus triggering an explosive immune response (Iliff et al., 2012). Having realized that the CNS has its own lymphatic drainage, we can now shift our thinking back to the yet unexplained pathophysiology of the immune-cell-mediated brain disorders, as well as the effects of these lymphatics on drainage of subdural haematomas and the effect of damage to these draining channels on traumatic brain injury (Hershenhouse et al., 2019; Liu et al., 2020).

It is necessary to emphasize that functional studies of mLVs have been restricted mostly to the animal models. Further research in human models will provide new insight in the future by explaining therapeutically exploitable etiological relations between the brain's fluid dynamics and its disorders. Further, the mapping of the complete meningeal lymphatic vessels, including glial-lymphatic system, will be required. Better understanding of the detailed anatomy of the meningeal vessels in human will propel the interventions to halt the progression of immune-mediated brain diseases where these vessels may plausibly be involved.

REFERENCES

ABSINTA M, HA S-K, NAIR G, SATI P, LUCIANO NJ, PALISOC M, LOUVEAU A, ZAGHLOUL KA, PITTALUGA S, KIPNIS J, REICH RS (2017) Human and nonhuman primate meninges harbor lymphatic vessels that can be visualized noninvasively by MRI. *Elife*, 6: e29738.

AHN JH, CHO H, KIM J-H, KIM SH, HAM J-S, PARK I, SUH SH, HONG SP, SONG J-H, HONG Y-K, JEONG Y, PARK S-H, KOH GY (2019) Meningeal lymphatic vessels at the skull base drain cerebrospinal fluid. *Nature*, 572(7767): 62-66.

ANTILA S, KARAMAN S, NURMI H, AIRAVAARA M, VOUTILAINEN MH, MATHIVET T, CHILOV D, LI Z, KOPPINEN T, PARK JH, FANG S (2017) Development and plasticity of meningeal lymphatic vessels. *J Exp Med*, 214(12): 3645-3667.

ASGARI MM, WANG W, IOANNIDIS NM, ITNYRE J, HOFFMANN T, JORGENSON E, WHITTEMORE AS (2016) Identification of susceptibility loci for cutaneous squamous cell carcinoma. *J Invest Dermatol*, 136(5): 930-937.

ASPELUND A, ANTILA S, PROULX ST, KARLSEN TV, KARAMAN S, DETMAR M, WIIG H, ALITALO K (2015) A dural lymphatic vascular system that drains brain interstitial fluid and macromolecules. *J Exp Med*, 212(7): 991-999.

BÁLINT L, OCSKAY Z, DEÁK BA, ARADI P, JAKUS Z (2020) Lymph flow induces the postnatal formation of mature and functional meningeal lymphatic vessels. *Front Immunol*, 10: 3043.

BOULTON M, FLESSNER M, ARMSTRONG D, HAY J, JOHNSTON M (1998) Determination of volumetric cerebrospinal fluid absorption into extracranial lymphatics in sheep. *Am J Physiol*, 274(1): R88-96.

BRADBURY MW, WESTROP RJ (1983) Factors influencing exit of substances from cerebrospinal fluid into deep cervical lymph of the rabbit. *J Physiol (Lond)*, 339: 519-534.

CHENG Y, WANG YJ (2020) Meningeal lymphatic vessels: a drain of the brain involved in neurodegeneration? *Neurosci Bull*, 36(5): 557-560.

DA MESQUITA S, FU Z, KIPNIS J (2018) The meningeal lymphatic system: a new player in neurophysiology. *Neuron*, 100(2): 375-388.

DISSING-OLESEN L, HONG S, STEVENS B (2015) New brain lymphatic vessels drain old concepts. *EBioMedicine*, 2(8): 776-777.

DUPONT G, IWANAGA J, YILMAZ E, TUBBS RS (2020) Connections between amyloid beta and the meningeal lymphatics as a possible route for clearance and therapeutics. *Lymphat Res Biol*, 18(1): 2-6.

FREDERICK N, LOUVEAU A (2020) Meningeal lymphatics, immunity and neuroinflammation. *Curr Opin Neurobiol*, 62: 41-47.

HERSHENHOUSE KS, SHAULY O, GOULD DJ, PATEL KM (2019) Meningeal lymphatics: a review and future directions from a clinical perspective. *Neurosci Insights*, 14: 1179069519889027.

ILIFF JJ, WANG M, LIAO Y, PLOGG BA, PENG W, GUNDERSEN GA, BENVENISTE H, VATES GE, DEANE R, GOLDMAN SA, NAGELHUS EA, NEDERGAARD M (2012) A paravascular pathway facilitates CSF flow through the brain parenchyma and the clearance of interstitial solutes, including amyloid β . *Sci Transl Med*, 4(147): 147ra111.

ILIFF JJ, LEE H, YU M, FENG T, LOGAN J, NEDERGAARD M, BENVENISTE H (2013) Brain-wide pathway for waste clearance captured by contrast-enhanced MRI. *J Clin Invest*, 123(3): 1299-1309.

JAFFE RJ, DAVE RS, BYRAREDDY SN (2019) Meningeal lymphatics in aging and Alzheimer's disease. *Ann Transl Med*, (Suppl 1): S2.

JIN B-J, SMITH AJ, VERKMAN AS (2016) Spatial model of convective solute transport in brain extracellular space does not support a "glymphatic" mechanism. *J Gen Physiol*, 148(6): 489-501.

LIU X, GAO C, YUAN J, XIANG T, GONG Z, LUO H, JIANG W, SONG Y, HUANG J, QUAN W, WANG D (2020) Subdural haematomas drain into the extracranial lymphatic system through the meningeal lymphatic vessels. *Acta Neuropathol Commun*, 8(1): 1-1.

LOUVEAU A, SMIRNOV I, KEYES TJ, ECCLES JD, ROUHANI SJ, PESKE JD, DERECKI NC, CASTLE D, MANDELL JW, LEE KS, HARRIS TH, KIPNIS J (2015) Structural and functional features of central nervous system lymphatic vessels. *Nature*, 523(7560): 337-341.

LOUVEAU A, PLOG BA, ANTILA S, ALITALO K, NEDERGAARD M, KIPNIS J (2017) Understanding the functions and relationships of the glymphatic system and meningeal lymphatics. *J Clin Invest*, 127(9): 3210-3219.

LOUVEAU A, HERZ J, ALME MN, SALVADOR AF, DONG MQ, VIAR KE, HEROD SG, KNOPP J, SETLIFF JC, LUPI AL, DA MESQUITA S, FROST EL, GAULTIER A, HARRIS TH, CAO R, HU S, LUKENS JR, SMIRNOV I, OVERALL CC, OLIVER

G, KIPNIS J (2018) CNS lymphatic drainage and neuroinflammation are regulated by meningeal lymphatic vasculature. *Nat Neurosci*, 21(10): 1380-1391.

MA Q, INEICHEN BV, DETMAR M, PROULX ST (2017) Outflow of cerebrospinal fluid is predominantly through lymphatic vessels and is reduced in aged mice. *Nat Commun*, 8(1): 1434.

PAL S, RAO S, LOUVEAU A (2020) Meningeal lymphatic network: The middleman of neuroinflammation. *Clin Exp Neuroimmunol*, 11(1): 21-25.

PAPADOPOULOS Z, HERZ J, KIPNIS J (2020) Meningeal lymphatics: from anatomy to central nervous system immune surveillance. *J Immunol*, 204(2): 286-293.

RAPER D, LOUVEAU A, KIPNIS J (2016) How do meningeal lymphatic vessels drain the CNS? *Trends Neurosci*, 39(9): 581-586.

SMITH AJ, YAO X, DIX JA, JIN B-J, VERKMAN AS (2017) Test of the “glymphatic” hypothesis demonstrates diffusive and aquaporin-4-independent solute transport in rodent brain parenchyma. *Elife*, 21: 6.

SONG E, MAO T, DONG H, BOISSERAND LS, ANTILA S, BOSENBERG M, ALITALO K, THOMAS JL, IWASAKI A (2020) VEGF-C-driven lymphatic drainage enables immunosurveillance of brain tumours. *Nature*, 577(7792): 689-694.

YANG L, KRESS BT, WEBER HJ, THIYAGARAJAN M, WANG B, DEANE R, BENVENISTE H, ILIFF JJ, NEDERGAARD M (2013) Evaluating glymphatic pathway function utilizing clinically relevant intrathecal infusion of CSF tracer. *J Trans Med*, 11(1): 107.

Morphometrics of the stapedius muscle: A systematic review of cadaveric studies

Bhagath Kumar Potu¹, Soubhagya R. Nayak², Ahmed A. Jaradat³

¹Department of Anatomy, College of Medicine & Medical Sciences, Arabian Gulf University, Kingdom of Bahrain

²Department of Anatomy, College of Medicine & J.N.M Hospital, WBUHS, Kalyani, West Bengal, India

³Department of Family and Community Medicine, College of Medicine & Medical Sciences, Arabian Gulf University, Kingdom of Bahrain

SUMMARY

The stapedius is the smallest skeletal muscle of the body, which has a significant importance in otology as one of the important muscles for sound wave modulation. Despite its functional importance, there is very little data available on the morphometrics of this muscle. Therefore, we have systematically reviewed the morphometrics of the stapedius muscle, specifically the length and width of the muscle belly and tendon. A systematic literature search was performed in databases such as Medline, Google Scholar, PubMed, ScienceDirect, SciELO and otology textbooks using search terms such as “stapedius muscle”, “stapedius tendon”, “morphometrics”, AND “size OR “length” OR “width”, which yielded more than 239 article links. All articles by their title and abstract were screened to see whether they included information relevant to our search terms. We also noted the distance between the stapedius tendon and the facial nerve. Of the eleven articles that met the inclusion criteria, only six studies comprising 106 stapedius muscles had the morphometric data. Pooled data (mean±SD, mm) of the stapedius showed: (i) total length 4.91 ± 0.88 , (ii) muscle belly length 3.77 ± 0.63 , (iii) tendon length 1.24 ± 0.42 , (iv) belly and tendon width 1.29 ± 0.20 , and 0.40 ± 0.09 respectively, and (v) distance of the

stapedius tendon with the facial nerve 1.26 ± 0.24 . Our pooled analysis from the available literature generated more representative values on the size of the stapedius muscle belly and tendon. This information might provide guidance in creating/reconstructing 3-dimensional models of the stapedius muscle and tendon in surgical intervention for otosclerosis.

Key words: Stapedius – Morphometrics – Systematic review

INTRODUCTION

The stapedius (ST) is the smallest skeletal muscle of the body, and consists of a muscle belly and tendon. The muscle belly originates from the inner wall of the pyramidal prominence, a tiny projection on the mastoid wall of the tympanic cavity, and the tendon attaches to the stapes neck (Figs. 1A, 1B) (Standing et al., 2008). Pieter Paaw (1615) first described the structure of the stapedius with more emphasis on an ossicle in its tendon. The ST muscle develops from the second pharyngeal arch by two anlagen: one for the tendon, which is derived from the internal segment of the interhyale; and another for the belly of the ST muscle, located in the second pharyngeal arch, medial to the facial nerve near

Corresponding author:

Potu Bhagath Kumar, Ph.D, Department of Anatomy, College of Medicine and Medical Sciences, Arabian Gulf University, Kingdom of Bahrain. E-mail: potubk@agu.edu.bh

Submitted: August 11, 2020. Accepted: October 14, 2020

interhylae (Rodriguez-Vazquez et al., 2010). He further postulated that the developmental variations of ST belly and tendon are likely due to the degree of angulation persistence between these two structures. Such structural variations of ST are accounting up to an incidence of 4.4% (Wright and Etholm, 1973).

According to Wright and Etholm (1973), the ST could be ectopic (along the facial nerve in facial canal), doubled, completely absent (or) lacking its tendon or belly. This muscle is important along with others for sound wave modulation. Its synchronized contraction with the tensor tympani muscle in a reflex manner dampens the high intensity and low frequency sounds to prevent excessive movements of the stapes; therefore, its paralysis leads to hyperacusis (Standring et al., 2008; Rubini et al., 2020). The morphometrics on the ST belly and tendon have gained so much importance in otology ever since Shea (1958) first introduced the procedure of stapedotomy. Since then many studies have discussed whether it is important to preserve the ST tendon during this procedure (Colletti et al., 1988; Gros et al., 2003; Arnold and Häusler, 2007; Elovikov et al., 2014; Rubini et al., 2020) and its possible role in conductive hearing loss and cholesteatoma (Zawawi et al., 2014; Rubini et al., 2020). Despite difficult access, considering the clinical importance of the stapedius, a few studies

in the literature have measured the dimensions of belly and tendon (Cheng and Gan, 2007; Ramirez-Aristeguieta et al., 2010; Beger et al., 2019; Prasad et al., 2019; Wojciechowski et al., 2020; Rubini et al., 2020; Beger et al., 2020). However, the morphometric data on ST remains vague and scarce. Hence, we felt it was important to have a quantitative synthesis from the available literature. Therefore, the aim of this systematic review is to generate more representative values on the size of ST muscle belly, tendon and their possible association with ethnicity, gender and side.

We comprehensively reviewed the literature that is available online regarding the morphometry of the ST muscle and critically interpreted the pooled data. We hope that these quantitative data on the dimensions of muscle belly and tendon may give a broader perspective to surgeons in avoiding iatrogenic injuries of the muscle and its intimate relations, such as the facial nerve (FN).

MATERIALS AND METHODS

Search methodology, extraction and selection criteria of studies

A thorough search was made mainly using the electronic databases such as Medline, Google Scholar, PubMed, ScienceDirect, SciELO and otologic textbooks. The keywords for search used

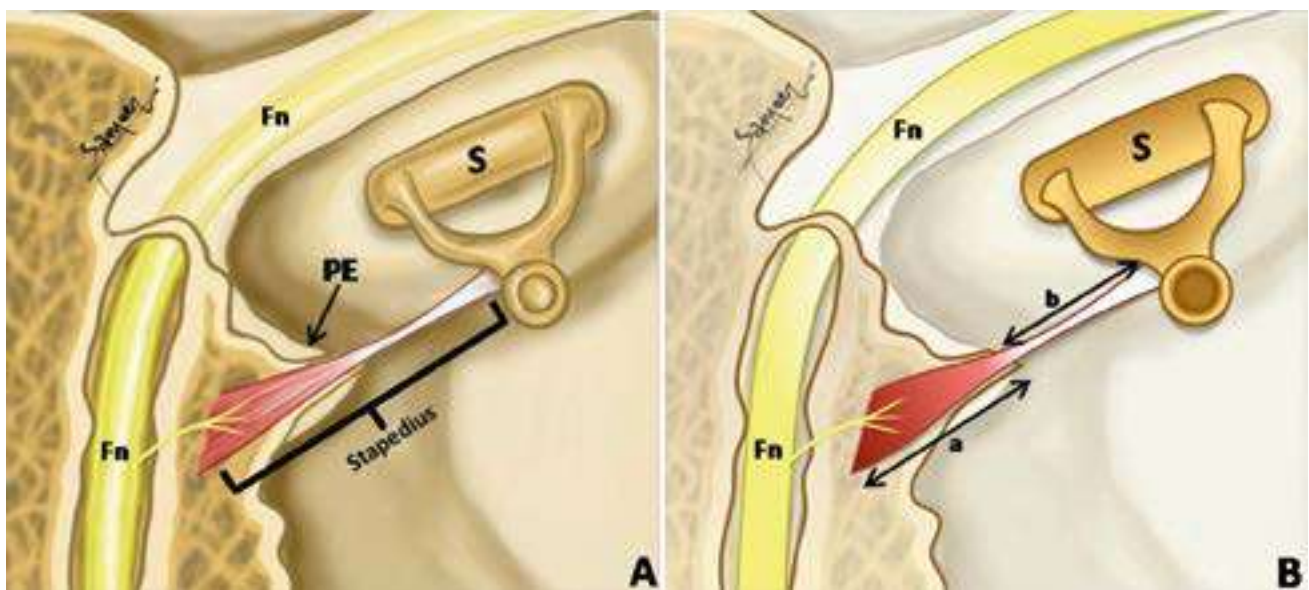


Fig. 1.- A) Schema of middle ear cavity showing the situation and extent of stapedius muscle. S- Stapes; PE- Pyramidal Eminence; Fn- Facial nerve. **B)** Schema of middle ear cavity showing the extent of stapedius muscle belly (Arrow "a") and stapedius tendon (Arrow "b"). S- Stapes; Fn- Facial nerve.

were as follows: “stapedius muscle”; “stapedius tendon”; “morphometrics” AND “size OR length OR width OR diameter”. We have limited our search criteria to the studies performed only on the cadavers. We have excluded all the case reports, case series, letters to editors and brief communications. The mean pooled ST belly length, ST tendon length, ST belly width, ST tendon width, total stapedius length, the mean pooled side and gender-based values were set to be the outcomes of our study. And also in the same articles, we have searched for the information on distance between ST tendon and FN. The references of the included articles were checked and duplicates were deleted. We have not set restrictions on date, language or age of the studies. Initial screening on titles and abstracts of the articles were done to obtain the full-text articles. The data collection was done using the guidelines of Preferred Reporting Items for Systematic reviews and MetaAnalyses (PRISMA) checklist (Moher et al., 2009).

Data analysis

Data extracted included the country of study, sample size and measurements related to the size of ST muscle belly and tendon. The mean \pm SD were calculated for all the outcomes. Then the mean values of all the outcomes were analyzed based on the geographical/population category using SPSS Version 23.0.

RESULTS

Outcome of Search

A total of 6 studies met the inclusion criteria (Fig. 2). One study that investigated the ST on cadavers was excluded (Prasad et al., 2019) due to incomplete data analysis on the measurements. The specimens are in range from 24.2 weeks fetus to 92 years age. We included a fetal study in our analysis due to a fact that the stapes and ST muscle do not grow according to increasing gestational weeks and attain the adult size in fetal period itself (Beger et al., 2019). The total sample comprised 106 ST muscles. Four studies (Cheng and Gan, 2007; Ramirez *Aristeguieta et al., 2010*; Beger et al., 2019; Beger et al., 2020) reported their

gender distribution with 38 males and 19 females. Tables 1 and 2 show the characteristics of the included studies and outcomes of the individual studies. Table 3 show the measurement methods of the ST muscle in the included studies.

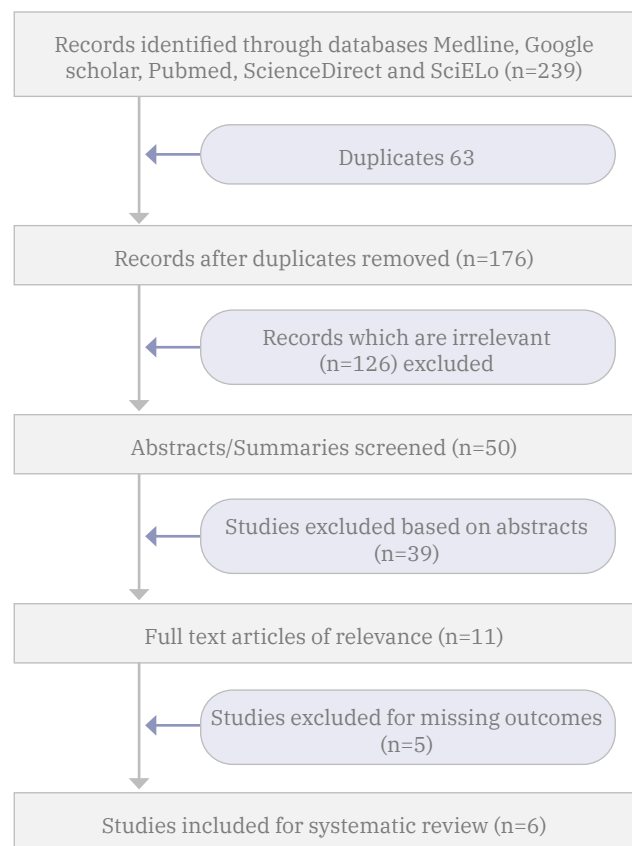


Fig 2.- Flowchart showing the application of selection criteria as per PRISMA guidelines.

Mean pooled ST belly length and width

Three studies (Ramirez Aristeguieta et al., 2010; Wojciechowski et al., 2020; Beger et al., 2020) reported the mean of ST belly length as 3.77 ± 0.63 mm, ranging from 2.98 ± 0.51 mm to 4.58 ± 0.34 mm. The sample from Poland had a lowest length value while the Colombian sample having a highest length value. Two studies (Wojciechowski et al., 2020; Beger et al., 2020) have reported the mean of ST belly width was 1.29 ± 0.20 mm, ranging from 1.19 ± 0.31 mm (Turkey) to 1.44 ± 0.32 mm (Turkey).

Mean pooled ST tendon length and width

Five studies (Cheng and Gan, 2007; Ramirez Aristeguieta et al., 2010; Beger et al., 2019; Wojciechowski et al., 2020; Beger et al., 2020)

reported the mean of ST tendon length as 1.24 ± 0.42 mm, ranging from 0.99 ± 0.09 mm (USA) to 1.40 ± 0.10 mm (Columbia). Four studies (Cheng and Gan, 2007; Beger et al., 2019; Wojciechowski et al., 2020; Beger et al., 2020) have reported the mean width of ST tendon was 0.40 ± 0.09 mm, ranging from 0.35 ± 0.12 mm (Poland) to 0.45 ± 0.08 mm (Turkey).

Mean pooled total length of Stapedius

Four studies (Ramirez Aristeguieta et al., 2010; Wojciechowski et al., 2020; Rubini et al., 2020; Beger et al., 2020) reported the mean of total length of stapedius as 4.91 ± 0.88 mm, ranging from 4.10 ± 0.90 mm (Italy) to 5.91 ± 0.37 mm (Columbia).

Mean pooled distance between ST tendon and FN

Only two studies (Beger et al., 2020 and Wojciechowski et al., 2020) have reported the mean distance between stapedius tendon and FN and it was 1.26 ± 0.24 mm, ranging from 1.14 ± 0.13 mm (Turkey) to 1.35 ± 0.30 (Poland).

Outcome values of Gender and Side

Two studies (Ramirez Aristeguieta et al., 2010 and Beger et al., 2020) reported SM belly length-width, tendon length-width, total stapedius length and one study (Beger et al., 2020) reported distance

between ST and FN for both sex. No significant differences ($P > 0.05$) were found between male and female morphometrics of the stapedius.

Three studies (Ramirez Aristeguieta et al., 2010; Beger et al., 2019; Beger et al., 2020) reported SM belly length-width, tendon length-width, total SM length and one study (Beger et al., 2020) reported distance between ST and FN for both sides. No significant differences ($P > 0.05$) were found between right and left stapedius.

DISCUSSION

Considering its location, size, and relationship with the adjacent structures, the ST muscle has always been a challenge for otologists. Due to its position, the ST muscle is known to pose procedural difficulties for otologists during cholesteatoma surgery or cochlear implantation (Rubini et al., 2020; Roberson et al., 2006). It is also reported in few cases that the ST along with its belly and tendon might be surgically removed to provide maximum exposure to the retrotympanic space (Rubini et al., 2020). And these procedures might cause iatrogenic injuries to the facial nerve due to its close anatomical relationship with the ST muscle (Rubini et al., 2020). Despite its high surgical relevance, studies regarding the morphometrics of ST muscle and its relationship with the FN are largely missing in the literature.

Table 1. Characteristics of the included studies.

Studies (year)	Region	Sample size of ST	Type of study & mode of measurement	Age (Years)	Male	Female	Left	Right
Cheng and Gan (2007)	USA	12	Adult cadaveric dissection	71 (51–92) years	6	6	NR	NR
Ramirez Aristeguieta et al. (2010)	Mestizo race, Columbia	23	Adult cadaveric dissection; manual	NR	21	2	12	11
Beger et al. (2019)	Turkey	24	Fetal cadaveric dissection; digital	24.27 ± 3.24 weeks	6	6	NR	NR
Wojciechowski et al. (2020)	Poland	16	Adult cadaveric dissection; MicroCT-digital	NR	NR	NR	NR	NR
Rubini et al. (2020)	Italy	11	Adult cadaveric dissection; endoscopic-digital	NR	NR	NR	NR	NR
Beger et al. (2020)	Turkey	20	Adult cadaveric dissection; digital	75.70 ± 13.75 years	5	5	10	10

ST: stapedius muscle; NR: not reported

Table 2. Outcomes of the different studies on ST size values.

Studies (year) & Region	Number of measured ST	Gender/ Side	ST belly length (mm)	ST tendon length (mm)	ST belly width (mm)	ST tendon width (mm)	Total Stapedius length (mm)	Distance between ST and Fn
Cheng and Gan (2007) - USA	12	Overall	NR	0.99±0.09	NR	0.40±0.07	NR	NR
Ramirez Aristeguieta et al. (2010) – COLUMBIA	23	Overall	4.52±0.41	1.27±0.20	NR	NR	5.80±0.61	NR
		Male	4.54±0.37	1.26±0.19	NR	NR	5.80±0.45	
		Female	4.25±0.25	1.40±0.10	NR	NR	5.65±0.15	
		Left	4.58±0.34	1.28±0.16	NR	NR	5.91±0.37	
		Right	4.54±0.61	1.28±0.21	NR	NR	5.79±0.45	
Beger et al. (2019) - TURKEY	24	Overall	NR	1.27±0.30	NR	0.45±0.08	NR	NR
		Left	NR	1.02	NR	0.35	NR	
		Right	NR	1.12	NR	0.46	NR	
Wojciechowski et al. (2020) - POLAND	16	Overall	2.98±0.51	1.29±0.50	1.26±0.29	0.35±0.12	4.34±0.74	1.35±0.30
Rubini et al. (2020) –ITALY	11	Overall	NR	NR	NR	NR	4.10±0.90	NR
Beger et al. (2020) – TURKEY	20	Overall	3.53±0.88	1.27±0.54	1.32±0.33	0.39±0.08	4.80±1.13	1.18±0.19
		Male	3.90±0.91	1.23±0.61	1.44±0.32	0.37±0.08	5.14±1.18	1.14±0.13
		Female	3.15±0.71	1.32±0.49	1.19±0.31	0.41±0.08	4.47±1.04	1.22±0.23
		Left	3.56±1.08	1.34±0.62	1.35±0.39	0.42±0.09	4.91±1.24	1.21±0.15
		Right	3.49±0.69	1.20±0.46	1.28±0.28	0.36±0.07	4.70±1.07	1.16±0.22

ST: stapedius muscle; Fn: Facial nerve; NR: not reported

Therefore we have done a quantitative synthesis on the stapedius muscle to derive a standard dataset. The main findings of our systematic review were as follows: (i) the mean ST muscle belly length and width were about 3.77 mm and 1.29 mm; (ii) the mean ST tendon length and width were 1.24 mm and 0.40 mm; (iii) the mean length of entire stapedius muscle was about 4.9 mm; (iv) the mean distance between ST tendon and FN was 1.26 mm; (v) there were no statistically significant differences between gender and sides of the outcomes.

Although the ST muscle with its tendon has been known for many years in humans, the classical anatomical textbooks failed to present standard measurements. It is very clear from our systematic review that the majority of studies have measured the length of the ST tendon from apex of the pyramidal prominence to neck of the stapes (Ramirez Aristeguieta et al., 2010; Beger et al., 2019; Wojciechowski et al., 2020; Rubini et al., 2020; Beger et al., 2020). While the muscle belly from reported studies was measured by standard procedures ranging from excavation of the pyramid (Beger et al., 2020), radiological

approach (Wojciechowski et al., 2020) and removal of the entire muscle complex (Prasad et al., 2019).

It was surprising to note that the ST tendon length (1.27 ± 0.30 mm) and width (0.45 ± 0.08 mm) in 24 fetal temporal bones seemed to have reached adult shape and size in the fetal period itself (Beger et al., 2019). These measurements are almost similar to the mean data presented (Table 2) from the adult sample (Ramirez Aristeguieta et al., 2010; Wojciechowski et al., 2020; Rubini et al., 2020; Beger et al., 2020). This interpretation give us a ground to argue that the muscle belly and tendon size does not change after birth and is similar to the size of adults as reported by few authors (Beger et al., 2019; Wojciechowski and Skadorwa, 2019). Our findings demonstrated that the ST muscle belly length was shown to vary between populations. While the Poland population had the shortest ST belly length, the Colombian population presented with the longest ST belly. However, the ST tendon length remained more or less same in all the studies. The reason for this variation in muscle belly length could be due to the methods of measurements they have used (Table 3).

Table 3. ST measurement methods used in the included studies.

Studies (year)	Points of the measurements of ST muscle
Cheng and Gan (2007) - USA	NR
Ramirez Aristeguieta et al., 2010 - COLUMBIA	Muscle belly: from the most dorso-lateral origin of the muscle to the pyramidal process Tendon: from pyramidal process to its insertion into the neck of the stapes.
Beger et al. (2019) - TURKEY	Muscle belly: was not measured Tendon: from the apex of the pyramidal eminence to the neck of the stapes and width of the tendon at the middle part.
Wojciechowski et al. (2020) - POLAND	Whole muscle was measured in the plane of the lateral semicircular canal from the pyramidal eminence to the neck of the stapes.
Rubini et al. (2020) - ITALY	Whole muscle was measured in antero-posterior distance from the posterior aspect of the stapes capitulum along the line of the ST tendon to the anterior aspect of the Fn in the descending portion.
Beger et al. (2020) - TURKEY	The pyramid was curetted or drilled with diamond burr to measure the muscle, tendon from the pyramidal eminence to the neck of the stapes.

NR: not reported; Fn: Facial nerve

Nevertheless, concordance was noticed between direct anatomical and radiological measurements. In relation to the width of the ST muscle belly and tendon, all included studies did not show any significant difference in values. For total length of the stapedius muscle, the Columbian population had the longest values with the Italian population having the shortest. Comparison between the measured parameters of the population may be relevant during surgery on the middle ear (Tccar et al., 2000; Silverstein et al., 1998), but also in the possible variations in the directions (or) distances between critical structures (Beger et al., 2020; Wojciechowski et al., 2020). Keeping this in mind, we analyzed the mean distance between ST tendon and FN. Only two studies, one based on dissection (Beger et al., 2020) and the other by microtomography (Wojciechowski et al., 2020) have reported the mean distance between ST and FN: it was 1.26 ± 0.24 mm, ranging from 1.14 ± 0.13 mm (Turkey) to 1.35 ± 0.30 (Poland) with no statistically significant differences despite the different measurement methods used.

These data might help surgeons to estimate how much space is there to operate or their choice on kinds of prosthesis or surgical tools they use in otosclerosis surgeries. Role of ST tendon in otosclerosis surgeries is controversial. Some studies stated that the ST tendon cut was quite common and results are satisfactory even without reconstruction of the tendon. However, preservation of the ST tendon was advocated by

several surgeons in the hope of obtaining better functional outcomes (Fowler, 1960; Causse et al., 1997; Silverstein et al., 1998). Few studies reported that ST-tendon-preserving is desirable when the pyramidal process is at the same or higher level than the attachment of the tendon onto the neck of the stapes (Colletti et al., 1988; Dubreuil et al., 1990). In two-thirds of cases; however, the pyramidal process is below the neck of the stapes. In these cases, reconstruction of the ST tendon is preferred (Causse et al., 1997). Our data on morphometrics of tendon will help in reconstructing ST tendon in all the above described cases.

Conclusions

It is important for surgeons to be aware of standard morphometric dataset of ST muscle and tendon. In this systematic review of the stapedius muscle, we confirm that the belly and tendon does not change from intrauterine period to adulthood. There is concordance between direct anatomic measurements and radiologic measurements of the stapedius muscle. The microarchitecture of stapedius muscle and its distance with facial nerve is also very important during both retrotympenic surgery and facial nerve surgery such as decompression and nerve grafting.

ACKNOWLEDGEMENTS

Authors would like to thank Dr. Sameer Qureshi, consultant orthopedic surgeon, CHL medical

center hospital, Ujjain for providing the schematic diagrams. We also thank Prof. Dr. Reginald P. Sequeira, Arabian Gulf University for reviewing our manuscript.

REFERENCES

- ARNOLD W, HÄUSLER R (2007) Otosclerosis and stapes surgery. *Adv Otorhinolaryngol*, 65: 119-126.
- BEGER O, KOÇ T, KARAGÜL Mİ, ÖZDEMİR DL, MÜDÜROĞLU F, CINTACIOIU DG, LE HT, VAYISOĞLU Y, YILMAZ SN, OLGUNUS ZK, TALAS DÜ (2019) Evaluation of the stapedial tendon growth dynamic in human fetuses. *Surg Radiol Anat*, 41(7): 833-839.
- BEGER O, VAYISOĞLU Y, AKBULUT Ş, TAGHIPOUR P, ÇAKIR S, TALAS DÜ (2020) Microsurgical anatomy of the stapedius muscle in adult cadavers. *Anat Sci Int*, 95(1): 540-547.
- CAUSSE V, VINCENT R, MICHAT M, GHERINI S (1997) Stapedius tendon reconstruction: technique and results. *Ear Nose Throat*, 76(4): 260-269.
- CHENG T, GAN RZ (2007) Mechanical properties of stapedial tendon in human middle ear. *J Biomech Eng*, 129(6): 913-918.
- COLLETTI V, SITTONI V, FIORINO F (1988) Stapedotomy with and without stapedius tendon preservation versus stapedectomy: long term results. *Am J Otol*, 9(2): 136-141.
- DUBREUIL C, DUMAREST D, BOULUD B (1990) Conservation du muscle de l'étrier dans le traitement de l'otospongiose. A propos de 48 cas. *Revue de Laryngologie*, 111(1): 23-26.
- ELOVIKOV AM, SELIANINOV AA, LILENKO SV, NIGMATULLINA SV (2014) The biomechanical prerequisites for the preservation of stapedius muscle tendon during stapedioplasty. *Vestn Otorhinolaryngol*, 5: 41-44.
- FOWLER E (1960) Anterior crurotomy with footplate fracture. *Arch Otolaryngol*, 71: 296-299.
- GROS A, VATOVEC J, ŽARGI M (2003) Preservation of the stapedial tendon in surgery for otosclerosis. *Int Congr Ser*, 1240: 89-92.
- MOHER D, LIBERATI A, TETZLAF J, ALTMAN DG, PRISMA GROUP (2009) Preferred reporting items for systematic reviews and metaanalyses: the PRISMA statement. *PLoS Med*, 6(7): e1000097.
- PAAW P (1615) *De Humani Corporis Ossibus*. Leiden. Publisher.
- PRASAD KC, AZEEM MOHIYUDDIN SM, ANJALI PK, HARSHITA TR, INDU VARSHA G, BRINDHA HS (2019) Microsurgical anatomy of stapedius muscle: anatomy revisited, redefined with potential impact in surgeries. *Indian J Otolaryngol Head Neck Surg*, 71(1): 14-18.
- RAMIREZ ARISTEGUIETA LM, BALLESTEROS ACUÑA LE, SANDOVAL ORTIZ GP (2010) Tensor veli palatini and tensor tympani muscles: Anatomical, functional and symptomatic links. *Acta Otorrinolaringol Esp*, 61: 26-33.
- ROBERSON JB, KUNDA LD, STIDHAM KR, INSERRA MM, CHOE W, TONOKAWA L (2006) Modifications of standard cochlear implantation techniques for children under 18 months of age. *Cochlear Implants Int*, 7: 207-213.
- RODRÍGUEZ VÁZQUEZ JF (2010) Morfodiferenciación del músculo del estribo. Aportación personal [Morph differentiation of the stapedius muscle. Personal contribution]. *Anales de la Real Academia Nacional de Medicina*, 127(1): 153-169.
- RUBINI A, JUFAS N, MARCHIONI D, SAXBY AJ, KONG JHK, PATEL N (2020) The endoscopic relationship of the stapedius muscle to the facial nerve: implications for retrotympanic surgery. *Otol Neurotol*, 41:64-69.
- SHEA J (1958) Fenestration of the oval window. *Ann Otol Rhinol Laryngol*, 67(4): 932-951.
- SILVERSTEIN H, HESTER TO, ROSENBERG SI, DEEMS DA (1998) Preservation of the stapedius tendon in laser stapes surgery. *Laryngoscope*, 108(10): 1453-1458.
- STANDRING S, BORLEY NR, COLLINS P, CROSSMAN AR, GATZOULIS MA, HEALY JC (2008) *Gray's Anatomy: The Anatomical Basis of Clinical Practice*. Elsevier, London.
- TCCAR E, TEKDEMIR I, ASLAN A, ELHAN A, DEDA H (2000) Radiological anatomy of the intratemporal course of facial nerve. *Clin Anat*, 13(2): 83-87.

WOJCIECHOWSKI T, SKADORWA T (2019) A few points regarding recent studies on stapedius muscle anatomy. *Surg Radiol Anat*, 41(9): 1099-1100.

WOJCIECHOWSKI T, SKADORWA T, NÈVE DE MÉVERGNIES JG, NIEMCZYK K (2020) Microtomographic morphometry of the stapedius muscle and its tendon. *Anat Sci Int*, 95(1): 31-37.

WRIGHT JL, ETHOLM B (1973) Anomalies of the middle-ear muscles. *J Laryngol Otol*, 87: 281-288.

ZAWAWI F, VARSHNEY R, SCHLOSS MD (2014) Shortened stapedius tendon: a rare cause of conductive hearing loss. *J Laryngol Otol*, 128(1): 98-100.

Morphometry of abductor pollicis longus relevant to surgical reconstruction of hand

Dhivyalakshmi Gnanasekaran, Raveendranath Veeramani, Aravindhan Karuppusamy, Grace Suganya

Department of Anatomy, Dhanvantri nagar, JIPMER, Puducherry, India 605006

SUMMARY

The thumb is considered a marvelous piece of machinery, performing many versatile functions. The thumb is more prone for external injuries apart from the other pathologies which comprises about 5% of the emergencies treated. The external injuries can be treated by several reconstructive procedures such as tendon graft, tendon transfer etc., for which the abductor pollicis tendon can be used. Hence it is essential to know the morphometry and anatomical variations of abductor pollicis longus. 28 freshly embalmed human cadavers of both genders, which included 55 upper limbs, were dissected. The length, thickness, variation in the number and insertion of the abductor pollicis longus tendon were noted. The overall length of the abductor pollicis longus tendon was 63.62 ± 13.74 mm. The thickness of the tendon at the proximal, middle and at the distal level of insertion were 1.15 ± 0.56 mm, 1.02 ± 0.49 mm and 0.89 ± 0.48 mm respectively. No significant morphometric differences of length and thickness were observed between genders and between right and left side at distal level, whereas statistically significant difference exist at the proximal and middle level between the left and the right side. The results obtained from this study regarding the variations and morphometry of the abductor pollicis longus may be helpful

for the surgeons in the various reconstructive procedures of the hand.

Key words: Abductor pollicis longus – Thumb – Thumb abductor – Abductor – Surgical reconstruction

INTRODUCTION

The abductor pollicis longus (APL), is one of the extrinsic muscles of the thumb, which provides dynamic stability to it (Tsiouri et al., 2009; Biant, 2016; Hirschmann et al., 2014). Variation in the APL tendons has been implicated in the development of de Quervain's tenosynovitis. Inadequate release of multiple tendons of APL in the extensor compartment of the wrist may result in the reoccurrence of de Quervain's tenosynovitis (Kulthanan and Chareonwat, 2007). Variable insertion of the accessory slips of APL have been implicated in the development of thumb carpometacarpal joint arthritis or subluxation (Bravo et al., 2010; Schulz et al., 2002). But at the same time the additional slips have been used as grafting material for various tendon reconstruction surgeries (Bravo et al., 2010). Although the APL muscle and its variations have been studied since long, all these studies were done in western populations (Stein, 1951; Coleman et al., 1953; Jackson et al., 1986; Oudenaarde, 1991; Khoury

Corresponding author:

Raveendranath Veeramani. Department of Anatomy, Dhanvantri nagar, JIPMER, Puducherry, India 605006. E-mail: dr_raveendra@rediffmail.com

Submitted: July 8, 2020. Accepted: October 14, 2020

et al., 1991; Brunelli and Brunelli, 1991; Godwin and Ellis, 1993; Bravo et al., 2010; El-Beshbishy et al. and Abdel-Hamid, 2013). Only a few studies have been carried out and there is paucity of knowledge regarding the variation of APL muscle, tendon and its dimension in the Indian literature (Joshi and Joshi, 2002; Tewari et al., 2015; Roy et al., 2012). The main objective of the present study is to find the incidence of variation in the APL muscle belly and the tendon, and also to document the detailed measurements of the APL tendon.

MATERIALS AND METHODS

The study was done in the department of anatomy, JIPMER, Puducherry from July 2016 to May 2018, after getting approval from the postgraduate research monitoring committee and the ethical clearance from the institute ethics committee. Twenty-eight formalin-fixed adult human cadavers of both genders available for undergraduate dissection in the Department of Anatomy, JIPMER, were taken up for the study. All embalmed cadavers without any damage were included in the study whereas, if there was any evidence of damage or loss of tissue in the region of the thumb, distal forearm and wrist were excluded. The right thumb of one of the female cadavers was amputated previously, hence a total sample of 55 upper limbs was included in the study.

The upper limb of the cadaver was kept abducted at the shoulder joint and in the supine position. The thumb was kept in extended position and the dissection was carried out. The distal forearm and hand were dissected in the dorsal aspect. The APL tendon inserted into the thumb was identified and traced backward. The course of the tendon and the muscle belly was traced by opening the first extensor retinaculum. Variations in the attachment of muscle, number of tendons and its site of insertion were noted. After dissection, the thumbs were photographed using a digital camera. Length of the tendon was measured from the distal end of the muscle fiber to the site of insertion of the tendon. The thickness of the tendon was measured at three places as follows: proximal— just after the ending of the muscle fibers at musculotendinous junction; middle—

at the middle of the first dorsal compartment; and distal— just before its insertion. All the measurements were taken using mitutoyo digital Vernier caliper to the nearest millimeters (mm) by one single investigator. The results were expressed in range, mean, standard deviation and inter-quartile range. In case of multiple slips, the mean of the measurements of the multiple tendons were calculated for each hand and then compared between the left and right hands of matched pairs (27 hands). All relevant data were recorded and analyzed using IBM_PASW STATISTICS ver. 19.0 (SPSS ver 19.0). For left- and right-side comparison of the mean of the abovementioned quantitative variables, paired t-test (normal distribution) or Wilcoxon signed-rank test (non-normal distribution) were used. And for comparison between genders independent student t-test (normal distribution) and Mann Whitney U test (non-normal distribution) were used.

RESULTS

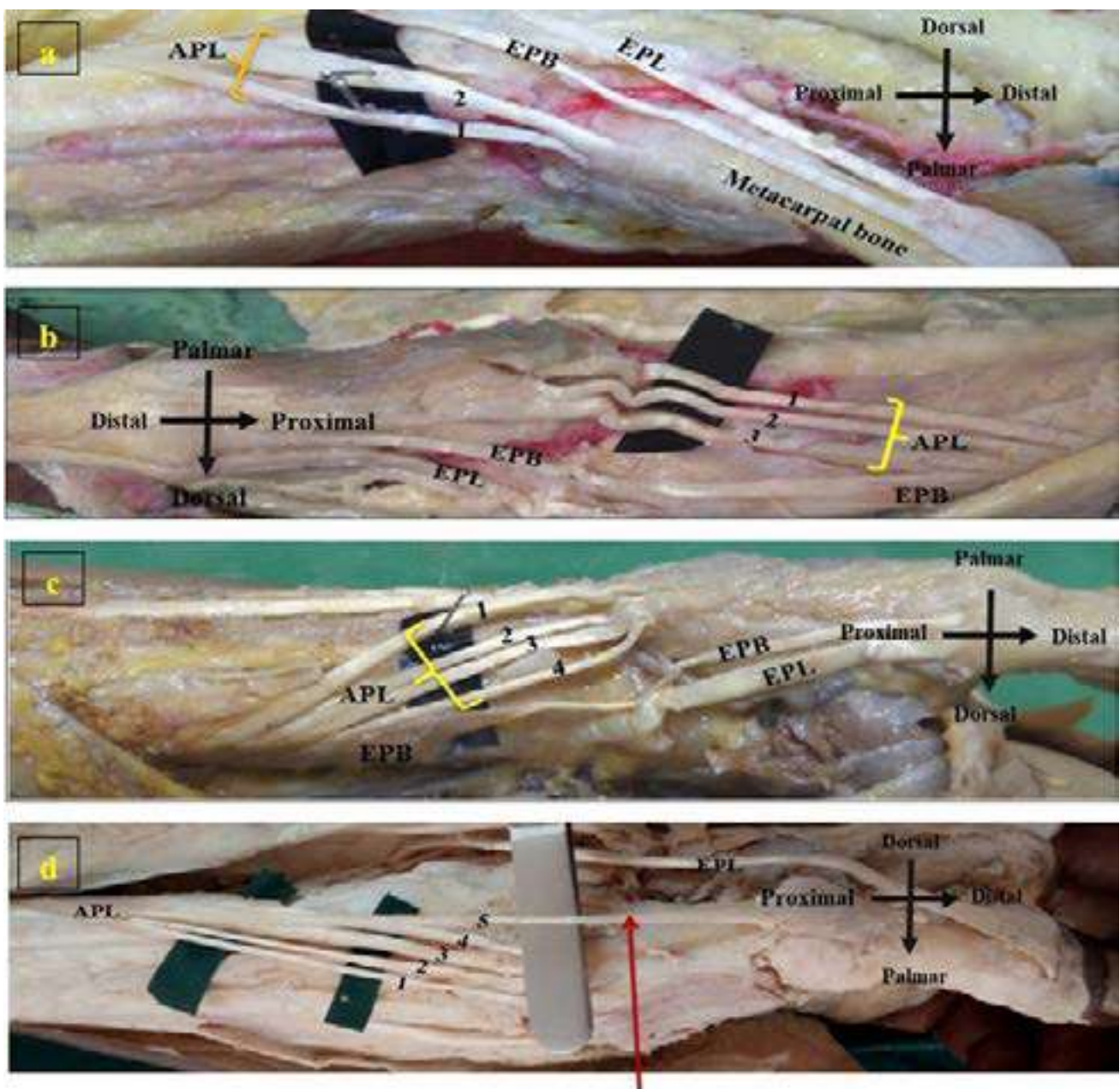
The APL muscle was present in all of the dissected hands (55 hands). The muscle was found to be fused with the extensor pollicis brevis (EPB) muscle to a variable degree from its origin until it gives rise to tendons in 54 hands. In one hand the EPB muscle belly and the tendon was absent, so an independent APL muscle belly was seen in this case (Fig. 1d). But in other 54 hands, an identifiable fascial plane separating both the APL and EPB muscle was found at least in the distal end of the muscle fiber. Hence no separate or distinct APL muscle belly was seen in 98% (54 hands). There was also no additional APL muscle belly.

Single APL tendon was not observed in any of the dissected hands. The number of APL tendons observed ranges from two to six (Fig. 1). The frequency distribution of number of APL tendon in each hand is given in Fig. 2.

The APL tendon inserts into the base of the first metacarpal in the majority of hands. Some of the tendons also get inserted into the thenar muscle (Fig. 3a), into the trapezium (Fig. 3b), part of tendon into the trapezium and partly into

the thenar muscle (Fig. 3.c), and sometimes it also gets inserted partly into the base of the first metacarpal and the remaining into the thenar muscle (Fig. 3d). In one hand where the EPB muscle and the tendon was absent, it was found that one of the five tendons of the APL muscle inserted into the base of the proximal phalanx instead of the normal EPB tendon (Fig. 1d). The frequency distribution of APL tendon based on the site of insertion is given in Fig. 4.

More than one APL tendon was present in 100% of the dissected hands (55 hands). Hence in total 186 tendons, measurements were taken up for the analysis. The overall length and thickness of the APL tendon is provided in Table 1. The average of the measurements such as length of the APL tendons and thickness of the tendons at proximal, middle and distal level showed no significant difference between male and female (Table 2).



APL tendon insertion into the base of the proximal phalanx instead of the EPB tendon

Fig. 1.- Variation in the number of APL tendons. a. Two, b. Three, c. Four, d. Five APL tendons. In figure d 5 independent APL muscle belly with absent EPB muscle belly and APL tendon number 5 attached to the base of the proximal phalanx instead of EPB tendon. APL - Abductor Pollicis Longus; EPB - Extensor Pollicis Brevis.

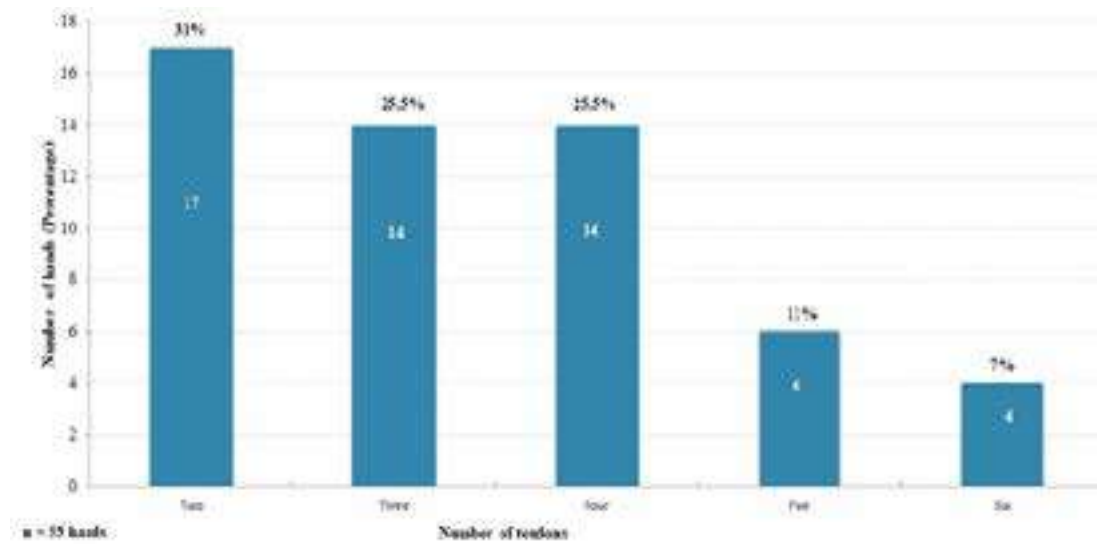


Fig. 2.- Distribution of number of abductor pollicis longus tendon per hand.

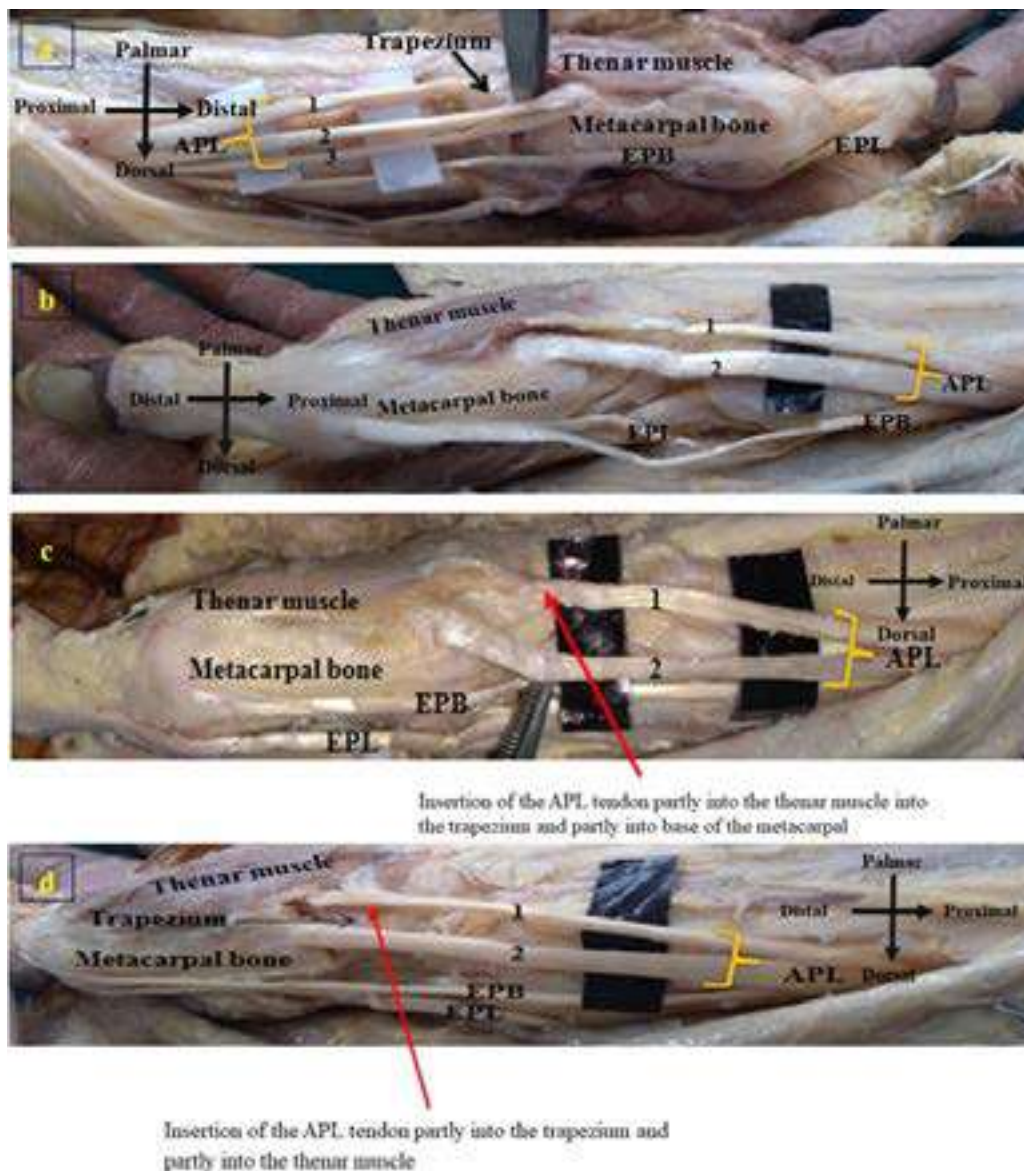


Fig. 3.- Variation in the insertion of APL tendons. a. Insertion of tendon 1 into thenar muscle. b. Insertion of tendon 1 into the trapezium. c. Insertion of tendon 1 partly into the thenar muscle and partly into the trapezium. d. Insertion of tendon 1 partly into the thenar muscle and partly into the metacarpal. APL - Abductor Pollicis Longus; EPB - Extensor Pollicis Brevis; EPL - Extensor Pollicis Longus.

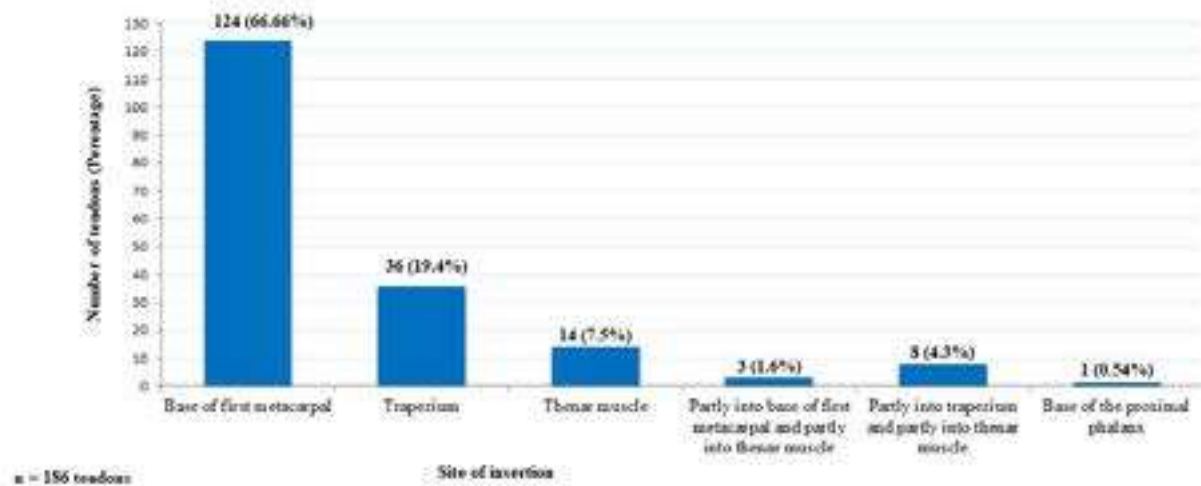


Fig. 4.- Distribution of abductor pollicis longus tendon based on the site of insertion.

Table 1. Overall length and thickness of the abductor pollicis longus tendon (mm); (Minimum, maximum, mean \pm standard deviation) n=186 tendons.

S.no	Parameters	Minimum	Maximum	Mean \pm Standard deviation
1	Length of the tendon	40.68	98.47	63.62 \pm 13.74
2	Thickness of the tendon at the proximal level	0.26	3.52	1.15 \pm 0.56
3	Thickness of the tendon at the middle level	0.31	2.85	1.02 \pm 0.49
4	Thickness of the tendon at the distal level	0.39	3.53	0.89 \pm 0.48

Table 2. Comparison of length and thickness of the abductor pollicis longus tendons between the genders (mm); Median (Interquartile range); n = 186 tendons; All the parameters measured showed non-normal distribution. Mann-Whitney U test was applied for statistical analysis.

S. No.	Parameters	Male (127 tendons)	Female (59 tendons)
1	Length of the tendon	59.4 (17.27)	66.40 (28.86)
2	Thickness of the tendon at proximal level	1.11 (0.80)	1.02 (0.63)
3	Thickness of the tendon at the middle level	0.88 (0.63)	0.97 (0.60)
4	Thickness of the tendon at distal level	0.69 (0.44)	0.74 (0.45)

The mean length of the APL tendon measured in the left side (94 tendons) and right side (92 tendons) was 65.22 mm and 61.50 mm. The thickness of the tendons measured at the proximal, middle and distal level on the left side were 1.23 mm, 1.08 mm, 0.91 mm and the same measured on the right side were 1.06 mm, 0.95 mm and 0.86 mm respectively.

The average of the measurements related to the APL tendons were compared between the matched pairs (27 hands). No significant differences were observed between the left and the right side related to the measurements such as length of the tendon and the thickness at distal level. But there exists significant difference in the thickness of the tendon at proximal and at middle level between the left and the right side (Table 3).

DISCUSSION

The present study involved dissection of 55 upper limbs to study the APL muscle. Out of these 55 limbs, the independent APL muscle was seen in only one of the dissected hands whereas the muscle was found to be fused with extensor pollicis brevis muscle to a variable extent in the remaining 54 hands. Fabrizio and Clemente (1996) observed variation in the APL muscle belly in 30% (15 out of 50 hands) of dissected hands. In all of these hands, an additional APL muscle belly was found to arise from the lateral aspect of distal portion of normal APL muscle

(Fabrizio and Clemente, 1996). In another study, two independent APL muscle bellies were found in 20% (16 out of 78 hands) (Bravo et al., 2010). Rarely, the APL having three independent muscle bellies have also been documented in the literature (Sarikcioglu and Abdel-Hamid, 2004). While in the other study, the APL muscle was identified with two muscle bellies with each one giving rise to an independent tendon. Of these two tendons, one tendon was inserted into the first metacarpal and the other tendon again split into three to insert into the abductor pollicis brevis, opponens pollicis, and flexor pollicis brevis muscles. The tendon slip inserted into the abductor pollicis brevis was described to have acquired muscular characteristics before insertion (Yuksel et al., 1992). Brandsma et al. (1996) suggested that such insertion of the APL into the abductor pollicis brevis can be considered a digastric muscle (one long muscle with two bellies).

Table 3. Comparison of mean length and thickness of the abductor pollicis longus tendon between paired limbs (mm); [Mean \pm Standard deviation/ Median (Interquartile range)]. * paired sample t-test; # Wilcoxon signed-rank test was applied for statistical analysis.

S. No.	Parameters	Left (27 hands)	Right (27 hands)	p-value
1	Length of the tendon *	67.59 \pm 11.0	65.6 \pm 14.10	0.45
2	Thickness of the tendon at the proximal level *	1.24 \pm 0.28	1.08 \pm 0.29	0.04
3	Thickness of the tendon at the middle #	1.19 (0.43)	1.01 (0.27)	0.02
4	Thickness of the tendon at the distal level #	0.95 (0.51)	0.89 (0.30)	0.76

In our study, single APL tendon was not seen in any of the dissected hands, similar to El-Beshbishy and Abdel-Hamid (2013). Two tendons were observed in 31%. Three tendons and four tendons were observed in 25% each. In 11% five tendons were observed and six tendons in 7% of the dissected hands. Variations in the number of the APL tendons were reported to be ranging from one to six in numbers. Some studies have even reported up from seven to nine APL tendon

slips (Sarikcioglu and Yildirim, 2004; Mansur et al., 2010). The incidence of the number of APL tendon slips in various studies is given in Table 4. Melling et al. (1996) stated that multiple slips of APL are also observed in other primates like gorillas and gibbons, suggesting the possibility of APL being an atavistic structure in humans.

Regarding the insertion of APL tendon, it was observed from this study that APL tendons inserted most commonly into the base of the first metacarpal bone (66%), similar to other studies. And insertion of the tendons into the trapezium was seen in only 19% in the present study, which is similar to the study by Roy et al. (2012). Tewari et al. (2015) reported such type of insertion was seen in 41% and on the other hand Khoury et al. (1991) could see it in 6% only. Brunelli and Brunelli (1992) opined from their cadaveric study that absence of insertion of the tendon into the trapezium should be regarded as normal as it was seen in 71% cases. It was claimed that absence of insertion into the trapezium could result in instability and arthritis of the trapeziometacarpal joint (Brunelli and Brunelli, 1992). Abnormal insertion of all four slips of APL into the fascia of APB muscle has resulted in laxity and recurrent subluxation of the trapeziometacarpal joint (Martinez and Omer, 1985). In the present study no insertion of the tendons into the thenar fascia was seen. Apart from insertion of the APL muscle into the base of first metacarpal, variable insertion site of these accessory tendons has been reported in the literature. Additional insertion sites of the APL tendon documented in the literature were the trapezium bone, the opponens pollicis or the abductor pollicis brevis muscle. Few cases have reported about insertion into the flexor pollicis brevis muscle, the scaphoid bone, fascia covering the thenar muscle, capsule of the trapeziometacarpal joint, anterior oblique ligament of this joint capsule and thumb proximal phalanx' base. Rarely, it was documented to insert into the wrist extensor retinaculum (Sarikcioglu and Yildirim, 2004, Kocabiyik et al., 2009). The tendons of the APL were considered to stabilize the carpometacarpal joint of the thumb (Fabrizio and Clemente, 1996). Sometimes the distal extension of APL muscle belly into the first

extensor compartment produces painful thumb and wrist on movement (Patel et al., 1988). In our study no such extension of APL muscle belly into the extensor compartment was observed. The variations in the site of insertion of the APL tendon in various studies are given in Table 5.

The embryological reasons of multiple slips and its variable distal attachments could be due to persistence of an early embryonic developmental state of APL muscle. In a human embryo with a crown-rump length of 20 mm the differentiating APL tendon is divided into three strips; the palmar slip blended with the opponens pollicis, middle

inserts into the trapezium and the dorsal into the base first metacarpal. Later, when the crown-rump length becomes 60 mm various new connections are established between the palmar strip and adjacent abductor pollicis brevis meanwhile the connection with the opponens pollicis is lost. This supports our study as more than one APL tendons was observed in all the 55 hands (Tewari et al., 2015).

Only very few studies have measured the dimensions of the APL tendons and they followed different methodology. There was difference in the grouping of the APL tendon slips. El-Beshbishy and Abdel-Hamid (2013) classified

Table 4. The incidence of the number of abductor pollicis longus tendon slips in various studies.

Number of tendons (Percentage)	Jackson et al., 1986, Texas & Toledo 300 hands	Oude-naarde, 1991, Netherland, 84 hands	Khoury et al., 1991, France, 54 hands	Brunelli & Brunelli, 1991, Italy, 100 hands	Bravo et al., 2010, Spain, 78 hands	Roy et al., 2012, India, 86 hands	El-Beshbishy & Abdel-Hamid, 2013, Saudi Arabia, 50 hands	Tewari et al., 2015, India, 50 hands	Present study
1	27.67	7.14	24.1	2	15	38.37	0	4	0
2	60.33	23.81	55.1	2	73	58.14	40	62	31
3	9.67	34.52	18.5	13	8	2.33	34	16	25.5
4	2	20.24	1.9	30	4	1.16	18	16	25.5
5	0.33	11.90	-	49	-	-	4	0	11
6	-	2.38	-	4	-	-	4	2	7

Table 5. Comparison of variation in the site of insertion of abductor pollicis longus tendon with other studies. APL - Abductor Pollicis Longus; AAPL - Accessory Abductor Pollicis Longus.

Site of insertion (Percentage)	Khoury et al., 1991, France, 54 hands	Joshi and Joshi, 2002, India, 50 hands		Bravo et al., 2010, Spain, 78 hands		Roy et al., 2012, India, 86 wrist	Tewari et al., 2015, India, 50 hands	Present study, India, 55 hands
	APL	APL	AAPL	APL	AAPL	AbPL	APL	APL
Base of the first metacarpal	71.2	100	-	98.72	1	60.14	53.97	66.66
Thenar muscle	22.7	-	-	1.28	-	-	-	7.5
Thenar fascia	-	-	20	-	-	-	2	-
Trapezium	5.9	-	30	-	41	22.38	41.27	19.4
Abductor pollicis brevis	-	-	44	-	22	12.59	-	-
Opponens pollicis	-	-	16	-	5	3.49	3.17	-
Both trapezium and thenar muscle	-	-	-	-	15	-	-	4.3
CMC joint	-	-	-	-	-	1.40	-	-
Partly into the base of metacarpal and partly into thenar muscle	-	-	-	-	-	-	-	1.6
Base of the proximal phalanx	-	-	-	-	-	-	-	0.54

the tendon slips into two groups. Those tendons that were lying adjacent to the EPB muscle were regarded as normal APL tendons (lateral group), while other tendons lying medially were regarded as the accessory tendons (medial group) (El-Beshbishy and Abdel-Hamid, 2013). Bravo et al. (2010) considered that the tendon slips radial to the main APL tendon and lying close to the EPB as the accessory ones. Bravo et al. (2010) measured the thickness and width of the main and accessory tendons at its insertion site. We could not compare our study results related to the tendons dimension with that of Bravo et al. (2010) and of El-Beshbishy and Abdel-Hamid (2013). Melling et al. (1996) suggested that the number, thickness and length of the accessory tendons of APL and EPB might have an important function in the development of de Quervain's disease.

Therefore, the knowledge of anatomical variations, arrangements, and prevalence of the multiple tendons of APL is of utmost importance for the physicians and surgeons to diagnose and treat various clinical conditions arising out of it, for repairing the injured tendons and during reconstructive surgery involving tendon transfer, tendon graft etc.

REFERENCES

- BIANT LC (2016) Elbow and forearm. In: Standring S (ed). *Gray's Anatomy: the anatomical basis of clinical practice*. 41st ed. New York: Elsevier Limited, pp 837-861.
- BRANDSMA JW, OUDENAARDE EV, OOSTENDROP R (1996) The abductores pollicis muscles: clinical considerations based on electromyographical and anatomical studies. *J Hand Ther*, 9(3): 218-222.
- BRAVO E, BARCO R, BULLON A (2010) Anatomic study of the abductor pollicis longus: a source for grafting material of the hand. *Clin Orthop Relat Res*, 468(5): 1305-1309.
- BRUNELLIG A, BRUNELLI GR (1992) Anatomy of the extensor pollicis brevis muscle. *J Hand Surg*, 17(3): 267-269.
- COLEMAN SS, McAFEE DK, ANSON BJ (1953) The insertion of the abductor pollicis longus muscle. an anatomical study of 175 specimens. *Quart Bull Northwestern Univ Med School*, 27(2): 117-122.
- EL-BESHBISHY RA, ABDEL-HAMID GA (2013) Variations of the abductor pollicis longus tendon: an anatomic study. *Folia Morphol (Warsz)*, 72(2): 161-166.
- FABRIZIO PA, CLEMENTE FR (1996) A variation in the organization of abductor pollicis longus. *Clin Anat*, 9(6): 371-375.
- GODWIN Y, ELLIS H (1993) Anatomical study of the symmetry of lateral extensor compartment of the wrist. *Clin Anat*, 6(4): 222-225.
- HIRSCHMANN A, SUTTER R, SCHWEIZER A, PFIRRMANN CW (2014) MRI of the thumb: anatomy and spectrum of findings in asymptomatic volunteers. *Am J Roentgenol*, 202(4): 819-827.
- JACKSON WT, VIEGAS SF, COON TM, STIMPSON KD, FROGAMENI AD, SIMPSON JM (1986) Anatomical variations in the first extensor compartment of the wrist. *J Bone Joint Surg Am*, 68(6): 923-926.
- JOSHI SS, JOSHI SD (2002) Applied significance of variations of the first extensor compartment of wrist. *J Anat Soc India*, 51(2): 159-161.
- KHOURY Z, BERTELLI J, GILBERT A (1991) The subtendons of the abductor pollicis longus muscle. *Surg Radiol Anat*, 13(3): 245-246.
- KOCABIYIK N, TATAR I, YALCIN B, YAZAR F, OZAN H (2009) Tendon variations of extensor digitorum and abductor pollicis longus muscles. *IJAV*, 2: 54-56.
- KULTHANAN T, CHAREONWAT B (2007) Variations in abductor pollicis longus and extensor pollicis brevis tendons in the Quervain syndrome: a surgical and anatomical study. *Scand J Plast Reconstr Surg Hand Surg*, 41(1): 36-38.
- MANSUR DI, KRISHNAMURTHY A, NAYAK SR, KUMAR CG, RAI R, D'COSTA S, PRABHU LV (2010) Multiple tendons of abductor pollicis longus. *IJAV*, 3: 25-26.
- MARTINEZ R, OMER JR (1985) Bilateral subluxation of the base of the thumb secondary to an unusual abductor pollicis longus insertion: a case report. *J Hand Surg Am*, 10(3): 396-399.

MELLING M, WILDE J, SCHNALLINGER M, SCHWEIGHART W, PANHOLZER M (1996) Supernumerary tendons of the abductor pollicis. *Acta Anat*, 155(4): 291-294.

MILETIN J, SUKOP A, BACA V, KACHLIK D (2017) Arterial supply of the thumb: systemic review. *Clin Anat*, 30(7): 963-973.

PATEL MR, DESAI SS (1988) Anomalous muscles of the first dorsal compartment of the wrist. *J Hand Surg Am*, 13(6): 829-831.

ROY AJ, ROY AN, DE C, BANERJID, DAS S, CHATTERJEE B, HALDER TC (2012) A cadaveric study of the first dorsal compartment of the wrist and its content tendons: anatomical variations in the Indian population. *J Hand Microsurg*, 4(2): 55-59.

SARIKCIOGLU L, YILDIRIM FB (2004) Bilateral abductor pollicis longus muscle variation: Case report and review of the literature. *Morphologie*, 88(282): 160-163.

SCHULZ CU, ANETZBERGER H, PFAHLER M, MAIER M, REFIOR HJ (2002) The relation between primary osteoarthritis of the trapeziometacarpal joint and supernumerary slips of the abductor pollicis longus tendon. *J Hand Surg Br*, 27(3): 238-241.

STEIN AD (1951) Variations of the tendons and insertions of the abductor pollicis longus and extensor pollicis brevis. *Anat Rec*, 110(1): 49-55.

TEWARI J, MISHRA PR, TRIPATHY SK (2015) Anatomical variation of abductor pollicis longus in Indian population: A cadaveric study. *Indian J Orthop*, 49: 549-553.

TSIOURI C, HAYTON MJ, BARATZ M (2009) Injury to the ulnar collateral ligament of the thumb. *Hand (NY)*, 4(1): 12-18.

VAN OUDENAARDE E (1991) Structure and function of the abductor pollicis longus muscle. *J Anat*, 174: 221.

YUKSEL M, ONDERAGLU S, ARIK Z (1992) Case of an abductor pollicis longus muscle: variation or differentiation? *Okajimas Folia Anat Jpn*, 69(4): 169-171.

Evaluation of the effect of n-hexane extract of *Leptadenia hastata* on the histomorphology of the liver in streptozotocin induced diabetic Wistar rat

Martha O.O. Attah¹, Tamunotonye W. Jacks², Sani H. Garba¹

¹ Department of Human Anatomy, Faculty of Basic Medical Sciences, University of Maiduguri, P.M.B. 1069, Maiduguri, Borno State, Nigeria

² Department of Human Anatomy, Rivers State University, Port-Harcourt, Rivers State, Nigeria

SUMMARY

Diabetes mellitus is becoming a serious health challenge to many individuals all over the world. The treatment and management of diabetes is geared towards keeping blood glucose levels as closely related as possible to that in healthy individuals. Medications used to treat diabetes are usually associated with complications and may cause different side effects, in addition to being unavailable in some rural areas. Many traditional anti-diabetic plants have become popular in the management of diabetes mellitus in such instances, and *Leptadenia hastata* has been used as locally as treatment for diabetes. The present study aimed at evaluating the effect of n-hexane extract of *Leptadenia hastata* on the histology of the liver in streptozotocin (STZ)-induced diabetic rats.

Diabetes mellitus was induced in 20 Wistar rats using a single injection of streptozotocin (50 mg/kg i.p.). The rats were divided into four groups of 5 rats each. Group III were untreated diabetic rats, Group IV and V were administered with 100mg/kg and 200mg/kg of the extract respectively, group VI was treated with insulin (6IU/kg) Groups I and II were non-diabetic rats. Group I rats were treated

with olive oil and group II rats were treated with 200mg/kg of the extract for 28 days. Histological observation revealed dilation of central veins, degeneration of hepatocytes, and reduced glycogen granules in the untreated diabetic group. These pathological changes were ameliorated in the *Leptadenia hastata* extract and insulin-treated rats. *Leptadenia hastata* extract may represent an alternative treatment to control diabetes mellitus and its associated hepatopathy.

Key words: Diabetes mellitus – *Leptadenia hastata* – Liver – Histology – n-Hexane extract

INTRODUCTION

Diabetes mellitus (DM) was once considered to be a disease of trivial significance but has now become a major public health challenge of the 21st century, especially in developing countries (Venkataramana et al., 2013). DM is defined as a clinical syndrome which is characterized by hyperglycemia due to absolute or relative deficiency of insulin, as well as disturbances of carbohydrate, fat and protein metabolism associated with absolute or relative deficiency in insulin secretion or insulin action (Jayakar and

Corresponding author:

Martha Orendu Oche Attah. University of Maiduguri, Department of Human Anatomy, Faculty of Basic Medical Sciences, University of Maiduguri, 60006 Maiduguri, Nigeria. E-mail: marthaorendua@uni-maid.edu.ng / marthaorendua@gmail.com

Submitted: July 18, 2020. Accepted: October 14, 2020

Suresh, 2003; World Health Organization 2013). DM can be divided into two principal forms: Type I diabetes mellitus (Type I DM) and Type II diabetes mellitus (Type II DM). Type I DM is characterized by loss of insulin producing beta cells of the islets of Langerhans in the pancreas leading to insulin deficiency. This type can be further classified as immune-mediated or idiopathic. The popular cause of Type I DM is of the immune-mediated nature, in which beta cell loss is a T-cell-mediated autoimmune attack (Rother, 2007). Type II DM is characterized by insulin resistance and/or abnormal insulin secretion. Individuals with Type II DM are not dependent on exogenous insulin, but may require it for control of blood glucose levels if this is not achieved with diet alone or with oral hypoglycemic agents (Venkataramana et al., 2013).

The past two decades has heralded an upsurge in the number of people diagnosed with DM worldwide (Ukwani and Igbokwu, 2015). It is one of the major causes of premature death worldwide. Every ten seconds, a person dies from diabetes-related causes, mainly from cardiovascular complications. In 2010, it was reported that about 6.6% people (representing 285 million people) suffer from diabetes (International Diabetes Federation, 2017, Cho et al., 2018). It is predicted that about 366 million people are likely to be diabetic by the year 2030 (Wild et al., 2004). In sub-Saharan Africa, Nigeria has the highest number of people with DM with an estimated 3.9 million people (World Health Assembly, 2013). In addition, there are about 1.8 million undiagnosed Nigerians suffering from DM (Dahiru et al., 2016). Treatment of DM has always included the administration of insulin and oral hypoglycemic agents in conjunction with dietary counselling and life style modification (Bella, 1990). Insulin therapy and oral hypoglycemic agents offer effective glycaemic control; yet, their shortcomings limit their usage (Anuradha et al., 2004). The disadvantages of oral and injected hypoglycemic agents include: injection-site pain or abscess, cost implications, decreased appetite, weight gain, risk of hypoglycemia and gastrointestinal discomfort (Valeron and de Pablos-Velasco, 2013). *Leptadenia hastata* (Pers) Decne (Family-Asclepiadaceae), commonly known as

yadiya, is an edible non-domesticated vegetable collected in wild throughout Africa. It is a voluble herb with creeping latex stems, glabrescent leaves, glomerulus and racemus flowers, as well as follicle fruits. Wild plants like *Leptadenia hastata* provide food security during seasonal changes and are used medicinally in many areas. The breeders commonly used the leaf and stems for their parasitic activity and against placental retention (Bello et al., 2011).

Ethno-botanical information obtained from traditional medical practitioners in northern Nigeria and during the course of this study revealed that it is used locally for the treatment of diabetes mellitus. Its antimicrobial effect has been also reported by Aliero and Wara (2009). DM induced by streptozotocin and alloxan in laboratory animals have been reported in causing pathological alterations in the liver, which vary from steatosis to steatohepatitis and liver fibrosis (Bilal et al., 2016). Currently available therapies for diabetes have a number of adverse effects, and as such there is an increased interest in the search for more effective and safer hypoglycemic agents to be administered in lieu of the existing medication. *Leptadenia hastata* is traditionally used in the management of DM and its hypoglycemic activities has been previously reported. However, there is the dearth of scientific evidence on the effects of the plant on organs like the liver, which serves as the body's primary organ for detoxification and metabolism. It is also a site for biotransformation by which a toxic compound gets transformed to less harmful form to reduce toxicity. However, toxic compounds could damage the liver cells and produce hepatotoxicity (Rajeshkumar, 2010). In view of the above, the present study was aimed to evaluate the effects of *Leptadenia hastata* on the histology of the liver in streptozotocin-induced diabetic rats.

MATERIALS AND METHODS

Collection, identification and extraction of plant material

Leptadenia hastata was collected from a garden, the leaves were harvested, washed and shade-dried for a period of two weeks, and then ground

to powder using a mortar and pestle. The powder was sieved to obtain the fine powder; it was then labeled and stored for use.

Maceration technique as described by Azwanida (2015) was used for extraction in the current study. The leaf powder weighing 500g was dissolved in 3 liters of n-hexane in a 5-liter stoppered container. Maceration involved soaking the plant, which is allowed to stand at room temperature for a period of 3 days at the minimum with periodic agitation. The process softened and broke the plant's cell wall to release the soluble phytochemicals. After 3 days, the mixture was filtered using Whatman's filter paper. The resulting n-hexane filtrate was concentrated to dryness in-vacuo using an evaporator and the resulting powder was kept in an air-tight container and refrigerated.

Experimental animals

All experiments were performed using Wistar albino rats of both sexes. A total of 30 albino rats weighing 135-190 g were used. The rats were obtained from the National Veterinary Research Institute (NVRI) Vom, Plateau State, Nigeria. They were kept in the Animal house of the Department of Human Anatomy, Faculty of Basic Medical Sciences, College of Medical Sciences, University of Maiduguri, Borno State for two weeks prior to the start of the experiment to acclimate to the new environment. The rats were weighed and maintained under controlled conditions of humidity (50-60%), temperature of 22°C±3°C, 12 hours light and 12 hours dark as well as adequate ventilation. They were fed with pelletized ECWA (Jos) feed and water *ad libitum*.

Experimental design

Diabetes was induced in twenty rats. These diabetic rats were divided into four groups (3-6) of 5 rats each. Rats in groups 3-6 received olive oil, 100 mg/kg of extract, 200 mg/kg of extract and insulin (6 IU/kg), respectively. In addition, 10 non-diabetic rats were grouped into 1 and 2. They received olive oil and 200 mg/kg of extract, respectively for 28 days. Olive oil was used as vehicle to dissolve the extract as it was not soluble in water.

Experimental induction of diabetes in rats

Hyperglycemia was induced in overnight fasted Wistar rats by a single intra-peritoneal injection of 50 mg/kg streptozotocin (Bristol-Sigma, Bristol Scientific Company, Missouri, United States of America) dissolved in 0.1M ice-cold sodium citrate buffer, (pH = 4.5), immediately before use in a volume of 1 ml/kg body weight as described by Etuk (2010). Hyperglycemia was confirmed by the elevated plasma glucose levels determined in tail blood sample using a glucometer (Roche, Germany). Rats whose fasting blood glucose levels exceeded 250 mg/dl (13 mmol/dl) after one week were considered as diabetic and used for the study. Urinalysis was also carried out to confirm diabetes in all groups according to a method adopted by Houcine et al. (2011).

Administration of the extract

The extract was given orally for a period of 28 days and administration was carried according to OECD guidelines (OECD TG 407) [European Chemicals Agency, 2016]. At the end of the experimental period, the animals were sacrificed by inducing sleep by injecting with ketamine hydrochloride (Rotexmedica, Trittau, Germany); the liver was removed and fixed in 10% formalin in preparation for routine histological processing.

Use of glucometer strips to determine blood glucose level

Serum glucose levels were determined weekly by testing the blood obtained from the tail of rats in all groups using Accucheck glucometer strips. The tip of the rat tail was swabbed with a disinfectant and then the tip of the tail pierced using an Accu-check Softclix lancet, and then the blood was applied to an Accu-check strip and then the strip, which was inserted into the Accu-check blood glucose meter to obtain a reading. The blood glucose level was read off the meter and the result recorded.

Analysis of serum glucose level

At the end of 28 days, the serum glucose levels were determined using Labkit protocol (Barcelona, Spain) kits using the glucose oxidase

method as described by Kanagasabapathy and Kumari (2000). The mass spectrometer was adjusted to zero with blank or reagent. The sample was pipetted into a curvette along with the following solutions: in the first test tube, 1.0 ml of the reagent was added, in the second test tube, 1.0 ml of reagent and 10 μ L of calibrator was added and in the third test tube, 1.0 ml of reagent and 10 μ L was added. These solutions were mixed and incubated for 5 minutes at 37°C or 10 minutes at room temperature (15-25°C). The absorbance of the samples and calibrator were observed against the blank and calculated if the color was observed to be stable for at least 30 minutes.

Calculations:

$$\text{Glucose (mg/dl)} = \frac{(\text{A}) \text{ Sample} \times 100 (\text{Calibrator conc})}{(\text{A}) \text{ Calibrat}}$$

or Calibrator Conversion factor: $\text{mg/dL} \times 0.555 = \text{mmol/L}$

Analysis of the histological sections

The images of the histological sections were obtained using an Amscope light microscope (MBJX-ISCOPE, Los Angeles) fitted with a digital camera (M500, X 64, version 3.7) under several magnifications. Images of the histological sections were obtained using 10X objective lens

and were also analyzed using Amscope Image software. An ocular micrometer, which was previously standardized with a stage micrometer, was also used to measure areas of interest in the histological slides. The results were analyzed using GraphPad Instat Software (Version 3.75).

The histological section of the liver in all groups were morphometrically analyzed to observe the following measurements.

- Diameter of the central vein (μm)
- Width of the sinusoids (μm)
- Width of the hepatocytes (μm)

RESULTS

Histological observations in the liver

The micrographs of the liver in all groups are represented by Figs. 1A-F and 2A-F. Liver sections obtained from normal group (group 1) revealed normal histological architecture with regular hepatic lobules with central veins, and peripheral portal areas were observed (Fig. 1A). Hepatocytes with sinusoidal spaces were extending radially from the central veins to the boundaries of portal areas. There was mild congestion of the hepatic

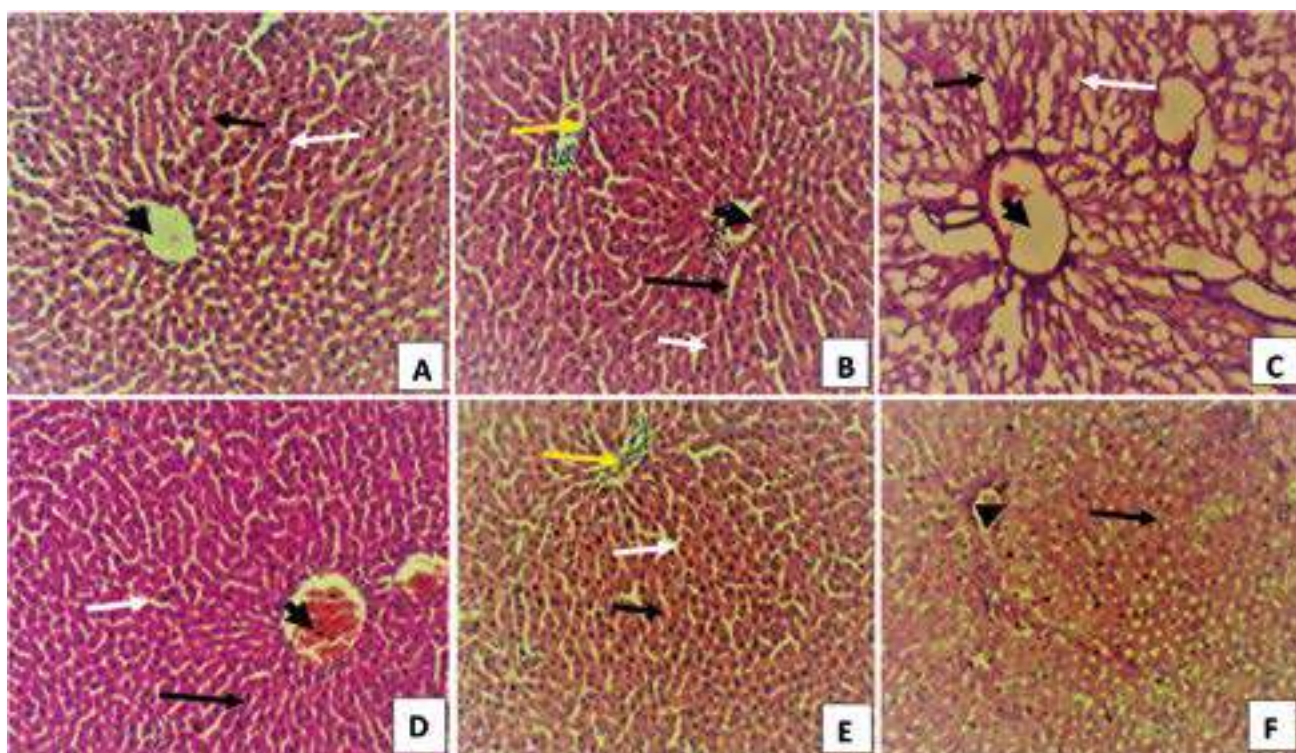


Fig. 1.- Photomicrographs of liver of rats in all groups after the 28 day oral toxicity study. Black arrow – cords of hepatocyte, white arrow – sinusoid, black arrow head – central vein, yellow arrow – portal triad. Groups I (A), II (B), III (C), IV (D), V (E) and VI (F). H&E staining. x 100.

vein in the rats in Group II. The rats in Group III showed wider sinusoids (white arrow) and degenerative changes to the hepatocytes (white arrow). The central veins (black arrow head) in this group were wider and more dilated than in the other groups. In Group IV, V and VI, the architecture of the liver was normal (Figs. 1D, E and F), with clear sinusoid (white arrow), hepatic cords (black arrow) and central vein (black arrow head).

Fig. 2A-F represents the micrographs of the liver stained with PAS to show the presence of glycogen in the hepatocytes. The presence of glycogen is indicated by a magenta-colored cytoplasm and blue-black nucleus. The micrograph of the liver tissue in all groups showed the presence of abundant distribution of glycogen in the cytoplasm of the hepatocytes in all groups, which was most marked in Group III rats (Fig. 2F).

Morphometric findings of the liver

The central vein diameter in the diabetic untreated rats (group III) showed a significantly ($P < 0.05$) wider sinusoids and central vein when compared to the extract treated (group IV and V), non-diabetic (groups I and II) and insulin-treated

group (VI). The hepatocytes in the extract treated group (IV) were significantly ($P < 0.05$) larger than the hepatocytes in other groups (Table 1).

Hypoglycemic activity of *Leptadenia Hastata*

The hypoglycemic/anti-diabetic activity of the extract was evaluated by demonstrating the effect of the extract on fasting blood glucose, and the results obtained are presented in Table 2 below. The extract demonstrated a progressive reduction in fasting blood glucose level in diabetic rats, which became noteworthy on days 21 and 28 for animals administered with 100 mg/kg and 200 mg/kg of the extract respectively. This was comparable to the reduction observed in animals injected with insulin (days 14, 21 and 28). However, no significant reduction was observed in the fasting blood glucose in normal non-diabetic rats. Non-diabetic rats that were administered the extract in group II also showed no significant change in blood glucose levels (Table 2).

DISCUSSION

Diabetes mellitus is a metabolic disorder characterized by hyperglycaemia, which predisposes sufferers to chronic complications

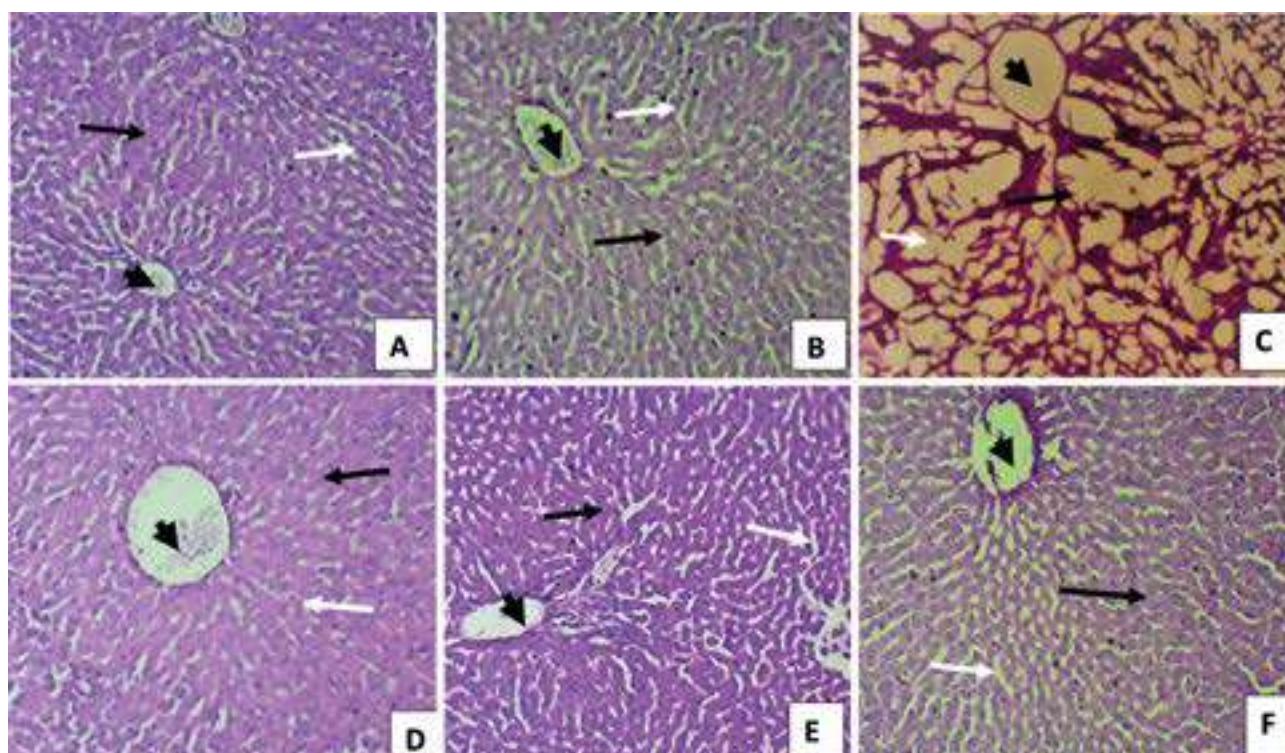


Fig. 2.- Photomicrographs of liver of rats in all groups after the 28 oral toxicity study. Black arrow – cords of hepatocyte, white arrow – sinusoid, black arrow head – central vein. Groups I (A), II (B), III (C), IV (D), V (E) and VI (F). PAS staining. x 100.

affecting several organs of the body, including the eye, blood vessels, kidneys, liver and nerves (Ahmed, 2005). The liver is an important organ that has its main function in maintaining and controlling blood glucose through the processes of glycogenesis and glycogenolysis. Hepatocyte damage and lipid peroxidation products induce an inflammatory response. Diabetes mellitus is considered to be one of the most common causes of liver damage (Manna et al., 2010). It has been correlated with the entire spectrum of liver diseases, including abnormal levels of liver enzymes, non-alcoholic fatty liver disease and liver cirrhosis and carcinoma (Kini et al., 2016; Al-Ani et al., 2017).

The anti-diabetic property of the extract was observed as it reduced blood glucose levels in the treated groups, while having no effect on the serum glucose levels in non-diabetic groups. The glucose-lowering property is well documented by several researchers like Bello et al. (2011),

Sanda et al., (2013), Umaru (2018) and Attah (2019a) have evaluated the hypo-glycaemic and hypolipidaemic effects of water and methanol and root extracts of *L. hastata* in normal and alloxan-induced diabetic rat models and found out that the plant has glucose lowering properties.

In the present study, the diabetic control group showed high level of cellular abnormalities including necrosis, cellular and vascular degeneration, vascular congestion, hyperplasia of the hepatocytes and vacuolation, which are features observed in a diabetic liver. This is similar to the result obtained in a study carried out by Salih et al., 2009 who observed hydrophobic changes, necrotic aggregation and aggregation of lymphocytes in the liver of rats induced with streptozotocin. There was also a severe reduction in glycogen content of hepatic cells in the untreated diabetic groups as evidenced by the degenerated hepatocytes. Histopathological evaluation of the liver after oral ingestion of 100 mg/kg and 200

Table 1. Morphometric findings of the liver.

Groups	Treatment	CV (μm^2)	SN (μm)	HEP (μm)
I	Olive Oil	177.3 \pm 16.5 ^a	19.8 \pm 1.8 ^a	19.8 \pm 1.8 ^a
II	Extract (200mg/kg)	175.4 \pm 11.2 ^a	12.6 \pm 2.2 ^c	16.2 \pm 1.8 ^a
III	Olive Oil	340.2 \pm 31.6 ^b	36.0 \pm 4.0 ^b	12.8 \pm 2.2 ^c
IV	Extract (100mg/kg)	158.0 \pm 15.6 ^a	9.0 \pm 0.0 ^c	25.2 \pm 1.8 ^b
V	Extract (200mg/kg)	224.1 \pm 16.9 ^c	18.0 \pm 2.8 ^a	12.6 \pm 2.2 ^c
VI	Insulin	169.2 \pm 17.8 ^a	9.0 \pm 0.0 ^c	12.6 \pm 2.2 ^c

Data are presented as mean \pm S.E.M. The values are expressed as mean \pm S.E.M expressed (n = 5). Values in the same column with different superscript are significantly different at P<0.05. Values in the same column with same superscript are not significant. CV- area central vein, SN- width of sinusoid, HEP- size of hepatocytes

Table 2. Effect of n-hexane extract of *Leptadenia hastata* on fasting blood glucose in experimental rats.

Groups	Treatment	Initial	Fasting Blood Glucose levels (mg/dl)				
			Day 1	Day 7	Day 14	Day 21	Day 28
I	Olive Oil	105.2 \pm 4.3 ^a	100.2 \pm 3.3 ^a	96.5 \pm 7.4 ^a	99.9 \pm 6.9 ^a	92.3 \pm 3.5 ^a	110.6 \pm 12.6 ^a
II	Extract (200 mg/kg)	108.3 \pm 6.6 ^a	112.3 \pm 4.8 ^a	114.2 \pm 5.5 ^a	108.8 \pm 8.1 ^a	119.2 \pm 7.3 ^a	105.0 \pm 9.3 ^a
III	Olive Oil	120.2 \pm 4.1 ^a	420.2 \pm 5.2 ^b	444.8 \pm 8.7 ^b	547.0 \pm 4.2 ^c	567.8 \pm 2.4 ^c	539.0 \pm 8.5 ^c
IV	Extract (100 mg/kg)	108.0 \pm 8.8 ^a	450.0 \pm 6.9 ^b	494.0 \pm 3.6 ^b	414.2 \pm 3.3 ^b	124.6 \pm 12.9 ^a	180.7 \pm 8.7 ^b
V	Extract (200 mg/kg)	116.8 \pm 5.4 ^a	440.8 \pm 5.6 ^b	446.0 \pm 4.7 ^b	391.4 \pm 4.7 ^b	214.4 \pm 6.3 ^b	93.4 \pm 8.9 ^a
VI	Insulin	113.4 \pm 3.7 ^a	462.4 \pm 6.8 ^b	441.0 \pm 9.3 ^b	374.4 \pm 3.3 ^b	291.7 \pm 6.0 ^b	222.4 \pm 3.0 ^b

This table is reproduced with permission from Sumerianz Journal of Medical and Healthcare. The values are expressed as mean \pm SEM (n=5). Values in the same column with different superscript are significantly different at p<0.05. Values in the same column with the same superscript are not significant. I – Non-diabetic and untreated with extract, II – non-diabetic but extracted treated, III – diabetic and untreated, IV – diabetic and treated with 100mg/kg extract, V – diabetic and treated with 200mg/kg of extract, VI – diabetic and treated with insulin

mg/kg of n-hexane extract indicated that the extract did not adversely affect the morphology of the liver, but preserved the histology of the liver to be similar to the control group. The results are similar to studies conducted by Waer and Helmy (2012), Oyebadejo et al. (2014) and Al-Ani et al. (2017), where plant extracts were observed to have ameliorated the adverse histopathological effects on the liver of diabetic rats.

The liver tissue treated with extract had significantly reduced sinusoid and central vein compared to the diabetic control group. The hepatocytes in the extract treated groups were also significantly larger than the diabetic group, and this increase may be the result of enlargement of metabolically active cells to be able to cope with the additional stress on the liver tissue.

Sinusoidal dilatation, which was present in the diabetic rats, has been suggested to represent the early stages of hyperplasia of the sinusoidal lining cells of the liver. It could be also caused by impaired portal perfusion or an inflammatory reaction. This feature is described by Marzano et al. (2015). The extract may have played a role in protecting the liver in the treated groups from an inflammatory reaction that was observable in the diabetic control group. The mechanism of the ameliorative effect of *Leptadenia hastata* extract on the histopathological changes in STZ-induced diabetic rats is still not clear. However, phytochemical analysis of *Leptadenia hastata* has revealed the presence of triterpenoids, which has been reported to be hepatoprotective (Mandal et al., 2015). Triterpenes isolated from *L. hastata* latex have also been known to possess anti-inflammatory activity (Nikiema et al., 2011). Zinc has been found to have insulin-like effect in that it enhances glucose uptake by inhibiting glycogen synthesis (Schlenger et al., 2014). Iron is an essential element for wide varieties of metabolic processes including playing pathogenic roles in diabetes mellitus and its complications. Some trace elements (Zn, Cr, and Mn) have important roles in metabolism and insulin action (Djama et al., 2012). These elements were found in trace amounts in the n-hexane extract of *Leptadenia hastata* when analysed (Attah et al., 2019b).

COMPLIANCE WITH ETHICAL STANDARDS

The experimental procedures were conducted in accordance with the University of Maiduguri Research and Ethical Committee guidelines, the ARRIVE guidelines (reporting of in vivo experiment), and the National Institutes of Health (NIH) guide for the CARE and use of laboratory animals (NIH Publications No. 8023, revised 1978). The research was also conducted in accordance with the Helsinki Declaration of 1975, as revised in 2000.

ACKNOWLEDGEMENTS

The Authors appreciate the support given by H.B. Ishaya Ph.D., N.I. Dibal, M.S. Chiroma Ph.D., J.V. Zirahei Ph.D. for the moral and academic support. The authors also appreciate the staff of the Histology Laboratory, Department of Human Anatomy, University of Maiduguri and the staff of Pharmacognosy Laboratory, Faculty of Pharmacy, University of Maiduguri for the endless hours of assistance during the experimental study.

REFERENCES

- ABDENNABIA R, BARDAAB S, MEHDIC M, RATEBD ME, RAABE A, ALENEZIF FN, SAHNOUNB Z, GHARSALLAHA N, BELBAHRI L (2016) *Phoenix dactylifera* L. sap enhances wound healing in Wistar rats: Phytochemical and histological assessment. *Int J Biol Macromol*, 88: 443-450.
- AHMED N (2005) Advanced glycation endproducts – role in pathology of diabetic complications. *Diabetes Res Clin Pract*, 67: 3-21.
- ALIERO A, WARA SH (2009) Validating the medicinal potential of *Leptadenia hastata*. *Afr J Pharm Pharmacol*, 3(6): 335-338.
- ANURADHA K, HOTA D, PANDHI P (2004) Investigation of central mechanism of insulin-induced hypoglycemic convulsions in mice. *Indian J Exp Biol*, 42: 368-372.
- ATTAH MOO, JACKS TW, GARBA SH, BALOGUN JB (2019a) Hypoglycemic and anti-diabetic profile of n-hexane extract of *Leptadenia hastata* leaves on streptozotocin-induced diabetes in albino rats. *Sumerianz J Med Healthcare*, 2(4): 42-46.

- ATTAH MOO, JACKS TW, GARBA SH, MSHELIA HE (2019b) Physico-chemical and phytochemical screening of n-hexane extract of *Leptadenia hastata* leaves: a proposed herbal remedy in the treatment of diabetes mellitus. *Int J Res - Granthaalayah*, 7(2): 45-57.
- AZWANIDA NN (2015) A review on the extraction methods used in medicinal plant: principles, strengths and limitations. *Med Arom Plants*, 4(196): 1-6.
- BILAL HM, RIAZ F, MUNIR K, SAQIB A, SARWAR MR, SCHUMACHER U (2016) Histological changes in the liver of diabetic rats: a review of pathogenesis of non-alcoholic fatty liver disease in type i diabetes mellitus. *Cogent Med*, 3(1).
- BELLA AF, ADETUYIBI A (1990) Insulin-binding antibodies in Nigerian diabetic patients. *West Afr J Med*, 9: 291-294.
- BELLO A, ALIERO AA, SAIDU Y, MUHAMMAD A (2011) Phytochemical screening, polyphenolic content and alpha-glucosidase inhibitory potential of *Leptadenia hastata* (Pers.) Decne, Nigeria. *Bayero J Pure Appl Sci*, 19(2): 181-186.
- CHO NH, SHAW JE, KARURANGA S, HUANG H, DA ROCHA JD, OHLROGGE AW, MALANDA B (2018) Diabetes research and clinical practice diabetes. *Res Clin Pract*, 138: 271-278.
- DAHIRU T, ALIYU A, SHEHU AUA (2016) Review of population-based studies on diabetes, mellitus in Nigeria. Downloaded from <http://www.ssajm.org> on Friday, September 15, 2017.
- DJAMA AAD, KOUASSI-GOFFRI, MC, OFOSU FG, ABOH JK (2012) Heavy metal analysis of some anti-diabetic medicinal plants in Côte d'Ivoire. *Curr Res J Biol Sci*, 4(5): 633-637.
- ETUK EU (2010) Animals models for studying diabetes mellitus. *Agric Biol J N Am*, 1(2): 130-134.
- HOUCINE B, RACHID A, RABAH D, FARID L, NABILA B, BOUFELDJA T (2011) Effect of saponosides crude extract isolated from *Citrullus Colocynthis* (L.) seeds on blood glucose level in normal and streptozotocin induced diabetic rats. *J Med Plants Res*, 5(31): 6864-6868.
- AL-ANI IM, ABIRED AN, MUSTAFA BE, WAHAB ENA, AZZUBAIDI MS (2017) Effect of flaxseed extract on the liver histological structure in streptozotocin induced diabetic rats. *Int Med J Malaysia*, 16(1): 1-8.
- INTERNATIONAL DIABETES ATLAS (2017) International diabetes atlas: global estimates of diabetes prevalence for 2017 and projections for 2045, 8th Edition.
- JAYAKARB, SURESHB (2003) Antihyperglycemic and hypoglycemic effect of *aporosa lindleyana* in alloxan-induced diabetic rats. *J Ethno-pharmacol*, 84: 247-249.
- KANAGASBAPATHY AS, KUMARI S (2000) Guidelines on standard procedures for clinical chemistry. *World Health Organization Regional Office, New Delhi*, pp 26-30, 45-49.
- KINI S, TRIPATHI P, AMARAPURKAR AD (2016) Histopathology of liver in diabetes mellitus - an autopsy study. *Int J Sci Stud*, 4(5): 110-113.
- MANDAL A, DAS V, GHOSH P, GHOSH S (2015) Anti-diabetic effect of freiedelan triterpenoids in streptozotocin induced diabetic rat. *Nat Prod Commun*, 10(10): 1683-1686.
- MARZANO C, CAZALS-HATEM D, RAUTOU EP, VALLA DC (2015) The significance of non-obstructive sinusoidal dilatation of the liver: impaired portal perfusion or inflammatory reaction syndrome. *Hepatology*, 62: 956-963.
- NIKIEMA JB, VANHAELEN-FASTRE R, VANHAELEN M, FONTAINE J, GRAEF CD, HEENEN M (2001) Effects of anti-inflammatory terpenes isolated from *Leptadenia hastata* latex on keratinocyte proliferation. *Phototherapy Resources*, 15(1): 131-134.
- ORGANIZATION FOR ECONOMIC CO-OPERATION AND DEVELOPMENT (OECD) (2008) Guidance document on acute oral toxicity testing 420; Organization for Economic Co-operation and Development: Paris, France.
- OYEBADEJO S, BASSEY E, OYEWUNMI A, ARCHIBONG V, USORO E (2014) Histopathological study of the liver of alloxan induced diabetic rats and macerated *Allium sativum* (garlic) ameliorative effect. *Asian J Biomed Pharm Sci*, 4(34): 72-77.
- RAJESHKUMAR D (2010) Evaluation of antioxidant property and toxicological assessment

of *Polyalthia Longifolia* var. *Pendula* Leaf. Thesis PhD, Saurashtra University.

ROTHERKI (2007) Diabetes treatment – bridging the divide. *New Eng J English*, 356(15): 1499-1501.

SALIH SD, MUSLIH RK, HAMOODI SR (2009) Histological liver changes in streptozotocin induced diabetic mice. *Int Med J Malaysia*, 8(1): 1-4.

SANDA KA, SANDABE UK, AUWAL MS, BULAMA I, BASHIR TM, SANDA FA, MAIRIGA A (2013) Hypoglycemic and antidiabetic profile of the aqueous root extracts of *Leptadenia hastata* in albino rats. *Pakistan J Biol Sci*, 16(4): 190-194.

SCHLIENGER JL, GRUNENBERGER F, MAIER EA (1998) Disorders of plasma trace elements in blood glucose equilibrium. *Press eMedicine*, 17: 1076-1079.

SWIMNATHAN S, FONSECA VA, ALAM MG, SHAH SV (2007) The role of iron in the diabetes and its complications. *Diabetes Care*, 30(12): 1923-1933.

UKWUANI AN, IGBOKWU MO (2015) In vitro anti-diabetic effect of *Leptadenia hastata* leaves fractions. *Biosci Res Today's World*, 1(1): 40-46.

UMARU IJ, BADRUDDIN FA, UMARU HA (2018) Phytochemical, antifungal and antibacterial potential of *Leptadenia hastata* stem-bark extract. *MOJ Toxicol*, 4(4): 263-268.

VALERON PF, DE PABLOS-VELASCO PL (2013) Limitations of insulin-dependant drugs in the treatment of type 2 diabetes mellitus. *Clin Med*, 2: 20-25.

VENKATARAMANA G, INDIRA P, RAO DVM (2013) Changes of plasma total proteins, albumin and fibrinogen in type 2 diabetes mellitus - a pilot study. *Ind J Basic Appl Med Res*, 7(2): 679-685.

WAER H, HELMY SA (2012) Cytological and histochemical studies in rat liver and pancreas during progression of streptozotocin induced diabetes and possible protection of certain natural antioxidants. *J Nutrion Food Sci*, 2: 165.

WILD S (2004) Global prevalence of diabetes: estimates for the year 2000 and projections for 2030. *Diabetes Care*, 27(10): 2568-9.

WORLD HEALTH ORGANIZATION (2013)

World Traditional Medicine EXPO Sancheong, Retrieved December 2017, from www.who.int/medicine/traditional_medicine.com World Health Organization. Fact Sheet No 312, 2013.

The effect of corn silk, as a hypoglycemic, on the congenital malformations caused by diabetes in mice: A morphological study

Dema Alsudairi, Fatma Al-Qudsi

Biological sciences department, science faculty, King Abdulaziz University

SUMMARY

Diabetes is an increasing health problem that could increase the rate of congenital malformations. Therefore, the burden on health care providers and society is increasing, which could be mitigated by providing treatments that are based on natural, available, and cheap materials. One of the natural hypoglycemic treatments that had been used is Corn Silk aqueous extract (CSE). One of the targeted beneficiaries from these treatments are diabetic pregnant women. The aim is to study the teratogenicity of CSE, as well as whether it reduces the effect of hyperglycemia on the offspring. Female mice were divided into four groups: Control, Treated, Diabetic Control, and Diabetic Treated. Pregnant mice of treated groups were given a daily dose of 4 g/kg of CSE orally, while control mice were given equal amounts of distilled water. Samples were collected on day 16.5 of pregnancy, birth (neonates), and 3 weeks postnatal. Whole body weight, length, and morphological malformations were recorded. The most frequent malformation observed was Intrauterine Growth Retardation (IUGR) among the diabetic groups' samples. The rate of malformations in fetuses of diabetic mothers was not decreased, but in 3-week-old mice of treated mothers we observed a significant increase in

whole body weight and length. We concluded that CSE consumption during pregnancy might not be favorable in the dose used, while it might have some benefits if used while nursing. More studies with different doses and their frequencies are needed. Also, the effect of the extract on lactation and nursing milk composition should be investigated.

Key words: Pre-gestational diabetes – Mouse embryo – Corn silk – Intrauterine growth retardation – Congenital malformations – Morphometry – Morphology

INTRODUCTION

Diabetes is an increasingly spreading disease all over the world (El-Abhar and Schaalán, 2014; International Diabetes Federation, 2017). Diabetes mellitus is classified into three main types. Type 1 diabetes mellitus (T1DM), which is characterized by the absence of insulin secretion due to the destruction of β -cells by the immune system or idiopathic reasons. Type 2 diabetes mellitus (T2DM), which is caused by insulin resistance and/or insufficient insulin production. Gestational Diabetes mellitus (GDM) is diabetes that begins during pregnancy (Chen, 2005). Women with GDM may be undiagnosed

Corresponding author:

Fatma Al-Qudsi, King Abdulaziz University, Dept. of Biology, PO Box 42650, 2551 Jeddah, Saudi Arabia. E-mail: dalsudairi@kau.edu.sa / falqudsi@kau.edu.sa

Submitted: August 18, 2020. Accepted: October 14, 2020

type 2 diabetics (Correa et al., 2008). Diabetes affects 2-5% of pregnant women. In 2013, more than 21 million diabetic pregnancies were reported. Maternal diabetes during pregnancy is either Pre-gestational (PGDM), type 1 or 2 existing before pregnancy, or Gestational (GDM), that occurs in mid gestation. 87.5% of diabetic pregnancies are GDM, while the remaining 12.5% result from PGDM (Dowling et al., 2014; Wahabi et al., 2017).

Saudi Arabia is named by International Diabetes Federation among the highest 10 countries in diabetes prevalence. It is also the highest among the Middle East countries (Lasheen et al., 2014; Wahabi et al., 2014). The Saudi Ministry of Health reported 0.9 million diabetic patients in 1992, compared to 2.5 million in 2010. This rapid increase in around 2 decades raised concern (Alotaibi et al., 2017). In 2014, 13.9% of the health expenditure was spent on the diabetic population in Saudi Arabia (Alwin Robert et al., 2017). Consequently, the burden on health care providers and society is increasing, which could be mitigated by providing treatments that are based on natural, available, and cheap materials. One of the targeted beneficiaries from these treatments are diabetic pregnant women.

Maternal hyperglycemia is associated with risk outcomes for the mother, fetus, child, and adult offspring. For the mother, there is an increased risk for premature and C-section delivery due to large sized infant, and higher possibility of developing gestational diabetes mellitus (GDM) in later pregnancies, and type 2 diabetes mellitus (T2DM) later in life. The fetus could be large for gestational age, develop metabolic problems, higher long-term risk for diabetes and obesity, and female offspring susceptibility of GDM in the future due to fetal genome epigenetic modifications (Monteiro et al., 2016; Stewart and Murphy, 2015). The risks associated with DM includes: macrosomia, congenital malformations, stillbirth, preterm delivery and birth asphyxia (Wahabi et al., 2014). Diabetes has a teratogenic effect on multiple organ systems, most commonly: cardiovascular, musculoskeletal and central nervous system (Correa et al., 2008; Mills, 2010).

Corn Silk (CS) is one of the medicinal herbs traditionally used by the Chinese and the natives of the Americas, as well as in Serbia, Turkey, and France, for hyperglycemia and a variety of diseases. *Stigma maydis* or corn silk is the thread-like yellow-brown or light-green style/stigmas that make the *Zea mays* L. (corn) female flower. Corn silk (CS) is used to treat disorders associated with the urinary system including edema, kidney stones, cystitis, prostate disorders, bedwetting and urinary infections. It relaxes the bladder's lining, increases the secretion of urine (due to its diuretic and kaliuretic properties (Velazquez et al., 2005), and reduces irritation. It is also used for gout, asthma, obesity and hypertension. CS possesses anti-depressant and anti-fatigue activity (Zhao et al., 2012), anti-fungal activity, and contains large amounts of antioxidants. The medicinal properties are attributed to its chemical compounds. It contains vitamins, proteins, carbohydrates, salts (Mg, K, Ca, and Na), volatile and fixed oils, alkaloids, steroids, tannins, saponins, and flavonoids (Guo et al., 2009; Hasanudin et al., 2012; Žilić et al., 2016). A toxicity study on mice done by Peng, Zhang, and Zhou, using three different doses of flavonoid-rich extract from CS (up to 10 g/Kg/day orally) for 28 days, showed that the extract has no toxicological effect or genotoxicity on either germ cells nor somatic cells. Therefore, it is safe to use it in the food industry and natural remedies (Peng et al., 2016).

In China, corn silk has been used as an antidiabetic treatment. Guo et al. (2009), studied the effect of CS extract on glycemic metabolism. They used 0.5, 1, 2, 4 g/kg body wt. doses of CS aqueous extract on alloxan-induced diabetic mice for 20 days. In mice groups which received the 2 and 4 g/kg doses, blood glucose levels decreased. They concluded that CS affected the glycemic metabolism via increasing insulin secretion and recovering damaged β -cells (Guo et al., 2009). In another study by Zhao et al. (2012), STZ-induced diabetic rats received 300, 400, 500 mg/kg body wt. of polysaccharides from CS extract (POCS) daily for 4 weeks. It had a hypoglycemic and hypolipidemic effect on diabetic rats, and no effect on normal ones (Zhao et al., 2012).

Maternal treatment with corn silk extract could reduce the pregestational diabetes teratogenicity.

This study will be focusing on the effect of Corn Silk aqueous Extract (CSE) on the fetus and offspring of diabetic and non-diabetic pregnant mice.

MATERIALS AND METHODS

All procedures took place at King Fahad Medical Research Center (KFMRC) and were approved by the biomedical ethics research committee in King Abdulaziz University (KAU) (reference Number 345-19).

In this study, Swiss white rodless (SWR) adult male and female mice weighing 25-30 g, obtained from KFMRC, were used.

Female mice were distributed in cages, 5 in each cage, while each male was isolated in a cage. The animals were acclimated for a week in a room with $22\pm 2^{\circ}\text{C}$, normal humidity and 12 hr. light/dark cycle, with free access to water and food (animal feed).

Corn silk (CS) was harvested from a local farm in Albadaiya (Duba, Tabuk Province, Saudi Arabia).

In this study, Streptozotocin was used to induce diabetes mellitus in experimental animals, as reviewed by Tripathi and Verma (2014). The used STZ (Sigma S0130-1G) was purchased from Bayouni Trading Co. LTD. Normal saline, formalin and diethyl ether were purchased from Al-Rowad Modern supply of medical equipment in Jeddah.

Preparation of corn silk extract

Corn silk (CS) was dried for a week in the farm, then transported to Jeddah. Corn silk was dried in a well-ventilated room for three weeks, then stored in a fridge (Fig. 1).

The method used to prepare the extract was based on previous studies (Velazquez et al., 2005; Guo et al., 2009) with slight modifications. First, the water extract was prepared by adding 100 ml of hot water to 10 g of dried CS and left for 20-30 min. Then the solution was filtered using filter paper (Whatman). The filtrate was frozen under -30°C in a deep freezer to prepare it for freeze-drying (lyophilization).

Lyophilization (Freeze-drying)

In order to measure exact amounts of the extract powder to prepare the doses, Freeze-Dryer (ilShinBioBase, Model FD8518) was used to dry (lyophilize) the extract. After drying, the samples were weighed and tightly sealed to be preserved in the freezer until needed. It was noticed that the dry extract absorbed water rapidly, so the water extract was placed in small plastic containers, which were placed in glass flasks.

Preparing the experimental solution

To prepare the dose freshly, we calculated the amount needed for each mouse (4 g/kg) and dissolved the extract powder in 0.5 ml of distilled water per mouse.

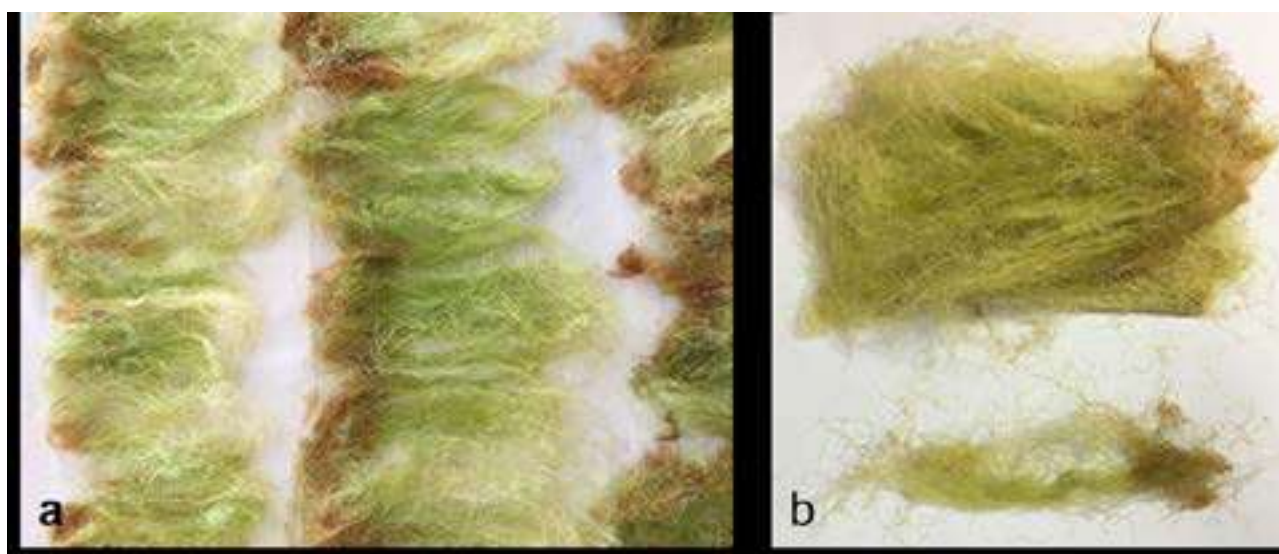


Fig. 1.- a. Drying CS in a well-ventilated room. b. CS after 3 weeks, notice the change in color when dried.

Working plan

The animals were divided into two main groups: non-diabetic and diabetic. Each group was divided into control and treated.

Group 1: Non-diabetic control (C), were given distilled water. Group 2: Non-diabetic treated (T), were given corn silk extract. Group 3: Diabetic control (DC), were given distilled water. Group 4: Diabetic treated (DT), were given corn silk extract.

Diabetes induction

Female mice were injected intraperitoneally with 75 mg/kg of STZ dissolved in cold normal saline, for three consecutive days (Martin et al., 2004; Deeds et al., 2011; Dowling et al., 2014). The dose was calculated and dissolved in 0.2 ml of normal saline for each mouse, making sure that the administration took place within 15 mins after preparation (STZ has a half-life of 15 min. and is cleared from the blood stream rapidly). After 10-14 days, blood glucose levels of the injected mice were checked using accu-check Performa (Roche Diabetes Care), if blood glucose levels were >200 mg/dL mice were considered diabetic (Loeken, 2005; Jawerbaum and White, 2010; Mostafa et al., 2014; Dong et al., 2015; Wang, Reece and Yang, 2015).

Mating

The estrus stages of diabetic and nondiabetic females were checked to determine readiness for mating (Caligioni, 2009; Byers et al., 2012). Females in the estrus and proestrus stages were gathered with males; 2 females with 1 male and left for 24 h., then checked in the next morning for vaginal plugs. Once the vaginal plug was seen, Embryonic day 0.5 of pregnancy (E0.5) would be established, so blood glucose and weight were recorded, and dose administration began.

Dose administration

Starting at E0.5, the mothers in the treated groups were given a dose of 4 g/kg CSE dissolved in 0.5 ml of distilled water, orally using a gavage (24G x 1" animal feeding needle, purchased from Pet Surgical), five days a week. Mothers in

the control groups were given equal amounts of distilled water (0.5 ml each).

Sample collection

At the age, E16.5, two mothers of each group were dissected. The uterus was taken out to extract the fetuses. Each fetus was numbered, photographed and weighed, then preserved in 10% formalin.

The neonates and 3-week-old offspring were numbered, photographed and weighed, then euthanized (using diethyl ether) to be preserved in 10% formalin.

For 3-week samples, the numbers were reduced especially in DC and DT groups due to death during lactation period (from birth till three weeks).

Photography

During dissection and sample collection videos and still photos were taken using a mobile (iPhone 6S) supported by a tripod. The distance and zooming were unified for each age treatment.

The preserved samples (E16.5 and neonates) were photographed under a dissecting microscope (Olympus SZX10) using an iPhone 6S held using an iPhone adapter (iDu Optics LabCam Microscope adapter for iPhone 6/6S) purchased from Amazon.com.

Morphology

The morphology of the control fetuses, neonates and 3-week-old offspring was examined and compared to the controls in previous literature (Theiler, 2013). Morphological malformations were recorded in all groups, including IUGR comparing sample weights to the lowest weight of control fetuses.

Morphometry

The photos were used for morphometrics using the image tool program, accessed and downloaded in 2019 from (<http://cme.msu.edu/cmeias/>). The whole length, starting from the tip of the nose to the beginning of the tail, as well as tail length were measured, in addition to placental diameters in E16.5 fetuses. (Fig. 2).

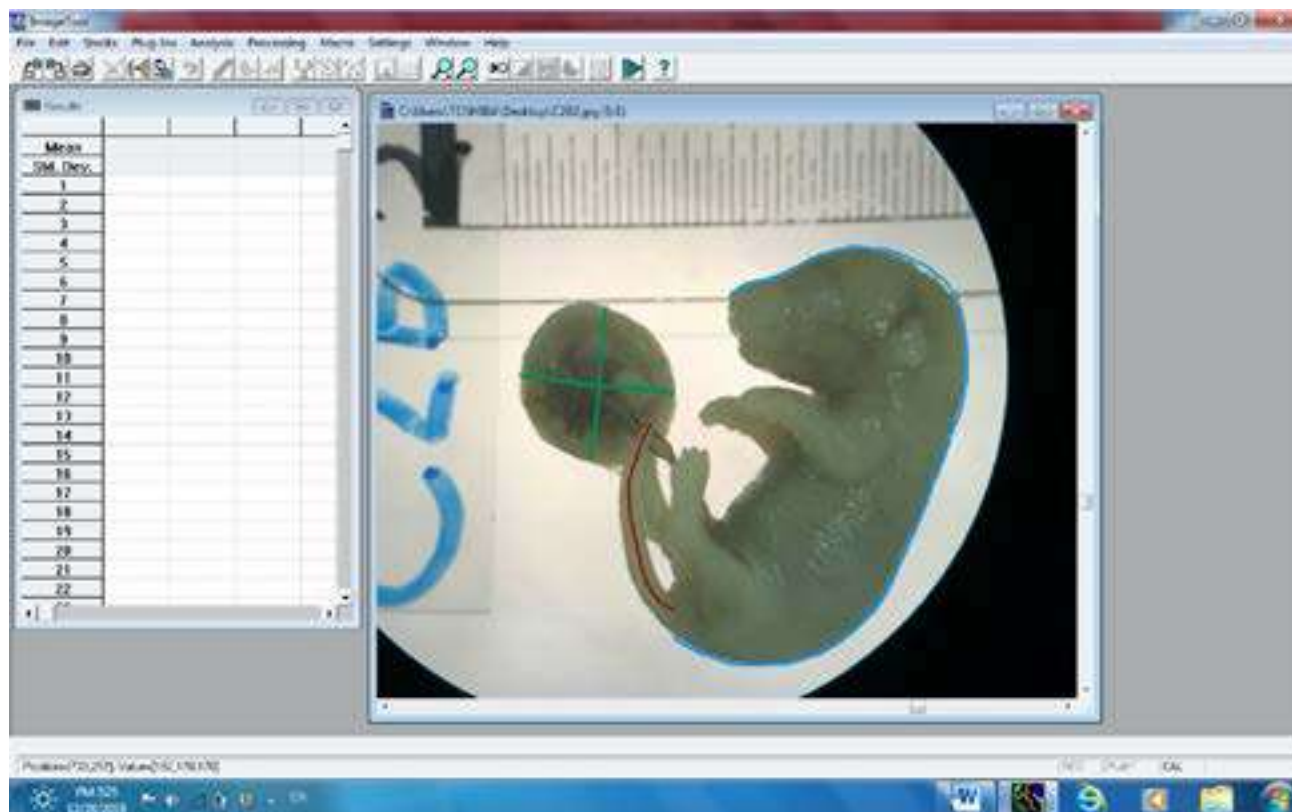


Fig. 2.- Morphometry method using image tool program. Blue line= whole body length. Red line= tail length. Green line= placental diameters.

Statistical analysis

The measurements and weights were statistically analyzed using SPSS program (IBM SPSS Statistics, v. 1.0.0.1275). Data were analyzed with One-way ANOVA, then Two-independent sample test (Mann-Whitney) was done to test the significance of differences between groups.

RESULTS

Morphology of E16.5 mouse fetus

Normal 16.5-day mouse fetuses were covered by wrinkled, transparent skin which subcutaneous veins could be seen through. The four limbs and tail were clearly seen. The eyes were covered with fused eyelids. The auricle of the ear was well-defined. The upper section of the back was straight. The snout had clear mouth and nose. The neck was too short, almost absent. Hair follicles could be seen all over the body and in an area in the snout where whiskers will grow (Fig. 3A, B). One control case was seen where the placentas of two adjacent fetuses were attached, although each had its own amnion sac (Fig. 3C, D).

Fetuses in all groups seemed similar to the control group. In the T group, fetuses were similar to the ones in the control groups, and no obvious malformations were observed.

However, some malformations were noticed in some groups. In the diabetic control group, a fetus had an exposed brain (Exencephaly) where the cerebral cortex and the cerebellum could be seen (Fig. 4G, H). Another fetus from the same group had underdeveloped auricle. In the diabetic treated group, a fetus had an exposed brain (exencephaly) with bleeding parts (Fig. 3I, J). Another fetus from the same group had an extreme case of IUGR, in which it seemed small, with short limbs, and had thin and clear skin (Fig. 3K, L).

Morphology of neonate mice

Normal newborn mice in this study had a well-defined body, a tail, and four limbs with clear digits. The skin, with visible hair follicles, covered the body. Stomach filled with milk could be seen through the skin from the left side, and the dark color of the liver could be seen from the right side. In the head, eyes could be seen through the closed eyelids, ears were closed, and a snout with

clear nasal openings and whiskers was visible. The neck was thick and short (Fig. 4A).

Neonates in all groups seemed similar to the control group. However, some malformations were noticed in different groups. In the treated group, one had an open left eyelid. Among the diabetic control group, the snout of one fetus seemed long and slightly narrow. One from the diabetic treated group was small and had a malformation in the posterior end of the body, where the tail was very short, thin, and almost transparent (caudal growth defect) (figure 4D).

Morphology of 3-week-postnatal mice

The 3-week old mice were similar to adult mice, with four limbs, a tail, and skin with white

hair. Fully developed eyes with open eyelids and open auricle were visible. Mice in all groups were similar to the control with variations in body size. Mice in the treated group seemed larger than the controls, while mice in the diabetic control group were smaller compared to the control group.

Morphometry results

The effect of CSE on the Whole-Body Weight of fetuses and offspring

In this study, the normal whole-body weight mean of mouse fetus was 0.89g at E16.5. Corn silk aqueous extract caused a very slight non-significant decrease in whole body weight (WBW) in the T group compared to the C group. Diabetes caused a significant decrease in WBW in DC

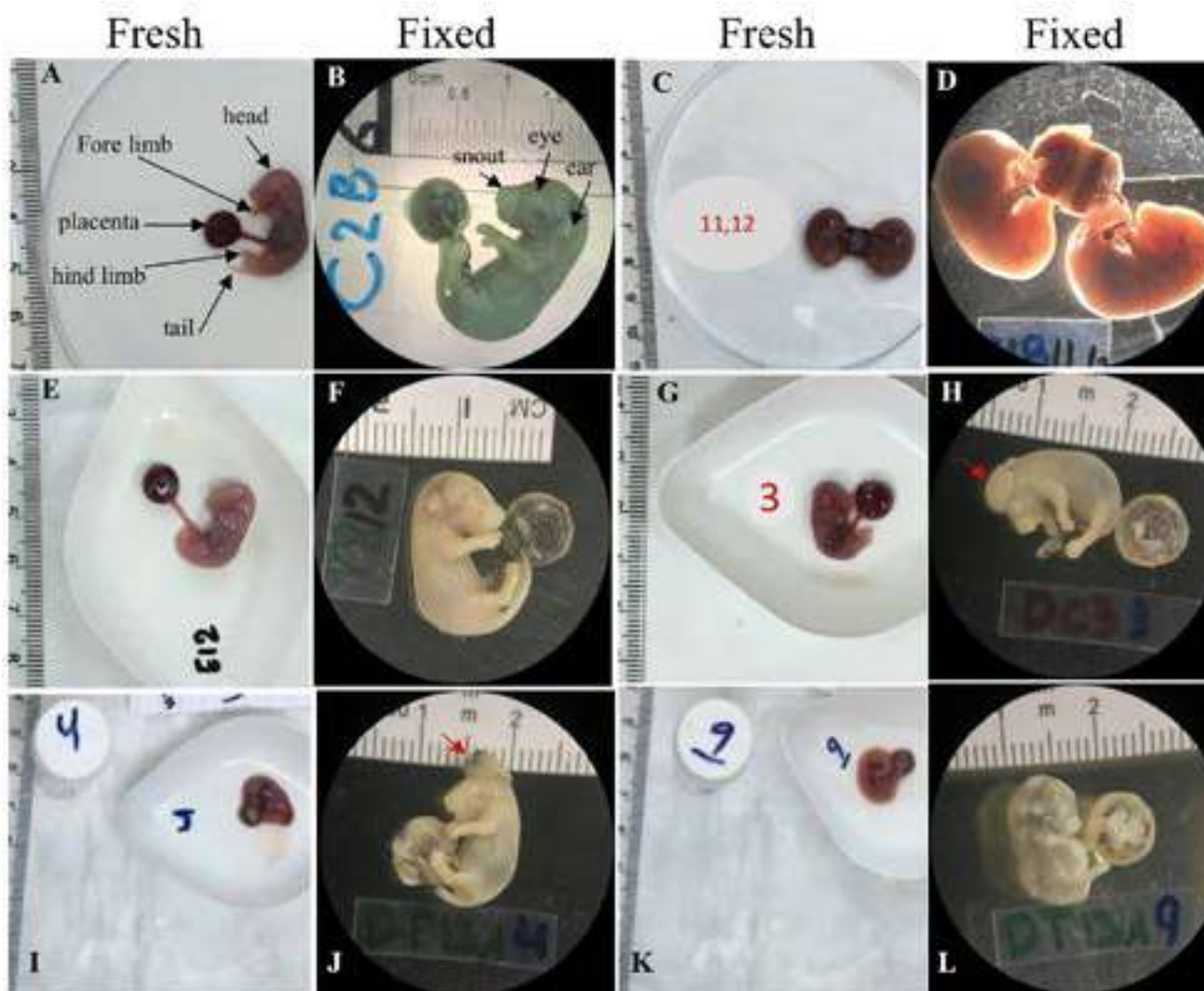


Fig. 3.- Fresh and fixed samples of E16.5 mice fetuses from all treatment groups. **A, B.** A fetus from the control group with normal morphological features. **C, D.** The case of the attached placentas in the control group. **E, F.** A fetus from the treated group with no seen malformations. **G, H.** A fetus from the diabetic control group with exencephaly malformation where the brain was clearly seen (red arrow). **I, J.** A fetus from the diabetic treated group with exencephaly malformation where the brain was clearly seen (red arrow). **K, L.** An extreme case of IUGR of a fetus from the diabetic treated group. The ruler in each photo was used as a scale. The photos of fixed fetuses were taken under a dissecting microscope with 6.3x magnification.

group compared to C group ($p=0.000$). It also caused a significant WBW decrease ($p=0.045$) in DT group compared to T group. CSE caused a significant decrease in DT ($p=0.034$) compared to C group while it caused a slight non-significant increase in WBW compared to DC group (figure 6). All fetuses in the T group weighed more than 0.77 g (the lowest control weight). While the percentage of fetuses in the DC group weighing less than 0.77 g was 68.2%, and 52.4% in the DT group (Table 1).

Table1. Showing the percentages of the main malformations observed in the study in E16.5 and neonate age groups. C= Control group. T= Treated group. DC= Diabetic Control group. DT= Diabetic Treated group.

Age	Malformation	C	T	DC	DT
E16.5	IUGR	-	-	68.2%	52.4%
	Exencephaly	-	-	4.5%	4.8%
Neo-nates	IUGR	-	68.8%	53.8%	66.7%
	Tail and hind-limbs (Caudal defect)	-	-	-	8.3%

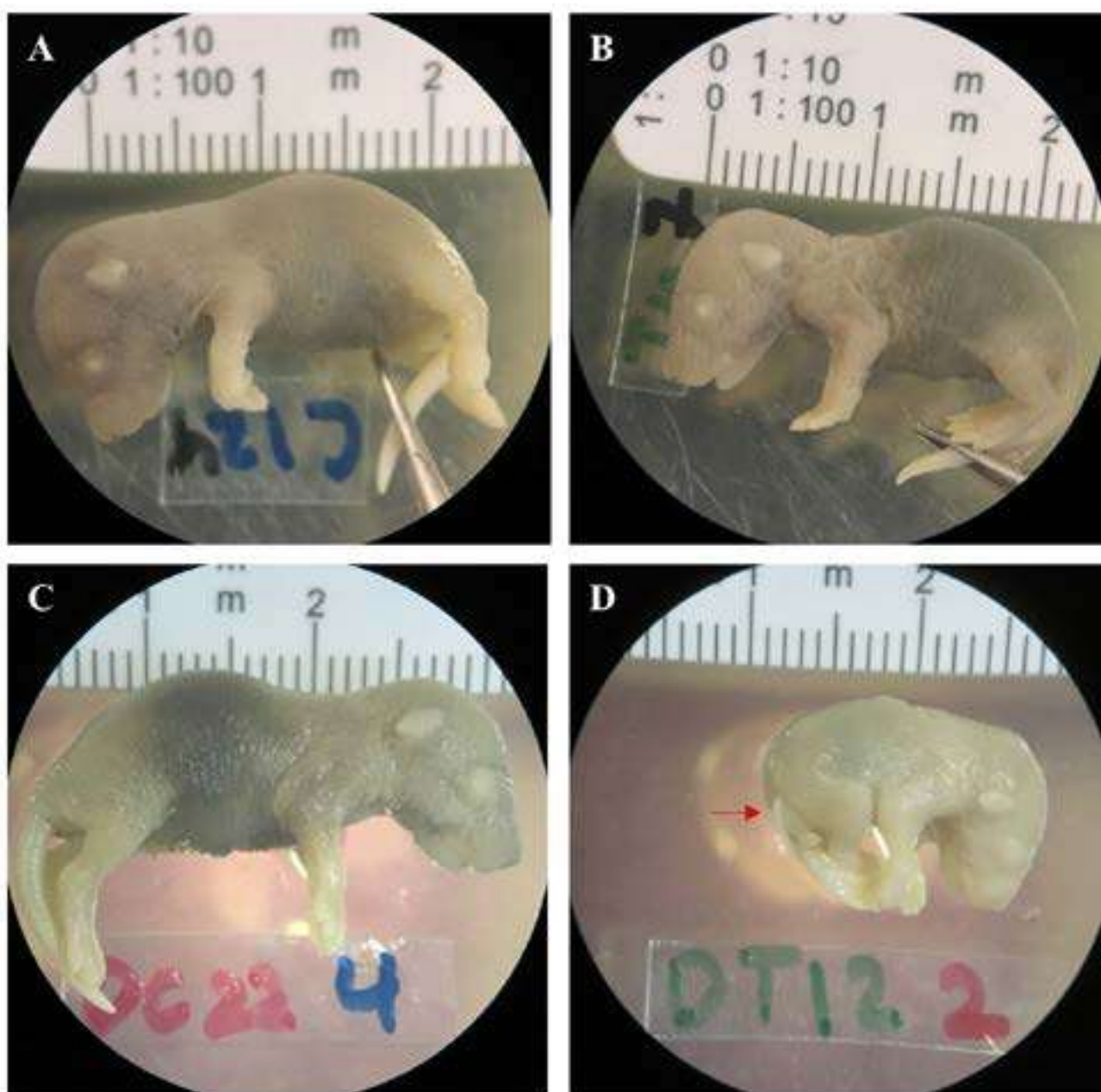


Fig. 4.- Samples of neonate mice from all treatment groups. The ruler in each photo was used as a scale. **A.** A normal neonate mouse from the control group. **B.** A neonate mouse from the treated group with IUGR. **C.** A neonate mouse from the diabetic control group with no obvious malformation. **D.** A neonate from the diabetic treated group with posterior end malformation (red arrow). The photos were taken under a dissecting microscope with 6.3x magnification.

The normal body weight mean of neonate mice in this study was 1.6035 g. Both CSE and diabetes caused significant decrease in neonates' WBW in T and DC (p=0.002), and DT (p=0.003) groups compared to C group. Diabetes and CSE also caused slight non-significant decreases in WBW of DT group compared to T group, and DT compared to DC (Fig. 5). The lowest weight of control fetuses was (1.43 g). In the T group, 68.8% had IUGR, while it occurred in 53.8% and 66.7% of DC and DT fetuses respectively.

At 3 weeks of age, the normal WBW mean of mice in this study was 7.0733 g. There was a significant increase in WBW caused by CSE in T group compared to the C (p=0.000), DT group compared to C (p=0.001) and in DT compared to DC group (p=0.002). On the other hand, diabetes

caused a significant decrease in WBW comparing DC with C group (p=0.000), and DT with T group (p=0.046) (Fig. 6).

The effect of CSE on the Whole-Body Length of fetuses and offspring

In this study, 16.5-day-old embryos' normal body length was 3.4887 cm. Comparing the T with C group, there was a non-significant decrease in whole body length caused by CSE. In addition, there was a non-significant decrease comparing DT to C. Body length significantly decreased due to diabetes in the DC group compared to C group (p=0.000). Diabetes also caused a non-significant decrease in DT compared to T. In the diabetic groups, CSE caused a non-significant increase comparing DT with DC (Fig. 5).

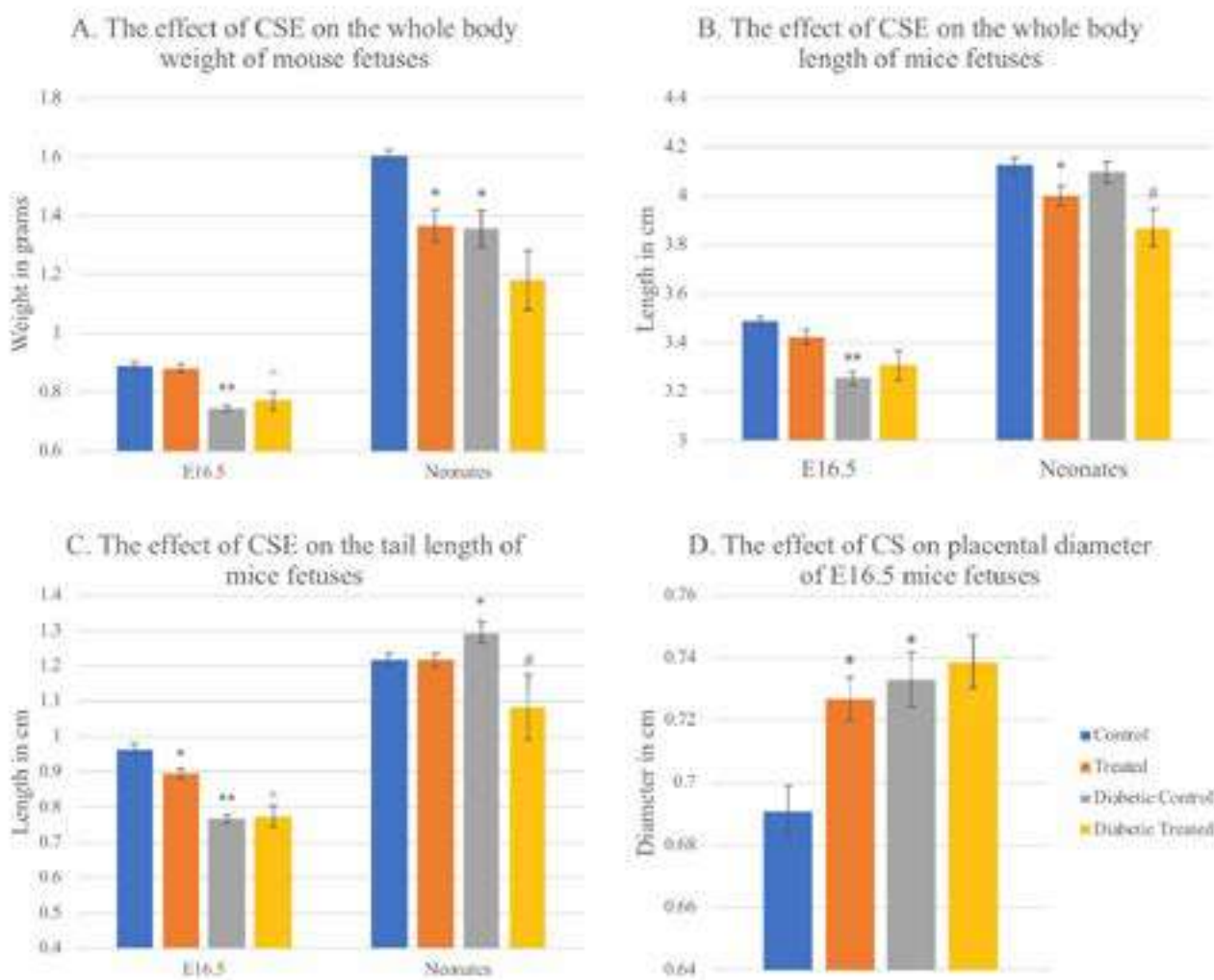


Fig. 5.- Graphs showing the effect of CSE on weight, length, and tail length of 16.5-day old mouse fetuses and neonates, in addition to the effect on placental diameter of E16.5 fetuses. Values are mean ± standard error taken from sample numbers shown in the chart D in figure 6, for each age group treatment. * = significant difference (p <0.05) compared to control group, ^ = sig. diff. compared to treated group, # = sig. diff. compared to diabetic control group, ** p<0.01.

Between neonates, the normal mean body length was 4.0977 cm in this study. There was CSE-related significant decrease in body length when T was compared with C group ($p=0.021$) also comparing DT and DC group ($p=0.014$). Comparing DT to C group there was a significant decrease ($p=0.004$) also. On the other hand, the comparison between DC with C, and DT with T group showed non-significant decreases related to diabetes (Fig. 5).

In this study, 8.108 cm was the normal mean body length for 3-week-old mice offspring. Comparing between T and C groups a significant increase in body length was associated with CSE ($p=0.001$), also in DT with DC ($p=0.001$) however DT group was slightly non significantly higher compared to C, while diabetes caused significant decreases in DC compared to C ($p=0.001$), and DT compared to T ($p=0.007$) (Fig. 6).

The effect of CSE on the Tail Length of fetuses and offspring

In this study in 16.5-day-old fetuses, the mean of normal tail lengths was 0.9643 cm. Among the groups of this age, CSE caused a significant decrease in tail length comparing T and C groups ($p=0.001$), but caused a non-significant increase comparing the diabetic groups DT with DC. Comparing DT to C ($p=0.000$), there was a significant decrease in the length of tails. The mean tail length in the DC was significantly decreased by diabetes compared to C group ($p=0.000$). Diabetes also caused a significant decrease in DT group tail length compared in T group ($p=0.009$) (Fig. 5).

The normal mean tail length of neonates in this study was 1.2175 cm. CSE caused a slight non-significant decrease in tail length in the T and DT groups compared to C. It also caused

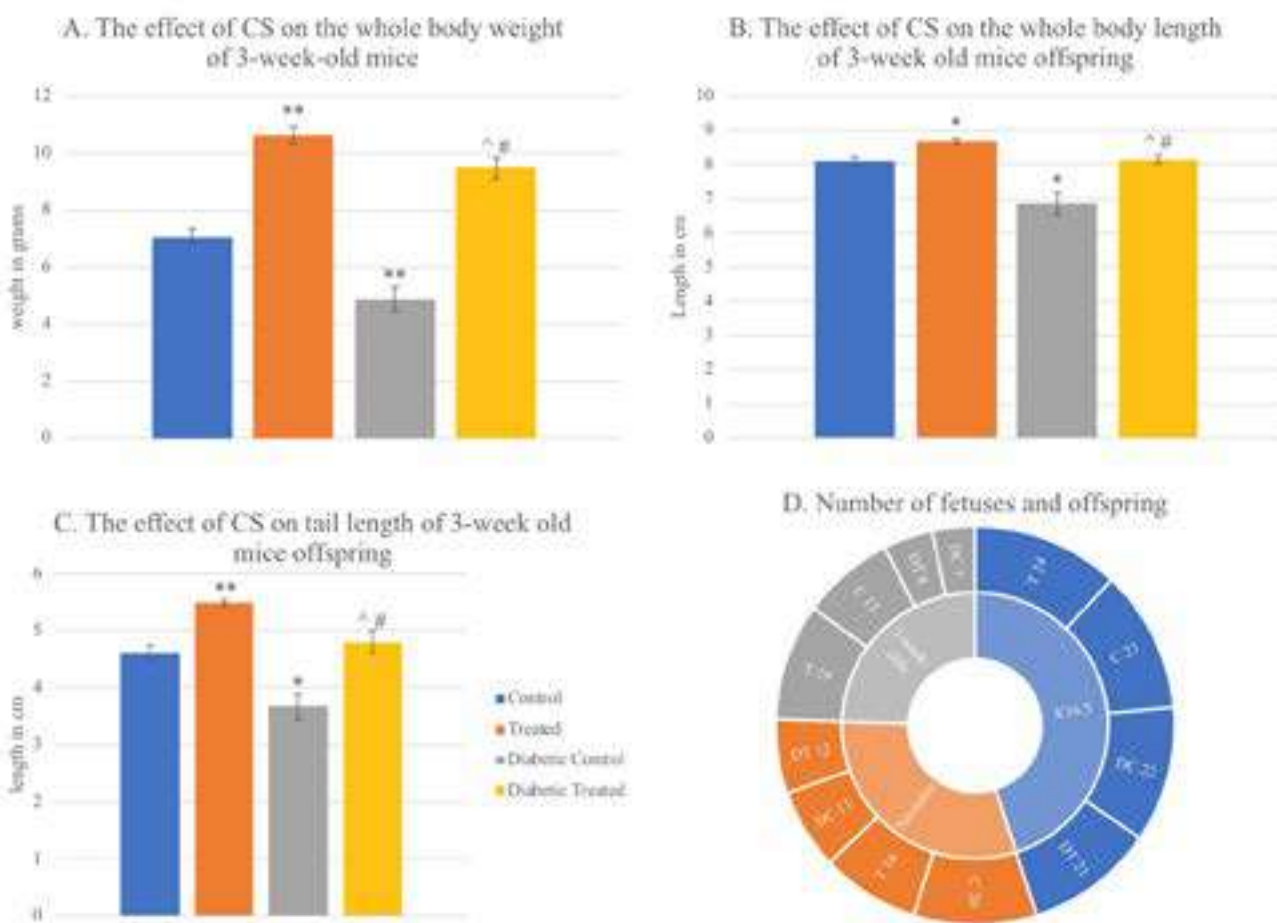


Fig. 6.- Graphs showing the effect of CSE on weight, length, and tail length of 3-week-old offspring, in addition to a chart D showing the number of fetuses and offspring in all age and treatment groups. Values are mean ± standard error taken from sample numbers shown in the chart D, for each group and treatment. * = significant difference ($p < 0.05$) compared to control group, ^ = sig. diff. compared to treated group, # = sig. diff. compared to diabetic control group, ** $p < 0.01$.

a significant decrease in DT compared to DC ($p=0.027$). Comparing DC with C, diabetes caused a significant increase in tail length ($p=0.032$). Diabetes caused a non-significant decrease among the diabetic groups DT and T (Fig. 5).

In 3-week-old mice offspring of this study, the normal mean tail length was 4.6227 cm. The treated group had significantly longer tails than the control group caused by CSE ($p=0.000$). However, DT group mice had longer tails, which were not significantly different compared to the controls. Also, CSE caused a significant increase in tail length in DT compared to DC ($p=0.011$). Comparing DC with C, diabetes caused a significant decrease in tail length ($p=0.003$). Diabetes also caused a significant decrease in tail length in DT compared to T ($p=0.001$) (Fig. 6).

The proportion of tail length to whole body length was reduced in all experimental groups in 16.5 fetuses compared to C. This reduction was significant in DC ($p=0.003$) and DT ($p=0.001$) groups compared to the controls. In neonates this proportion had a very slight non-significant increase in T and DC groups, while it stayed non-significantly reduced in DT group compared to the controls. In 3-week-old offspring, CSE caused a significant increase in the proportion of tail length to whole body length in T group ($p=0.00$), while there was a non-significant increase in DT compared to C. Diabetes clearly caused a significant decrease in DC ($p=0.00$) compared to C group.

The effect of CSE on placental diameter of fetuses

In this study, the mean of normal placenta diameter of E16.5 embryos was 0.695 cm. Compared to the control group of this age, CSE caused a significant increase in the T group placental diameter ($p=0.008$) and DT group ($p=0.001$). Diabetes caused a significant increase in the diameter of the placenta of DC compared to C group ($p=0.004$). It also non-significantly increased DT placental diameter compared to T group. CSE had non-significantly increased the placenta diameter in DT compared to DC (Fig. 5).

It was also noticed that the number of neonates and 3-week-old mice was reduced in the diabetic

groups. The rate of major malformations observed on our study are listed in Table 1.

DISCUSSION

Diabetes mellitus during pregnancy is considered a teratogen that increases the rate of birth defects in humans and animal models (Savion et al., 2004). In this study, female mice were used as a model for diabetes mellitus during pregnancy to study the effect of corn silk extract, as a hypoglycemic agent, on fetal development with and without diabetes. It was noticed that diabetes in general seemed to decrease growth in postnatal, natal, and prenatal mice. On the other hand, the effect of CSE on growth varied between age groups, as growth was reduced during in 16.5 fetuses and neonates, while it was significantly increased in 3 weeks offspring. It seems that diabetes and CSE increased the diameters of the placenta of E16.5 fetuses. Few morphological anomalies were observed in different groups.

In this study, the main malformation seen in the DC group was Intrauterine Growth Retardation (IUGR). The CSE seemed to decrease the amount of IUGR as seen from the morphometric results. However, CSE was not able to get rid of IUGR completely, or reduce the congenital malformations seen as exencephaly. On the other hand, CSE seemed to significantly boost the growth of T and DT 3-week-old progeny compared to C and DC groups.

Many factors could affect the weight of the fetus, including: hormones, genetic, nutrition, placental, and growth factors (Li et al., 2015) and could play a role in IUGR. As Padmanabhan and Shafiullah (2001) reviewed in their literature, earlier studies showed an association between maternal diabetes and IUGR, a number of malformations, and increased placental weight. Anomalous changes in metabolism, fuel, and fuel-related compounds in diabetic mothers' pregnancies (such as elevated glucose levels, ketones, and free radicals among others) may affect fetal growth and could cause congenital defects. The rate of Macrosomia incidents is higher in GDM, since hyperglycemia affects the fetus in the mid-gestation period, leading to fetal hyperglycemia and consequent

abnormal fetal weight gain. IUGR, on the other hand, is more frequent in the case of PGDM, where hyperglycemia affects the embryo in the preimplantation stages. In that case, glucose receptors formation might be reduced by DM in the blastula, causing insufficient energy supply. It also increases apoptosis, leading to a reduction in cell number, which contribute in manifestation of birth defects including IUGR or embryonic death (Padmanabhan and Shafiullah, 2001).

From the results of this study, CSE caused a slight decrease in WBW and WBL in the treated group compared to controls in E16.5 fetuses and a significant decrease in neonates.

Although studies showed that CSE did not cause hypoglycemia to normal mice (Zhao et al., 2012), it might be that giving the normal pregnant females daily doses of CSE might have reduced their blood sugar temporarily, thus exposing embryos to low glucose supply for a short period environment for a short period, might have caused the reduced growth seen in the T group compared to the controls. On the other hand, CSE caused an increase in growth parameters in the diabetic treated group compared to the diabetic controls in E16.5 fetuses but a slight insignificant decrease in neonates. The proportion of tail length to body length followed the WBW and WBL pattern. This shows that CSE could have a slight role in reducing the effect of diabetes on fetuses and neonate growth. DM caused a decrease in growth in all ages: this decrease was significant except WBL in neonates. This result is contestant with previous studies (Kappen et al., 2011).

The placenta plays a vital role in providing the fetus in subsequent and stable oxygen and nutrient supply. Changes in placental dimensions might lead to instability in blood and nutrient supply to fetuses (Moore et al., 2018). Many factors might lead to an increase in placental diameter, causing instability in blood and nutrient supply.

In a study on the effect of diabetes on placental cellular composition, the weight of placentas from uncontrolled diabetic pregnancy were elevated compared to controlled diabetic and normal pregnancies. This elevation seemed to be due to more glycogen storage rather than increased

cellularity, since the amounts of DNA and proteins were similar in all three groups (Husain et al., 2001). This is supported by Padmanabhan and Shafiullah's (2001) study, in which they noticed that these changes are correlated with fetal growth retardation and other developmental delays.

In this study, both corn silk extract and diabetes caused an increase in placental diameters for E16.5 fetuses, even though growth parameters decreased. It seems that some factors present in CSE increased placental diameters, which might be caused by glycogen accumulation.

As for the 3-week-old progeny in this study, CSE significantly increased growth in both diabetic and nondiabetic treated groups, which enhanced the decrease that diabetes caused in the DC group. This could be due to increased mothers' lactation or changing milk components. These results could lead to explore the benefits of using CSE extract in early life after diabetic pregnancy. More research is needed to explore these probabilities.

As mentioned in the non-diabetic groups results of E16.5 fetuses (C and T), CSE did not seem to affect the morphology of fetuses. On the other hand, among the DC and DT groups, each had one incident of a major malformation exencephaly, which is a neural tube defect that diabetes could induce (Loeken, 2005; Wilde et al., 2014). The fact that this defect was manifested in the diabetic groups only is consistent with earlier studies, which concluded that diabetes increased the rate of NTDs (Sugimura et al., 2009; Kappen et al., 2011), especially exencephaly (Bohuslavova et al., 2013). Loeken (2005) reviewed that hyperglycemia could induce embryonic oxidative stress, which inhibits the expression of Pax3 gene, which is important for neural tube closure. The exencephaly seen in DT group seemed different than the one seen in the DC group, as the head opening that the brain was protruding from seemed smaller.

In the neonates' results of this study, an incident of caudal growth defect was manifested in the DT group, where the posterior end of the fetus was malformed (Fig. 5). This case could be named caudal regression, a NTD. It is a defect affecting the lower spine vertebrae ranging from agenesis to hypogenesis of the caudal vertebrae and

associated parts. This defect is rare in normal pregnancies, but its rate increases 250 times in pregnancies affected by diabetes (Chan et al., 2002; Sugimura et al., 2009; Mills, 2010; Kappen, 2013). One cause could be oxidative stress, since maternal diabetes increases it. Oxidative stress induces DNA damage that activate DNA damage response (DDR) pathway during neurulation stage. Excess DNA damage leads to cell apoptosis (Dong et al., 2015). Another possible mechanism could be due to downregulation of a gene in the tail bud in response to retinoic acid, causing the malformation as reported by Chan et al. (2002). In their study, they injected diabetic and non-diabetic pregnant mice with two doses of retinoic acid (Vit. A), a known teratogen. They found that vitamin A significantly increased the vulnerability of fetuses of diabetic mothers to caudal regression compared to non-diabetic ones. They noticed that the amount of downregulation in low-dose diabetic mice is comparable to high-dose non-diabetics. This suggested that diabetes increases the amount of vitamin A transferred to the fetus (Chan et al., 2002). In this study, it seems that other factors might have affected the expression of the gene responsible for the tail formation.

To our knowledge, this is the first study on the effect of CSE on the fetuses and offspring. More studies should be done to detect the mechanisms of the CSE effect on Neural Tube (NT) closure. It seems that the CSE dose given to pregnant females in this study was not enough to antagonize the effect of DM as it was 4 g/kg a day for 5 days per week only.

REFERENCES

- ALOTAIBI A, PERRY L, GHOLIZADEH L, ALGANMI A (2017) Incidence and prevalence rates of diabetes mellitus in Saudi Arabia : An overview. *J Epidemiol Glob Health*, 7(4): 211-218.
- ALWIN ROBERT A, AL DAWISH MA, BRAHAM R, MUSALLAM MA, AL HAYEK AA, AL KAHTANY NH (2017) Type 2 diabetes mellitus in Saudi Arabia: major challenges and possible solutions. *Curr Diabetes Rev*, 13(1): 59-64.
- BOHUSLAVOVA R, SKVOROVA L, SEDMERA D, SEMENZA GL, PAVLINKOVA G (2013) Increased susceptibility of HIF-1 α heterozygous-null mice to cardiovascular malformations associated with maternal diabetes. *J Mol Cell Cardiol*, 60: 129-141.
- BYERS SL, WILES MV, DUNN SL, TAFT RA (2012) Mouse estrous cycle identification tool and images. *PLoS One*, 7(4): e35538.
- CALIGIONI CS (2009) Assessing reproductive status/stages in mice. *Curr Protoc Neurosci*, Appendix 4:Appendix 4I.
- CHAN BWH, CHAN K-S, KOIDE T, YEUNG S-M, LEUNG MBW, COPP AJ, LOEKEN MR, SHIROISHI T, SHUM ASW (2002) Maternal diabetes increases the risk of caudal regression caused by retinoic acid. *Diabetes*, 51(9): 2811-2816.
- CHEN C-P (2005) Congenital malformations associated with maternal diabetes. *Taiwan J Obstet Gynecol*, 44(1): 1-7.
- CORREA A, GILBOA SM, BESSER LM, BOTTO LD, MOORE CA, HOBBS CA, CLEVES MA, RIEHLE-COLARUSSO TJ, WALLER DK, REECE EA (2008) Diabetes mellitus and birth defects. *Am J Obstet Gynecol*, 199(3): 237.e1-237.e9.
- DEEDS MC, ANDERSON JM, ARMSTRONG AS, GASTINEAU DA, HIDDINGA HJ, JAHANGIR A, EBERHARDT NL, KUDVA YC (2011) Single dose streptozotocin-induced diabetes: considerations for study design in islet transplantation models. *Lab Anim*, 45(3): 131-140.
- DONG D, YU J, WU Y, FU N, ARIAS VILLELA N, YANG P (2015) Maternal diabetes triggers DNA damage and DNA damage response in neurulation stage embryos through oxidative stress. *Biochem Biophys Res Commun*, 467(2): 407-412.
- DOWLING D, CORRIGAN N, HORGAN S, WATSON CJ, BAUGH J, DOWNEY P, MCAULIFFE FM (2014) Cardiomyopathy in offspring of pregestational diabetic mouse pregnancy. *J Diabetes Res*, 2014: 624939.
- EL-ABHAR HS, SCHAALAN MF (2014) Phytotherapy in diabetes: review on potential mechanistic perspectives. *World J Diabetes*, 5(2): 176-197.
- GUO J, LIU T, HAN L, LIU Y (2009) The effects of corn silk on glycaemic metabolism. *Nutr Metab*, 6(1): 47.

- HASANUDIN K, HASHIM P, MUSTAFA S (2012) Corn silk (*Stigma maydis*) in healthcare: a phytochemical and pharmacological review. *Molecules*, 17(8): 9697-9715.
- HUSAIN SM, FROST R, MUGHAL ZM (2001) Effect of diabetes mellitus on rat placenta cellularity. *Early Hum Dev*, 60(3): 207-214.
- INTERNATIONAL DIABETES FEDERATION (2017) IDF Diabetes Atlas. 8th edn. Brussels, *International Diabetes Federation (IDF)*.
- JAWERBAUM A, WHITE V (2010) Animal models in diabetes and pregnancy. *Endocr Rev*, 31(5): 680-701.
- KAPPEN C, KRUGER C, MACGOWAN J, SALBAUM JM (2011) Maternal diet modulates the risk for neural tube defects in a mouse model of diabetic pregnancy. *Reprod Toxicol*, 31(1): 41-49.
- KAPPEN C (2013) Modeling anterior development in mice: diet as modulator of risk for neural tube defects. *Am J Med Genet C Sem Med Genet*, 163C(4): 333-356.
- LASHEEN AE, ABDELBASIT OB, SEIDAHMED MZ, HUSSEIN KA, MIQDAD AM, AL ZAHRANI MH, FARID GH, BADR HA (2014) Infants of diabetic mothers. A cohort study. *Saudi Med J*, 35(6): 572-577.
- LI J, CHEN L, TANG Q, WU W, GU H, LIU L, WU J, JIANG H, DINGH, XIA Y, CHEN D, HUY, WANG X (2015) The role, mechanism and potentially novel biomarker of microRNA-17-92 cluster in macrosomia. *Sci Rep*, 5: 17212.
- LOEKEN MR (2005) Current perspectives on the causes of neural tube defects resulting from diabetic pregnancy. *Am J Med Genet C Sem Med Genet*, 135C(1): 77-87.
- MARTIN PM, ROON P, VAN ELLS TK, GANAPATHY V, SMITH SB (2004) Death of retinal neurons in streptozotocin-induced diabetic mice. *Invest Ophthalmol Vis Sci*, 45(9): 3330-3336.
- MILLS JL (2010) Malformations in infants of diabetic mothers. *Teratology* 25:385-94. 1982. *Birth Defects Res A Clin Mol Teratol*, 88(10): 769-778.
- MONTEIRO LJ, NORMAN JE, RICE GE, ILLANES SE (2016) Fetal programming and gestational diabetes mellitus. *Placenta*, 48 Suppl 1: S54-S60.
- MOORE KL, PERSAUD TVN, TORCHIA MG (2018) *The Developing Human-E-Book: Clinically Oriented Embryology*. Elsevier Health Sciences.
- MOSTAFA AM, MOHAMED WS, SERWAH AHA, SERWAH MA. (2014) Effect of diclofenac on plasma glucose level, insulin resistance, inflammatory markers and hepatocytes in diabetic albino rats. *Egypt J Hosp Med*, 15(54): 117-128.
- PADMANABHAN R, SHAFIULLAH M (2001) Intrauterine growth retardation in experimental diabetes: possible role of the placenta. *Arch Physiol Biochem*, 109(3): 260-271.
- PENG K-Z, ZHANG S-Y, ZHOU H-L (2016) Toxicological evaluation of the flavonoid-rich extract from *Maydis stigma*: Subchronic toxicity and genotoxicity studies in mice. *J Ethnopharmacol*, 192: 161-169.
- SAVION S, GIDON-DABUSH S, FEIN A, TORCHINSKY A, TODER V (2004) Diabetes teratogenicity is accompanied by alterations in macrophages and T cell subpopulations in the uterus and lymphoid organs. *Int Immunopharmacol*, 4(10): 1319-1327.
- STEWART ZA, MURPHY HR (2015) Gestational diabetes. *Medicine*, 43(1): 44-47.
- SUGIMURA Y, MURASE T, OYAMA K, UCHIDA A, SATO N, HAYASAKA S, KANO Y, TAKAGISHI Y, HAYASHI Y, OISO Y, MURATA Y (2009) Prevention of neural tube defects by loss of function of inducible nitric oxide synthase in fetuses of a mouse model of streptozotocin-induced diabetes. *Diabetologia*, 52(5): 962-971.
- THEILER K (2013) *The house mouse: atlas of embryonic development*. Springer Science & Business Media.
- TRIPATHI V, VERMA J (2014) Different models used to induce diabetes: a comprehensive review. *Int J Pharm Pharm Sci*, 6(6): 29-32.
- VELAZQUEZ DVO, XAVIER HS, BATISTA JEM, DE CASTRO-CHAVES C (2005) *Zea mays* L. extracts modify glomerular function and potassium urinary excretion in conscious rats. *Phytomedicine*, 12(5): 363-369.
- WAHABI H, FAYED A, ESMAEIL S, MAMDOUH H, KOTB R (2017) Prevalence and complications

of pregestational and gestational diabetes in Saudi women: analysis from Riyadh mother and baby cohort study (RAHMA). *Biomed Res Int*, 2017: 6878263.

WAHABI HA, FAYED A, ESMAEIL SA (2014) Maternal and perinatal outcomes of pregnancies complicated with pregestational and gestational diabetes mellitus in Saudi Arabia. *J Diabetes Metab*, 5(7): 1-5.

WANG F, REECE EA, YANG P (2015) Oxidative stress is responsible for maternal diabetes-impaired transforming growth factor beta signaling in the developing mouse heart. *Am J Obstet Gynecol*, 212(5): 650.e1-650.e11.

WILDE JJ, PETERSEN JR, NISWANDER L (2014) Genetic, epigenetic, and environmental contributions to neural tube closure. *Ann Rev Genet*, 48: 583-611.

ZHAO W, YIN Y, YU Z, LIU J, CHEN F (2012) Comparison of anti-diabetic effects of polysaccharides from corn silk on normal and hyperglycemia rats. *Int J Biol Macromol*, 50(4): 1133-1137.

ŽILIC S, JANKOVIĆ M, BASIĆ Z, VANČETOVIĆ J, MAKSIMOVIĆ V (2016) Antioxidant activity, phenolic profile, chlorophyll and mineral matter content of corn silk (*Zea mays* L): Comparison with medicinal herbs. *J Cereal Sci*, 69: 363-370.

Histological evaluation of L-arginine-mediated exocrine pancreatic injury in rats and the potential implication of the probiotic (*Lactobacillus Acidophilus*)

Dalia A. Mandour, Asmaa M. Tolba

Department of Human Anatomy and Embryology, Faculty of Medicine, Zagazig University, Postal Code: 44519, Egypt

SUMMARY

The acute exocrine pancreatic injury was induced by L-arginine in rats and the potential prophylactic/therapeutic role of probiotics was evaluated in a histological, immunohistochemical, and molecular study. Thirty adult male rats were used and randomly divided into five groups. Group I (Control group). Group II (Probiotic group): supplemented orally with 2×10^8 CFU/kg *Lactobacillus Acidophilus* for 5 days. Group III (Acute pancreatitis, AP) group: received double intraperitoneal injections of 250mg/100g BW L-arginine with one hour apart. Group IV (Prophylactic group): before induction of AP, the rats were supplemented orally with 2×10^8 CFU/kg *Lactobacillus Acidophilus* for 5 days. Group V (Therapeutic group): after induction of AP, the rats were supplemented orally with 2×10^8 CFU/kg *Lactobacillus Acidophilus* for 5 days. Pancreatic specimens were processed for histological and biochemical studies, and assessment of deoxyribonucleic acid (DNA) fragmentation by gel electrophoresis. Serum amylase, lipase and IL-1 β were determined. Also, pancreatic malondialdehyde (MDA), reduced glutathione (GSH) and myeloperoxidase (MPO) were assessed. In AP group, the histological architecture of the

exocrine pancreas was distorted with acinar cell necrosis, inflammatory cellular infiltration, interstitial edema, and hemorrhage. Inducible nitric oxide synthase (iNOS) was highly expressed in the cytoplasm of acinar cells. Moreover, AP group displayed much DNA fragmentations and a significant increase of amylase, lipase, IL- β , MDA, MPO, and a decrease of GSH. Most deleterious effects of the AP were alleviated more with the prophylactic than therapeutic use of *Lactobacillus Acidophilus*. In conclusion: The prophylactic regimen of probiotics has a supreme beneficial effect over the therapeutic one in ameliorating the AP.

Key words: Exocrine pancreas – L-arginine – Histology – Probiotics – Rats

INTRODUCTION

Acute pancreatitis (AP) is a devastating life-threatening inflammatory disease of the pancreas, and it constitutes the most common cause of hospital admission among gastrointestinal diseases (Melo et al., 2010; Mirmalek et al., 2016). Over the last few years, the incidence of AP was increased worldwide due to the high prevalence of gallstone-related

Corresponding author:

Asmaa M. Tolba, Department of Human Anatomy and Embryology, Faculty of Medicine, Zagazig University, Postal Code: 44519, Egypt.
E-mail: amtolba@zu.edu.eg / a_toba2009@yahoo.com

Submitted: September 5, 2020. Accepted: October 14, 2020

disorders together with alcohol abuse, which represent two major risk factors in developing AP (Krishna et al., 2017; Esteban-Zubero et al., 2018). AP is a multifactorial disease, whose exact etiology has not been fully elucidated. However, some proposed causes are documented in the literature including trypsin reflux, a viral infection like coxsackievirus, hypercalcemia, hyperlipidemia, drugs like furosemide, thiazides, and sulfonamides or developmental anomalies particularly the pancreatic divisum (Vinklerová et al., 2010; Biradar and Veeresh, 2013). Also, the cause of the AP may be idiopathic (Muddana et al., 2009). Clinically, the presentation of AP varies from a mild self-limiting form to a severe form, necrotizing pancreatitis, which is usually encountered with systemic complications like systemic inflammatory response syndrome (SIRS) and multiple organ dysfunction syndromes (MODS), which are responsible for high AP-induced mortality (Pan et al., 2017). The overall estimated mortality rate in patients with AP is approximately 5%, which reaches 30% in patients with severe form (Shah et al., 2018). In the past decades, intense efforts have been devoted by the scientists to clarify the pathogenesis of AP. However, the exact mechanism has not been fully elucidated yet (Goodchild et al., 2019). Nevertheless, a hypothesis has argued that the pathogenesis is related to acinar cell response to the premature activation of pancreatic proenzymes, particularly trypsinogen into trypsin, which triggers a chain of activation of other pancreatic precursors that ultimately cause intracellular autodigestion of the gland (Bhatia et al., 2005; Pan et al., 2017). This process harbors many histological alterations, local inflammatory reactions, and the release of a vast array of inflammatory mediators in conjunction with free radicals in the pancreatic parenchyma. These histochemical cross talks eventually lead to acinar cell necrosis (Bhatia et al., 2005). Unfortunately, there is no specific treatment for the AP, so far and the currently available medical treatment is limited only to some supportive symptomatic drugs like analgesics, anti-inflammatories and steroids (Muddana et al., 2009; Biradar and Veeresh, 2013). These synthetic drugs were reported to be neither

specific nor implemented for all patients due to the increased frequency of their complications and their high economic burden. Therefore, the search continues for novel strategies of natural compounds that are recommended based on their cost-effectiveness and pursued as prophylactic or therapeutic agents for the management of AP. In that regard, a naturally-occurring probiotic (*Lactobacillus Acidophilus*) was tried in this study. According to the definition adopted by Food and Agriculture Organization (FAO) and World Health Organization (WHO), probiotics are “living non- pathogenic microorganisms which when administered in adequate amounts confer a health benefit to the host”. Therefore, they have been incorporated in various fermented milk products (Zielińska and Kolożyn-Krajewska, 2018). Interestingly, probiotics involve many species of microorganisms, of which *Lactobacillus acidophilus* (*L. acidophilus*) is the most beneficial species, and it has been studied widely in animals and humans (Wang et al., 2017a). This species exerts potent anti-inflammatory, antioxidant, immune-modulatory, and bacteriostatic functions (Lutgendorff et al., 2008; Spyropoulos et al., 2011; Kechagia et al., 2013). Taking into account the potential implication of inflammatory mediators and free radicals in the pathophysiology of AP, together with the above-mentioned biological functions of the probiotics, consequently this study was settled down as a trial to explore the possible prophylactic and therapeutic role of *L. acidophilus* supplementation in an experimental model of AP induced by L-arginine in the adult male rats.

MATERIALS AND METHODS

Chemicals and Drugs

L-Arginine

L-arginine (a semi-essential amino acid) was provided in the form of a powder (L-arginine, Cat. No. A5006, Sigma Aldrich Company, St. Louis, MO, USA). It was dissolved in a freshly prepared normal saline (0.9% NaCl) whose pH was adjusted to 7.0 by 5.0 N HCL with a final concentration of 500 mg/ml.

***Lactobacillus acidophilus* (*L. acidophilus*)**

L. acidophilus strain of probiotics was used. It was provided as tablets. Each tablet was 0.5 mg containing 10^8 colony-forming units (CFU) of *L. acidophilus* (Puritan's Pride, INC., Holbrook, NY 11741, USA). Each tablet was dissolved in one ml of distilled water.

Experimental animals

Thirty adult male Sprague Dawley albino rats of 180-220 gm body weight (BW) were used in this study. They were obtained from the animal house of the Faculty of Medicine, Zagazig University, Egypt. The rats were left to acclimatize for one week prior to the start of the experiments. The animals were housed in clean, well-ventilated cages at a constant room temperature of $23\pm 2^\circ\text{C}$ under the natural 12-hour day/night cycles with free access to a standard commercial rodent pellets chow and water *ad libitum*. The rats were kept under the same environmental conditions throughout the whole study period. The experimental protocol and all experimental procedures of this study were revised and approved by the ethical guidelines established by the Institutional Animal Care and Use Committee of Zagazig University, Egypt (reference number ZU-IACUC/3/F/106/2019) in compliance with and in according to the international guidelines for the care and use of the research laboratory animals.

Experimental design

The rats were randomly divided into 5 groups, each comprising 6 rats.

Group I (Control group): The rats of this group were injected intraperitoneally (I.P) with a double dose of 1 ml normal saline with one-hour interval and left without any medication for 5 days; then they were sacrificed.

Group II (Probiotic group): The rats of this group were supplemented orally with *L. acidophilus* in a dose of 2×10^8 CFU/kg, once a day for 5 consecutive days; then they were sacrificed (Muftuoglu et al., 2006).

Group III (AP group): Induction of AP was performed by injecting the rats with double I.P doses of L-arginine with one hour apart, each of

which was 250 mg/100 g BW. The animals were sacrificed 5 days after the second L-arginine injection (Pezzilli and Fantini, 2006).

Group IV (Prophylactic group): The rats were supplemented orally with *L. acidophilus* in a dose of 2×10^8 CFU/kg, daily for 5 successive days, then AP was induced as in group III and the animals were sacrificed 5 days after the second L-arginine injection.

Group V (Therapeutic group): In this group, AP was induced as in group III and after the second L-arginine injection, the rats were supplemented orally with *L. acidophilus* in a dose of 2×10^8 CFU/kg, daily for 5 successive days, after which they were sacrificed.

Induction of AP

In this study, an experimental model of AP was induced in rats via double I.P injections of L-arginine (250 mg/100g BW) with one hour apart. To confirm a successful induction of AP, two blood samples were withdrawn from the retro-orbital venous plexus of the rats; the first sample was obtained immediately before induction of AP, while the second sample was obtained 24 hours after the second injection of L-arginine. AP was biochemically insured when the serum level of amylase and lipase enzymes in the second sample was double or more than their normal basal level of the first sample (Pacheco et al., 2003).

Experimental procedures

The experimental procedures of this study were performed in the animal house of the Faculty of Medicine, Zagazig University, Egypt. At the end of the experimental schedule, the animals were subjected to overnight fasting, after which they were weighed, and then anesthetized by I.P injection of sodium pentobarbital (40 mg/kg BW). Afterward, blood samples were collected from the rats of all groups and left to be coagulated at room temperature, then centrifuged at 3000 r.p.m for 10 min. The serum was separated and collected in dry clean Eppendorf tubes, and frozen immediately at -20°C until further biochemical analysis of serum amylase, lipase, and interleukin-1beta (IL-1 β).

Thereafter, the rats were sacrificed by cervical dislocation, then a midline abdominal incision was performed and tissue fixation was carried out by means of intracardiac injection of 2.5% phosphate-buffered glutaraldehyde

solution (pH 7.4). Then, the whole pancreas was quickly excised outside the rats' body, trimmed free of fat and peripancreatic tissues and blotted on filter paper, and weighed. Thereafter, the harvested pancreas was sharply divided into two halves. The half including the head was processed for light and electron microscopic examinations, while the other half was preserved in buffered saline at -80°C for later homogenization.

Pancreatic weight/body weight ratio (PW/BW ratio)

This ratio was calculated (mg/g) as a crude index of pancreatic edema (Biradar and Veeresh, 2013).

Histological study

Light microscopy (LM)

Pancreatic specimens were fixed overnight in 10% neutral buffered formalin, dehydrated in ascending grades of ethanol, cleared with xylene and embedded in paraffin wax. Paraffin sections of 5 µm thick were cut and stained with Hematoxylin and Eosin (H&E) to study the histological architecture of the exocrine pancreas (Bancroft and Layton, 2013). Finally, the stained sections were examined under a light microscope (Leica Microsystems, Schweiz, AG, Heerbrugg, CH-9435, Switzerland) and photographed using a digital camera coupled to that microscope in the Department of Anatomy, Faculty of Medicine, Zagazig University, Egypt.

Transmission electron microscopy (TEM)

Specimens from the head of the pancreas, about 1 mm³ in size, were taken, fixed in 2.5% phosphate-buffered glutaraldehyde solution (pH 7.4) for 24 hours at 4°C. Thereafter, the specimens were post-fixed in 1% osmium tetroxide at 4°C for one hour, then dehydrated in ascending grades of ethanol and finally embedded in epoxy resin. Afterward, semithin sections of about 1 µm thick were cut with an ultramicrotome (Leica Reichert, Ultracut, S, Germany), to be stained with 1% toluidine blue, and examined under a light microscope. Then, ultrathin sections of 70 nm were cut, mounted on copper grids, and double-stained with uranyl acetate and lead citrate (Bozzola and Russel, 1999). Finally, the obtained ultrathin sections were photographed using a JEOL JEM-1400

transmission electron microscope at Electron Microscopy Unit in the Research Center, Faculty of Agriculture, Cairo University, Egypt.

Immunohistochemical study

Inducible nitric oxide synthase (iNOS) enzyme expression in the pancreatic tissue was assessed by immunohistochemical staining technique. Paraffin pancreatic sections of 4 µm thick were mounted on a positively charged slide. These tissue sections were deparaffinized with xylene then rehydrated in descending grades of ethanol. Antigen retrieval was accomplished and endogenous peroxidase activity was blocked by 0.3% hydrogen peroxide (H₂O₂). Non-specific protein binding sites were blocked by 5% goat serum in phosphate-buffered saline (PBS) for 30 min. The sections were then incubated overnight at 4°C with primary rabbit anti-iNOS polyclonal antibody (Thermo Fisher Scientific, Massachusetts, USA) diluted 1:200 with PBS. Then, the slides were incubated with 2% biotinylated goat anti-rabbit secondary antibody in PBS (EnVision™/AP, K1396; Dako, Carpinteria, CA, USA) for 30 min. followed by the addition of a streptavidin-peroxidase solution. Afterward, diaminobenzidine (DAB) chromogen solution was added. Finally, the sections were counterstained with Mayer's hematoxylin. The negative control slides were prepared following the same staining procedures, but with omitting the primary antibody. Positive iNOS immunostaining reaction was identified under the light microscope as brown coloration in the cytoplasm of the pancreatic acinar cells (Ramos-Vara et al., 2008).

Histomorphometric study

The mean optical density of iNOS immunoreaction was quantitatively assessed in five non-overlapped high-power fields (X400) of immune stained pancreatic sections from each animal of all groups. This measuring technique was performed using the image analyzer computer system (Leica Qwin plus microsystem version 3, Switzerland) at the Image Analyzing Unit of the Oral Pathology Department, Faculty of Dentistry, Cairo University, Egypt. The obtained data were represented as

Mean±Standard deviation (Mean±SD) and were statistically analyzed.

Homogenization of pancreatic tissue

The buffered saline-preserved pancreatic tissue was blotted dry, weighed and homogenized 5% (w/v) in a freshly prepared ice-cold PBS (50 mM, pH 7.4) using an electronic tissue homogenizer (Model silent crusher-M; Heidolph Instruments, Donau, Germany). The resulting pancreatic homogenate was centrifuged at 4000 r.p.m for 15 min. at 4°C (Mirmalek et al., 2016). Then, the supernatant was separated and stored at -80°C in aliquots until the assessment of DNA fragmentation by gel electrophoresis and measuring the pancreatic tissue level of malondialdehyde (MDA, a marker of oxidative stress and lipid peroxidation), reduced glutathione (GSH, a marker of tissue antioxidant activity), myeloperoxidase enzyme activity (MPO, a marker of neutrophil sequestration and infiltration in pancreatic tissue).

Molecular study (Assessment of DNA fragmentation)

DNA fragmentation of the pancreatic tissue was assessed by the agarose gel electrophoresis technique adopted by Kratz and Siegfried (2010), in which DNA fragments were separated and then assessed qualitatively according to their size. Briefly, DNA was isolated from the previously prepared pancreatic homogenate of different groups, and loaded into wells at one end of agarose gel, and then an electric current was applied, DNA fragments being negatively charged; they phoresis (migrate) in lanes corresponding to their wells towards the positive electrode, where small fragments move faster than large ones through the gel. The gel-containing DNA was stained with ethidium bromide and DNA fragments were visualized as bands (each representing a group of the same sized fragments) under ultraviolet light (UV transilluminator, BIORAD, USA). Finally, DNA fragmentation was assessed based on the size of each band compared to a standard “yardstick” ladder made up of DNA fragments of known size.

Biochemical study

Serum amylase (U/L) was determined by the colorimetric method using an amylase commercial assay kit (Ultra diagnostics, Cairo, Egypt) (Ceska et al., 1969). *Serum lipase* (U/L) was determined by the colorimetric method using lipase commercial assay kit (Accurex diagnostics, Cairo, Egypt) (Whitaker, 1973). *Serum IL-1 β* (pg/mL) was measured by the enzyme-linked immunosorbent assay (ELISA), following the manufacturer’s manual of instructions, using an ELISA kit (R&D Systems, Minneapolis, MN USA). The results were calculated from a standard curve and expressed as (pg/mL) (Moody et al., 2001). *Pancreatic tissue MDA* (nmol/g protein) was measured by thiobarbituric acid colorimetric method using MDA assay kit (Bio-diagnostic, catalog no. MD 2529, Cairo, Egypt) (Ohkawa et al., 1979). *Pancreatic tissue GSH* (μ mol/g protein) was measured colorimetrically using GSH commercial assay kit (Bio Diagnostic, catalog no. GR 2511; Cairo, Egypt) (Beutler et al., 1963). *Pancreatic tissue MPO activity* (U/g protein) was assessed colorimetrically according to the manufacturer’s instructions, using MPO commercial assay kit (Nanjing Jian cheng Corp., China) (Bradley et al., 1982).

Statistical analysis

The morphometric and biochemical studies were statistically analyzed using the statistical package of Social Science Program, Version 19 for Windows (SPSS Inc., Chicago, Illinois, USA). The data were expressed as Mean±SD. Statistical significance was calculated by using one-way ANOVA, followed by post hoc Tukey’s test for multiple comparisons. P-value ≤ 0.05 was considered statistically significant (Petrie and Sabin, 2005).

RESULTS

During the experiment, no mortality was recorded among the rats of all groups.

Light microscopic

Examination of (H&E) stained pancreatic sections of the control and probiotic groups revealed a normal histological architecture of

the pancreas, which appeared to be divided into lobules by thin interlobular connective tissue septa containing interlobular ducts. The lobules contained closely packed exocrine acini, which

appeared rounded or triangular in cross-section with basal basophilia and apical eosinophilia. The acini have central lumen contained centroacinar cells. Among the acini, the endocrine islets of

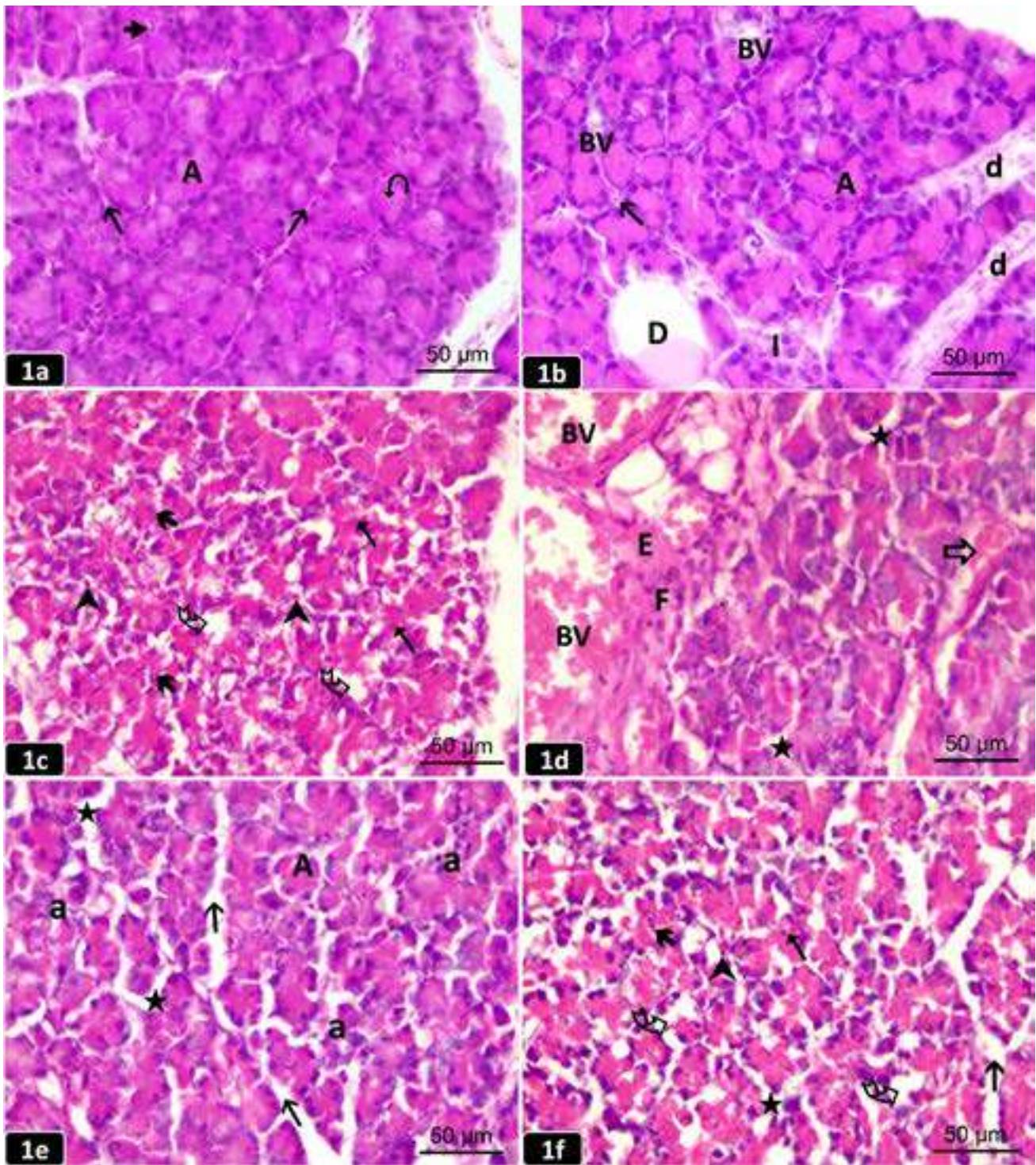


Fig. 1.- Pancreatic sections from the studied groups of rats (H&E; x 400). **[1a]:** The control group showing a normal histological architecture of the pancreatic lobules separated by thin interlobular septa (†). The lobules contain closely packed exocrine acini (A) having basal basophilia and apical acidophilia (◡). Centroacinar cells (↔) appear inside the lumen of the acini. **[1b]:** The probiotic group showing normal closely packed exocrine acini (A) separated by scanty connective septa (†) having blood vessels (BV). Interlobular duct (D) containing eosinophilic material and intralobular ducts (d) are observed. An Islet of Langerhans (I) is embedded among the acini. **[1c]:** The AP group showing focal areas of acinar cell necrosis in the form of pyknotic (▲), karyorrhectic (⚡), and karyolytic (◡) nuclei with diffuse eosinophilic cytoplasm that exhibits multiple vacuoles (⊖) giving a moth-eaten appearance. **[1d]:** The AP group showing dilated congested blood vessels (BV), inflammatory cellular infiltrate (F), extravasation of red blood cells within an inflammatory exudate (E), and destructed BV with microscopic foci of hemorrhage (⇨). Distorted acini are separated by wide interacinar spaces (★). **[1e]:** The prophylactic group showing some preserved acini (A) and others are distorted (a) with a widening of both interacinar (★) and interlobular (†) spaces. **[1f]:** The therapeutic group showing necrotic changes in some acini including vacuoles (⊖) in diffuse eosinophilic cytoplasm, karyolytic (◡), pyknotic (▲), and karyorrhectic (⚡) nuclei. Widening of both interacinar (★) and interlobular (†) spaces. Scale bars (a-f) = 50 μm.

Langerhans were embedded and appeared as clusters of pale staining cells intermingled with blood sinusoids with no apparent capsule (Figs. 1a, 1b). Moreover, toluidine blue-stained sections of the control and probiotic groups revealed pancreatic acini lined with pyramidal-shaped

cells that had basal rounded vesicular nuclei with many apical, densely-stained, secretory zymogen granules (ZG). The acinar cell boundaries were regular and well defined, and the acini were separated from each other by thin inter-acinar connective tissue septa (Figs. 2a, 2b).

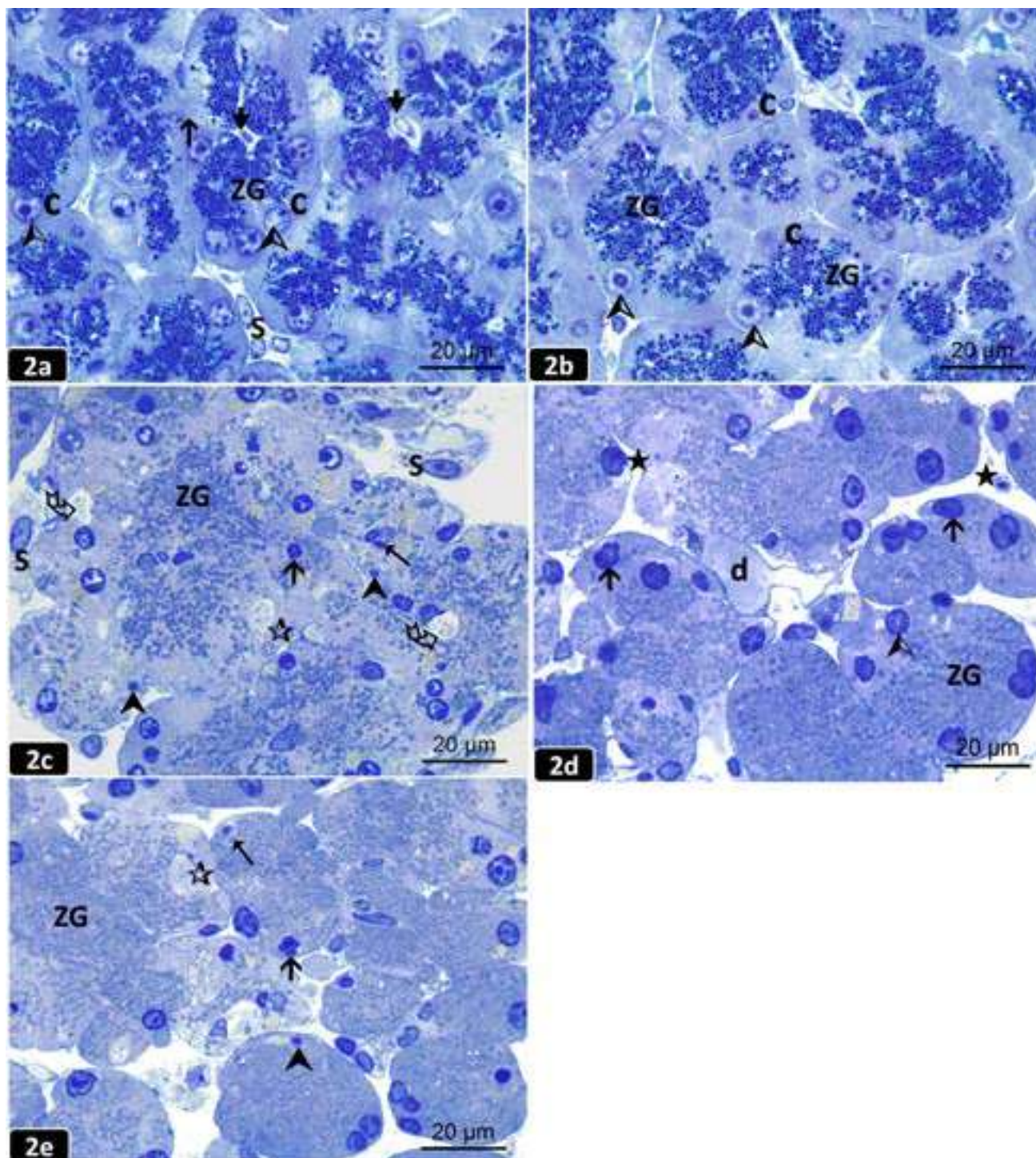


Fig. 2.- Semithin pancreatic sections from the studied groups of rats (Toluidine blue; x 1000). [2a]: The control group showing normal acini lined with pyramidal-shaped cells (C) having basal rounded nuclei (A) and many apical densely stained zymogen granules (ZG) toward the lumen (V) of the acini. The acini are separated by thin interacinar septa (↑). Interstitial stromal cells (S) are observed. [2b]: The probiotic group showing pyramidal-shaped cells (C) lining the acini with basal rounded nuclei (A) and many apical densely stained ZG. [2c]: The AP group showing loss of acinar cell boundaries with an intermingling of their few ZG, cytoplasmic vacuolation (Ψ) with small irregular (↑), pyknotic (▲), and karyolytic (∞) nuclei. Some acini appear anucleated (⊙). Stromal cells (S) are noticed in a wide interlobular space. [2d]: The prophylactic group showing some preserved acinar cells with basal vesicular nuclei (A) and many apical ZG. Some acini have irregular (↑) nuclei and separated by wide interacinar spaces (★). An intralobular duct (d) is noticed. [2e]: The therapeutic group revealing the loss of cell boundaries of some acini with an intermingling of their ZG. Most acini have irregular (↑), pyknotic (▲), and karyolytic (∞) nuclei. Some acini appear anucleated (⊙). Scale bars (a-e) = 20 μm.

Examination of H&E-stained sections of the AP group demonstrated a massive distortion of the histological architecture of the pancreatic acini, with focal areas of acinar cell necrosis in the form of multiple vacuoles in diffuse eosinophilic cytoplasm, giving the tissue a moth-eaten appearance with pyknotic, karyorrhectic, and karyolytic nuclei (Fig. 1c). Also, there were wide interlobular septa containing dilated, congested blood vessels (BVs) with inflammatory cellular infiltrate and extravasation of inflammatory exudate entangled with red blood cells. The distorted acini were separated by wide inter-acinar spaces with microscopic foci of interstitial hemorrhage from destructed blood vessels (Fig. 1d). Furthermore, toluidine blue sections of the AP group demonstrated loss of acinar cell boundaries, and the cytoplasm contained few or depleted ZG. The nuclei appeared small irregular, pyknotic and karyolytic. Some acini were anucleated (Fig. 2c).

Examination of H&E sections of the prophylactic group showed preserved pancreatic architecture, where the pancreatic lobules revealed some intact acini, while some appeared distorted with wide inter-acinar and interlobular spaces (Fig. 1e). Moreover, toluidine blue sections of this group revealed some preserved acinar cells with basal vesicular nuclei and many secretory ZG. However, some acini showed irregular nuclei (Fig. 2d).

Examination of H&E sections of the therapeutic group revealed somewhat comparable changes to that of the AP group, where some acini showed necrotic changes in the form of vacuolations in diffuse eosinophilic cytoplasm with pyknotic, karyolytic, and karyorrhectic nuclei (Fig. 1f). Additionally, toluidine blue of this group exhibited loss of the cell boundaries of some acini with an intermingling of their ZG. Most of the acini showed irregular, pyknotic and karyolytic nuclei (Fig. 2e).

Transmission electron microscopic

TEM examination of the pancreatic acinar cells of the control and probiotic groups displayed nearly the same ultrastructural picture of the normal acinar cells, having rounded euchromatic nuclei with dispersed chromatin and prominent nucleoli. The cytoplasm contained a heavy basal

arrangement of the rough endoplasmic reticulum (rER) with parallel-arranged cisternae yielding a lamellar profile, surrounding the nucleus. Mitochondria of normal shape and size were interspersed within rER. The apical part of the acinar cells was occupied by numerous ZG that appeared homogenous electron-dense (Figs. 3a, 3b, and 3c).

TEM examination of pancreatic acinar cells of the AP group showed small, irregular, fragmented and heterochromatic nuclei with dark peripheral condensed chromatin. Most acinar cells showed ZG of variable size and electron-density. Also, dilated fragmented cisternae of rER and swollen mitochondria were observed. Some acinar cells had rarified electron-lucent areas of cytoplasm that were nearly devoid of organelles. Congested BVs with perivascular inflammatory exudates were observed (Figs. 3d, 3e, and 3f).

Ultrathin sections of the acinar cells of the prophylactic group revealed a cytoplasm with less electron-dense ZG, apparently normal mitochondria, and heterochromatic nuclei surrounded by some regularly arranged cisternae of rER with other dilated and disarranged ones (Fig. 4a). Ultrathin sections of the acinar cells of the therapeutic group revealed irregular small heterochromatic nuclei, dilated fragmented cisternae of rER, swollen mitochondria, ZG of variable size, and electron density (Figs. 4b, 4c).

Immunohistochemical results

Examination of the iNOS immunohistochemical-stained sections from the control and probiotic groups appeared nearly similar, where a negative immunostaining reaction for iNOS in the cytoplasm of the normal acini with a weak immunoreaction in the cytoplasm of islets of Langerhans cells in the form of faint brown staining was noticed (Figs. 5a, 5b). AP group showed a strong positive immunostaining reaction for iNOS with a high intense brown coloration of the cytoplasm of the acinar cells and the wall of BVs compared with the control and probiotic groups (Fig. 5c).

However, the prophylactic group showed a mild immunostaining reaction for iNOS in the cytoplasm of both acinar cells and the

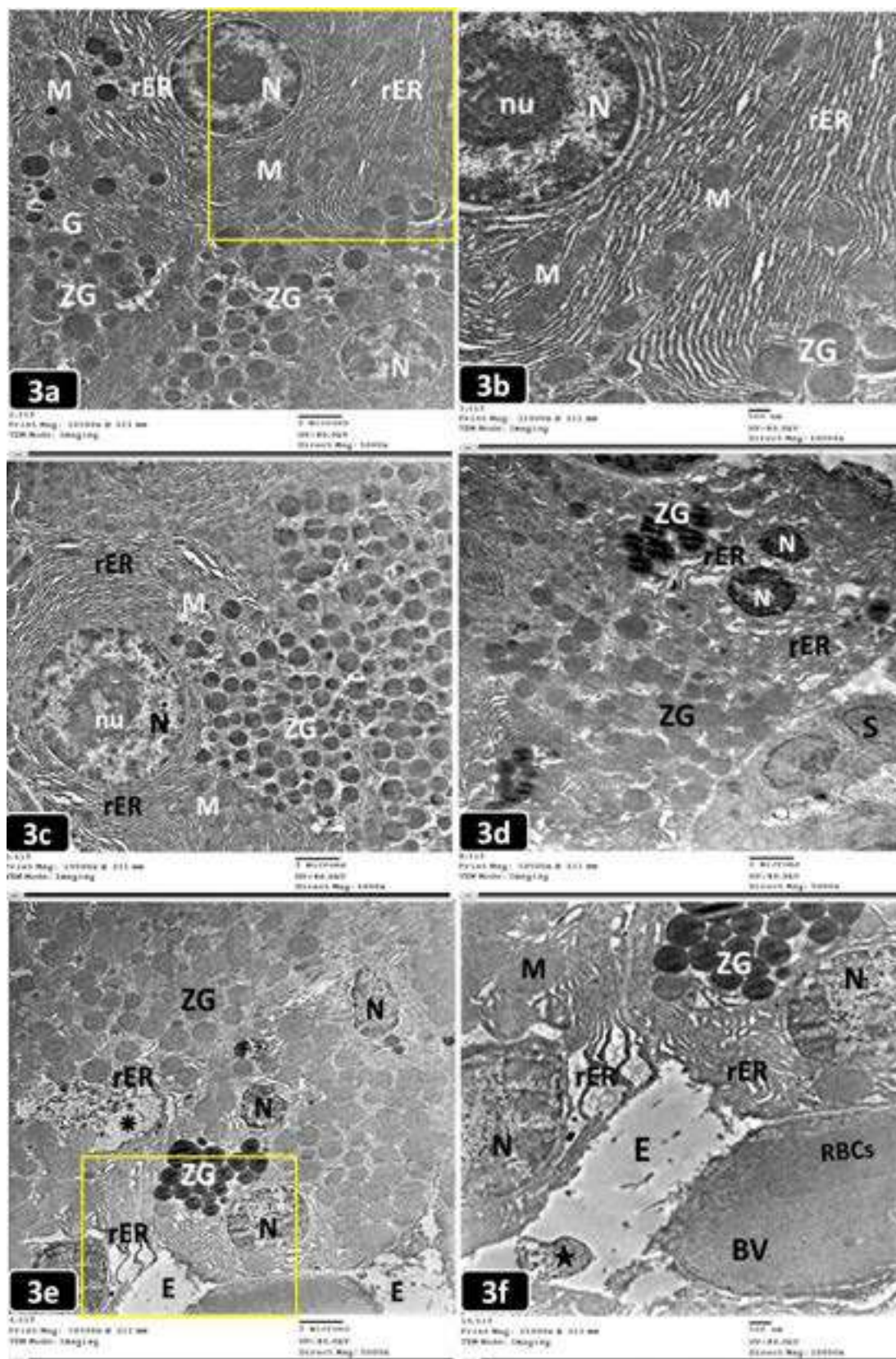


Fig. 3.- Electron micrographs of an ultrathin pancreatic sections from the studied groups of rats. 3a,c,d,e (TEM; x 5,000) and 3b,f (TEM; x 10,000). [3a]: The control group showing normal acinar cells with rounded nuclei (N), perinuclear rough endoplasmic reticulum (rER) with interspersed mitochondria (M). Supranuclear Golgi complex (G) and many homogenous electron-dense zymogen granules (ZG) are observed. [3b]: A higher magnification of the boxed area of (Fig. 3a) showing the euchromatic nucleus (N) and prominent nucleolus (nu). Well-arranged cisternae of rER with interspersed mitochondria (M) of normal shape and size with electron-dense ZG are observed. [3c]: The probiotic group showing a rounded euchromatic nucleus (N) and a prominent nucleolus (nu) of the normal acinar cell. The nucleus is surrounded by well-organized cisternae of rER with normal mitochondria (M). Numerous apical electron-dense ZG are observed. [3d]: The AP group showing a fragmented heterochromatic nucleus (N) surrounded by dilated disarranged rER and ZG of variable size and electron-density. Stromal cells (S) are noticed. [3e]: The AP group showing ill-defined acinar cell boundaries with small irregular heterochromatic nuclei (N), dilated fragmented rER, a rarified area of cytoplasm (*) with the debris of disintegrated organelles, and ZG of variable electron-density. Perivascular areas of electron-lucent exudate (E) are noticed. [3f]: A higher magnification of the boxed area of (Fig. 3e) showing small heterochromatic nuclei (N), dilated disarranged cisternae of rER, swollen mitochondria (M) and ZG. A congested blood vessel (BV) containing red blood cells (RBCs) with an electron-lucent exudate (E) and cellular debris (★) are noticed. Scale bars (a,c,d,e) = 2 μ m; (b,f) = 500 nm.

islets of Langerhans with less intense brown coloration compared with that of the AP group, but more intense coloration when compared with the control and probiotic groups (Fig. 5d). The therapeutic group showed a moderate immunostaining reaction for iNOS in the cytoplasm of both acinar cells and islets of Langerhans, with less intense brown coloration than AP but more intense than the control and probiotic groups (Fig. 5e).

Histomorphometric results

The mean value of iNOS in the cytoplasm of the acinar cells of the AP group was 71.28 ± 8.32 , which was statistically significantly higher ($P < 0.0001$) compared with those of the control group (7.57 ± 1.19) and probiotic group (7.24 ± 1.30). The mean values of iNOS in both prophylactic and therapeutic groups were 44.66 ± 2.14 and 59.18 ± 4.18 respectively, which were statistically significantly lower ($P < 0.0001$ and $P < 0.001$), compared with that of the AP group (Fig. 6).

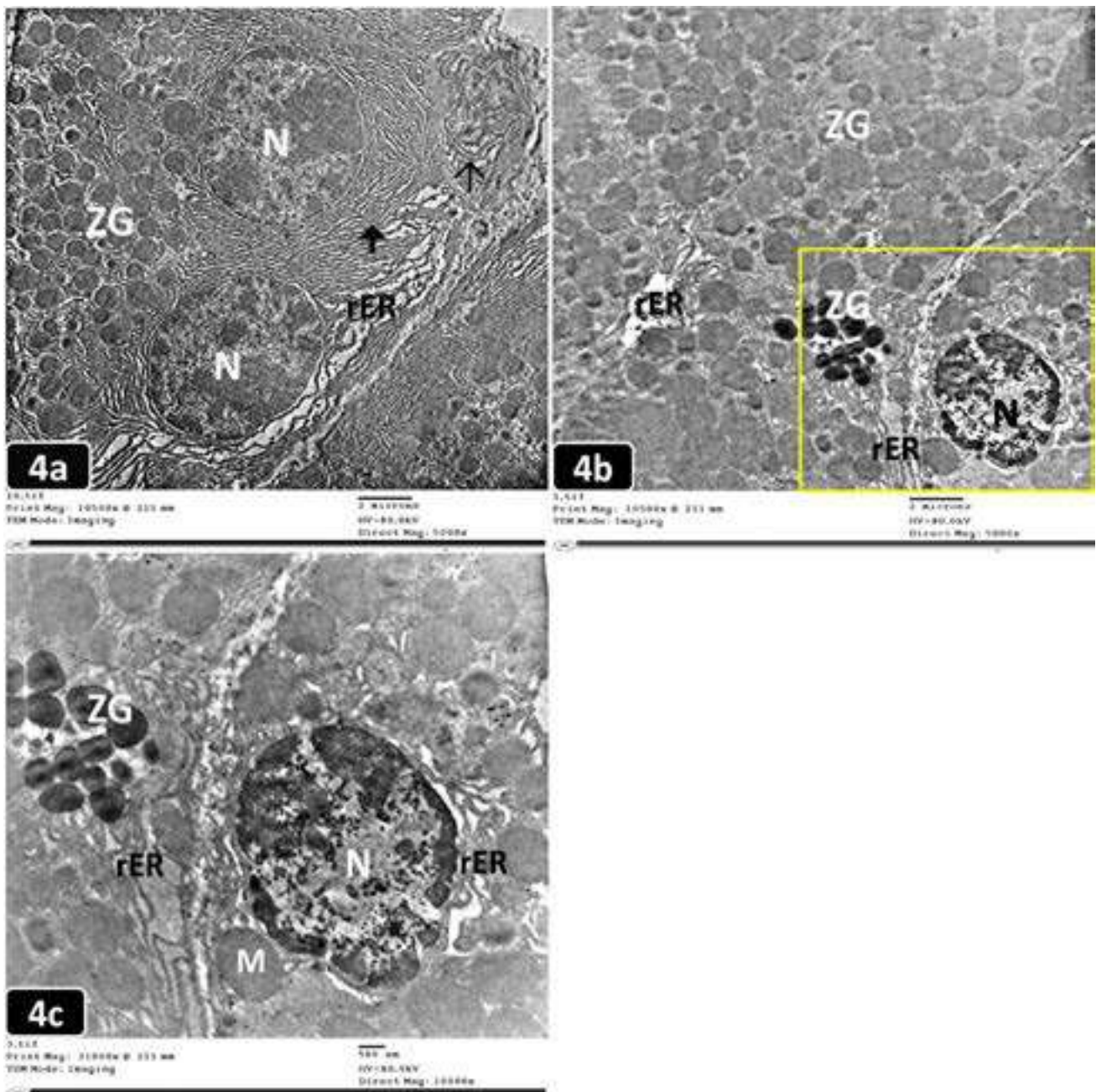


Fig. 4.- Electron micrograph of ultrathin pancreatic sections from the studied groups of rats. 4a,b (TEM; x 5,000) and 4c (TEM; x 10,000). [4a]: The prophylactic group showing acinar cells with heterochromatic nuclei (N), apparently normal mitochondria (M), and less electron-dense ZG. Some cisternae of rER are dilated and others are disarranged in whorls (↑). [4b]: The therapeutic group showing ZG of variable size and electron density, a small heterochromatic nucleus (N), and dilated fragmented cisternae of rER. [4c]: A higher magnification of the boxed area of (Fig.4b) showing an irregular heterochromatic nucleus (N), ZG of variable size & electron density, dilated cisternae of rER, and swollen mitochondria (M). Scale bars (a,b) = 2 μm; (c) = 500 nm.

DNA fragmentation results

The results of the gel electrophoresis displayed five DNA bands in lanes corresponding to their wells, which were regularly arranged from I to V, corresponding to the experimental groups of this study. The wells I (control group) and II (probiotic group) showed clear sharp normal DNA bands.

Well III (AP group) revealed a swarming of the DNA band with many fragmentations. Well IV (prophylactic group) showed a DNA band with minor fragmentation. Well V (therapeutic group) showed a comparable DNA band to that of the AP group, but with lesser fragmentation (Fig. 7).

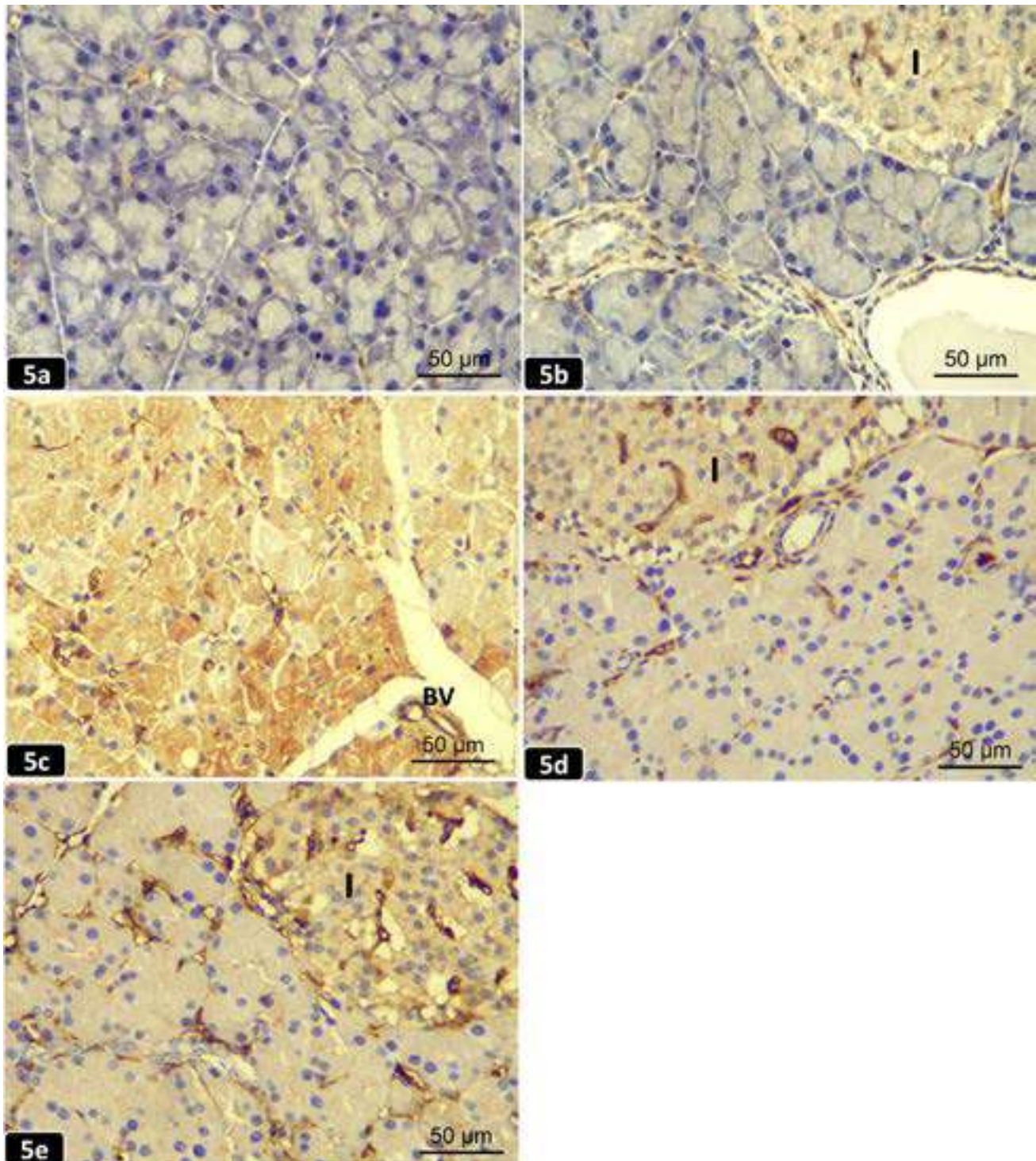


Fig. 5.- Pancreatic sections from the studied groups of rats (iNOS immunohistochemical staining; x 400). [5a]: The control group showing a negative immunostaining reaction for inducible nitric oxide synthase (iNOS) in the cytoplasm of normal acini. [5b]: The probiotic group showing a negative immunostaining reaction for iNOS in the cytoplasm of the normal acini. While a weak immunoreaction in the cytoplasm of islets of Langerhans cells (I) is noticed in the form of faint brown staining. [5c]: The AP group showing a strong positive immunostaining reaction for iNOS in the form of dark brown staining of the acinar cell cytoplasm and the wall of blood vessels (BV). [5d]: The prophylactic group showing a mild immunostaining reaction for iNOS in the cytoplasm of both acinar cells and islets of Langerhans (I). [5e]: The therapeutic group showing a moderate immunostaining reaction for iNOS in the cytoplasm of both acinar cells and islets of Langerhans (I). Scale bars (a-e) = 50 µm.

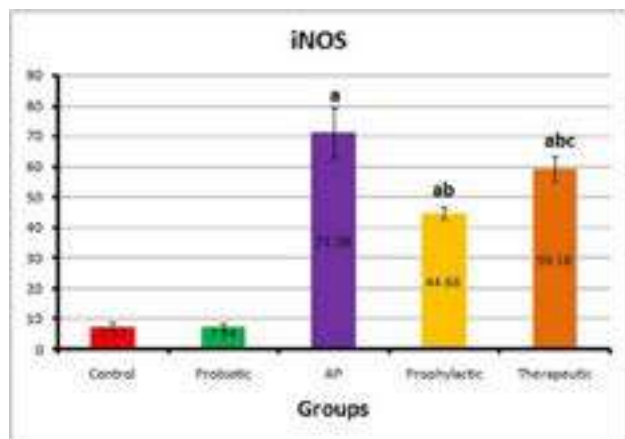


Fig. 6.- Histogram of the optical density of iNOS in different animal groups (Mean±SD). AP: Acute pancreatitis; iNOS: Inducible nitric oxide synthase. Statistical significance was set at p values≤0.05. ^aP≤0.05 vs control group. ^bP≤0.05 vs AP group. ^cP≤0.05 vs prophylactic group.

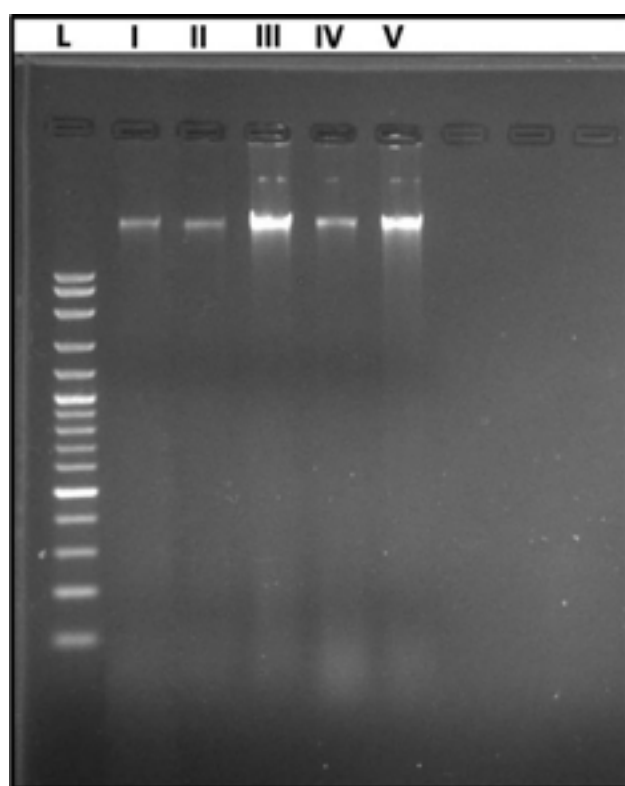


Fig. 7.- Agarose gel electrophoresis of DNA extracted from the pancreas of different animal groups. Five DNA bands in lanes I to V corresponds to the studied groups (I: Control, II: Probiotic, III: AP, IV: Prophylactic, and V: Therapeutic). The wells I and II showed clear sharp DNA bands. Well III revealed a swarming of the DNA band with many fragmentations. Well IV showed a DNA band with minor fragmentation. Well V showed a comparable DNA band to that of AP group but with lesser fragmentation. L: ladder of DNA fragments.

PW/BW ratio results

The mean value of the PW/BW ratio in the AP group was 9.51 ± 0.67 , which was statistically significantly higher ($P < 0.0001$) compared with those of the control group (6.08 ± 1.02) and the probiotic group (5.91 ± 0.85). The mean values of the PW/BW ratio in both prophylactic and therapeutic groups were 7.60 ± 0.55 and 7.95 ± 1.20

respectively, which were statistically significantly lower ($P < 0.008$ and $P < 0.04$) compared with that of the AP group (Fig. 8).

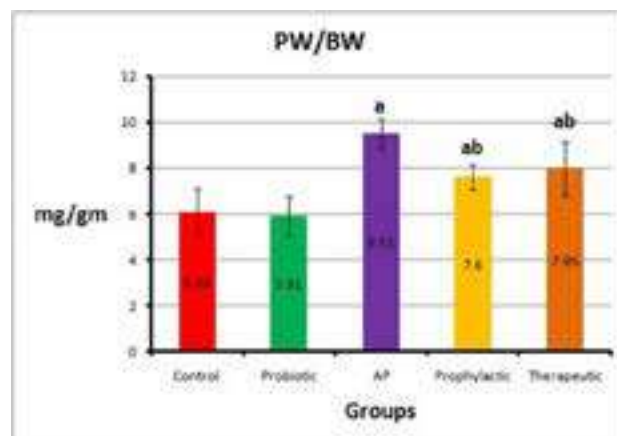


Fig. 8.- Histogram of PW/BW ratio in different animal groups (Mean±SD). AP: Acute pancreatitis; PW/BW: Pancreatic weight/body weight ratio. Statistical significance was set at p-value ≤0.05. ^aP≤0.05 vs control group. ^bP≤0.05 vs AP group. ^cP≤0.05 vs prophylactic group.

Biochemical results

The results of serum amylase, lipase, and IL-1β were depicted in the Table 1. Statistical comparison between the control and the probiotic groups revealed insignificant change ($P > 0.05$) regarding all the measured biochemical parameters. In the AP group, the mean serum amylase, lipase, and IL-1β levels were significantly higher ($P = 0.0001$) when compared with the corresponding values of the control group. In the prophylactic group, the serum level of these three biochemical parameters decreased significantly ($P = 0.0001$, $P = 0.002$, and $P = 0.004$), respectively when compared with the AP group. In the therapeutic group, the serum level of the above-mentioned three parameters showed insignificant differences ($P = 0.47$, $P = 0.74$, and $P = 0.12$), respectively when compared with the AP group. In the therapeutic group, the mean serum amylase and lipase were significantly higher ($P = 0.015$ and $P = 0.041$), while the mean serum IL1B was insignificantly changed ($P = 0.535$) when compared with the corresponding values of the prophylactic group.

The results of the pancreatic tissue level of MDA, GSH, and MPO were depicted in the Table 2. In the AP group, the mean pancreatic tissue MDA was significantly higher ($P = 0.0001$) when compared with the corresponding values of the control group. In the prophylactic and therapeutic groups, the MDA level decreased significantly ($P = 0.0001$

and $P=0.024$), respectively when compared with the AP group. The mean pancreatic tissue level of GSH in the AP group was significantly lower ($P=0.0001$) than those of the control group. In the prophylactic and therapeutic groups, GSH levels displayed insignificant change ($P=0.48$ and $P=0.78$), respectively compared with the AP group. In the AP group, the mean pancreatic tissue MPO was significantly higher ($P=0.0001$) when compared with the corresponding value of the control group. In the prophylactic group, the MPO level decreased significantly ($P=0.0001$) when compared with the AP group, while in the therapeutic group, MPO displayed insignificant change ($P=0.27$) when compared with the AP group. In the therapeutic group, the mean serum MDA and MPO were significantly higher ($P=0.032$ and $P=0.001$), while the mean serum GSH was insignificantly changed ($P=0.98$) when compared with the corresponding values of the prophylactic group.

DISCUSSION

Acute pancreatitis (AP) is a major inflammatory disease of the pancreas that, to date, has neither satisfactory settled underlying pathogenesis nor conventional successful therapy. So far it is thus usually associated with a high rate of morbidity and mortality (Esteban-Zubero et al., 2018). In this study, an experimental model of AP was produced

by I.P injection of a high dose of L-arginine: this amino acid was reported to produce selective dose-dependent necrosis of the exocrine part of the pancreas without a major morphological change in the endocrine part or other organs (Su et al. 2006 and Dawra; Saluja, 2012).

This model was chosen because it is an easy, highly reproducible, and a non-invasive model. Besides, it produces histological and biochemical alterations in the acinar cells resembling those of acute necrotizing pancreatitis in humans (Su et al. 2006). In a trial to ameliorate such histochemical changes during AP, *L.acidophilus* species of the probiotics were tried in this study. The results of the present study revealed a marked distortion of the histological architecture of the pancreatic acini of the AP group and focal areas of acinar cell necrosis associated with interstitial edema, microscopic foci of hemorrhage, and inflammatory cellular infiltration. These findings were in line with Melo et al. (2010); Chen et al. (2012), and Wang et al. (2017b), who reported that a large dose of L-arginine in different experimental animals resulted in pancreatic histopathological changes nearly similar to those observed in this study.

The mechanism by which L-arginine produced the above-mentioned pancreatic histological alterations has been attributed partly to the excessive production of nitric oxide (NO) in the

Table 1. Serum amylase, lipase and IL-1 β in different animal groups (Mean \pm SD). Number of rats in each group (n=6). Statistical analysis was carried out by One-way ANOVA followed by Tukey's intergroup multiple comparison test. Statistical significance was set at p value \leq 0.05. AP: Acute pancreatitis; IL1 β : interleukin-1 beta. a significant P value vs control group. b significant P value vs AP group. c significant P value vs prophylactic group.

Groups	Control	Probiotic	AP	Prophylactic	Therapeutic
Amylase (U/L)	593.96 \pm 62.82	584.08 \pm 60.36	1437.16 \pm 94.39a	1221.70 \pm 86.36ab	1367.16 \pm 48.98ac
Lipase (U/L)	31.80 \pm 7.40	28.75 \pm 5.20	91.36 \pm 6.47a	74.00 \pm 8.40ab	86.40 \pm 7.54ac
IL-1 β (Pg/ml)	11.05 \pm 2.08	10.30 \pm 1.52	41.43 \pm 6.30a	30.90 \pm 4.79ab	34.96 \pm 5.68a

Table 2. Pancreatic tissue level of MDA, GSH and MPO in different animal groups (Mean \pm SD). Number of rats in each group (n=6). Statistical analysis was carried out by One-way ANOVA followed by Tukey's intergroup multiple comparison test. Statistical significance was set at p value \leq 0.05. AP: Acute pancreatitis; MDA: Malondialdehyde; GSH: Reduced glutathione; MPO: Myeloperoxidase. a significant P value vs control group. b significant P value vs AP group. c significant P value vs prophylactic group.

Groups	Control	Probiotic	AP	Prophylactic	Therapeutic
MDA (nmol/ gm)	27.16 \pm 5.33	24.73 \pm 4.88	114.51 \pm 9.19a	86.30 \pm 8.60ab	100.13 \pm 8.94abc
GSH (μ mol/ gm)	2.66 \pm 0.57	2.90 \pm 0.44	0.69 \pm 0.05a	1.00 \pm 0.05a	0.91 \pm 0.07a
MPO (U/gm)	31.38 \pm 4.199	29.91 \pm 4.53	98.20 \pm 11.39a	71.31 \pm 7.27ab	89.88 \pm 5.30ac

pancreatic tissue. NO is a potential free radical, and is one of the most important inflammatory mediators generated from L-arginine in a reaction catalyzed by a family of three NO synthase (NOS) isoforms, including neuronal NOS (nNOS), endothelial NOS (eNOS), and inducible NOS (iNOS) (Takacs et al., 2002). On the contrary to nNOS and eNOS, which are a normal cellular constituent and form a small amount of NO, iNOS is not a cellular constituent, but it is cytokine-inducible and forms a large amount of NO in a sustained and uncontrolled manner in cases of inflammatory condition of a wide variety of tissues, particularly the pancreas (Tanjoh et al., 2007; Förstermann and Sessa, 2011).

The sustained overproduction of NO imparts a direct toxic effect on the pancreatic acinar cells, and mediates diverse inflammatory responses like interstitial edema, and inflammatory cellular infiltration (Tanjoh et al., 2007). Additionally, much evidence implicated that excessive NO reacts with superoxide anion radicals ($O_2^{\cdot-}$), resulting in the formation of peroxynitrite anions ($ONOO^-$), which are highly reactive nitrogen species (RNS) and represent powerful oxidants and cytotoxic agents that have been incriminated indirectly in the pathogenesis of acinar cell injury (Bhatia et al., 2005; Dawra and Saluja, 2012). In the present study, the increased iNOS activity in the pancreatic tissue of the AP group was evident, where there were strong positive immunohistochemical staining reactions and an increase in the mean morphometric optical density of antibody-iNOS reaction inside the cytoplasm of the acinar cells and the wall of microvasculature, compared with the negative reaction seen in the control group. However, the latter group showed a weak staining reaction in the cytoplasm of the islet cells.

These results were explained by Qader et al. (2003), who reported that iNOS is not a normal constituent in the exocrine compartment of the pancreas, but it is weakly expressed in the islets of Langerhans. Apparently in this study, there was a decrease of iNOS expression upon probiotic supplementation, particularly in the prophylactic group of rats that might mitigate NO production. This finding could explain how the pancreatic histopathological changes were indirectly

ameliorated by these natural non-pathogenic microorganisms. The iNOS was reported to be highly induced by tissue inflammatory cytokines and endotoxins (Al-Mufti et al., 1998). Therefore, the downregulation of iNOS elicited by the currently used *L. acidophilus* could be due to their anti-inflammatory effects (Kechagia et al., 2013) and their ability to inhibit bacterial endotoxins (Markowiak and Śliżewska, 2017). Determinately, not only NO and RNS, but also reactive oxygen species (ROS) produced from the injured acinar cells are reported to be strongly implicated in the pathogenesis of L-arginine-induced AP. It was cited that these ROS, in a positive feedback manner, cause more acinar cell injury via oxidative denaturation of the proteins of acinar cell membranes, leading to loss of their structural integrity, with subsequent extracellular leakage of pancreatic protease enzymes that ultimately lead to necrosis of the gland (Esrefoglu, 2012). Also, ROS cause denaturation of cytoplasmic proteins, cellular organelles, and the cytoskeleton yielding more necrosis (Urunuela et al., 2002).

Correspondingly, in this study, upon examining LM and TEM pancreatic sections in the AP group, a full-blown picture of acinar cell necrosis was observed in the form of loss of acinar cell boundaries, vacuolated rarified cytoplasm, and even acinar cell loss giving the tissue a moth-eaten appearance. Also, pyknotic, karyolytic, and karyorrhectic nuclei were encountered. The later changes in the nuclei were reported to be mostly due to ROS-induced strand breaks, abnormal cross-linking, and fragmentation of DNA (Meher et al., 2015). Furthermore, ROS lead to peroxidation of polyunsaturated fatty acids of the acinar cell membranes, resulting in the formation of toxic byproducts metabolites such as MDA (Özkan et al., 2012). In that regard, in the present study, pancreatic MDA was measured, and its level was significantly high in the AP group. Likewise, Mirmalek et al. (2016) have found that the MDA level increased significantly in rats with L-arginine-induced AP. On the other hand, in this study, *L. acidophilus* supplementation prior to induction of AP resulted in a stronger reduction of MDA than with the post induction regimen of the therapeutic group. This result might emphasize

the antioxidant effect of probiotics (Spyropoulos et al., 2011).

In this study, redox imbalance was evident in the AP group, where not only the pancreatic MDA was increased, but also GSH, the main intracellular non-enzymatic antioxidant, was significantly decreased compared to the control group. In support of our findings, Pérez et al. (2015) have documented an early depletion of GSH in pancreatic tissue in AP. This depletion is presumably due to overconsumption of GSH in catalyzing premature activation of pancreatic proenzymes into active enzymes (Lüthen et al., 1998). Nevertheless, in this study, there was a mild increase in GSH that did not reach a significant level in the prophylactic and therapeutic groups compared with the AP group. This implied mostly that the chosen dose of *L. acidophilus* had a moderate capability in reducing oxidative stress (Lutgendorff et al., 2008).

In this study, one of the main histological findings in the AP group was the perivascular inflammatory cellular infiltration in the pancreatic tissue. Pathologically, in acute inflammation, the leucocytes, in particular the neutrophils, are known to be recruited and activated within hours to the inflammatory sites by the chemotactic effect of the cytokines, released from both injured pancreatic tissue and the resident pancreatic macrophages (Bhatia et al., 2005; Cosen-Binker and Gaisano, 2007). Once activated, the neutrophils start their strong phagocytic activity and degranulate their granules, particularly the primary (azurophilic) granules that contain an ample amount of myeloperoxidase (MPO) enzyme (Selders et al., 2017).

Therefore, biochemical assessment of the tissue activity of MPO is used as an indirect biomarker of the neutrophil infiltration and as an index of acute inflammation of different tissues (Biradar and Veeresh, 2013). Correspondingly, in this study, neutrophils' trafficking to the inflamed pancreatic tissues in the AP group was confirmed biochemically by the elevated pancreatic tissue level of MPO. Obviously in the present study, upon histological examination of the pancreatic tissue of the AP group, the pancreatic acini were separated by wide inter-acinar and interlobular

spaces and inflammatory exudate. Widening of these spaces was secondary to the encountered necrosis of the pancreatic acini (Melo et al, 2010; Chen et al., 2012). Whilst, the exudate may reflect the presence of interstitial pancreatic edema (Wang et al. 2017b). The later histological finding was broadly supported by what was obtained in this work on measuring the PW/BW ratio, which represents a rough index in evaluating the degree of pancreatic edema. The cause of such edema is the increase of microvascular permeability, which is caused presumably by the potent vasodilator effect of NO and by the proinflammatory cytokines released from the injured pancreatic acini (Takacs et al., 2002). Also, in this study, microscopic foci of interstitial hemorrhage were observed in the histological sections of the AP group. The cause of such hemorrhage is the proinflammatory cytokines that cause vascular endothelial injury with extravasation of blood in the interstitium (Wang et al., 2017b).

Keeping in view the above-mentioned deleterious roles of the cytokines in the pathogenesis of the AP, consequently in the present study, the serum level of the proinflammatory cytokine IL-1 β was measured and its level was significantly higher in the AP group compared with the control one. This was consistent with Özkan et al. (2012) and Mirmalek et al. (2016), who found that serum IL-1 β level increased in different rat models of AP. On the other side, IL-1 β decreased significantly more in the prophylactic than in the therapeutic group, denoting a more beneficial anti-inflammatory effect of *L. acidophilus* pretreatment.

In light of the pathophysiology of AP, emerging evidence has shown that many cytokines rather than IL-1 β such as tumor necrosis factor alpha (TNF- α) and IL-6 are produced during AP from the injured acini, macrophages, and recruited leucocytes (Cosen-Binker and Gaisano, 2007). Uncontrolled release of these cytokines induces premature activation of the pancreatic proenzymes (zymogens) (Tsang et al., 2016). Also, ROS causes denaturation of the membrane proteins of lysosomes and ZG yielding, their co-localization forming cytoplasmic vacuoles in which the lysosomal hydrolase enzymes such as cathepsin-B causes premature activation of the

pancreatic zymogens (Waterford et al., 2005). Moreover, ROS causes thiol oxidation of cysteine residues of ryanodine receptors (RyR) and inositol trisphosphate receptors (IP3R) of calcium (Ca²⁺) channels on the smooth endoplasmic reticulum (sER), resulting in hastening the activity of these channels with subsequent active efflux of Ca²⁺ into the cytosol. This rise of the intracellular Ca²⁺ induces premature activation of pancreatic zymogens (Husain et al., 2005). In this premature activation process, trypsinogen, in particular, is activated into trypsin, which is the most potent pancreatic proteases in the initiation of the AP. Once activated, trypsin is capable of converting other zymogen forms of pancreatic enzymes to their active forms (Tsang et al., 2016).

For instance, activation of chymotrypsin, carboxypeptidase, and aminopeptidases cause denaturation of cytoplasmic proteins; activation of phospholipases disrupts the membrane phospholipids; activation of endonucleases causes DNA chromatin damage, and activation of elastase disrupts the elastic fibers in the wall of BVs, causing interstitial hemorrhage (Kumar et al., 2018). These inappropriately activated pancreatic enzymes elicit autodigestion (autolysis) of the gland (Bhatia et al., 2005 and Wang et al. 2017b). This autodigestion process is an overwhelming necrotic process, particularly of the exocrine pancreas, in which the cytoplasm showed diffuse eosinophilia, which is attributable partly to increased binding of eosin stain to the denatured cytoplasmic proteins, and partly to the loss of basal basophilia secondary to denatured ribonucleoproteins in rER.

On the contrary, in normal acinar cells, eosinophilia is restricted only to the apical part due to abundant ZG (Kumar et al., 2018). Interestingly, premature activation of pancreatic enzymes with subsequent autodigestion of the gland represents hallmarks in the pathogenesis of experimental AP (Pan et al., 2017). In the present study, in addition to the above-mentioned histological findings, the development of AP was confirmed biochemically by a significant increase in the serum amylase and lipase enzyme levels that decreased with *L. acidophilus* administration. In agreement with these results, Melo et al. (2010) and Chen et al.

(2012) have found that the serum amylase and lipase increased significantly in animal models of AP. The cause beyond such rise of these two enzymes could be attributed to the proteolysis of ZG and cytoskeleton proteins of the acinar cells, with the subsequent escape of these enzymes locally into the pancreatic interstitium, and thereafter into the bloodstream (Urunuela et al., 2002 and Tsang et al., 2016).

Notably in this study, the prophylactic regimen of *L. acidophilus* yielding a more beneficial effect over the therapeutic one in ameliorating most of the histological and biochemical results encountered with AP. This beneficial protective role of *L. acidophilus* could be due to its ability in preventing secondary bacterial infection of the necrotic pancreatic tissue which is a pathological hallmark during AP (Pan et al., 2017). This secondary bacterial infection is presumably due to bacterial translocation which is a process in which intestinal microbiota crosses a dysfunctional intestinal mucosal barrier and reaches the necrotic tissue of the pancreas via systemic circulation (Guarner and Malagelada, 2003) and via mesenteric lymphatics (Mittal et al., 2009).

The prevention of secondary bacterial infection was reflected upon MPO that significantly decreased in the pancreatic tissue of the prophylactic group in comparison with that of the AP group in this study. It was reported that pre-treatment with probiotics reduced bacterial translocation through releasing many antimicrobial substances like defensins and bacteriocins (Penner et al., 2005) and exerting a potent immune-modulatory effect (Pan et al., 2017). Also, they strengthen the intestinal mucosal barrier by increasing mucosal IgA, enhance tight junction protein expression, prevent epithelial cell apoptosis, and release cytoprotective molecules such as heat shock protein (Madsen 2012). This prophylactic dogma of probiotics in maintaining gut integrity was documented in the literature, in particular with *L. acidophilus* species (Wang et al., 2017a). In vitro, these species were found to increase mucin secretion from human intestinal epithelial cells, which block pathogenic *E. coli* adherence and invasion (Mack

et al., 2003). In addition, *L. acidophilus* produces lactic, acetic, and propionic acids, which lower the intestinal pH, thus suppressing the growth of various pathogenic bacteria and keep the balance of the gut flora (Doron and Gorbach, 2006). Based upon their above-mentioned roles, probiotics have been used in the management of infectious and antibiotic-associated diarrhea, *Clostridium difficile* infections, lactose intolerance, inflammatory bowel diseases, and necrotizing enterocolitis (Knight and Girling, 2003).

Conclusion

The findings of this study have shown that the prophylactic regimen of *L. acidophilus* has a supreme beneficial effect over the therapeutic one in ameliorating some histopathological changes of the pancreatic tissue, and in attenuating the markers of oxidative stress and inflammation in an experimental model of the AP. This crucial prophylactic effect is presumably due to the antioxidant, anti-inflammatory, and immunomodulatory effects of *L. acidophilus* in addition to their role in preventing secondary bacterial infection of the injured pancreatic tissue. These findings provided a basis for future clinical studies that may constitute a novel strategy in the prophylaxis against the AP in humans.

ACKNOWLEDGEMENTS

The authors are grateful to the team of Zagazig Scientific and Medical Research Center (ZSMRC) for helping the authors in accomplishing the experiments.

Author contributions: All authors contributed to the study conception and design. Material preparation, data collection, and analysis were performed by [Dalia A. Mandour]. The first draft of the manuscript was written by [Asmaa M. Tolba] and all authors commented on previous versions of the manuscript. All authors read and approved the final manuscript.

REFERENCES

Al-MUFTI RA, WILLIAMSON RCN, MATHIE RT (1998) Increased nitric oxide activity in a rat model of acute pancreatitis. *Gut*, 43 (4): 564-570.

BANCROFT JD, LAYTON C (2013) The hematoxylin and eosin. In: Suvarna SK, Layton C, Bancroft JD (eds). *Theory Practice of histological techniques*, 7th ed. Churchill Livingstone, Elsevier, Philadelphia, USA, pp 179-220.

BEUTLER E, DURON O, KELLEY BM (1963) Improved method for the determination of blood glutathione. *J Lab Clin Med*, 6: 882-888.

BHATIA M, WONG FL, CAO Y, LAU HY, HUANG J, PUNEET P, CHEVALI L (2005) Pathophysiology of acute pancreatitis. *Pancreatology*, 5(2-3): 132-144.

BIRADAR S, VEERESH B (2013) Protective effect of lawson on L-Arginine induced acute pancreatitis in rats. *Indian J Exp Biol*, 51(3): 256-261.

BOZZOLA J, RUSSEL L (1999) *Electron microscopy: Principles and techniques for biologists*. 2nd ed. Sudbury MA, Jones and Bartlett Publishers, Toronto, Canada, pp 17-48.

BRADLEY PP, PRIEBAT DA, CHRISTENSEN RD, ROTHSTEIN G (1982) Measurement of cutaneous inflammation: Estimation of neutrophil content with an enzyme marker. *J Invest Dermatol*, 78: 206-209.

CESKA M, BIRATH K, BROWN B (1969) A new and rapid method for the clinical determination of alpha-amylase activities in human serum and urine. Optimal conditions. *Clin Chim Acta*, 26: 437-744.

CHEN J, CAI QP, SHEN PJ, YAN RL, WANG CM, YANG DJ, FU H-B, CHEN X-Y (2012) Netrin-1 protects against L-Arginine-induced acute pancreatitis in mice. *PLoS One*, 7(9): e46201.

COSEN-BINKER LI, GAISANO HY (2007) Recent insights into the cellular mechanisms of acute pancreatitis. *Can J Gastroenterol*, 21(1): 19-24.

DAWRA R, SALUJA AK (2012) L-arginine-induced experimental acute pancreatitis. *Pancreapedia Exocrine Pancreas Knowledge Base*, 1: 1-6.

DORON S, GORBACH SL (2006) Probiotics: Their role in the treatment and prevention of disease. *Expert Rev Anti Infect Ther*, 4(2): 261-275.

ESREFOGLU M (2012) Experimental and clinical evidence of antioxidant therapy in acute

pancreatitis. *World J Gastroenterol*, 18(39): 5533-5541.

ESTEBAN-ZUBERO E, CABRERA-FALCÓN E, RIBAGORDA-TEJEDOR S, ALATORRE-JIMÉNEZ MA, LÓPEZ-GARCÍA CA, MARÍN-MEDINA A, VILLEDA-GONZÁLEZ R, ALONSO BARRAGÁN SA, GÓMEZ-RAMOS JJ (2018) Current trends in management of acute pancreatitis. *Ann Gastroenterol Dig Syst*, 2(1006): 1-7.

FORSTERMANN U, SESSA WC (2011) Nitric oxide synthases: regulation and function. *Eur Heart J*, 33(7): 829-837.

GOODCHILD G, CHOUHAN M, JOHNSON GJ (2019) Practical guide to the management of acute pancreatitis. *Frontline Gastroenterol*, 10(3): 292-299.

GUARNER F, MALAGELADA JR (2003) Gut flora in health and disease. *Lancet*, 361(9356): 512-519.

HUSAIN SZ, PRASAD P, GRANT WM, KOLODECİK TR, NATHANSON MH, GORELICK FS (2005) The ryanodine receptor mediates early zymogen activation in pancreatitis. *Proc Natl Acad Sci USA*, 102(40): 14386-14391.

KECHAGIA M, BASOULIS D, KONSTANTOPOULOU S, DIMITRIADI D, GYFTOPOULOU K, SKARMOUTSOU N, FAKIRI EM (2013) Health benefits of probiotics: A review. *ISRN Nutr*, 2013: 481651.

KNIGHT DJW, GIRLING KJ (2003) Gut flora in health and disease. *Lancet*, 361(9371): 1831.

KRATZ RF, SIEGFRIED DR (2010) Using gel electrophoresis to separate molecules. In: *Biology for dummies*. 2nd ed. Hoboken, NJ: John Wiley and Sons, USA, pp 132-133.

KRISHNA SG, KAMBOJ AK, HART PA, HINTON A, CONWELL DL (2017) The changing epidemiology of acute pancreatitis hospitalizations: a decade of trends and the impact of chronic pancreatitis. *Pancreas*, 46(4): 482-488.

KUMAR V, ABBAS AK, ASTER JC (2018) Robbins Basic Pathology. 10th ed. Elsevier Philadelphia, Pennsylvania, USA, pp 680-689.

LUTGENDORFF F, TRULSSON LM, VAN MINNEN LP, RIJKERS GT, TIMMERMAN HM, FRANZEN LE, GOOSZEN HG, AKKERMANS LMA, SÖDERHOLM

JD, SANDSTRÖM PA (2008) Probiotics enhance pancreatic glutathione biosynthesis and reduce oxidative stress in experimental acute pancreatitis. *Am J Physiol Gastrointest Liver Physiol*, 295(5): G1111-G1121.

LUTHEN R, GRENDALL JH, NIEDERAUC, HAUSSINGER D (1998) Trypsinogen activation and glutathione content are linked to pancreatic injury in models of biliary acute pancreatitis. *Int J Pancreatol*, 24(3): 193-202.

MACK DR, AHRNE S, HYDE L, WEI S, HOLLINGSWORTH MA (2003) Extracellular MUC3 mucin secretion follows adherence of Lactobacillus strains to intestinal epithelial cells in vitro. *Gut*, 52(6): 827-833.

MADSEN KL (2012) Enhancement of epithelial barrier function by probiotics. *J Epith Biol Pharmacol*, 5(1): 55-59.

MARKOWIAK P, ŚLIZEWSKA K (2017) Effects of probiotics, prebiotics, and synbiotics on human health. *Nutrients*, 9(9): 1021-1050.

MEHER S, RATH S, SHARMA R, ROUT B, MISHRA TS, SASMALPK, SINHAMK (2015) Pathophysiology of oxidative stress and antioxidant therapy in acute pancreatitis. *J Mol Biomark Diagn*, 6(6): 1-7.

MELO CM, CARVALHO KMMB, DE SOUSA NEVES JC, MORAIS TC, RAO VS, SANTOS FA, DE-CASTRO BRITO GA, CHAVES M-H (2010) α , β -amyrin, a natural triterpenoid ameliorates L-arginine-induced acute pancreatitis in rats. *World J Gastroenterol*, 16(34): 4272-4280.

MIRMALEK SA, GHOLAMREZAEI BA, YAVARI H, KARDEH B, PARS A, SALIMI-TABATABAEE SA, JANGHOLI E (2016) Antioxidant and anti-inflammatory effects of coenzyme Q10 on L-arginine-induced acute pancreatitis in rat. *Oxi Med Cell Long*, 2016: 5818479.

MITTAL A, PHILLIPS AR, MIDDLEDITCH M, RUGGIERO K, LOVEDAY B, DELAHUNT B, COOPER GJS, WINDSOR JA (2009) The proteome of mesenteric lymph during acute pancreatitis and implications for treatment. *JOP*, 10(2): 130-142.

MOODY MD, ARSDELL SV, MURPHY KP, ORENCOLE SF, BURNS C (2001) Array-based ELISAs for high-throughput analysis of human cytokines. *Biotech*, 31: 186-194.

- MUDDANA V, WHITCOMB DC, PAPACHRISTOU G (2009) Current management and novel insights in acute pancreatitis. *Expert Rev Gastroenterol Hepatol*, 3(4): 435-444.
- MUFTUOGLU MAT, ISIKGOR S, TOSUN S, SAGLAM A (2006) Effects of probiotics on the severity of experimental acute pancreatitis. *Eur J Clin Nutr*, 60(4): 464-468.
- OHKAWA H, OHISHI W, YAGAI K (1979) Assay for lipid peroxides in animal tissues by thiobarbituric acid reaction. *Biochem*, 95: 351-358.
- ÖZKAN E, AKYUZK C, DULUNDU E, TOPALOGLU Ü, ŞEHIRLI AÖ, ERCAN F, SENER G (2012) Protective effects of lycopene on cerulein-induced experimental acute pancreatitis in rats. *J Surg Res*, 176(1): 232-238.
- PACHECO RC, NISHIOKA SA, DE OLIVEIRA LC (2003) Validity of serum amylase and lipase in the differential diagnosis between acute/acute-chronic pancreatitis and other causes of acute abdominal pain. *Arq Gastroenterol*, 40(4): 233-238.
- PAN LL, LI J, SHAMOON M, BHATIA M, SUN J (2017) Recent advances on nutrition in treatment of acute pancreatitis. *Front Immunol*, 8: 1-10.
- PENNER R, FEDORAK RN, MADSEN KL (2005) Probiotics and nutraceuticals: non-medicinal treatments of gastrointestinal diseases. *Curr Opin Pharmacol*, 5(6): 596-603.
- PEREZ S, PEREDA J, SABATER L, SASTERJ (2015) Redox signaling in acute pancreatitis. *Redox Biol*, 5: 1-14.
- PETRIE A, SABIN C (2005) In: Sugden M, Moore K (eds). *Medical statistics at a glance*, 2nd ed. Blackwell Publishing Ltd. USA, pp 55-56.
- PEZZILLI R, FANTINI L (2006). Probiotics and severe acute pancreatitis. *J Pancreas (JOP)*, 7(1): 92-93.
- QADER SS, EKELUND M, ANDERSSON R, OBERMULLER S, SALEHI A (2003) Acute pancreatitis, expression of inducible nitric oxide synthase and defective insulin secretion. *Cell Tissue Res*, 313(3): 271-279.
- RAMOS-VARAJA, KIUPEL M, BASZLERT, BLIVEN L, BRODERSEN B, CHELACK B, CZUB S, DEL PIERO F, DIAL S, EHRHART EJ, GRAHAM T, MANNING L, PAULSEN D, VALLI VE, WEST K (2008) Suggested guidelines for immunohistochemical techniques in veterinary diagnostic laboratories. *J Vet Diagn Invest*, 20: 393-413.
- SELDERS GS, FETZ AE, RADIC MZ, BOWLIN GL (2017) An overview of the role of neutrophils in innate immunity, inflammation and host-biomaterial integration. *Regen Biomater*, 4(1): 55-68.
- SHAH AP, MOURAD MM, BRAMHALL SR (2018) Acute pancreatitis: current perspectives on diagnosis and management. *J Inflamm Res*, 11: 77-85.
- SPYROPOULOS BG, MISIAKOS EP, FOTIADIS C, STOIDIS CN (2011) Antioxidant properties of probiotics and their protective effects in the pathogenesis of radiation-induced enteritis and colitis. *Dig Dis Sci*, 56(2): 285-294.
- SU KH, CUTHBERTSON C, CHRISTOPHI C (2006) Review of experimental animal models of acute pancreatitis. *HPB*, 8(4): 264-286.
- TAKACS T, CZAKO L, MORSCHL E, LASZLO F, TISZLAVICZ L, RAKONCZAY ZJR, LONOVICS J (2002) The role of nitric oxide in edema formation in L-arginine-induced acute pancreatitis. *Pancreas*, 25 (3): 277-282.
- TANJOH K, TOMITA R, IZUMI T, KINOSHITA K, KAWAHARA Y, MORIYA T, UTAGAWA A (2007) The expression of the inducible nitric oxide synthase messenger RNA on monocytes in severe acute pancreatitis. *Hepatogastroenterology*, 54(75): 927-931.
- TSANG SW, GUAN YF, WANG J, BIAN ZX, ZHANG HJ (2016) Inhibition of pancreatic oxidative damage by stilbene derivative dihydro-resveratrol: implication for treatment of acute pancreatitis. *Sci Rep*, 6: 22859-22873.
- URUNUELA A, SEVILLANO S, De LA MANOAM, MANSO MA, ORFAO A, de DIOS I (2002) Time-course of oxygen free radical production in acinar cells during acute pancreatitis induced by pancreatic duct obstruction. *Biochim Biophys Acta*, 1588(2): 159-164.
- VINKLEROVA I, PROCHAZKA M, PROCHAZKA V, URBANEK K (2010) Incidence, severity, and etiology of drug-induced acute pancreatitis. *Dig Dis Sci*, 55(10): 2977-2981.

WANG Y, WU Y, WANG Y, XU H, MEI X, YU D, WANG Y, LI W (2017a) Antioxidant properties of probiotic bacteria. *Nutrients*, 9(5): 521-535.

WANG N, ZHANG F, YANG L, ZOU J, WANG H, LIU K, WANG K (2017b) Resveratrol protects against L-arginine-induced acute necrotizing pancreatitis in mice by enhancing SIRT1-mediated deacetylation of p53 and heat shock factor1. *Int J Mol Med*, 40(2): 427-437.

WATERFORD SD, KOLODECİK TR, THROWER EC, GORELICK FS (2005) Vacuolar ATPase regulates zymogen activation in pancreatic acini. *J Biol Chem*, 280(7): 5430-5434.

WHITAKER JF (1973) A rapid and specific method for the determination of pancreatic lipase in serum and urine. *Clin Chim Acta*, 44: 133-138.

ZIELINSKA D, KOŁOZYN-KRAJEWSKA D (2018) Food-origin lactic acid bacteria may exhibit probiotic properties. *Biomed Res Int*, 2018: 5063185.

Ponticulus Posticus prevalence in Uruguayan population: dry bone and cervical CT imaging

Fernando Martínez¹, Juan Del Castillo^{2,3}, Santiago Hermosilla⁴, Juan Kenny⁴, Nicolás Sgarbi⁵, Juan Emmerich⁶

¹ Departamento de Anatomía, Facultad de Medicina UCLAEH. Clínica de Neurocirugía, Universidad de la República, Uruguay

² Departamento de Anatomía, Universidad de la República, Uruguay

³ Clínica de Traumatología y Ortopedia, Universidad de la República, Uruguay

⁴ Departamento de Anatomía, Universidad de la República, Uruguay

⁵ Centro de Alta tecnología, Mutualista Círculo Católico

⁶ Neurocirugía, Hospital de Niños de La Plata, Argentina

SUMMARY

To investigate the prevalence of ponticulus posticus (PP) in Uruguay, as well as its anatomoclinic characteristics, we used dry bone pieces and CT scans of the first cervical vertebrae. Seventy-seven dry bone pieces from Facultad de Medicina de la Universidad de la República (Montevideo, Uruguay) and UCLAEH (Maldonado, Uruguay) were analyzed macroscopically. Posteriorly, 55 CT scans of the cervico-occipital junction were analyzed with 3D reconstruction.

Out of the 77 analyzed atlases, 30 presented PP (38.9%), 12 were bilateral cases and 18 were unilateral. Out of the 42 bony bridges, 20 were situated on the right (47.6%) and the other 22 (52.4%) on the left, 14 were complete (33.3%) and 28 were incomplete (66.7%). The analyzed CT corresponded to 25 men and 30 women, with a mean age of 49 years. Nineteen pieces presented PP (34.5%), 11 were bilateral cases and 8 were unilateral. This totalize 30 bridges, 12 (40.0%) were situated on the right and the other 18 (60.0%) on the left, 15 (50.0%) were complete PP and 15 (50.0%) were incomplete. In the CT

analysis, the male gender showed statistical association with PP presence ($p=0.013$). PP is an anatomical variation with high prevalence in our population, usually overlooked if systematic search is not performed. Its great surgical and clinical implications make it of great interest to know its presence and characteristics.

Key words: Atlas – C1 vertebrae – Arcuate foramen – Ponticulus posticus – Kimmerle anomaly

INTRODUCTION

Ponticulus posticus (PP) is an anatomical variation from the first cervical vertebra (Atlas) in which a bony bridge joins the lateral mass to the posterior arch: it has been an object of study and included in photographic atlas (Mann et al., 2016). This definition corresponds to the complete ponticulus posticus, being more frequent to find an incomplete bridge.

Its prevalence varies between the populations under study or according to the study method that is employed, having an incidence range from 1%

Corresponding author:

Santiago Hermosilla. Departamento de Anatomía, Universidad de la República, 8 de Octubre 3061, Montevideo, 11600 Uruguay. E-mail: santiagoherac123@gmail.com

Submitted: July 15, 2020. Accepted: November 3, 2020

to 46%, according to different authors (Bayrakdar et al., 2018; Donald et al., 2017; Giri et al., 2017; Lo Giudice et al., 2018).

The authors present a study about the presence of the ponticulus posticus in dry bone pieces and imaging studies.

MATERIALS AND METHODS

A total of 77 dry bone pieces from Facultad de Medicina, Universidad de la República (Montevideo, Uruguay) and UCLAEH (Maldonado, Uruguay) were examined. In these, the presence of the PP was searched macroscopically registering whether it was present or not. If present, its corresponding side of appearance, and whether it was complete or incomplete. Other variations of the atlas were also registered. To reduce the inter observer bias, the 77 dry bone pieces were evaluated by the same examiner.

Simultaneously, 55 computed tomography (CT) multi detector of normal cervical spine were collected randomly, including the totality of the cervico-occipital junction. The obtained images were reprocessed with the Volume Rendering (VR) protocol for the study of the 3D images in different approaches, and were reviewed by a radiology physician with expertise. The age and gender of the patients were registered. In these CT images, presence of PP, side, and complete/incomplete status were also assessed.

In the identification of the PP, we adopted the classification applied by Lo Giudice, which defines complete PP when a full osseous ring was formed above the posterior arch, and incomplete PP when the extension of the bridge was larger than half the distance between the posterior arch and the articular process of the atlas (Lo Giudice et al., 2018). This author only applied this to imaging studies, while we applied this to the 55 imaging studies and the macroscopic analysis of the 77 pieces.

Data were registered in Microsoft Office Excel, and Chi-square test and Z-test for proportion comparisons were used to identify associations and differences between variables. A p-value under 0.05 was considered statistically significant.

RESULTS

Out of the 77 analyzed dry bone pieces, 30 presented bony bridges (38.9% of the pieces). The corresponding data is shown in Table 1 and few examples appear in Fig. 1.

Table 1. Population and PP characterization in dry bone pieces and TC 3D reconstruction.

	Dry bone	TC 3D reconstruction	p value
n	77	55	-
PP presence	30 (38.9%)	19 (34.5%)	0.518
Male/Female (PP presence)	-	25 (13)/30 (6)	-
Unilateral/Bilateral	18/12	8/11	0.223
Number of bridges	42	30	1.000
Complete/Incomplete (bridges)	14/28	15/15	0.156
Right/Left (bridges)	20/22	12/18	0.522

Twelve atlases presented bilateral bony bridges (15.6% of the total, 40.0% of the vertebrae with bridges) while 18 presented unilateral bridges (23.4% of the total, 60.0% of the vertebrae with bridges).

Because of this, a total of 42 bridges were accounted, whether they were complete (14 bridges, 33.3% of the pieces with PP) or incomplete (28 cases, 66.7% of the pieces with PP).

The side of the bony bridges and the presence of a complete or incomplete bridge did not show a statistically significant association ($p=0.827$) (Table 2).

Table 2. Complete PP presence frequency depending on side (dry bone pieces only).

	Incomplete	Complete	Total
Right side	13 (30.9%)	7 (16.7%)	20 (47.6%)
Left side	15 (35.7%)	7 (16.7%)	22 (52.4%)
Total	28 (66.7%)	14 (33.3%)	42 (100%)

The sole other variation found was the presence of 3 pieces with absence of laminar fusion in the posterior middle line. Of these 3 pieces, 1 presented bilateral incomplete bridges (Fig. 1E), 1 presented bilateral complete bridges (Fig. 1F) and 1 presented no bony bridges.

Regarding the analysis of the 3D CT images (Table 1) (Fig. 2), studies from both genders were analyzed (25 male and 30 female), ages ranged between 16 and 83 years, with a mean of 49 years. Nineteen pieces presented bony bridges (34.5% of the analyzed images) from which 11 were bilateral cases (20.0% of the total, 57.9% of the vertebrae with bridges) and 8 were unilateral cases (14.6% of the total, 42.1% of the vertebrae with bridges). This totalize 30 ponticulus posticus, 12 were located on the right side and 18 on the left side (no statistically significant difference). A total of 15 complete and 15 incomplete PP were found.

Out of the 25 men, 13 presented bony bridges (52.0%), while in the 30 women only 6 presented PP (20.0%). A statistically significant association was found between the presence and male gender ($p=0.013$) (Table 3).

Table 3. PP presence frequency depending on gender (TC 3D reconstruction only).

	PP presence	PP absence	Total
Male	13 (23.6%)	12 (21.8%)	25 (45.5%)
Female	6 (10.9%)	24 (43.6%)	30 (54.5%)
Total	19 (34.6%)	36 (65.5%)	55 (100%)

When we compare the PP prevalence between the dry bone material and imaging studies, 38.9% and 34.6% were the obtained values respectively, with no statistically significant difference.

Finally, no statistically significant differences were found when comparing the proportions for number of bridges, bilateral or unilateral bridges, and complete or incomplete bridges between the dry bone material and the imaging studies (Table 1).

DISCUSSION

The presence of bony bridges in the posterior sector of the atlas has called the attention of investigators and physicians due to its potential association with many pathologic states.

The ponticulus posticus is a bony bridge, complete or incomplete, extended from the posterior aspect of the articular process of the atlas to its posterior arch. Although it is sometimes considered an “anomaly”, it is relatively frequent, being found in up to 46% of the cases (Giri et al., 2017), and most of the times it may not be discovered since it could not produce pathology. Three or four variants of the PP are described, depending of the consulted author.

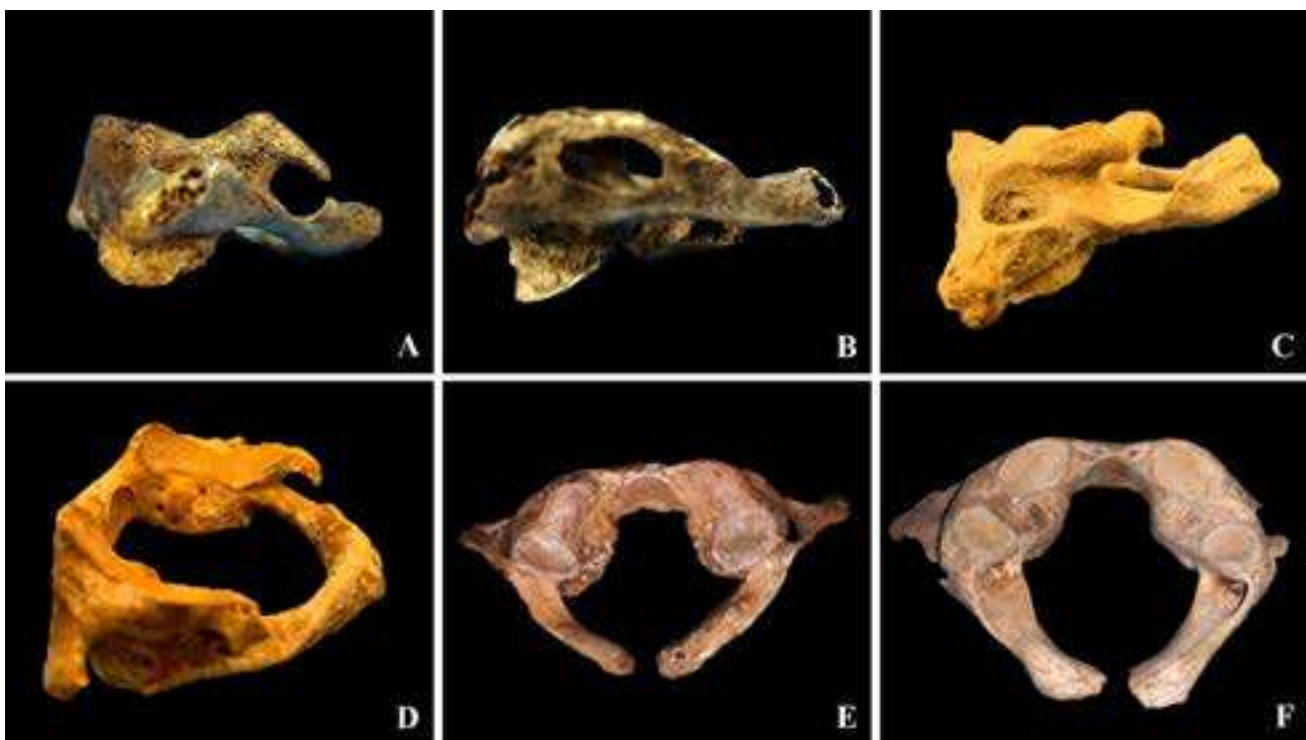


Fig. 1.- Examples of dry bone pieces with PP. **A.** Left lateral view of incomplete unilateral PP. **B.** Left lateral view of complete unilateral PP. **C.** Left lateral view of incomplete bilateral PP. **D.** Oblique view of incomplete bilateral PP. **E.** Superior view of incomplete bilateral PP with absence of laminar fusion. **F.** Superior view of complete bilateral PP with absence of laminar fusion.

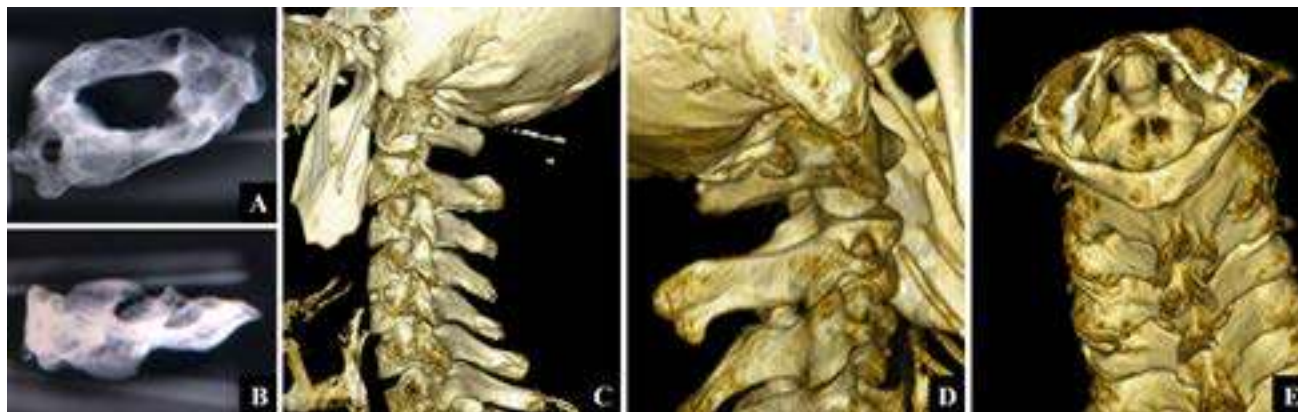


Fig. 2.- Examples of TC analyzed PP. **A.** Oblique view of complete unilateral PP. **B.** Lateral view of incomplete unilateral PP. **C.** Left lateral view of 3D reconstruction showing complete unilateral PP. **D.** Right lateral view of 3D reconstruction showing incomplete bilateral PP. **E.** Superior view of 3D reconstruction showing complete bilateral PP.

Miki et al. state 3 variants: complete bridge, incomplete bridge or calcification. The latter is a bony spicule that raises from the lateral mass. In our pieces, we only consigned whether the bridge was complete or incomplete, as we believe there is no major clinical impact in discriminating the calcification from the incomplete bridge (Donald et al., 2017).

A lateral bridge extended from the lateral mass to the transverse process may be found, among other common variations, such as an accessory foramina. These findings should be differentiated from the PP (Mann et al., 2016).

The prevalence of PP is very variable according to the study method. This one can vary from the review of skeletal material, the dissection of fresh or fixated corpse material and the utilization of imaging studies, such as radiographies, computed tomography or magnetic resonance images (Hauser and De Stefano, 1989). Likewise, the variations could be due to the population under study, as it may be linked to their genetic background (Baraykdar et al., 2018). As far as we are concerned, there is no previous study of prevalence of the PP in Uruguayan population. The frequency of PP in our bone pieces and in the imaging studies (38.9% and 34.6%, respectively) shows no statistical difference between these two resources, and rate among the highest incidences reported. According to Baraykdar et al. (2018) the PP is more frequent in European and North American populations than the ones reported from Asian populations and it is more frequent in males than females. The Uruguayan population is

constituted from the ethnic point of view, by more than 85% of European descendants, around 10% of Afro-American population, and approximately 5% that manifests having indigenous descent (Klüver et al., 2019). Taking this into account, it is not striking that our results are comparable to those of European population. In a regional study from Peru, 1056 lateral cephalograms of Peruvian population were reviewed and an incidence of 19.8% of the PP was observed (Pérez et al., 2014). This incidence differs significantly from our results (p -value < 0,001) and could be explained because of a different ethnic constitution of the Peruvian population.

In our series of bone pieces, we could not determine the gender of the analyzed atlases, but in the imaging series gender was assessed. We found that men have a higher incidence of PP and that this association is statistically significant. This is consistent with authors such as Baraykdar et al. (2018). Arslan et al. (2018) observed the opposite, finding a higher incidence in female gender unlike our series; this author could also register a greater incidence of the PP in the right side, both these results with statistically significant difference.

About the unilaterality/bilaterality, the reports are dissimilar. In fact, our study showed greater unilateral proportion in the dry bone pieces while the CT analysis showed greater bilateral proportion (with no significant difference). Series presented by Tripodi et al. (2019) reported that 74,3% of the bridges were bilateral. A study including 181 patients showed results more

similar to our TC analysis: 43.9% of patients with unilateral bridges against 56.1% of bilateral bridges (Bayrakdar et al., 2018).

In the consulted literature, the presence of complete bridges ranges between 0.9% and 18%. Predominantly, the series show a higher frequency of incomplete bridges than complete bridges (Bayrakdar et al., 2018; Giri et al., 2017; Tripodi et al., 2019). Our general results are comparable to the majority of the consulted literature, and we also found higher rates of incomplete PP in our bone pieces.

Regarding the origin of PP, it is not clear, and several theories have been presumed. The most discussed ones describe the PP as the result of post traumatic exposure, as a variation appeared due to evolutionary or genetic factors, or as the ossification of the occipito-atlantoid ligament, these being considered normal ontogenetic processes (Bayrakdar et al., 2018). About the latter, the relatively high incidence in pediatric population is against it. Tripodi et al. (2019), having analyzed 524 CT scans from children up to 17 years old, founds complete and incomplete bony bridges in 28.2% of the cases. The ontogenetic theory due to aging and calcification of the ligament does not match with this incidence in the pediatric population.

Several clinical implications of the PP have been described in the bibliographic research. It has been associated with cervicogenic headache, tinnitus, migraine, vestibular symptoms, vertebrobasilar insufficiency, photophobia, eye pain, brachialgia, omalgia, oculomotor disorders, diplopia, strokes or even dysphagia and hearing loss (Arslan et al., 2018; Bayrakdar et al., 2018; Donald et al., 2017; Giri et al., 2017; Tripodi et al., 2019). Having its location into account, its relationships, and the incidence of PP in populations of all ages, the authors of this study believe it to be unlikely that all these clinical manifestations can be related to the PP. Nevertheless, it does have clinical and surgical implications in some scenarios.

When there is a complete PP, it forms an osseous ring in which the vertebral artery and the first spinal nerve can be found. So, anatomically, it is difficult to explain oculomotor disorders,

dysphagia or vestibular symptoms if not by an ischemic mechanism or a diminishment of blood flow to the nucleus, via, or cranial nerves implicated in those functions. If we suppose that due to the PP the blood flow has been compromised, then the other vertebral artery could supply (Prinzo et al., 2006). Thus, it seems unlikely that the PP is responsible for these symptoms, especially having into consideration its high incidence in general population.

Another scenario in which it is of interest to know in advance the presence of the PP is in the surgery of tumoral injuries of the occipito-atlantoid region (Fig. 3). In some of these injuries, it can be necessary to move the vertebral artery during the procedure, or even the tumor itself can displace the vertebral artery, as it is shown in Fig. 3, where the expansive process (schwannoma of C1) has displaced the vertebral artery upwards and laterally. The presence of a bony bridge modifies the surgical strategies since the surgeon could angle the artery against the bridge and decrease its blood flow.

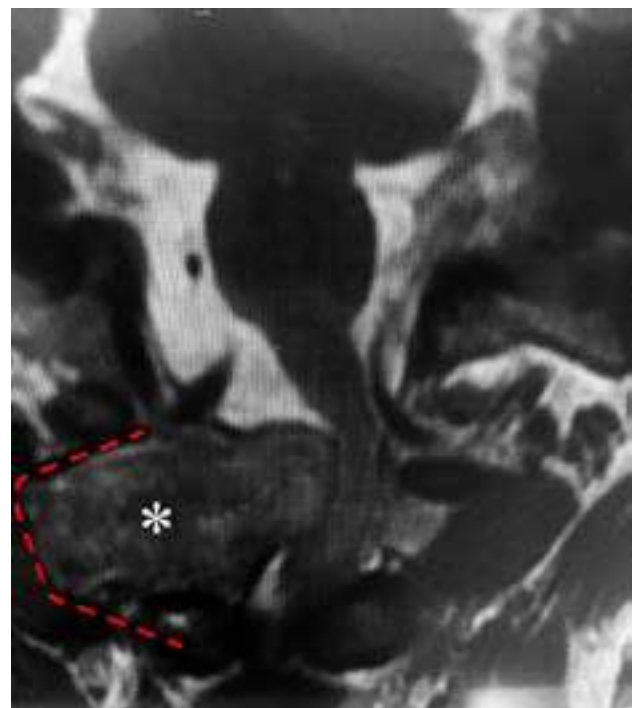


Fig. 3.- Coronal RM T2 image showing C1 schwannoma (*) and the consequent vertebral artery deviation (dotted line).

In a local study about the configuration of the posterior sector of the cerebral arterial circle, 35 adult encephala were dissected. In this sector, a 57.1% of variations were registered. We highlight

that the caliber of the left vertebral artery was larger in 45% of the cases, 50% the calibers were similar and only in 5%, the caliber of the right vertebral artery was larger (Martínez et al., 2003). These considerations are essential along with the consideration of the PP. If for example, the schwannoma compresses the left vertebral artery against the PP, and this artery is responsible for the vast blood flow of the posterior fossa, the right vertebral artery may not be capable to supply in case of having a small caliber.

In case of occipito-atlantoid instability, it may be necessary to collocate a fixation system with screws and bars. In the presence of PP, during the intra operative procedure, the surgeon can misinterpret that he is in front of a wide posterior arch, and collocate a screw through the bony bridge, with the risk of injuring the vertebral artery and first cervical nerve (Sharma et al., 2010). Song et al. investigated the impact of present PP in two high cervical surgeries (arthrodesis of posterior arch to lateral mass and occipito-condylar arthrodesis), both with screws. They concluded that both techniques were feasible and secure in presence of PP, and even stated that when increasing the distance between the vertebral artery and the occipital, in the case of occipito-condylar fixation, the presence of the PP could mean an anatomic advantage in this procedure. Nevertheless, in female patients such dimensions are smaller and surgeon should be cautious, according to the investigators (Song et al., 2017). Findings by Arslan et al. (2018) suggest that the presence of the PP does not alter the feasibility and security of lateral mass fixation; contrarily, these researchers state that this bony bridge is associated with narrower vertebral arteries. These are some of the reasons why it is handy to know in advance the presence of the PP, especially to identify it before surgical procedures.

Zhang et al. (2016) carried out a retrospective study about screw fixation in patients with atlantoaxial instability. They included 28 patients with atlas variations, which they defined in three groups depending on the height of the arterial groove and height of the posterior arch, being these groups of interest because this fixation technique is not suggested when any of these measures <4,0 mm,

since these reduced distances could increase the difficulty of the procedure of fixation. The presence of a bony bridge in the posterior arch should be taken into account, as it may lead to misinterpretation of its height, and therefore surgical planning would have the wrong anatomical bases with the consequent wrong surgical procedure.

Conclusions

Ponticulus posticus is a high prevalence variation, that usually goes unnoticed if its systematic research is not carried out. Our results rate among the higher prevalence reported. Clinical and surgical implications justify why knowing its presence is of great interest either as a numerous medical condition-associated variation, or as a condition to take into account in surgery planification.

ACKNOWLEDGEMENTS

The authors express their recognition to all who, in life, decide to donate their body to our Faculty, for teaching and research of Anatomy.

REFERENCES

- ARSLAN D, OZER MA, GOVSA F, KITIS O (2018) The ponticulus posticus as risk factor for screw insertion into the first cervical lateral mass. *World Neurosurg*, 113: 579-585.
- BAYRAKDAR IŞ, MILOĞLU Ö, YEŞİLTEPE S, YILMAZ AB (2018) Ponticulus posticus in a cohort of orthodontic children and adolescent patients with different sagittal skeletal anomalies: A comparative cone beam computed tomography investigation. *Folia Morphol (Warsz)*, 77: 65-71.
- DONALD PM, NAGRAJ SK, PALLIVATHUKKAL RG, ISMAIL ARB (2017) Ponticulus posticus of atlas vertebrae: An incidental finding in Malaysian orthodontic patients. *BMJ Case Rep* 2017: bcr2017220851.
- GIRI J, POKHAREL PR, GYAWALI R (2017) How common is ponticulus posticus on lateral cephalograms? *BMC Res Notes*, 10: 1-5.
- HAUSER G, DE STEFANO GF (1989) Epigenetic variants of the human skull. Schweizerbart'sche Verlagsbuchhandlung. Stuttgart, Germany, p 111.

KLÜVER C, NARANJA M (2019) Ascendencia - Étnica y seguridad social en Uruguay. *Banco de Previsión Social - Asesoría General En Seguridad Social*: 1-49.

LO GIUDICE A, CACCIANIGA G, CRIMI S, CAVALLINI C, LEONARDI R (2018) Frequency and type of ponticulus posticus in a longitudinal sample of non-orthodontically treated patients: Relationship with gender, age, skeletal maturity, and skeletal malocclusion. *Oral Surg Oral Med Oral Pathol Oral Radiol*, 126: 291-297.

MANN RW, HUNT DR, LOZANOFF S (2016) Photographic regional atlas of non-metric traits and anatomical variants in the human skeleton. *Charles C Thomas*, Springfield, USES, pp 568-572.

MARTINEZ F, SGARBI N, ARMAND UGON G, PRINZO H, SORIA VR (2003) Estudio anatómico del polígono de Willis. Parte II: sector posterior. *Arch Inst Neurol*, 6(1): 23-30.

PÉREZ IE, CHÁVEZ AK, PONCE D (2014) Frequency of ponticulus posticus in lateral cephalometric radiography of Peruvian patients. *Int J Morphol*, 32: 54-60.

PRINZO H, MARTÍNEZ F, SGARBI N, SORIA VR (2006) Anatomía microquirúrgica de la arteria cerebral posterior. *Rev Mex Neuroci*, 7: 364-374.

SHARMA V, CHAUDHARY D, MITRA R (2010) Prevalence of ponticulus posticus in Indian orthodontic patients. *Dentomaxillofac Radiol*, 39: 277-283.

SONG MS, LEE HJ, KIM JT, KIM JH, HONG JT (2017) Ponticulus posticus: morphometric analysis and its anatomical implications for occipito-cervical fusion. *Clin Neurol Neurosurg*, 157: 76-81.

TRIPODI D, TIERI M, DEMARTIS P, PERÒ G, MARZO G, D'ERCOLE S (2019) Ponticulus posticus: Clinical and CBCT analysis in a young Italian population. *Eur J Paediatr Dent*, 20: 219-223.

ZHANG QH, LI HD, MIN JK (2016) Pedicle screw placement in patients with variant atlas pedicle. *J Int Med Res*, 44: 931-939.

Origin and branching pattern of external carotid artery - a cadaveric study

Aby S. Charles¹, Suganthy Rabi², Anjali Jain³, Parminder K. Rana⁴

¹ Christian Medical College, Ludhiana*

² Christian Medical College, Vellore

³ Christian Medical College, Ludhiana

⁴ Christian Medical College, Ludhiana**

Present affiliation:

* Christian Medical College, Vellore

** Adelaide Medical School, Adelaide

SUMMARY

The vascular supply to the head and neck is chiefly derived from the carotid system of arteries. Numerous variations have been reported regarding the level of origin of the external carotid artery and its branching pattern. Clinically, the branches of the external carotid artery are important in head and neck surgeries involving the thyroid, oro-facial reconstruction, diagnosis and treatment of tumors of the head and neck. This study aimed to observe the origin and branching pattern of the external carotid artery in the Indian Punjabi population. The study was done on both sides of 15 formalin-fixed adult human cadavers, thus making up to 30 carotid systems. The level of origin of the external carotid artery and its individual branches were measured. Out of the 30 carotid systems studied, only four showed the typical level of origin at the upper border of the thyroid cartilage, with trifurcations seen in eight cases and one case showing tetrafurcation. 53.33% of the external carotid systems showed the presence of at least one common trunk of origin, of which linguo-facial trunk was seen in 26.67%, pharyngo- occipital trunk in 23.33%

and auriculo-occipital trunk in 13.33% cases. Moreover, an aberrant ascending pharyngeal artery was noticed, with communication to the internal carotid artery.

Key words: Carotid bifurcation – Common carotid artery – Linguo-facial trunk – Pharyngo-occipital trunk – Auriculo-occipital trunk

INTRODUCTION

The vascular supply to the head and neck is chiefly derived from the carotid system of arteries. Additional supply comes from the branches of the subclavian artery, most importantly the vertebral artery. The carotid system of arteries begins as the common carotid artery (CCA), which bifurcates into the external carotid artery (ECA) and the internal carotid artery (ICA) (Mata et al., 2012; Hollinshead et al., 1968). The level of carotid bifurcation cannot be predicted by any known clinical sign. Most of the literature states that bifurcation of the common carotid artery occurs at the level of the superior border of the thyroid cartilage (Lo et al., 2006).

Corresponding author:

Parminder Kaur Rana. Adelaide Medical School, Dept. of Anatomy, Faculty of Health and Medical Sciences, 5005 Adelaide, Australia. E-mail: parminderk083@gmail.com

Submitted: January 28, 2020. Accepted: November 11, 2020

The ECA has eight branches, namely the superior thyroid artery, the ascending pharyngeal artery, the lingual artery, the facial artery, the occipital artery, the posterior auricular artery, the superficial temporal artery and the maxillary artery (Hollinshead et al., 1968). A good knowledge of the normal anatomy and variations of ECA and its branches are of prime importance in both surgical and medical specialties. Both carotid endarterectomy and carotid stenting to prevent recurrence of stroke warrant a thorough knowledge of the carotid system (Rajamani and Chaturvedi, 2011). Extracranial-intracranial bypass procedure for revascularization uses the ECA or one of its branches as donor vessels (Germans and Regli, 2014). Radiologists must have a good preexisting knowledge of the external carotid arterial system and expected variations in order to identify the various arteries. This applies specially to tests like CT angiography, which are done prior to major surgeries (Acar et al., 2013). Hence, this study aims at observing the origin and branching pattern of the external carotid artery in the Indian Punjabi population.

MATERIALS AND METHODS

Ethical approval was obtained from the Institutional Review Board of the Christian Medical College, Ludhiana, where the study was conducted. Fifteen formalin-fixed adult cadavers of unknown age, ten male and five females, were obtained from the Department of Anatomy of the institution. These cadavers were being used by medical students as part of their training and was obtained through a body donation program. Bilateral dissection was done. Thus, 30 ECAs were studied for their origin and branching pattern. Cadavers with any obvious congenital anomaly of the head and neck region or those in which the carotid system was used for embalming purposes were excluded from the study.

The cadaver was dissected in a supine position with the neck extended. The skin and superficial fascia containing platysma with nerves and the deep fascia were reflected. The boundaries of the carotid triangle were ascertained. The inferior attachment of the sternocleidomastoid muscle was detached to better expose the area. Fat and

fascia from the area between the posterior belly of the digastric and the superior belly of the omohyoid were removed, exposing the CCA and ICA medially and the internal jugular vein laterally. The ECA was identified lying anteromedial to the ICA. The hypoglossal nerve was identified and followed forwards across the ECA. Ansa cervicalis was identified and removed. The posterior belly of the digastric, stylohyoid, and thyrohyoid muscles was reflected. The carotid sheath was dissected to expose the CCA and its bifurcation into ICA and ECA. The ECA was traced in the digastric triangle. The hypoglossal nerve was preserved to serve as landmark.

In the parotid gland, the ECA was traced after removing the gland piecemeal. The termination of the ECA was studied by division of the zygomatic arch and removal of part of the mandible along with the attached muscles. The branches of the ECA were identified and followed to confirm their identity and course. This was verified by a second investigator.

The level of bifurcation of the CCA was noted in relation to the highest point of the upper border of the thyroid cartilage with a scale, and then this distance was measured using Vernier calipers. The distance of origin of the individual branches of the ECA from the point of carotid bifurcation was measured along the tortuosity of the vessel using an inelastic thread and measured by the Vernier calipers. The variations in the branching pattern, if any, were documented. Descriptive statistics were used and analyzed using SPSS Version 23.

RESULTS

Carotid bifurcation

In the present study, the carotid bifurcation was seen at a mean distance of 1.28 ± 0.93 cm above the level of the upper border of the thyroid cartilage in 25 out of 30 (83.33%) cases, out of which 11 were on the left side, and 14 on the right side (Fig. 1A). The eleven cases on the left were at a mean distance of 1.55 ± 0.96 cm, while the 14 cases on the right were at a mean distance of 1.06 ± 0.86 cm from the upper border of the thyroid cartilage. Only in four out of 30 (13.33%) cases, the carotid bifurcation occurred at the level of the upper

border of the thyroid cartilage, three cases on the left and one case on the right side. In one case (3.33%), on the left side, the bifurcation occurred 1.2 cm below the level of the upper border of the thyroid cartilage (Fig. 1B).

In the present study, the branches of ECA took origin not only from the ECA, but also from the CCA or at the level of bifurcation. A trifurcation, meaning a branch arising from the carotid bifurcation, was noted in eight cases. In three cases, the superior thyroid artery took origin from the carotid bifurcation; in four cases, the ascending pharyngeal artery took origin from the carotid bifurcation, and in one case the occipital artery took origin at the level of the carotid bifurcation (Fig. 2A). One case of tetrafurcation was observed, where both the superior thyroid artery and the ascending pharyngeal artery took origin from the carotid bifurcation.

Of the 30 cases studied, in 13 cases the superior thyroid artery took origin from the CCA.

In one case, on the left side, the ascending pharyngeal artery took origin from the CCA, after which it travelled upwards and medially along with the ICA. In this particular case, in addition to the ascending pharyngeal artery, a linguo-facial trunk arose from the CCA. At a distance of 1.2 cm from its origin, the artery communicated with the ICA by a very short communicating branch, before continuing on its course. The ICA gave off two branches in the neck just above this level. On following these branches, they appeared to be entering the cranial cavity at the base of the skull (Fig. 2B).

Length of ECA

The ECA terminated as the maxillary artery and superficial temporal artery in all cases. The mean length of the ECA was 6.15 ± 1.22 on the left and 6.28 ± 1.2 on the right (Table 1). Table 1 shows the mean distance of origin of the arteries from the carotid bifurcation.

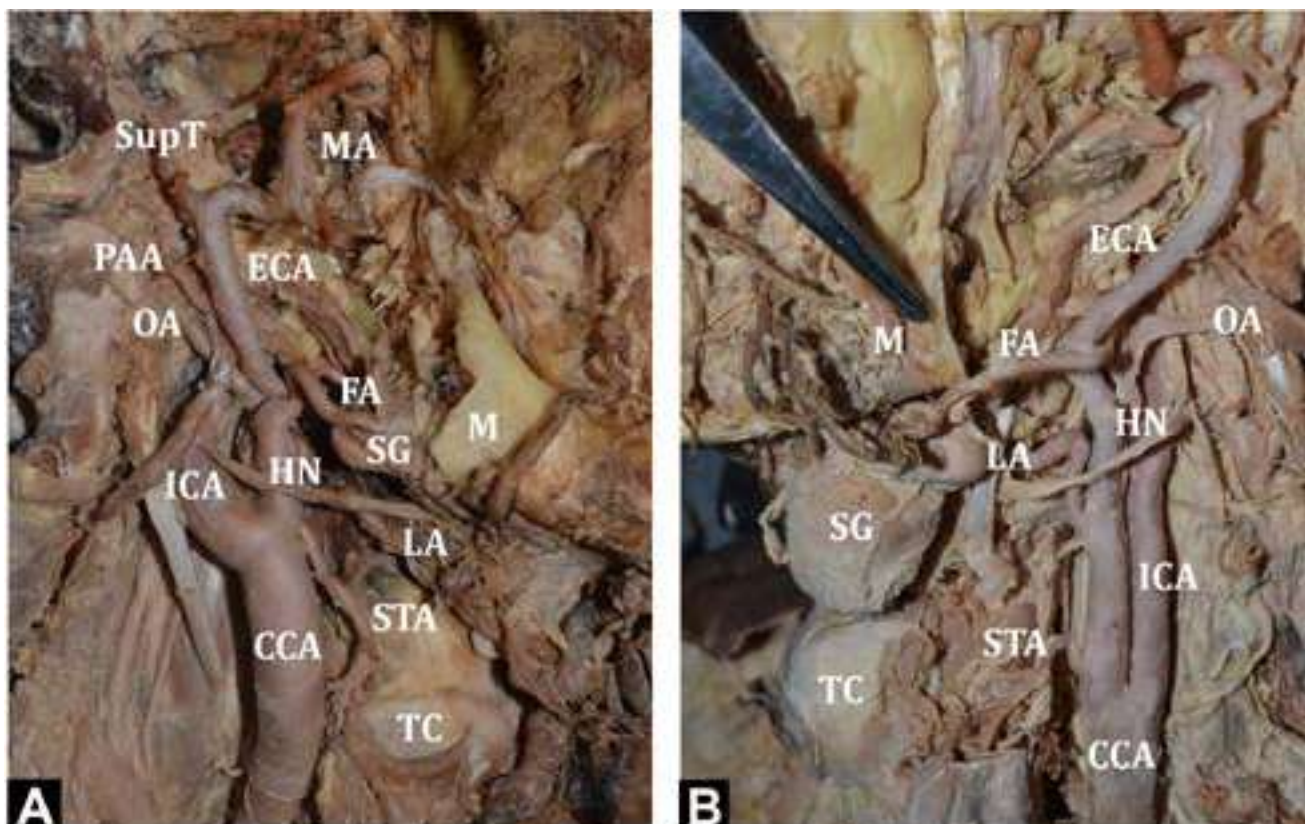


Fig. 1.- A) Showing the bifurcation of CCA above the level of TC (right side). **B)** Bifurcation of CCA below the upper border of TC (left side). TC - Thyroid cartilage; CCA - Common carotid artery; ECA - External carotid artery; ICA - Internal carotid artery; OA - Occipital artery; APA - Ascending pharyngeal artery; ComB - Communicating branch to ICA; BriCA - Branches arising from ICA; STA - Superior thyroid artery; LA - Lingual artery; FA - Facial artery; LFT - Linguo-facial trunk; AOT - Auriculo-occipital Trunk; PAA - Posterior auricular artery; SupT - Superficial temporal artery; MA - Maxillary artery; POT - Pharyngo-occipital trunk HN - Hypoglossal nerve; SG - Submandibular gland.

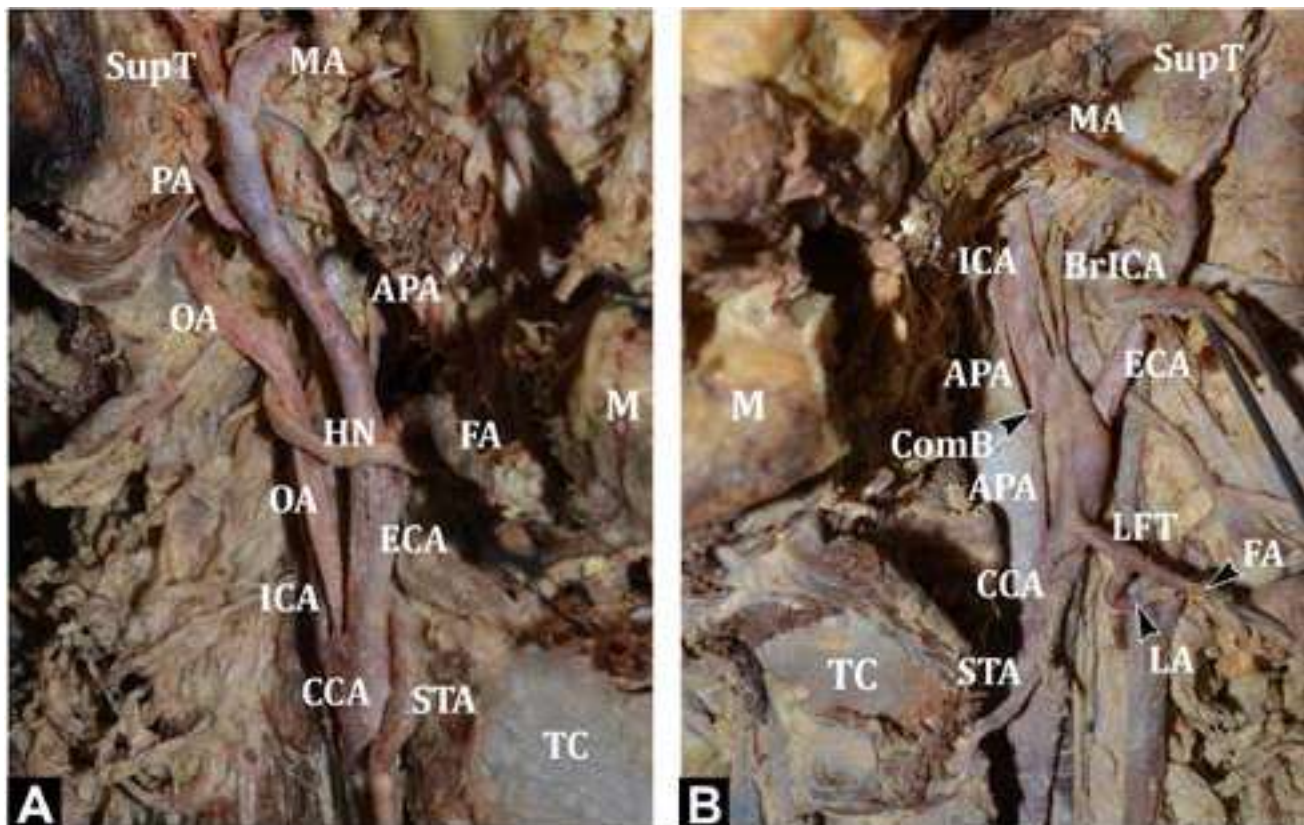


Fig. 2.- A) Showing the OA arising at the level of carotid bifurcation (right side). **B)** Showing APA arising from CCA with a communicating branch to ICA. In addition, LFT is seen arising from the CCA. ICA gives two cervical branches (left side). TC - Thyroid cartilage; CCA - Common carotid artery; ECA - External carotid artery; ICA - Internal carotid artery; OA - Occipital artery; APA - Ascending pharyngeal artery; ComB - Communicating branch to ICA; Br-ICA - Branches arising from ICA; STA - Superior thyroid artery; LA - Lingual artery; FA - Facial artery; LFT - Linguo-facial trunk; AOT - Auriculo-occipital Trunk; PAA - Posterior auricular artery; SupT - Superficial temporal artery; MA - Maxillary artery; POT - Pharyngo-occipital trunk HN - Hypoglossal nerve; SG - Submandibular gland.

Common trunks of origin

In this study, there were several instances of branches of the ECA sharing common trunks of origin. Three types of common trunks were noted:

Linguo-facial trunk: between the lingual artery and the facial artery (Figs. 2B and 3A).

Pharyngo-occipital trunk: between the ascending pharyngeal artery and the occipital artery (Fig. 3B).

Auriculo-occipital trunk: between the posterior auricular artery and the occipital artery (Fig. 3A).

Linguo-facial trunk was the most common, present in 26.67% (8/30) cases at a mean distance of 1.3 ± 0.31 cm from the carotid bifurcation. Five cases were seen on the left side, at a mean distance of 1.42 ± 0.33 cm from the carotid bifurcation at a range of 0.9-1.8 cm. Three cases were seen on the right side, at a mean distance of 1.1 ± 0.1 cm from the carotid bifurcation at a range of 1-1.2 cm. The linguo-facial trunk took origin from the ECA in all cases except one, where it took origin from the CCA.

Pharyngo-occipital trunk was seen in 23.33% (7/30) cases, at a mean distance of 2.23 ± 0.97 cm from the carotid bifurcation. Four cases were seen on the left side, at a mean distance of 2 ± 1.25 cm from the carotid bifurcation at a range of 0.7-3.6 cm. Three cases were seen on the right side, at a mean distance of 2.53 ± 0.47 cm from the carotid bifurcation at a range of 2-2.9 cm. The pharyngo-occipital trunks took origin from the ECA in all cases.

Auriculo-occipital trunk was seen in 13.33% (4/30) cases at a mean distance of 3.48 ± 0.57 cm from the carotid bifurcation. Two cases were seen on the left side, at a mean distance of 3.2 ± 0.2 cm from the carotid bifurcation at a range of 3-3.4 cm. Two cases were seen on the right side, at a mean distance of 3.75 ± 0.78 cm from the carotid bifurcation at a range of 3.2-4.3 cm. The auriculo-occipital trunk took origin from the ECA in all cases.

53.33% (16/30) cases showed the presence of at least one common trunk of origin. Presence of

Table 1. Origin of branches of the external carotid artery.

	Left				Right		
	Source of origin	Number of cases	Mean distance from CB (in cm)	Range (in cm)	Number of cases	Mean distance from CB (in cm)	Range (in cm)
Superior Thyroid Artery	CCA	9	0.73±0.65	0.2–2.2	4	0.38±0.15	0.3–0.6
	CB	2			2		
	ECA	4	0.38±0.17	0.2–0.6	9	0.27±0.11	0.2–0.5
	Total	15	0.54±0.57		15	0.26±0.16	
Ascending Pharyngeal Artery	CCA	1	2.2		0		
	CB	2			3		
	ECA	12	1.5±0.9	0.2–3.6	12	1.7±0.62	1–2.9
	Total	15	1.35±0.98		15	1.36±0.89	
Lingual Artery	CCA	1	1.4		0		
	ECA	14	1.44±0.82	0.7–4	15	1.18±0.42	0.4–2.1
	Total	15	1.43±0.79		15	1.18±0.42	
Facial Artery	CCA	1	1.4		0		
	ECA	14	1.65±0.88	0.5–3.6	15	1.9±1.11	1–5.4
	Total	15	1.63±0.85		15	1.9±1.11	
Occipital Artery	CB	0			1		
	ECA	15	1.83±0.91	0.7–3.6	14	1.95±1.06	0.4–4.3
	Total	15	1.83±0.91		15	1.82±1.14	
Posterior Auricular Artery	ECA	15	4.01±1.09	1.9–5.7	15	4.01±0.69	2.6–5.4
Length of ECA		15	6.15±1.22	3.8–8.9	15	6.28±1.2	4.8–9.2

common trunks of origin was more common on the left side. These 16 cases included three, which showed the presence of more than one common trunk, two on the left and one on the right.

DISCUSSION

Surgeries like thyroidectomy, laryngectomy, faciomaxillary surgeries, tonsillectomy, glossectomy and other neck surgeries involve areas supplied by or related to branches of the ECA (Sanjeev et al., 2010). Preoperative appreciation of variations of the ECA can help in maintaining a bloodless field (Hansdak et al., 2015). Oro-facial reconstruction surgeries, including scalp transplantation, depend on the superior thyroid, lingual and facial arteries for their technical applicability, feasibility, and flap survival (Li et al., 2013; Siemionow and Kulahci, 2007).

Preoperative arteriograms are used to map out the vascularity and true extent of the head and neck tumors, while selective arterial embolization helps reduce their vascularity (Byun et al., 2012).

Super-selective intra-arterial chemotherapy, aimed at treating head and neck tumors, like oral cancer, demands accurate knowledge of the arteries supplying the region (Tohnai, 2006).

Carotid bifurcation

The CCA bifurcates into the ECA and ICA at the level of the superior border of the lamina of the thyroid cartilage. Previous literature shows that the level of carotid bifurcation is highly variable (Table 2). Cases of high bifurcation, low bifurcation, intrathoracic bifurcation and even the absence of CCA have been reported by various authors (Bergman et al., 1998; Cakirer et al., 2002; Chan et al., 2013; Gailloud et al., 2000; Gomez and Arnuk, 2013; Uzun et al., 2013). The present study showed a high number of high bifurcations, which were comparable to a study done by Ozgur et al. (2008a, b) in the Turkish population. In the present study, the distance of the bifurcation from the upper border of the thyroid cartilage was 1.22±1.03 cm on the left side, in comparison

to 0.99 ± 0.89 cm on the right side. According to Ribeiro et al. (2006), the carotid bifurcation levels were symmetrical on both sides.

Trifurcation of the CCA into ECA, ICA and a branch of ECA has been reported by various authors (Altinbas et al., 2015; Gürbüz et al., 2001). In the present study, trifurcation of CCA was seen in eight cases (26.67%). This included four cases of ascending pharyngeal artery, three cases of superior thyroid artery and one case of occipital artery taking origin from the carotid bifurcation. One case (3.33%) of tetrafurcation was seen in a female cadaver, where on the right side the superior thyroid artery and ascending pharyngeal artery took origin from the carotid bifurcation.

Superior thyroid artery

While most Indian authors have reported a low incidence of superior thyroid artery arising from the CCA, a higher incidence of 43.33% was seen in the present study done on the Punjabi

population from India, which was similar to certain foreign authors (Table 3). This variation has been noted in classically referenced studies, with Quain (1844) reporting 14% cases, Livini (1903) reporting 9% cases and Adachi (1928) reporting 13% cases. The superior thyroid artery took origin from the CCA more commonly on the left side. The origin of the superior thyroid artery was at a mean distance of 0.4 ± 0.43 cm from the carotid bifurcation, which was in accordance with Ozgur et al. (2009), who observed a similar result with a mean of 0.33 ± 0.43 cm.

Ascending pharyngeal artery

In the present study, the ascending pharyngeal artery took origin from the ECA in 80% (24/30) cases. Variant origin from the carotid bifurcation was seen in 16.67% (5/30) cases and from CCA in 3.33% (1/30) cases (Fig. 2B).

The ascending pharyngeal artery took origin at a mean distance of 1.35 ± 0.92 cm from the carotid bifurcation with a range of 0-3.6 cm, which was

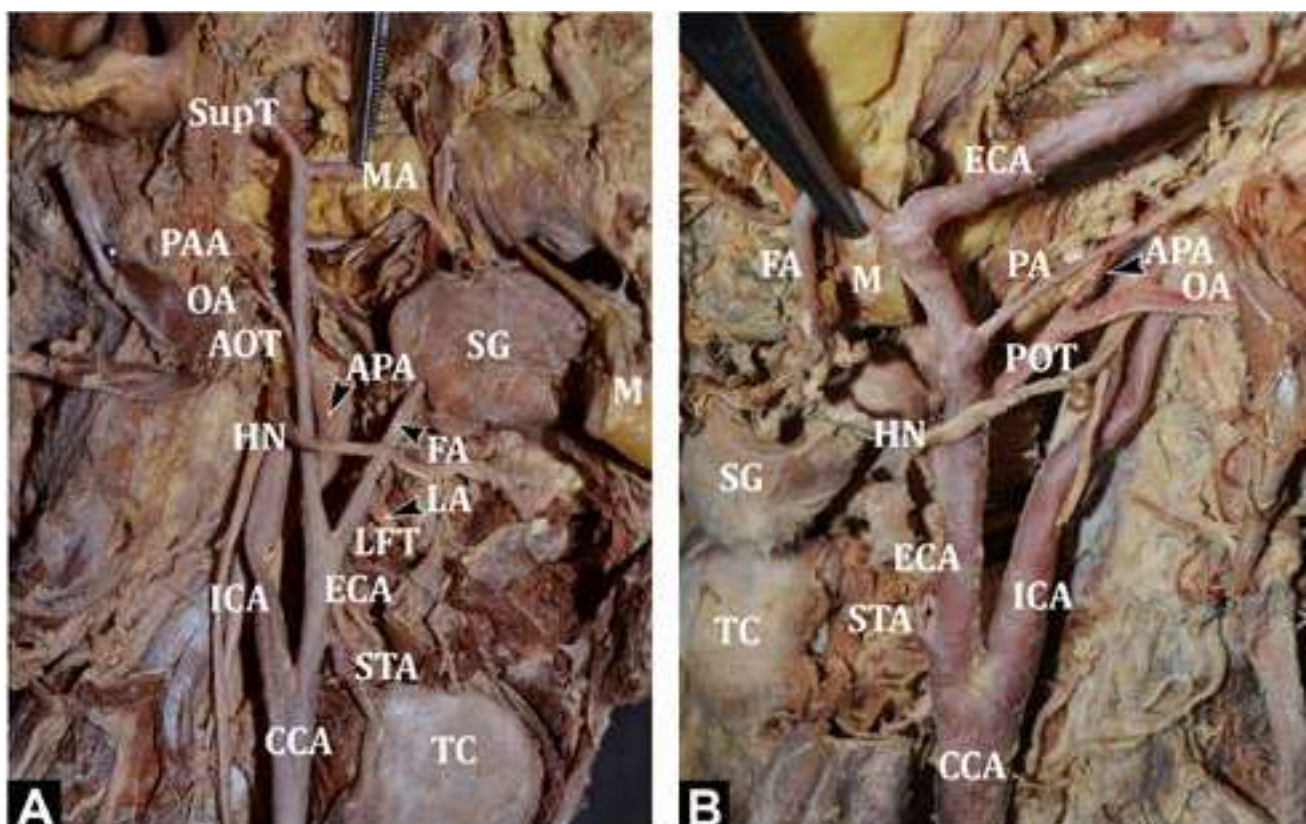


Fig. 3.- A) Showing the LA and FA arising from the LFT and OA and PAA arising from the POT (left side). TC - Thyroid cartilage; CCA - Common carotid artery; ECA - External carotid artery; ICA - Internal carotid artery; OA - Occipital artery; APA - Ascending pharyngeal artery; ComB - Communicating branch to ICA; BrICA - Branches arising from ICA; STA - Superior thyroid artery; LA - Lingual artery; FA - Facial artery; LFT - Linguo-facial trunk; AOT - Auriculo-occipital Trunk; PAA - Posterior auricular artery; SupT - Superficial temporal artery; MA - Maxillary artery; POT - Pharyngo-occipital trunk HN - Hyoglossal nerve; SG - Submandibular gland.

Table 2. Cadaveric studies comparing level of carotid bifurcation in relation to thyroid cartilage.

Author and Year	Number of cases	Level of bifurcation		
		Below	At level	Above
Lučev et al. (2000)	40	12.5% (5/40)	50% (20/40)	37.5% (15/40)
Ozgun et al. (2008)	40	22.5% (9/40)	5% (2/40)	72.5% (29/40)
Sanjeev et al. (2010)	37	27.03% (10/37)	56.76% (21/37)	16.22% (6/37)
Al-Rafiah et al (2011)	60	5% (3/60)	48.3% (29/60)	46.6% (28/60)
Ambali and Yadhav (2012)	200	1% (2/200)	57% (114/200)	42% (84/200)
Mompeó and Bajo (2015)	38	-	63.15% (24/38)	36.85% (14/38)
Present Study	30	3.33% (1/30)	13.33% (4/30)	83.33% (25/30)

Table 3. Cadaveric studies comparing origin of superior thyroid artery in relation to carotid bifurcation from different regions.

Author and Year	Population studied	Number of cases	Level of origin		
			CCA	CB	ECA
Lučev et al. (2000)	Croatian	40	47.5% (19/40)	22.5% (9/40)	30% (12/40)
Patel et al. (2013)	Indian	100	-	23% (23/100)	77% (77/100)
Shivaleela et al. (2016)	Indian	84	2.38% (2/84)	21.34% (18/84)	76.19% (64/84)
Won (2016)	Korean	30	40% (12/30)	40% (12/30)	20% (6/30)
Present Study	Indian	30	43.33% (13/30)	13.33% (4/30)	43.33% (13/30)

similar to Cavalcanti et al. (2009), who observed a similar result in the North American population with a mean of 1.53 ± 0.83 cm with a range of 0-3.2 cm. The branches of the ascending pharyngeal artery anastomose with branches of ICA, maxillary artery, vertebral artery and occipital artery, thus providing important collateral circulation (Hacein-Bey et al., 2002).

Lingual artery

The lingual artery took origin from the ECA in all cases, except one, where it stemmed from the CCA along with the facial artery as a common trunk (Fig. 2B). Lučev et al. (2000) and Troupis et al. (2014), each observed a case where the lingual artery took origin from the carotid bifurcation, whereas Ambali and Jadhav (2012) observed a case in their study where the lingual artery took origin from the CCA. In the present study, the distance of origin of the lingual artery from the carotid bifurcation ranged from 0.4-4 cm, similar to the findings of Lins et al. (2005) and Lučev et al. (2000), where the range of origin was 0.5-3.7 cm and 0.5-4 cm respectively. The lingual artery was at a distance of 1.31 ± 0.63 cm from the carotid

bifurcation. Yonenaga et al. (2011) observed a mean distance of 2.13 ± 0.85 cm in their study.

Facial artery

In the present study, the facial artery took origin from the CCA in one case (Fig. 2B). A Japanese study reported a mean distance of 3.08 ± 1.18 cm from the carotid bifurcation, while in the present study, this distance was 1.77 ± 0.98 cm (Yonenaga et al., 2011).

Occipital artery

In the present study, the occipital artery took origin from the ECA in all cases except one, where it took origin from the carotid bifurcation (Fig. 2A). Various authors have observed the occipital artery arising from the ICA (Adachi, 1928; Cappabianca et al., 2012; Small et al., 2014). Such a finding was absent in the present study. The origin of the occipital artery was at a mean distance of 1.83 ± 1.01 cm from the carotid bifurcation with a range of 0-5.4 cm, indicating a wide range in the origin of occipital artery, whereas the observation made by Alvernia et al. (2006) showed a range of 0.7-2.8 cm with a mean of 1.74 cm.

Table 4. Cadaveric studies comparing prevalence of common trunks of origin among branches of ECA.

Author and Year	Population studied	Number of cases	Common trunks				
			Thyro-lingual trunk	Thyro-linguo-facial trunk	Linguo-facial trunk	Auriculo-occipital trunk	Pharyngo-occipital trunk
Shintani et al. (1999)	Japan	58	3.5%	-	31%	-	-
Hayashi et al. (2005)	Japan	98	1%	-	18%	-	19%
Lins et al. (2005)	Brazil	48	-	-	25%	-	-
Vázquez et al. (2009)	English	330	0.6%(2/330)	0.3% (1/330)	-	-	-
Ozgur et al. (2008)	Turkey	40	2.5%	-	7.5%	-	-
Sanjeev et al. (2010)	Indian	37	2.7%(1/37)	-	18.92% (7/37)	2.7% (1/37)	24.32% (9/37)
Yonenaga et al. (2011)	Japan	56	1.8% (1/56)	-	28.6% (16/56)	-	-
Mata et al. (2012)	Brazil	36	2.8%(1/36)	-	19.4% (7/36)	-	-
Present Study	Indian	30	-	-	26.67% (8/30)	13.33% (4/30)	23.33% (7/30)

Posterior auricular artery

In the present study the posterior auricular artery took origin from the ECA in all cases. In addition, the distance of origin of the posterior auricular arteries was similar on both sides.

Termination of external carotid artery

In the present study, all ECAs terminated as superficial temporal arteries and maxillary arteries. In one case observed by Sanjeev et al. (2010), the ECA trifurcated into the superficial temporal, maxillary and posterior auricular arteries. In the present study, the mean length of ECA was similar to the study by Sanjeev et al. (2010), who reported a mean length of 6 cm. A Japanese study by Yonenaga et al. (2011) showed the length to be 7.78 ± 0.9 cm.

Common trunks of origin

Three varieties of common trunks were seen in the present study: linguo-facial trunks, pharyngo-occipital trunks and auriculo-occipital trunks.

As seen in Table 4, studies report a varying prevalence of branches of the ECA, originating through common trunks. This may depict a geographical variation in the branching pattern.

The vasculature of the head and neck is derived from two dorsal aortic arches along with two ventral pharyngeal arteries during early embryogenesis. These communicate through six aortic arches, which disappear variably during development. The carotid arterial system and its branches, with their variations, develop from this early system of arteries (Troupis et al., 2014).

Conclusions

In conclusion, differences in the branching pattern of the ECA are prevalent in the Indian Punjabi population. These include variations in the level of origin and common trunks. The typical level of origin at the upper border of the thyroid cartilage was seen only in four cases out of 30, with trifurcations seen in eight cases and tetrafurcation in one case. Linguo-facial trunk was seen in 26.67%, pharyngo-occipital trunk in 23.33% and auriculo-occipital trunk in 13.33% cases. Knowledge of these aberrations in the branching pattern of the ECA is crucial to clinicians and anticipating them will help in better diagnosis and treatment of patients.

REFERENCES

- ACAR M, SALBACAK A, SAKARYA ME, ZARARSIZ I, ULUSOY M (2013) The morphometrical analysis of the external carotid artery and its branches with multidetector computerized tomography angiography technique. *Int J Morphol*, 31: 1407-1414.
- ADACHI B (1928) *Das arteriensystem der Japaner*. Maruzen, Kyoto, pp 54-82.
- AL-RAFIAH A, EL-HAGGAGY AA, AAL IHA, ZAKI AI (2011) Anatomical study of the carotid bifurcation and origin variations of the ascending pharyngeal and superior thyroid arteries. *Folia Morphol*, 70: 47-55.
- ALTINBAS NK, UNAL S, PEKER A, UZUN C, AKKAYA Z, PEKER E (2015) Trifurcation of the left common carotid artery. *Pol J Radiol*, 80: 376-378.
- ALVERNIA JE, FRASER K, LANZINO G (2006) The occipital artery: a microanatomical study. *Oper Neurosurg*, 58: 114-122.
- AMBALI M, JADHAV SJ (2012) Variations in bifurcation point and branching pattern of common carotid arteries: a cadaveric study. *J Pharm Biomed Sci*, 25: 147-151.
- BERGMAN RA, THOMPSON SA, AFIFI AK, SAADEH (1998) *Compendium of human anatomic variation*. Urban & Schwarzenberg, Baltimore-Munich, pp 28-31.
- BYUN H, CHO YS, CHU HS (2012) Glomus faciale: primary paraganglioma of the facial canal. *J Int Adv Otol*, 8: 137-142.
- CAKIRER S, KARAARSLAN E, KAYABALI M, ROZANES I (2002) Separate origins of the left internal and external carotid arteries from the aortic arch: MR angiographic findings. *Am J Neuroradiol*, 23: 1600-1602.
- CAPPABIANCA S, SCUOTTO A, IASELLI F, SPINAZZOLA NPD, URRARO F, SARTI G, MONTEMARANOM, GRASSIR, ROTONDO A (2012) Computed tomography and magnetic resonance angiography in the evaluation of aberrant origin of the external carotid artery branches. *Surg Radiol Anat*, 34: 393-399.
- CAVALCANTI DD, REIS CVC, HANEL R, SAFAVI-ABBASI S, DESHMUKH P, SPETZLER RF, PREUL MC (2009) The ascending pharyngeal artery and its relevance for neurosurgical and endovascular procedures: *Oper Neurosurg*, 65 ONS Suppl 1: ons114-ons120.
- CHAN YC, WONG WH, CHENG SW (2013) Successful carotid endarterectomy in a patient with an aberrant branch from the common carotid artery. *Ann R Coll Surg Engl*, 95: e17-e19.
- GAILLOUD P, MURPHY KJ, RIGAMONTI D (2000) Bilateral thoracic bifurcation of the common carotid artery associated with Klippel-Feil anomaly. *Am J Neuroradiol*, 21: 941-944.
- GERMANS MR, REGLI L (2014) Posterior auricular artery as an alternative donor vessel for extracranial-intracranial bypass surgery. *Acta Neurochir (Wien)*, 156: 2095-2101.
- GOMEZ CK, ARNUK OJ (2013) Intrathoracic bifurcation of the right common carotid artery. *BMJ Case Rep*, 2013: bcr2012007554.
- GÜRBÜZ J, CAVDAR S, OZDOĞMUŞ O (2001). Trifurcation of the left common carotid artery: a case report. *Clin Anat*, 14: 58-61.
- HACEIN-BEY L, DANIELS DL, ULMER JL, MARK LP, SMITH MM, STROTTMANN JM, BROWN D, MEYER GA, WACKYM PA (2002) The ascending pharyngeal artery: branches, anastomoses, and clinical significance. *Am J Neuroradiol*, 23: 1246-1256.
- HANSDAK R, RUSTAGI SM, LOH HK, PAKHIDDEY R, SURI RK, MEHTA V (2015) Variant topography of the carotid arteries - a clinicoanatomical appraisal. *Int J Adv Res*, 3: 1-6.
- HAYASHI N, HORI E, OHTANI Y, OHTANI O, KUWAYAMA N, ENDO S (2005) Surgical anatomy of the cervical carotid artery for carotid endarterectomy. *Neurol Med Chir (Tokyo)*, 45: 25-30.
- LINS CCDSA, CAVALCANTI JS, NASCIMENTO DLD (2005) Extraoral ligature of lingual artery: anatomic and topographic study. *Int J Morphol*, 23: 271-274.
- LIVINI F. (1903) Le type normal et les variations de l'A. carotis externa. *Arch Ital Biol*, 39: 486-487.
- LO A, OEHLEY M, BARTLETT A, ADAMS D, BLYTH P, AL-ALI S (2006) Anatomical variations

of the common carotid artery bifurcation. *ANZ J Surg*, 76: 970-972.

LUČEV N, BOBINAC D, MARIĆ I, DREŠČIK I (2000) Variations of the great arteries in the carotid triangle. *Otolaryngol Head Neck Surg*, 122: 590-591.

MATA JR, MATA FR, SOUZA MCR, NISHIJO H, FERREIRA TAA (2012) Arrangement and prevalence of branches in the external carotid artery in humans. *Ital J Anat Embryol*, 117: 65-74.

MOMPEÓ B, BAJO E (2015) Carotid bifurcation - clinical relevance. *Eur J Anat*, 19: 37-45.

OZGUR Z, GOVSA F, OZGUR T (2008a) Anatomic evaluation of the carotid artery bifurcation in cadavers: implications for open and endovascular therapy. *Surg Radiol Anat*, 30: 475-480.

OZGUR Z, GOVSA F, OZGUR T (2008b) Assessment of origin characteristics of the front branches of the external carotid artery. *J Craniofac Surg*, 19: 1159-1166.

OZGUR Z, GOVSA F, CELIK S, OZGUR T (2009) Clinically relevant variations of the superior thyroid artery: an anatomic guide for surgical neck dissection. *Surg Radiol Anat*, 31: 151-159.

PATEL JP, DAVE RV, SHAH RK, KANANI SD, NIRVAN AB (2013) A study of superior thyroid artery in 50 cadavers. *Int J Biol Med Res*, 4: 2875-2878.

QUAIN R (1844) The anatomy of the arteries of the human body. *Taylor and Walton*, London, pp 55-112.

RAJAMANI K, CHATURVEDI S (2011) Stroke prevention-surgical and interventional approaches to carotid stenosis. *Neurother J Am Soc Exp Neurother*, 8: 503-514.

RIBEIRO RA, RIBEIRO JADS, FILHO OAR, CAETANO AG, FAZAN VPS (2006) Common carotid artery bifurcation levels related to clinical relevant anatomical landmarks. *Int J Morphol*, 24: 413-416.

SANJEEV IK, ANITA H, ASHWINI M, MAHESH U, RAIRAM GB (2010) Branching pattern of external carotid artery in human cadavers. *J Clin Diag Res*, 4: 3128-3133.

SHINTANI S, TERAKADO N, ALCALDE RE, TOMIZAWA K, NAKAYAMA S, UYAMA Y, ICHIKAWA H, SUGIMOTO T, MATSUMURA T (1999) An anatomical study of the arteries for intraarterial chemotherapy of head and neck cancer. *Int J Clin Oncol*, 4: 327-330.

SHIVALEELA C, ANUPAMA D, LAKSHMI PSR (2016) Study of anatomical variations in the origin of superior thyroid artery. *Int J Anat Res*, 4: 1765-1768.

SIEMIONOW M, KULAHCI Y (2007) Facial transplantation. *Semin Plast Surg*, 21: 259-268.

SMALL JE, HARRINGTON J, WATKINS E (2014) Prevalence of arterial branches arising from the extracranial internal carotid artery on CT angiography. *Surg Radiol Anat*, 36: 789-793.

TOHNAI I (2006) Chemotherapy using intra-arterial infusion for oral cancer. *Nagoya J Med Sci*, 68: 101-108.

TROUPIS T, MICHALINOS A, DIMOVELIS I, DEMESTICHA T, VLASIS K, SKANDALAKIS P (2014) Bilateral abnormal origin of the anterior branches of the external carotid artery. *Ann Vasc Surg*, 28: 494.e5-494.e7.

UZUN L, KOKTEN N, KILICASLAN A, TASEL B, KALCIOGLU MT, TEKIN M (2013) Bilateral lower cervical bifurcation of the common carotid artery. *Case Rep Otolaryngol*, 2013: 1-3.

VÁZQUEZ T, COBIELLA R, MARANILLO E, VALDERRAMA FJ, MCHANWELL S, PARKIN I, SAÑUDO JR (2009) Anatomical variations of the superior thyroid and superior laryngeal arteries. *Head Neck*, 31: 1078-1085.

WON SY (2016) Anatomical considerations of the superior thyroid artery: its origins, variations, and position relative to the hyoid bone and thyroid cartilage. *Anat Cell Biol*, 49: 138-141.

YONENAGA K, TOHNAI I, MITSUDO K, MORI Y, SAIJO H, IWAI T, YONEHARA Y, OTA Y, TORIGOE K, TAKATO T (2011) Anatomical study of the external carotid artery and its branches for administration of superselective intra-arterial chemotherapy via the superficial temporal artery. *Int J Clin Oncol*, 16: 654-659.

Influence of each hesperidin and insulin on diabetes-induced testicular alterations in adult albino rats

Maha S. Abd Elsamie, Mona H. Mohammed Ali, Omayma M. Mahmoud, Eman M. Kamel

Anatomy Department, Faculty of Medicine, Suez Canal University, Egypt

SUMMARY

Diabetes mellitus is a chronic metabolic disorder that adversely affects male reproductive organs, resulting in infertility due to testicular atrophy. Hyperglycemia and oxidative stress are considered the main factors implicated in the pathogenesis of diabetic complication. Hesperidin is a natural flavonoid with wide pharmacological effects such as hypoglycemic, antioxidant and anti-inflammatory. This work aims to study the ability of hesperidin to counteract diabetes-induced testicular alterations. 50 rats were used in this experiment, divided equally and randomly into five groups: control C, diabetic DM, diabetic +hesperidin DM+H, diabetic +insulin DM+In and hesperidin group H. At the end of the experiment, the rats were sacrificed and evaluated for body weight, blood sugar level, testicular weight, histopathological, immunohistochemistry, morphometric analyses, and spermatozoa analysis. Results revealed that DM significantly reduced the body and testicular weights, produced drastic histopathological, morphometric adverse changes of the testicular tissues and morphological abnormalities of the spermatozoa. Hesperidin produced valuable hypoglycemic effect, increased the body and testicular weights, ameliorated the histopathological changes, restored normal germinal epithelium and spermatogenesis, restored morphometric parameters and significantly decreased the morphological abnormalities of the spermatozoa caused by DM. Insulin could improve some parameters that were adversely changed

by DM, but less than the hesperidin. We conclude that treatment with hesperidin appeared to be more effective in counteracting the toxic effects of diabetes on testes than insulin.

Key words: Diabetes – Testis – Hesperidin – Insulin – Albino rats

INTRODUCTION

Diabetes mellitus is associated with reproductive impairment in both men and women. Its impact on reproduction can be profound, by a decrease in fertility and increase in reproductive failures (Ramalho-Santos et al., 2008). Male reproductive functions can be affected at multiple levels, including increased apoptosis in testicular germ cells, altered spermatogenesis, variation in sperm quality and quantity, decreased testicular weight, and ejaculatory dysfunction and reduced libido (Ricci et al., 2009; Jain and Jangir, 2014). Men with DM have low testosterone levels, associated with decreased luteinizing hormone and follicle-stimulating hormone concentrations. Therefore, diabetes-induced reproductive dysfunction is an important challenge (Ebong et al., 2014). Many articles explained that diabetic complications are due to hyperglycemia and overproduction of reactive oxygen species (ROS) that exceeds natural antioxidant defenses of the body, resulting in cell apoptosis (Ghlassi et al., 2012). Both testicular and sperm cells have increased susceptibility to free radical damage due to higher levels of

Corresponding author:

Omayma M. Mahmoud, Anatomy Department, Faculty of Medicine, Suez Canal University, Egypt. E-mail: omima34@hotmail.com

Submitted: August 16, 2020. Accepted: October 26, 2020

polyunsaturated fatty acids, low oxygen tension and lack of antioxidant defense mechanisms (Idris et al., 2012). Many natural products have hypoglycemic activity and significant antioxidant capacity (Ebong et al., 2014).

Intake of citrus fruits and their constituting flavonoids can reduce the risk of certain chronic diseases and increase survival (Jasmin and Jaitak, 2019). Hesperidin is the predominant flavonoid in lemons and oranges. Hesperidin had a wide range of biological effects including hypolipidemic, antioxidant, anti-inflammatory, hypoglycemic, anticarcinogenic activities and has anti-apoptotic efficacy (Elshazly et al., 2018). Hesperidin showed significant antioxidant potential in terms of scavenging free radicals produced by various *in vitro* assays. Hesperidin showed optimum protection against free-radical-induced cellular damage (Kalpana et al., 2009). Moreover, studies have shown that hesperidin is nontoxic and causes no allergic reactions in male or female mice (Acipayam et al., 2014). So, the present study was conducted in order to compare the effects of hesperidin and insulin in counteracting diabetes-induced testicular alterations in adult albino rats.

MATERIAL AND METHODS

Animals

Fifty adult male Sprague Dawley albino rats weighing 200-250 g were obtained from the animal house of Faculty Veterinary Medicine, Suez Canal University. The rats were acclimatized two weeks before drug administration, housed in a separate cage (10 rats each). The experiment was performed at the Animal and Experimental House, Anatomy department, Faculty of Medicine, Suez Canal University. All experiments were carried out in accordance with the guidelines of the Institutional Animals Ethics Committee of Suez Canal University.

Chemicals

Streptozotocin (STZ) and Insulin were purchased from Sigma pharmaceutical, Egypt. Hesperidin was purchased from Sigma Chemical, Co., St. Louis, Mo., USA

Experimental design

The rats were randomly divided into five groups (10 rats each), as follows:

- **Group I:** Control group (**C**), which was subdivided into:
 - Group IA: rats received nothing and served as negative control.
 - Group IB: rats received distilled water (the vehicle for hesperidin) orally, through an oral gavage, at a dose of 200 mg/kg/day for 10 consecutive days and served as positive control I (Arafa et al., 2009).
 - Group IC: rats received citrate buffer (the vehicle for STZ) intraperitoneally at a dose of 40 mg/kg just once and served as positive control II (Kassab et al., 2019; Ricci et al., 2009).
- **Group II:** Diabetes-induced group (**DM**), rats received STZ dissolved in citrate buffer intraperitoneally at a dose of 40 mg/kg just once. Seven days after STZ injection, rats were screened for fasting blood glucose levels (through blood obtained from a puncture of the tail vein). The rats having fasting blood glucose levels higher than 200 mg/dl were selected for experimentation (Kassab et al., 2019).
- **Group III:** Diabetes-induced group treated with hesperidin (**DM+H**). Diabetic rats received hesperidin dissolved in distilled water orally, through an oral gavage, at a dose of 200 mg/kg/day for 10 consecutive days once hyperglycemia was confirmed (Arafa et al., 2009).
- **Group IV:** Diabetes-induced group treated with insulin (**DM+In**). Diabetic rats received insulin subcutaneously at a dose of 15 IU/kg daily for 10 consecutive days, once hyperglycemia was confirmed (Moir and Zammit, 1994).
- **Group V:** Hesperidin-treated group (**H**). Rats received hesperidin dissolved in distilled water orally, through an oral gavage, at a dose of 200 mg/kg/day for 10 consecutive days (Arafa et al., 2009).

Animals weighed daily, and drug doses were adjusted accordingly. Rats were sacrificed 24 hours after the last dose of drugs. Testes were extracted, weighed, fixed in Bouin's solution,

embedded in paraffin and sectioned at 5 μm thickness (Mahmoud et al., 2014). Left testes were used to obtain testicular weight, processed for histopathological staining, immunohistochemical and morphometric measurements.

Immunohistochemistry

- Proliferating cell nuclear antigen (PCNA): Specific monoclonal anti- PCNA antibody was used to estimate the degree of cell proliferation. Positive PCNA labeling was detected in cells located at or near the basement membrane of the seminiferous tubules (Kanter et al., 2012).
- B cell leukemia/lymphoma-2 (Bcl-2): Bcl-2 is an anti-apoptotic protein. It expressed in most tubular cells with preferential expression in cytoplasm of the spermatids close to the luminal surface (Oldereid et al., 2001).

Morphometry

The seminiferous tubules' slides were examined at x400 magnification, captured using a light microscope coupled to a digital camera (Olympus, Japan). Thirty seminiferous tubules were randomly chosen and analyzed with ImageJ software (Schneider et al., 2012; Mahmoud et al., 2014; Kianifard et al., 2011). H&E-stained sections were used for measuring thickness of tunica albuginea, diameter of the seminiferous tubules, thickness of the basement membrane of the seminiferous tubules and seminiferous epithelium height (μm). PCNA-stained sections were analyzed for measuring the number of proliferating nuclei (Kanter et al., 2012). Bcl-2-stained sections of the testis were analyzed for measuring percentage area positively stained with Bcl-2 protein (Schiller et al., 2002).

Preparation of rat sperms

Spermatozoa were collected from rats' left cauda epididymis, according to methods described by (Suresh et al., 2010).

Statistical analysis

Results were analyzed using the Statistical Package of Social Science (SPSS) computer software, version 21. All data were reported as mean \pm standard deviation (SD). To evaluate significant differences, the comparison of means between each two experimental groups was done by One-way analysis of variance (ANOVA) and Post hoc Bonferroni tests. P value <0.05 was considered statistically significant and P value <0.01 was considered highly statistically significant.

RESULTS

Body weight, testicular weights and GSI

The rats in the DM, DM+H and DM+In groups showed a highly statistically significant decrease in the final body weight, testicular weight and GSI when compared to the C group. The final body weight and testicular weight of the rats in the H group show statistically insignificant difference when compared to the C group (Table 1).

Blood glucose levels

The rats in the DM, DM+H and DM+In groups showed a highly statistically significant increase in the blood glucose levels when compared to the C group. DM+H and the DM+In groups showed a highly statistically significant decrease in the blood glucose levels when compared to the DM group (Table 2).

Table 1. Means \pm SD of the body weight (initial and final), the testicular weight and GSI of the rats in the different study groups.

Parameter	Body weight (gm)			Testicular weight (gm)	GSI (%)
	Initial body weight	Final body weight	Changes (gain or loss)		
C	221.40 \pm 18.88	223.60 \pm 19.28	1.90 \pm 1.52	1.51 \pm 0.23	0.67 \pm 0.05
DM	218.10 \pm 16.36	181.80 \pm 8.70 ^{**a}	-36.20 \pm 13.16 ^{**a}	0.84 \pm 0.04 ^{**a}	0.45 \pm 0.01 ^{**a}
DM+H	218.20 \pm 12.00	204.40 \pm 8.47 ^{**a, **b}	-14.30 \pm 8.56 ^{**a, **b}	1.2 \pm 0.1 ^{**a, **b}	0.58 \pm 0.04 ^{**a, **b, c}
DM+In	217.90 \pm 16.41	190.10 \pm 8.86 ^{**a}	-27.80 \pm 19.75 ^{**a}	1.0 \pm 0.08 ^{**a, *b}	0.52 \pm 0.03 ^{**a, *b}
H	222.70 \pm 18.00	224.80 \pm 17.36 ^{**b}	2.10 \pm 1.79 ^{**b}	1.57 \pm 0.23 ^{**b}	0.68 \pm 0.05 ^{**b}

(*) P <0.05 ; (**) P <0.01 ; ^a compared to the C group; ^b compared to the DM group; ^c compared to the DM+In group

Table 2. Means ± SD of the blood glucose levels of the rats in the different study groups.

Group	Blood glucose levels (mg/dl)
C	85.9±13.27
DM	256.30±21.26 ^{**a}
DM+H	169.70±6.79 ^{**a, **b}
DM+In	183.50±3.92 ^{**a, **b}
H	74.9±2.42 ^{**b}

(*) P <0.05; (**) P <0.01; ^a compared to the C group; ^b compared to the DM group

Histopathological results of the testicular tissues

Control group:

The rat testes of the C group showed a normal histological architecture. Homogenous tunica albuginea surrounded closely packed seminiferous tubules, enveloped with normal basement membrane and myoid cells having flat nuclei. The tubules were lined by multiple layers of distinct germinal epithelial cells with normal shape and size. Spermatogonia appeared small with oval nucleus. 1ry spermatocytes appeared as the largest cells of all spermatogenic cell series, having large vesicular nucleus. 2ry spermatocytes were of a small size and vesicular nucleus. Spermatids also appeared as small cells with vesicular nucleus. Normal spermatozoa appeared filling the lumen of the seminiferous tubules. Sertoli cells, extending between the basal lamina and the tubular lumen, were normal in size and having oval nuclei. The interstitial tissue showed clusters of Leydig cells with distinct round nucleus and pale cytoplasm. Interstitial blood vessels were of normal wall thickness and normal diameter (Fig. 1).

PCNA: PCNA-positive cells were markedly detected in basal tubular compartment, presenting a single layer of brown PCNA-positive nuclei along the basement membrane of the seminiferous tubules (Fig. 5).

Bcl-2: marked cytoplasmic expression of brown Bcl-2 protein in most tubular cells with preferential staining close to the tubular lumen (staining mainly spermatids) (Fig.6).

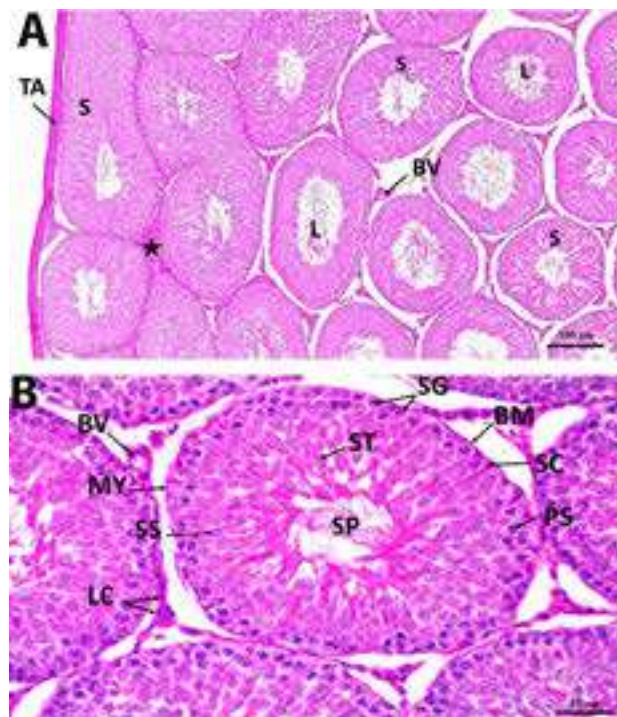


Fig. 1. Photomicrograph section in control rat testis group showing (A) homogenous tunica albuginea of normal thickness (TA), closely packed seminiferous tubules (S), germinal epithelium of normal height, lumen (L) full of spermatozoa, Normal interstitium (★) containing Leydig cells and normal blood vessels (BV)(H&E x 100). (B) normal different cells of the germinal epithelium, Spermatogonia (SG), 1ry spermatocytes (PS), 2ry spermatocytes (SS), spermatids (ST) and spermatozoa (SP). Normal sertoli cells (SC) are observed between the germinal cells. The seminiferous tubules are surrounded with a basement membrane of a normal thickness (BM) and myoid cells (MY). Interstitium shows clusters of Leydig cells (LC) and normal blood vessels (BV) (H&E x 400).

Hesperidin-treated group:

Sections of the testicular tissues of the H group showed no difference from the C group Diabetes-induced group:

The testes of the rats of the DM group showed a disrupted histological architecture. There was marked thickening of the tunica albuginea with cystic degeneration. The basement membranes surrounding the seminiferous tubules was also thickened. The seminiferous tubules decreased markedly in size. The germinal epithelium was strongly reduced in height with disrupted morphology, even atrophied in some tubules. Vacuolization was seen within the germinal epithelium. Marked decrease in the number of spermatozoa in the tubular lumen was detected. Some seminiferous tubules were even devoid completely of spermatozoa. The interstitial tissue showed marked edema and hemorrhage with dilated and congested thick-walled blood vessels. Leydig cells were remarkably damaged and decreased (Fig. 2).

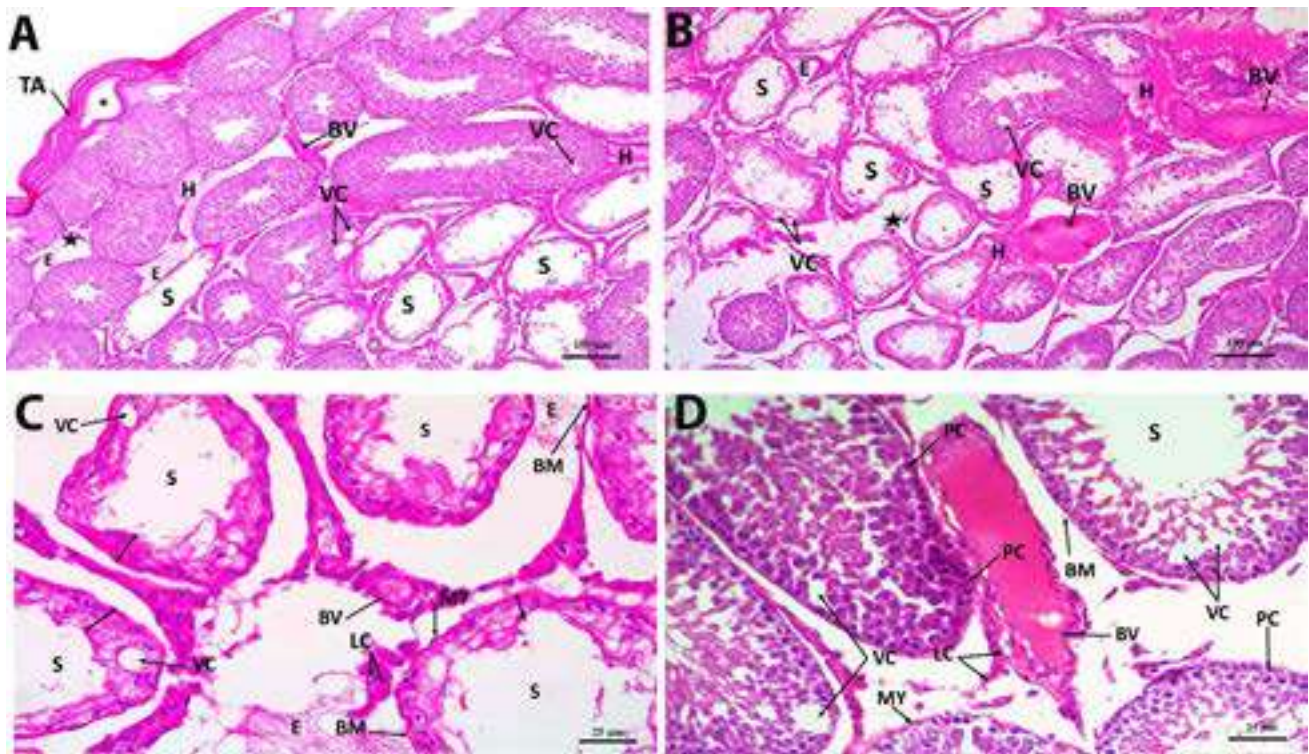


Fig. 2. Photomicrograph section in DM rat testis showing (A& B) thick tunica albuginea (TA) with cystic degeneration (*). Many seminiferous tubules show atrophied germinal epithelium (S), vacuolization (VC), lumen devoid of spermatozoa, Edema (E) and hemorrhage (H) are seen widely separating the tubules. Decreased interstitial mass is observed (*), dilated and congested thick-walled blood vessels (BV) (H&E x 100). (C) seminiferous tubules (S) having almost completely atrophied germinal epithelium (double-headed arrow), vacuolization (VC) and a lumen devoid of spermatozoa. The tubules are surrounded with detached thick basement membrane (BM) and myoid cells (MY). Leydig cells are distorted (LC), Edema (E), dilated congested thick-walled blood vessels (BV) (H&E x 400). (D) seminiferous tubule (S) with a lumen devoid of spermatozoa. The epithelium of other tubules shows pyknotic cells (PC). Vacuolization (VC) is found within the germinal epithelium. Detached basement membrane (BM) and myoid cells (MY) are seen surrounding the seminiferous tubules. Leydig cells are distorted (LC). Dilated congested, thick-walled blood vessel (BV) (H&E x 400).

PCNA: The number of brown PCNA-positive cells was more markedly decreased in the DM group than in the C group, even absent in some seminiferous tubules (Fig. 5).

Bcl-2: Testicular tissues obtained from the diabetic rats showed a weak expression of brown Bcl-2 protein in comparison to the C group (Fig. 6).

Diabetes-induced group treated with hesperidin:

Administration of hesperidin to the diabetic rats resulted in restoration of a near-normal morphology of the testicular tissues. The tunica albuginea was of homogenous morphology and appeared thinner than that observed in the DM group. The basal lamina surrounding the seminiferous tubules also appeared thinner when compared to that of the DM group. The germinal epithelium showed marked increased height when compared to the DM group. Almost all cell types of the germinal epithelium were noticed lining the seminiferous tubules. Spermatozoa were filling

the tubular lumen. However, some vacuolization was still seen within the germinal epithelium. The interstitial tissue showed a decrease in the edema and hemorrhage, and the blood vessels were much less congested with thinner walls than those observed in the DM group. Leydig cells were increased (Fig. 3).

PCNA: There was a moderate increase in the expression of brown PCNA-positive cells in the testicular tissues of the DM+H group in comparison to the DM group (Fig. 5).

Bcl-2: There was a moderate increase in brown Bcl-2 protein expression in the testicular cells of the DM+H group in comparison to the DM group (Fig. 6).

Diabetes-induced group treated with insulin:

Testicular tissues of diabetic rats treated with insulin showed some improvement when compared to that of DM group. The tunica albuginea appeared thinner, although sub-capsular hemorrhage was observed. Many

seminiferous tubules showed increased diameter and increased germinal epithelial height with restoration of the different types of cells; other tubules were lined with disorganized epithelium, devoid of spermatozoa and showed degenerative changes. Vacuolization was still seen within the germinal epithelium. Some interstitial edema and hemorrhage were still observed. The interstitial blood vessels showed congestion and thick walls. Increased number of Leydig cells was observed (Fig. 4).

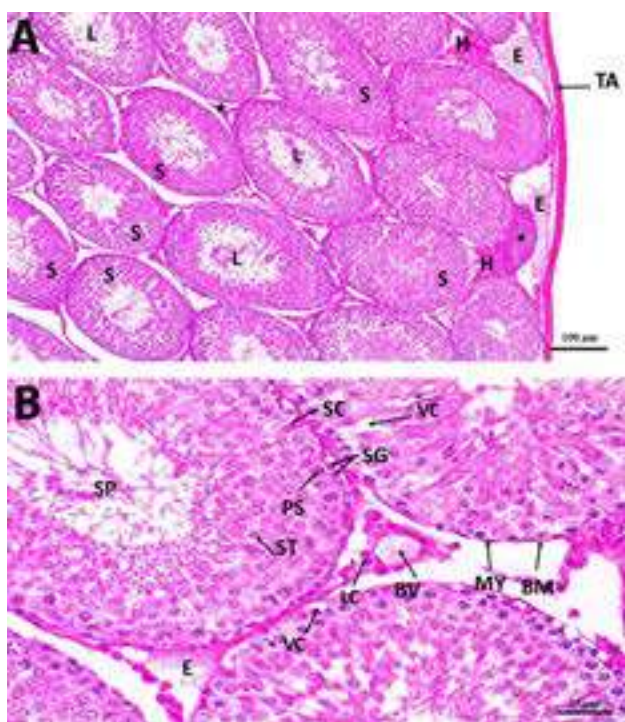


Fig. 3. Photomicrograph section in DM+H rat testis showing (A) homogenous tunica albuginea of an almost normal thickness (TA), closely packed seminiferous tubules (S) with regeneration of their germinal epithelium. The tubular lumen (L) is filled with spermatozoa. Degenerated seminiferous tubule is observed (*). Increase in the interstitial mass, containing Leydig cells, (★), edema (E) and hemorrhage (H) are still observed (H&E x 100). (B) The seminiferous tubules are surrounded with a basement membrane of a near-normal thickness (BM) and lined with almost regular germinal epithelium containing different types of cells. Spermatogonia (SG), 1ry spermatocytes (PS), spermatid (ST), spermatozoa (SP) and Sertoli cells (SC). Myoid cells are also seen surrounding the tubules (MY). Vacuolization (VC) is still found within the seminiferous tubules. Interstitium shows normal Leydig cells (LC), edema (E) and thin-walled dilated blood vessels (BV) (H&E x 400).

PCNA: There was a mild expression of brown PCNA-positive cells in the testicular tissues of the DM+In group when compared to the DM group (Fig. 5).

Bcl-2: There was a mild expression of brown Bcl-2 protein in the testicular tissues of the DM+In group when compared to the DM group (Fig. 6).

Morphometric results

1. Thickness of the tunica albuginea:

The rats of the DM, DM+H and DM+In groups showed a highly statistically significant increase in the thickness of the tunica albuginea when compared to the C group. On the other hand, the DM+H and DM+In groups showed a highly statistically significant decrease when compared to the DM group. The DM+H showed a highly statistically significant decrease in the thickness of the tunica albuginea when compared to the DM+In group. In the H group, the thickness of the tunica albuginea shows statistically insignificant difference from the C group (Table 3).

2. Tubular diameter:

The rats in the DM, DM+H and DM+In groups showed a highly statistically significant decrease in the tubular diameter in comparison to the C group. The DM+H and DM+In groups showed a highly statistically significant increase in the tubular diameter when compared to the DM group. Moreover, the DM+H showed a highly statistically significant increase in the tubular diameter when compared to the DM+In group. The rats in the H group showed a statistically insignificant difference in the tubular diameter when compared to the C group (Table 3).

3. Germinal epithelial height:

The rats in the DM, DM+H and DM+In groups showed a highly statistically significant decrease in the germinal epithelial height when compared to the C group. The DM+H group showed a highly statistically significant increase in the germinal epithelial height when compared to the DM group, while the DM+In group showed a statistically significant increase when compared to the DM group. The DM+H showed a highly statistically significant increase in the germinal epithelial height when compared to the DM+In group. The germinal epithelial height of the H group shows statistically insignificant difference from the C group (Table 3).

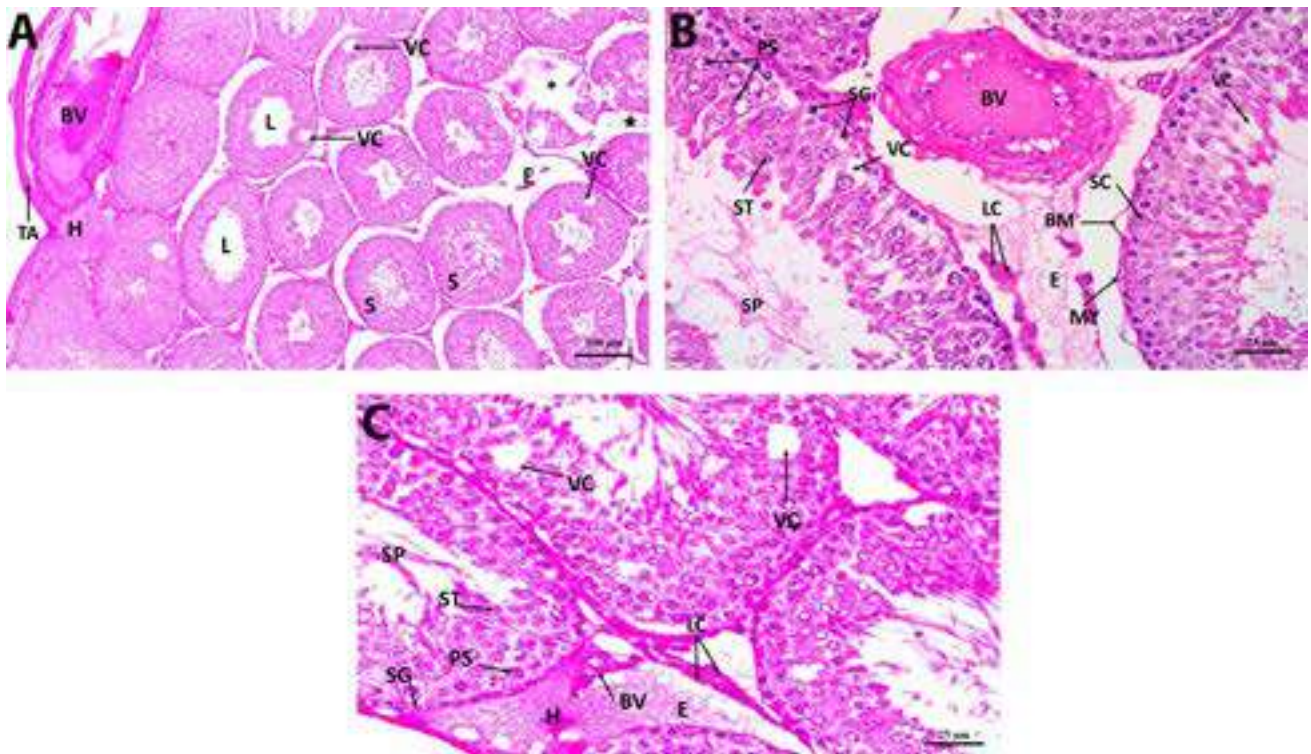


Fig. 4. Photomicrograph section in DM+In rat testis showing (A) thick tunica albuginea (TA), some seminiferous tubules appear normal (S), other tubules show vacuolization (VC), a lumen devoid of spermatozoa (L) and are degenerated (*). Distorted interstitial cells (\star), hemorrhage (H), edema (E) are still observed, dilated, congested thick-walled blood vessels appear in the tunica vasculosa (BV) (H&E x 100). (B) disorganized germinal epithelial cells lining the seminiferous tubules. Spermatogonia (SG), Iry spermatocytes (PS), spermatids (ST) and spermatozoa (SP) are seen. Sertoli cells (SC) are occasionally seen within the disrupted germinal cells. Vacuolization (VC) is still found within the seminiferous tubules. The tubules are surrounded with detached basement membrane (BM). Myoid cells (MY). Interstitium shows abnormal Leydig cells (LC), edema (E) and dilated, congested thick-walled blood vessels (BV) (H&E x 400). (C) disorganized germinal epithelial cells lining the seminiferous tubules. Spermatogonia (SG), Iry spermatocytes (PS), spermatids (ST) and spermatozoa (SP) are seen. Vacuolization (VC) is still found within the seminiferous tubules. Interstitium shows some regeneration of Leydig cells (LC), edema (E), hemorrhage (H) and thick-walled blood vessels (BV) (H&E x 400).

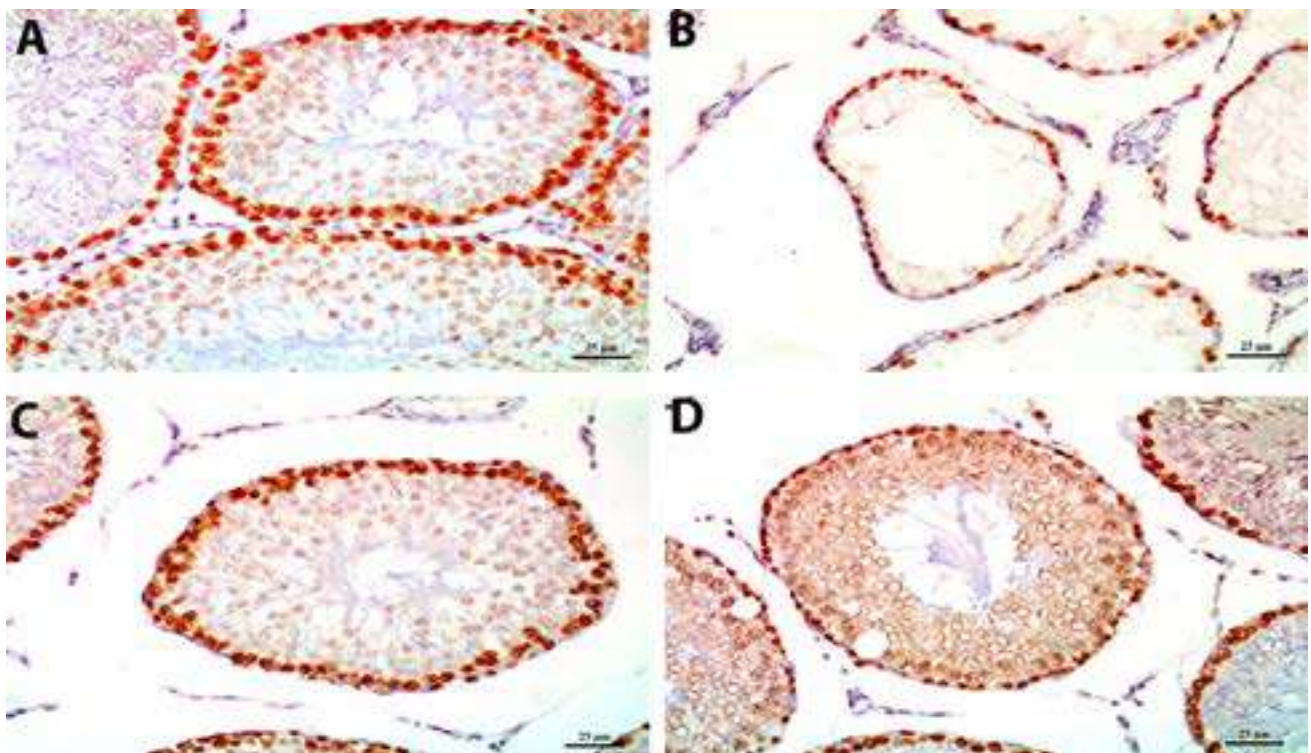


Fig. 5. A photomicrograph of a section of the rat seminiferous tubules with PCNA immuno-stain showing (A) **control group:** brown PCNA-positive nuclei that are markedly detected in the spermatogonia and early-stage spermatocytes. (B) **DM group:** marked decrease in the expression of brown PCNA-positive nuclei. (C) **DM+H group:** moderate expression of brown PCNA-positive nuclei. (D) **DM+In group:** mild expression of brown PCNA-positive nuclei (PCNA immuno-stain x 400).

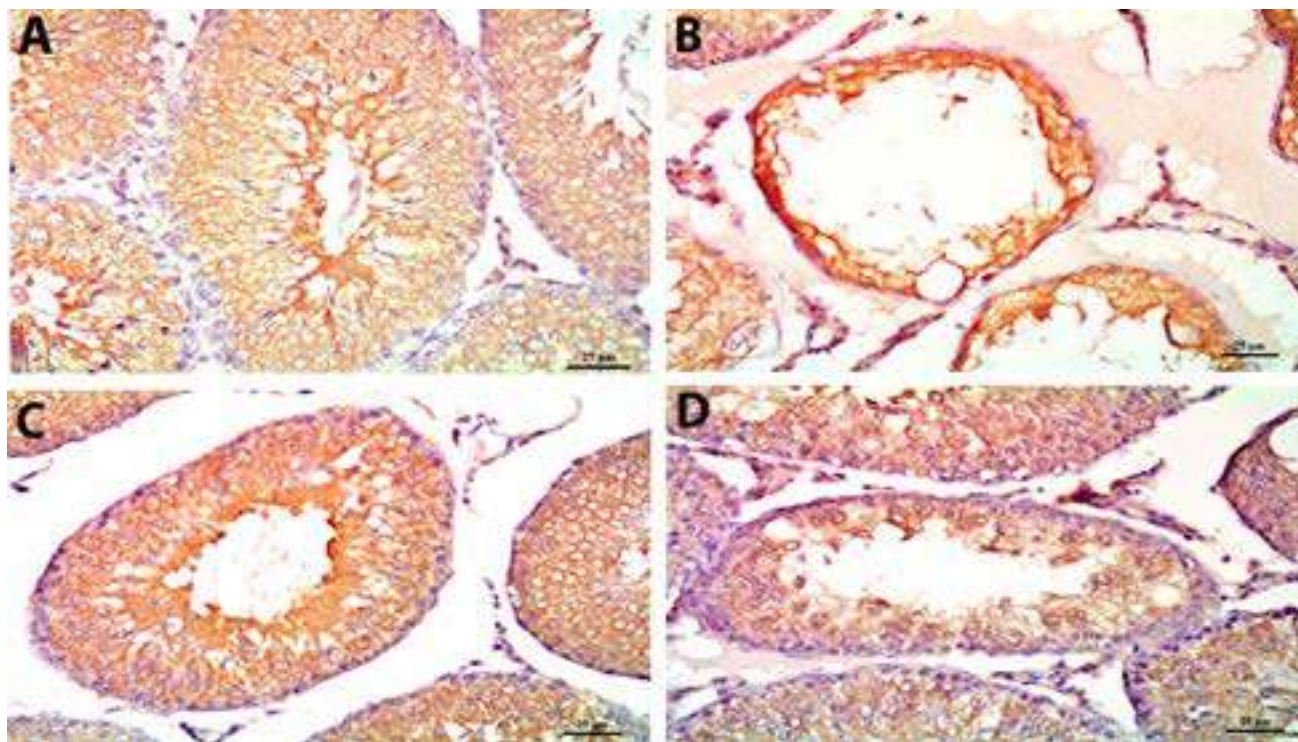


Fig. 6. A photomicrograph of a section of the rat seminiferous tubules with Bcl-2 immuno-stain showing (A) control group: marked expression of brown Bcl-2 protein in most tubular cells, mainly near the tubular lumen. (B) DM group: marked decrease in the expression of brown Bcl-2 protein in the tubular cells. (C) DM+H group: moderate expression of brown Bcl-2 protein in the tubular cells. (D) DM+In group: mild expression of brown Bcl-2 protein in the tubular cells (Bcl-2 immuno-stain x 400).

4. Thickness of the tubular basement membrane:

The rats in the DM, DM+H and DM+In groups showed a highly statistically significant increase in the thickness of the tubular basement membrane when compared to the C group. The DM+H and DM+In groups showed a statistically significant decrease in the thickness of the tubular basement membrane when compared to the DM group. The DM+H showed a statistically significant decrease in the thickness of the tubular basement membrane when compared to the DM+In group. The thickness of the tubular basement membrane of the H group show statistically insignificant change from the C group (Table 3).

5. Number of PCNA-positive cells:

The rats in the DM, DM+H and DM+In groups showed a highly statistically significant decrease in the number of PCNA-positive cells in comparison to the C group. The DM+H and DM+In groups showed a highly statistically significant increase in the number of PCNA-positive cells when compared to the DM group. The DM+H showed a highly statistically significant increase in the

number of PCNA-positive cells when compared to the DM+In group. The number of PCNA-positive cells of the H group did not show a statistically significant difference from the C group (Table 3).

6. Percentage area positively stained with Bcl-2:

The rats in the DM, DM+H and DM+In groups showed a highly statistically significant decrease in the percentage area positively stained with Bcl-2 in comparison to the C group. The DM+H and DM+In groups showed a highly statistically significant increase in the percentage area when compared to the DM group. The DM+H showed a highly statistically significant increase in the percentage area when compared to the DM+In group. The percentage area positively stained with Bcl-2 of the H group show a statistically insignificant difference from the C group (Table 3).

Sperm morphology

Normal sperm morphology was demonstrated in Fig. 7a. The normal sperm consists of head, neck, and tail. The current results showed a highly statistically significant decrease in the total

number of normal spermatozoa in the DM, DM+H and DM+In groups when compared to the C group. Head abnormalities were in the form of an absent head (Fig. 7b), a flat hook-less head (Fig. 7c) and an amorphous head (Fig. 7d). Neck abnormalities were mostly represented as a bent neck, either a backward bent (Fig. 7e) or a forward bent (Fig. 7f). Tail abnormalities detected were either a bent tail (Fig. 7g) or a ring tail (Fig. 7h). Also, a single sperm may exhibit multiple abnormalities (Fig. 7i) (Table 4).

DISCUSSION

DM is one of the most common endocrine metabolic disease. It affects numerous organs, system complications and dysfunction, including

reproductive system. Nearly 90% of patients with DM suffer from sexual dysfunction which includes impotence, reduced libido, impaired ejaculation, and impaired semen parameters. Hyperglycemia and oxidative stress were the main factors implicated in the pathogenesis of the diabetic complications. Oxidative stress in diabetic rats causes testicular DNA damage, depletion of spermatogenic cells and delay of spermatogenesis (Long et al., 2018). The current widespread hypoglycemic agents, besides causing several side effects, have no antioxidant effect and cannot prevent the progression of the diabetic complications (Ebong et al., 2014). Thus, a regimen that can cause hypoglycemia, target oxidative stress and improve diabetic complications is required.

Table 3. Means \pm SD of the morphometric parameters of the t in the different study groups.

Parameter Group	Tunica albuginea thickness (μ m)	Tubular diameter (μ m)	Germinal epithelial height (μ m)	Basement membrane thickness (μ m)	Number of PCNA-positive nuclei	Percentage area positively stained with Bcl-2 (%)
C	79.61 \pm 0.88	597.86 \pm 3.91	210.27 \pm 3.14	2.96 \pm 0.23	70.06 \pm 3.80	49.86 \pm 0.94
DM	97.83 \pm 2.46 ^{**a}	384.05 \pm 7.86 ^{**a}	80.49 \pm 16.10 ^{**a}	8.93 \pm 0.48 ^{**a}	40.30 \pm 1.78 ^{**a}	10.69 \pm 1.84 ^{**a}
DM+H	86.27 \pm 2.09 ^{**a, **b, **c}	558.40 \pm 6.19 ^{**a, **b, **c}	186.64 \pm 1.22 ^{**a, **b, **c}	6.12 \pm 0.50 ^{**a, **b, **c}	59.56 \pm 3.72 ^{**a, **b, **c}	32.91 \pm 1.33 ^{**a, **b, **c}
DM+In	89.48 \pm 2.11 ^{**a, **b}	412.84 \pm 6.35 ^{**a, **b}	142.04 \pm 11.01 ^{**a, **b}	7.64 \pm 0.58 ^{**a, **b}	50.03 \pm 2.88 ^{**a, **b}	23.19 \pm 1.15 ^{**a, **b}
H	79.46 \pm 1.19 ^{**b}	596.06 \pm 5.30 ^{**b}	210.76 \pm 2.55 ^{**b}	2.90 \pm 0.16 ^{**b}	69.90 \pm 3.73 ^{**b}	49.62 \pm 0.90 ^{**b}

(*) P <0.05; (**) P <0.01; ^a compared to the C group; ^b compared to the DM group; ^c compared to the DM+In group

Table 4. Means \pm SD of the different morphological abnormalities detected in the spermatozoa in the different study groups.

Parameter Group	Normal	Head			Neck	Tail		Multiple
		Absent head	Hook-less	Amorphous		Bent	Ring	
C	75 \pm 4.47	2 \pm 0.7	0.2 \pm 0.44	0.00 \pm 0.00	2.6 \pm 1.34	17.8 \pm 2.77	2.2 \pm 1.64	0.2 \pm 0.44
		Total=2.2\pm0.51				Total=20\pm4.41		
DM	6.8 \pm 2.28 ^{a**}	15 \pm 3.8 ^{a**}	6.2 \pm 2.48 ^{a**}	2.2 \pm 0.83 ^{a**}	5.2 \pm 1.78	47 \pm 4.06 ^{a**}	10 \pm 0.7 ^{a**}	9.8 \pm 1.64 ^{a**}
		Total=23.4\pm7.11				Total=57\pm4.76		
DM+H	51.6 \pm 5.59 ^{a**, b**}	5.2 \pm 1.64 ^{b**, c*}	1.8 \pm 1.3 ^{b**, c*}	0.6 \pm 0.54 ^{b**}	2.2 \pm 0.38 ^{b*}	26 \pm 5.45 ^{a**, b**, c**}	5.6 \pm 1.14 ^{a**, b*}	4.8 \pm 1.3 ^{a**, b**}
		Total=7.6\pm3.48				Total=31.6\pm6.59		
DM+In	28.6 \pm 7.75 ^{a**, b**}	7.8 \pm 2.16 ^{a**, b**}	3.6 \pm 2.3 ^{a**}	1.2 \pm 0.44 ^{a**, b**}	4 \pm 2.12	38.8 \pm 3.89 ^{a**, b*}	8 \pm 2.91 ^{a**}	6.8 \pm 0.83 ^{a**, b**}
		Total=12.6\pm4.9				Total=46.8\pm6.8		
H	78.2 \pm 5.06 ^{b**}	3.2 \pm 1.48 ^{b**}	1.2 \pm 0.83 ^{b**}	0.00 \pm 0.00 ^{b**}	0.8 \pm 0.83 ^{b**}	15.04 \pm 4.3 ^{b**}	1.8 \pm 0.83 ^{b**}	0.00 \pm 0.00
		Total=4.4\pm2.31				Total=21.84\pm13.87		

(*) P <0.05; (**) P <0.01; ^a compared to the C group; ^b compared to the DM group; ^c compared to the DM+In group

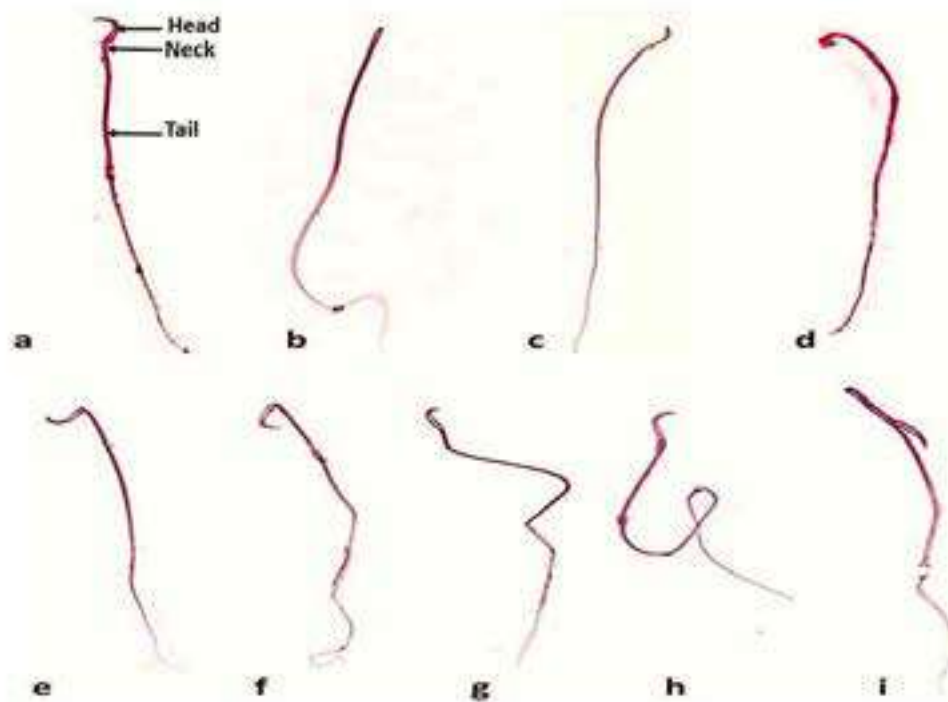


Fig. 7. A photomicrograph illustrating sperm morphology. a: normal (showing head, neck and tail), b: absent head abnormality, c: hook-less head abnormality, d: amorphous head abnormality, e: abnormal backward bent of the neck, f: abnormal forward bent of the neck, g: bent tail abnormality, h: ring tail abnormality and i: multiple abnormalities in a single sperm (note the hook-less head and the bent tail) (Eosin x 400).

In the current study, we compared the effect of hesperidin, a natural antioxidant, with the effect of insulin in counteracting testicular complications caused by DM.

The current results showed that the final body weight of the diabetic rats was reduced in a statistically significant way when compared to control group. Hesperidin administration increase body weight significantly while insulin did not significantly increase body weight of the rats. Weight loss of the rats observed in STZ-induced DM is not caused directly by the toxicity of STZ, but by the induction of DM (Jain and Jangir, 2014; Dkhil et al., 2016). Weight loss can be explained by loss of tissue proteins and increased muscle wasting that accompany DM (Cheng et al., 2013). STZ possibly prevents secretion of testosterone and growth hormone that results in disrupted anabolic activities, resulting in loss of weight (Long et al., 2018). The improvement of the body weight was attributed to the antioxidant effects of hesperidin and its capacity to enhance insulin secretion by pancreas, improve glucose metabolism, increase uptake of glucose by tissues and reverse most of the toxic effects of

DM (Visnagri et al., 2014). Administration of exogenous insulin does not increase the rate of muscle protein synthesis (Sudha et al., 2000; Trommelen et al., 2015).

The current study showed a statistically significant decrease in the testicular weight of DM group. Administration of hesperidin caused a highly significant increase in the testicular weight. Administration of insulin increased the testicular weight significantly. Oxidative stress and hyperglycemia had a marked destructive effect on the testicular cells, causing apoptotic death, damage of the tubular epithelial lining led to marked thinning of the epithelium and atrophy. This destruction of the testicular interstitial tissue results in testicular atrophy, reduction of weight and dysfunction (Idris et al., 2012; Long et al., 2018). Administration of hesperidin increased the testicular weight significantly and ameliorated testicular weight loss (Arafa et al., 2009; Kaya et al., 2015). The protective effects of hesperidin could be ascribed to its antioxidant potentials through scavenging free radicals, improving the antioxidant defense mechanisms in testicular tissues, which in turn inhibit apoptosis, enhance

spermatogenesis, regeneration of Leydig cells and restore testicular weight (Vijaya Bharathi et al., 2015). The restoration of testicular weight with insulin treatment is through its beneficial effect on the hypothalamic-pituitary-testicular axis, thus normalizing the secretion of testosterone by Leydig cells (Schoeller et al., 2012; Dkhil et al., 2016).

GSI is used to assess the damage to the testes in relation to the body (Latif et al., 2008). In the current study, the diabetic rats showed decrease in GSI when compared to the C group. Hesperidin treatment significantly increase GSI. Insulin treatment also showed a significant increase in GSI values, but less than hesperidin group. This may be due to the fact that testes were markedly affected in diabetic rats, and that the testicular weight decreased more than the total body weight (Sangameswaran and Jayakar, 2008). Controversially, some researchers found that GSI did not change in diabetic groups. This may be due to proportional decrease in the body and testicular weights. Hesperidin increase both body weight and testicular weight, thus increasing GSI (Alluanan Adelson do Nascimento et al., 2014; Ugarte et al., 2012).

STZ in this study produced a significant elevation of the blood glucose levels. Both hesperidin and insulin significantly lowered blood glucose levels. STZ hyperglycemia is explained by beta cell destruction and alters glucose metabolism (Ahmed et al., 2012; Ugarte et al., 2012). Hesperidin effects may be through attenuation of oxidative stress, decreasing production of pro-inflammatory cytokines, increasing the sensitivity of insulin receptors, inhibiting gluconeogenesis and ameliorating pancreatic damage (Ahmed et al., 2012; Mahmoud et al., 2015). Insulin can decrease blood glucose levels through stimulating glucose uptake by skeletal muscles and adipose tissue (Ramnanan et al., 2012; Newsholme and Dimitriadis, 2001).

Concerning the current results, testicular histopathological examination of DM group showed marked thickening of the tunica albuginea and the basal lamina, and widely separated seminiferous tubules with a significant decrease in their tubular diameter. Severe loss of the germinal epithelium with abnormal arrangement and morphology of the

remaining cells, widening of the tubular lumen and severe decrease in the number of spermatozoa in the tubular lumen were also seen. Damage to Leydig cells was observed. Interstitial tissues showed signs of inflammation in the form of edema, hemorrhage and dilated thick-walled blood vessels. Morphometric measurements of the testicular sections of the DM group confirmed the histopathological changes. Hesperidin administration markedly restored the structure of the testicular tissues and improved the morphometric measurements of the seminiferous tubules in diabetic rats. Insulin treatment caused mild improvement of the testicular architecture and significant improvement of the morphometric measurements. These alterations seen in the DM group could be explained by hyperglycemia which increase of cellular oxidative stress due to the overproduction of ROS and decreasing the antioxidant mechanisms. These high levels of ROS had a direct damaging effect on the tubular epithelium and Leydig cells, markedly increasing their apoptosis and atrophy, and consequently affecting sperm quantity and function (Kianifard et al., 2011; Alves et al., 2013). The diabetes-related hyperinsulinemia decreases LH levels, together with the destruction of Leydig cells, cause a decrease in the androgen biosynthesis and a decrease in the serum testosterone levels leading to a delayed abnormal spermatogenesis and a reduction in sperm output and fertility. The decreased tubular diameter is due to the atrophy of the germinal epithelium and the pressure caused by the surrounding interstitial edema and hemorrhage. The inflammatory process occurring in testis is due to the occurring oxidative stress and apoptosis, causing destruction of blood vessels, edema and hemorrhage (Ballester et al., 2004). Thick tunica albuginea and tubular basal lamina were explained by either increased collagen content, due to dysfunction of fibroblasts or glycation of the collagen. This thickness impairs blood supply to the testicular cells, thus increasing their damage and atrophy (Kianifard et al., 2011). The effects of hesperidin were attributed to its capacity to ameliorate the toxic effects of DM through its powerful antioxidant, hypoglycemic action, down-regulation of the pro-inflammatory cytokines, its beneficial effects on the capillary permeability and blood flow, it reduces diabetes-induced inflammatory edema, hemorrhage and

congested dilated blood vessels (Belhan et al., 2017). Insulin was unable to reverse the oxidative process and apoptosis in DM as it lacks the antioxidant/anti-apoptotic actions (Dkhil et al., 2016).

In the present study, PCNA-positive cells in the testicular tissues of the diabetic rats ranged from few cells in some seminiferous tubules to complete absence of positive cells in other tubules. The administration of hesperidin increased expression of PCNA-positive cells compared to DM group. The insulin-treated rats showed mild improvement in comparison to the DM group, but less than the hesperidin-treated group. The ability of hesperidin to stimulate the proliferation of cells in DM is attributed to its antioxidant/hypoglycemic, leading to enhanced cellular proliferation and survival stated by (Mahmoud and Hussein, 2014; Dkhil et al., 2016).

In this study, Bcl-2 sections of diabetic rats showed a marked decrease in the expression of the anti-apoptotic protein Bcl-2. Hesperidin markedly upregulated expression of Bcl-2 in the testicular tissues. Insulin was noticed to mildly increase Bcl-2 expression. This can be explained by increased testicular cell apoptosis accompanying DM (Jiang et al., 2015). Hesperidin provide evidence for the anti-apoptotic properties.

In the current work, sperm morphological abnormalities were increased significantly in the diabetic rats, in which tail abnormalities were the most common, followed by head abnormalities, then multiple abnormalities. Neck abnormalities were the least common. Administration of hesperidin to the diabetic rats greatly improved sperm abnormalities. Insulin treatment also lessened many sperm abnormalities. Increased abnormal sperm forms in the diabetic rats is attributed to disrupted glucose metabolism and the damaging effect of ROS to the spermatozoa. The susceptibility of the spermatozoa to ROS is high, particularly in the epididymis, because spermatozoa produced in the testis are reasonably more protected by the microenvironment of SCs, but they are less protected against oxidation in the epididymis, where they are stored. Oxidative stress led to DNA damage of the sperm cells, altered membrane functions, impaired motility, and decreased fertilization capacity. As insulin cannot

work as an antioxidant, some abnormalities were still seen with insulin treatment.

Conclusion

Treatment with hesperidin appeared to be more effective in counteracting the toxic effects of diabetes on testes than insulin.

Author contributions

All authors have been personally, equally and actively involved in substantive work leading to the manuscript and will hold themselves jointly and individually responsible for its content.

REFERENCES

- ACIPAYAM C, BAYRAM I, DAGLIOGLU K, DORAN F, YILMAZ S, SEZGIN G, TOTAN ATEŞ B, OZKAN A, TANYELI A (2014) The protective effect of hesperidin on methotrexate-induced intestinal epithelial damage in rats: an experimental study. *Medical Principles and Practice*, 23(1): 45-52.
- AHMED OM, MAHMOUD AM, ABDEL-MONEIM A, ASHOUR MB (2012) Antidiabetic effects of hesperidin and naringin in type 2 diabetic rats. *Diabetologia Croatica*, 41(2): 53-67.
- ALLUANAN ADELSON DO NASCIMENTO S, JESSICA SANTANA DE O, RODRIGO RIBEIRO DE O, SÍLVIA REGINA ARRUDA DE M, VALDEMIRO AMARO DA SILVA J, ELIZABETH NEVES DE M (2014) Evaluation of quantitative parameters of Leydig cell in diabetic adults rats. *Acta Scientiarum Biol Sci*, 36(4): 483-489.
- ALVES MG, MARTINS AD, RATO L, MOREIRA PI, SOCORRO S, OLIVEIRA PF (2013) Molecular mechanisms beyond glucose transport in diabetes-related male infertility. *Biochim Biophys Acta - Molecular Basis of Disease*, 1832(5): 626-635.
- ARAFI H, ALY H, ABD-ELLAH M, EL-REFAEY H (2009) Hesperidin attenuates benzo[α] pyrene-induced testicular toxicity in rats via regulation of oxidant/antioxidant balance. *Toxicol Industrial Health* 25(6): 417-427.
- BALLESTER J, MUÑOZ MC, DOMÍNGUEZ J, RIGAU T, GUINOVART JJ, RODRÍGUEZ-GIL JE (2004) Insulin-dependent diabetes affects testicular function by FSH- and LH-linked mechanisms. *J Androl*, 25(5): 706-719.

- BELHAN S, ÖZKARACA M, KANDEMİR FM, GÜLYÜZ F, YILDIRIM S, ÖMÜR AD, YENER Z (2017) Effectiveness of hesperidin on methotrexate-induced testicular toxicity in rats. *Kafkas Üniversitesi Veteriner Fakültesi Dergisi*, 23(5): 789-796.
- CHENG D, LIANG B, LI Y (2013) Antihyperglycemic effect of Ginkgo biloba extract in streptozotocin-induced diabetes in rats. *Biomed Res Int*, 2013: 162724.
- DKHIL MA, ZRIEQ R, AL-QURAI SHY S, ABDEL MONEIM AE (2016) Selenium nanoparticles attenuate oxidative stress and testicular damage in streptozotocin-induced diabetic rats. *Molecules*, 21(11): 1517.
- EBONG PE, EFIONG EE, MGBEJE BI, IGILE GO, ITAM EH (2014) Combined therapy of Moringa oleifera and Ocimum gratissimum reversed testicular damage in diabetic rats. *J Adv Med Medical Res*, 4(11): 2277-2290.
- ELSHAZLY SM, ABD EL MOTTELEB DM, IBRAHIM IAAEH (2018) Hesperidin protects against stress induced gastric ulcer through regulation of peroxisome proliferator activator receptor gamma in diabetic rats. *Chemico-Biological Interactions*, 291: 153-161.
- GHLISSI Z, HAMDEN K, SAOUDI M, SAHNOUN Z, ZEGHAL KM, EL FEKI A, HAKIM A (2012) Effect of Nigella sativa seeds on reproductive system of male diabetic rats. *Afr J Pharm Pharmacol*, 6 (20): 1444-1450.
- IDRIS MHM, BUDIN SB, OSMAN M, MOHAMED J (2012) Protective role of Hibiscus sabdariffa calyx extract against streptozotocin induced sperm damage in diabetic rats. *Excli Journal*, 11: 659- 669.
- JAIN G, JANGIR R (2014) Modulation of diabetes-mellitus-induced male reproductive dysfunctions in experimental animal models with medicinal plants. *Pharmacognosy Rev*, 8: 113-121.
- JASMIN, JAITAK V (2019) A review on molecular mechanism of flavonoids as antidiabetic agents. *Mini Reviews Med Chem*, 19 (9): 762-786.
- JIANG X, CHEN J, ZHANG C, ZHANG Z, TAN Y, FENG W, SKIBBA M, XIN Y, CAI L (2015) The protective effect of FGF21 on diabetes-induced male germ cell apoptosis is associated with up-regulated testicular AKT and AMPK/Sirt1/PGC-1 α signaling. *Endocrinology*, 156(3): 1156-1170.
- KALPANA KB, SRINIVASAN M, MENON VP (2009) Evaluation of antioxidant activity of hesperidin and its protective effect on H₂O₂ induced oxidative damage on pBR322 DNA and RBC cellular membrane. *Mol Cell Biochem*, 323(1): 21-29.
- KANTERM, AKTASC, ERBOGAM (2012) Protective effects of quercetin against apoptosis and oxidative stress in streptozotocin-induced diabetic rat testis. *Food Chemical Toxicol*, 50(3-4): 719-725.
- KASSAB BM, HUSSEIN HH, MAHMOUD OM, ABDEL-ALRAHMAN G (2019) Effects of insulin and metformin on fetal kidney development of streptozotocin-induced gestational diabetic albino rats. *Anat Cell Biol*, 52(2): 161-175.
- KAYA K, CIFTCI O, CETIN A, DOĞAN H, BAŞAK N (2015) Hesperidin protects testicular and spermatological damages induced by cisplatin in rats. *Andrologia*, 47(7): 793-800.
- KIANIFARD D, SADRKHANLOU RA, HASANZADEH S (2011) The histological, histomorphometrical and histochemical changes of testicular tissue in the metformin treated and untreated streptozotocin- induced adult diabetic rats. *Vet Res Forum*, 2 (1): 13-24.
- LATIF R, LODHI GM, ASLAM M (2008) Effects of amlodipine on serum testosterone, testicular weight and gonado-somatic index in adult rats. *J Ayub Med Coll, Abbottabad JAMC*, 20 (4): 8-10.
- LONG L, QIU H, CAI B, CHEN N, LU X, ZHENG S, YE X, LI Y (2018) Hyperglycemia induced testicular damage in type 2 diabetes mellitus rats exhibiting microcirculation impairments associated with vascular endothelial growth factor decreased via PI3K/Akt pathway. *Oncotarget*, 9 (4): 5321-5336.
- MAHMOUD AM, HUSSEIN OE (2014) Hesperidin as a promising anti-diabetic flavonoid: the underlying molecular mechanism. *Int J Food Nutr Sci*, 3 (3): 1.
- MAHMOUD AM, AHMED OM, ASHOUR MB, ABDEL-MONEIM A (2015) In vivo and in vitro

antidiabetic effects of citrus flavonoids; a study on the mechanism of action. *Int J Diabetes Dev Countries*, 35 (3): 250-263.

MAHMOUD OM, AL BADAWI MH, SALEM NA (2014) Role of Ginseng on mercury chloride-induced testicular lesions in adult albino rat: a histological and immunohistochemical study. *Egypt J Histol*, 37 (3): 506-513.

MOIR AMB, ZAMMIT VA (1994) Effects of insulin treatment of diabetic rats on hepatic partitioning of fatty acids between oxidation and esterification, phospholipid and acylglycerol synthesis, and on the fractional rate of secretion of triacylglycerol in vivo. *Biochem J*, 304 (1): 177-182.

NEWSHOLME EA, DIMITRIADIS G (2001) Integration of biochemical and physiologic effects of insulin on glucose metabolism. *Exp Clin Endocrinol Diabetes*, 109 (Suppl 2): S122-S134.

OLDEREIDNB, ANGELIS PD, WIGER R, CLAUSEN OP (2001) Expression of Bcl-2 family proteins and spontaneous apoptosis in normal human testis. *Mol Human Reprod*, 7 (5): 403-408.

RAMALHO-SANTOS J, AMARAL S, OLIVEIRA PJ (2008) Diabetes and the impairment of reproductive function: possible role of mitochondria and reactive oxygen species. *Current Diabetes Rev*, 4 (1): 46-54.

RAMNANAN CHRISTOPHER J, EDGERTON DALE S, CHERRINGTON ALAN D (2012) Evidence against a physiologic role for acute changes in CNS insulin action in the rapid regulation of hepatic glucose production. *Cell Metab*, 15 (5): 656-664.

RICCI G, CATIZONE A, ESPOSITO R, PISANTI FA, VIETRI MT, GALDIERI M (2009) Diabetic rat testes: morphological and functional alterations. *Andrologia*, 41 (6): 361-368.

SANGAMESWARAN B, JAYAKAR B (2008) Anti-diabetic, anti-hyperlipidemic and spermatogenic effects of *Amaranthus spinosus* Linn. on streptozotocin-induced diabetic rats. *J Nat Med*, 62 (1): 79-82.

SCHILLERAB, CLARK WS, COTSONISG, LAWSON D, DEROSE PB, COHEN C (2002) Image cytometric bcl-2:bax and bcl-2:bcl-x ratios in invasive breast

carcinoma: correlation with prognosis. *Cytometry*, 50 (4): 203-209.

SCHNEIDER CA, RASBAND WS, ELICEIRI KW (2012) NIH Image to ImageJ: 25 years of image analysis. *Nature Methods*, 9 (7): 671-675.

SCHOELLER EL, ALBANNA G, FROLOVA AI, MOLEY KH (2012) Insulin rescues impaired spermatogenesis via the hypothalamic-pituitary-gonadal axis in Akita diabetic mice and restores male fertility. *Diabetes*, 61 (7): 1869.

SUDHA S, VALLI G, JULIE PM, ARUNAKARAN J, GOVINDARAJULU P, BALASUBRAMANIAN K (2000) Influence of streptozotocin-induced diabetes and insulin treatment on the pituitary-testicular axis during sexual maturation in rats. *Exp Clin Endocrinol Diabetes*, 108 (01): 14-20.

SURESH S, PRITHIVIRAJ E, PRAKASH S (2010) Effect of *Mucuna pruriens* on oxidative stress mediated damage in aged rat sperm. *Int J Androl*, 33 (1): 22-32.

TROMMELEN J, GROEN B, HAMER HM, GROOT CPGMD, LOON LJC (2015) Exogenous insulin does not increase muscle protein synthesis rate when administered systemically: a systematic review. *Eur J Endocrinol*, 173: R25-R34.

UGARTE M, BROWN M, HOLLYWOOD KA, COOPER GJ, BISHOP PN, DUNN WB (2012) Metabolomic analysis of rat serum in streptozotocin-induced diabetes and after treatment with oral triethylenetetramine (TETA). *Genome Medicine*, 4 (4): 35.

VIJAYA BHARATHI B, JAYA PRAKASH G, KRISHNA KM, RAVI KRISHNA CH, SIVANARAYANA T, MADAN K, RAMA RAJU GA, ANNAPURNA A (2015) Protective effect of alpha glucosyl hesperidin (G-hesperidin) on chronic vanadium induced testicular toxicity and sperm nuclear DNA damage in male Sprague-Dawley rats. *Andrologia*, 47 (5): 568-578.

VISNAGRI A, KANDHARE AD, CHAKRAVARTY S, GHOSH P, BODHANKAR SL (2014) Hesperidin, a flavanoglycone attenuates experimental diabetic neuropathy via modulation of cellular and biochemical marker to improve nerve functions. *Pharmaceutical Biol*, 52 (7): 814-828.

Anatomical study of the external pudendal artery at the anatomy laboratory of Bamako

Tata Touré¹, Babou Ba¹, Abdoulaye Kanté^{1,2}, Moumouna Koné¹, Gaoussou Simpara¹, Ousmane I. Touré¹, Mahamadou Daou¹, Falé Traoré¹, Demba Yatera¹, Nouhoum Ongoïba^{1,2}

¹ Anatomy laboratory of the Faculty of Medicine and Odontostomatology of Bamako, Mali

² Surgery Department B of the University Hospital Center of Point-G, Bamako, Mali

SUMMARY

The aim of this work was to specify the number of the external pudendal arteries and describe its origin as well as its relationship with the arch of the great saphenous vein. We dissected the external pudendal artery 72 times in 36 cadaveric subjects (29 men and 7 women) in the anatomy laboratory of the Faculty of Medicine and Odontostomatology in Bamako. There was a single external pudendal artery in 40 cases (55.56%). Two external pudendal arteries existed in 30 cases (41.67%). In 2 cases, three external pudendal arteries were present. The most common origins of the external pudendal artery were the common and superficial femoral arteries. In 1 case, the external pudendal artery originated from the quadricipital artery. The most common relationship of the external pudendal artery with the arch of the great saphenous vein was the sub-crossing of the latter by the single external pudendal artery. This report was noted in 32 cases (44.44%). In 7 cases (9.72%), the single external pudendal artery passed in front of the great saphenous vein and behind the lateral accessory saphenous vein. Most often there is only one EPA. When there are two EPA, they can be born in isolation or through a common core. The EPA contracts variable and close relationships with the butt of the GSV. Since lesions of the EPA can lead to sexual impotence, its origin

and these relationships with the buttocks of GSV must be known by surgeons to avoid damaging it during surgical treatment of varicose veins of the pelvic limb.

Key words: External pudendal artery – Great saphenous vein arch – Femoral artery

Abbreviations:

CFA = Common femoral artery

EPA = External pudendal artery

GSV = Great saphenous vein

SFA = Superficial femoral artery

INTRODUCTION

There are two external pudendal arteries (formerly called external shame arteries), superficial (or upper) and deep (or lower), which arise from the medial side of the common femoral artery (Bouchet and Cuilleret, 1996).

The branches of the external pudendal artery (EPA) incidentally supply the penis. The latter is mainly vascularized by the branches of the internal pudendal artery (Droupy et al, 1997). Due to an acquired or congenital cause, the vascularization of the penis can be provided exclusively by the

Corresponding author:

Tata Touré. Anatomy laboratory of the Faculty of Medicine of Bamako, Mali. Phone: (00223)78008900. E-mail: ttbaba@gmail.com

Submitted: November 5, 2020. Accepted: November 29, 2020

branches of the EPA; in this case, degenerative involvement during a chronic illness or trauma, for example surgical, of a dominant EPA can lead to erection difficulty by reducing the flow of blood in the corpora cavernosa (Macchi et al, 1996).

Anatomically, the EPA has variable but very close relationships with the arch of the great saphenous vein (GSV) (Henriet, 1987). In vascular surgery, the latter is dissected and sectioned as part of surgery for varicose veins of the pelvic limb. Thus, at the time of approaching the femoral trigone or dissecting the butt and trunk of the GVS, the EPA can be ligated with the afferents of the butt or completely severed (Gaye et al, 2016).

In plastic surgery, the flaps based on the superficial EPA have been used in the repair of skin defects of the penis rod after fitting prosthesis, in vulvar reconstruction, and in reconstruction of skin lesions of the hand (Thate et al, 1986; Mayer and Rodriguez, 1991; Abe et al, 1992; George et al, 1996).

There has not been much study on the EPA and data are lacking for the Malian population. We undertook this work with the objective of:

- specify the number of the EPA;
- describe the variations of origin of the EPA;
- and describe the relationship of the EPA with the arch of GSV.

MATERIALS AND METHODS

It was a prospective study carried out at the anatomy laboratory of the Faculty of Medicine and Odontostomatology of Bamako during a period of 20 months going from July 26, 2018 to March 14, 2020. We dissected the external pudendal artery 72 times (36 times on the left and right) in 36 corpses including 29 men and 7 women. We included in this study all fresh corpses bearing no trace of trauma or operative scar in the upper half of the anterior aspect of the thigh. We excluded from this study all corpses showing traces of trauma or operative scar in the upper half of the anterior aspect of the thigh. The dissection was performed at the femoral trigone by making 3 skin incisions. The first, oblique incision extended from the anterosuperior iliac spine to the upper medial part of the anterior aspect of the thigh

via the pubic spine. The second vertical incision started from the middle of the first incision to the junction of the upper 1/3 and the lower 2/3. The third, transverse incision passed through the lower end of the previous incision. After these incisions, the skin was peeled off, 3 skin flaps were obtained and folded down inside, outside and above. Then, the subcutaneous cell tissue was dissected for GSV. The latter was dissected with the tributary veins of its butt. The EPA was sought at the saphenofemoral junction and dissected to its origin. The femoral artery and vein were also dissected. After these dissections, the photos were taken with the camera of a Samsung Galaxy J6 + phone. The following parameters were noted: the sex of the cadaveric subject; the dissected side; the number, origin and mode of birth of the EPA, and finally the relationship of the EPA with the butt of the GSV.

The data were entered and analyzed using the Epi info software. A comparison between men and women, and between the left and right sides, was made with the Fischer test.

Concerning the ethical aspect, during this work the respect for the anonymity of cadaveric subjects and the confidentiality of information were required.

RESULTS

Number

The EPA was visible in all cases. There was only one EPA in 40 cases (55.56%), including 22 cases on the right and 18 cases on the left. According to sex, the presence of a single EPA was observed 33 times in men and 7 times in women. The presence of two APE, superficial and deep, was noted in 30 cases (41.67%); depending on the side, it was observed in 13 cases on the right and in 17 cases on the left; by sex, it was observed in men in 24 cases and in women in 6 cases. In 2 cases, there were 3 EPA, superficial, middle and deep; one case was observed in a man on the right; the other case was seen in a woman on the left.

The difference was not significant between men and women or between the right and left sides, because $P > 0.05$. The number of EPA is summarized in Fig. 1.

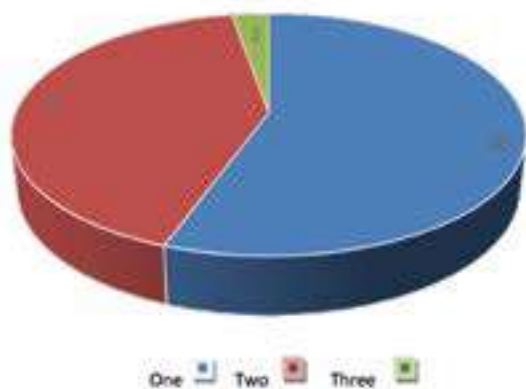


Fig. 1.- Number of EPA.

Origin

In the 40 cases where there was only one EPA, it came from the common femoral artery (CFA) (Fig. 2) in 18 cases and from the superficial femoral artery (SFA) (Fig. 3) in 22 cases. According to the side, it came from the CFA in 10 cases on the right and in 8 cases on the left; it came from SFA in 12 cases on the right and 10 cases on the left. According to sex, the presence of a single EPA which came from CFA was observed 15 times in men and 3 times in women, the presence of a single EPA which came from SFA was observed 18 times in men and 4 times in women.

In the 30 cases where there were two EPA, we noted 4 types of origin of superficial and deep EPA:

- First, the two superficial and deep EPA are both from the CFA. This type of origin was noted in 17 cases. Depending on the side, it was observed in 6 cases on the right and in 11 cases on the left; by sex, it was observed in 13 cases in men and in 4 cases in women.
- Second, the superficial EPA comes from the CFA and the deep EPA from the AFS (Fig. 4). This type of origin of the EPA was observed in 7 cases. Depending on the side, it was observed in 4 cases on the right and in 3 cases on the left; by sex, it was observed in 6 cases in men and in 1 case in women.
- Third, the superficial EPA and deep EPA both come from the SFA. This type of origin of the EPA was noted in 5 cases. Depending on the side, it was observed twice on the right and three times on the left; by sex, it was observed 4 times in men and 1 time in women.
- The fourth type of origin was the origin of the superficial EPA of the quadricipital artery and the deep EPA of the SFA (Fig. 5). This type of origin has been observed in a man on the right.

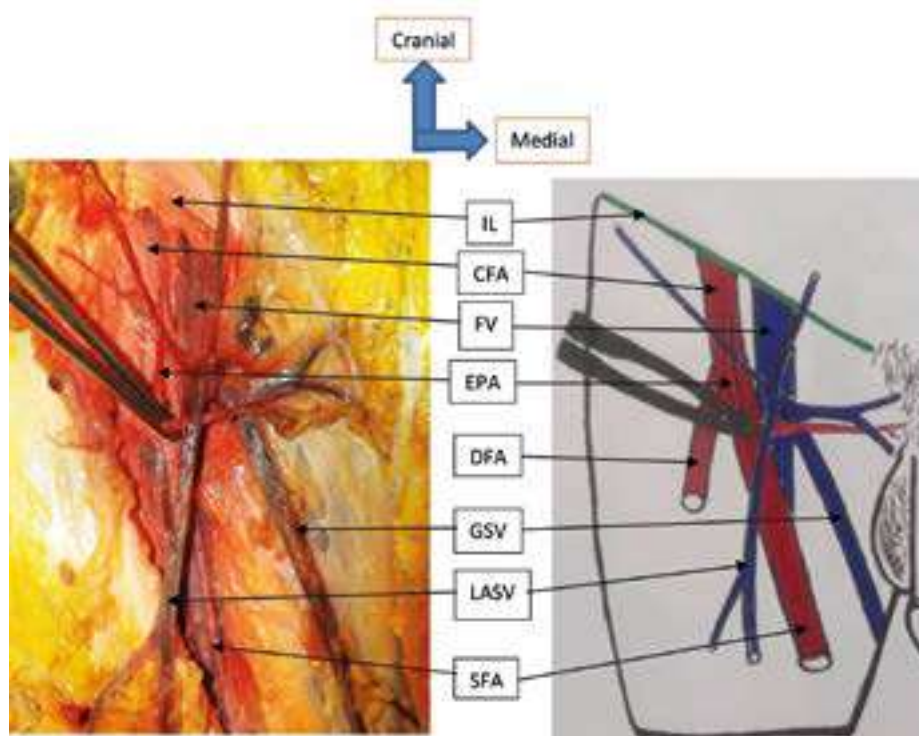


Fig. 2.- Unique EPA which came from the CFA and which pre-crossed the GSV passing behind the LSVA. CFA=Common femoral artery, DFA=Deep femoral artery, EPA=External pudendal artery, FV=Femoral vein, GSV=Great saphenous vein, IL=Inguinal ligament, LASV=Lateral accessory saphenous vein, SFA=Superficial femoral artery.

- In the 2 cases where there were 3 EPA, the superficial EPA came from the CFA and the middle and deep EPA came from by a common trunk of the SFA. One of these 2 cases was observed in a man on the right; the other case was observed in a woman on the left.

Original mode

In all cases where there was only one EPA, it was born in isolation (Figs. 2 and 3). Among the cases where there were 2 EPA, in 15 cases (20, 83) the superficial EPA and the deep EPA originated in isolation (Fig. 4). This mode of birth was observed 7 times on the right and 8 times on the left. According to sex, it has been observed 13 times in men 2 times in women. In 13 cases (18.06%), the superficial EPA and the deep EPA originated through a common trunk (Fig. 6). Depending on the side, this mode of birth was observed 4 times on the right and 9 times on the left. By sex, it has been observed 9 times in men and 4 times in women. In 2 cases, the superficial EPA originated through a common trunk with the superficial epigastric

artery, and the deep EPA originated in isolation. These 2 cases were observed in men on the right.

Among the 2 cases where there were 3 EPA, in 1 case the superficial EPA originated by a common trunk with the superficial epigastric and iliac circumflex arteries; the middle and deep EPA originated by a common trunk. This disposition was noted in a man on the right. In the other case, the superficial EPA originated by a common trunk with the inferior epigastric artery; the middle and deep EPA were born by a common trunk. This disposition was observed in a woman on the left.

Reports of the external pudendal artery with the arch of the great saphenous vein

The most frequent relationship of the EPA with the arch of the GSV was the sub-crossing of the arch of the GSV by the single EPA (Fig. 3). This disposition was observed in 32 cases (44.44%). Depending on the side, it was observed in 17 cases on the right and in 15 cases on the left; by sex, it was observed in 25 cases in men and in 7 cases in women.

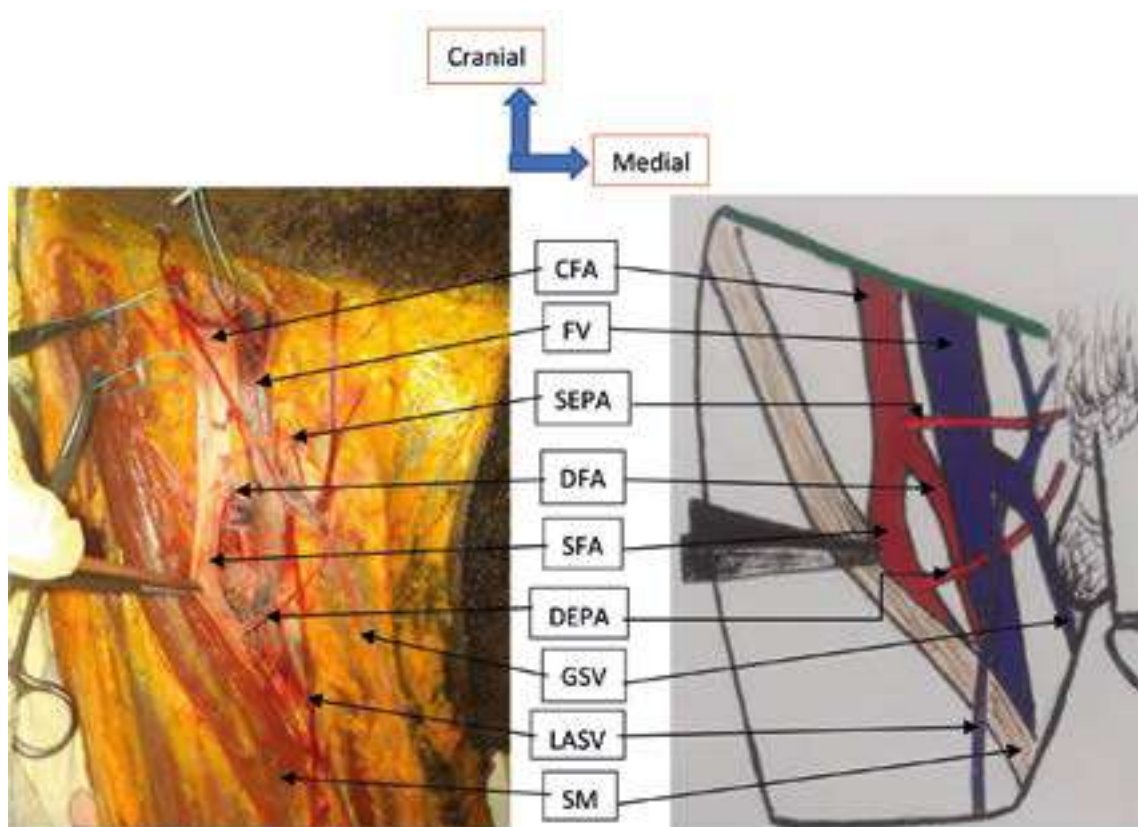


Fig. 3.- Presence of single EPA which came from the SFA and which sub-crossed the arch of GSV. CFA=Common femoral artery, DFA=Deep femoral artery, EPA=External pudendal artery, FV=Femoral vein, GSV=Great saphenous vein, LASV=Lateral accessory saphenous vein, SFA=Superficial femoral artery.

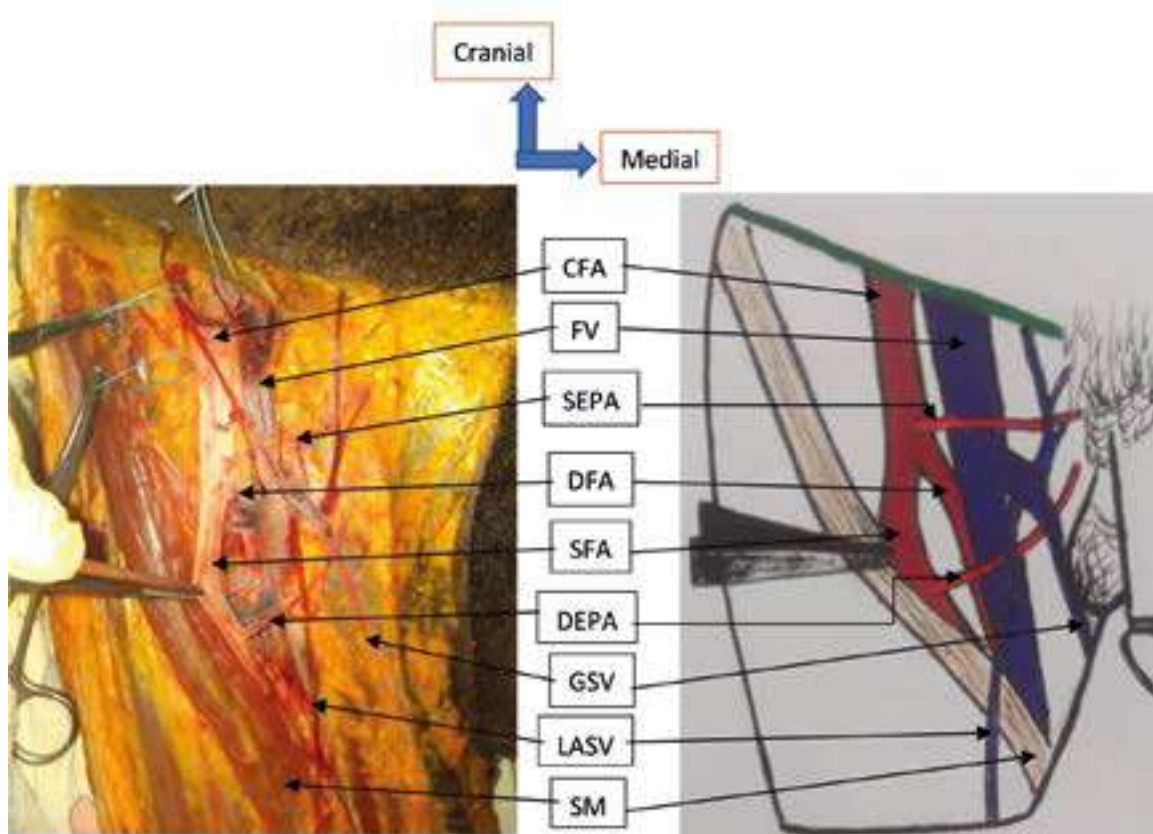


Fig. 4.- Presence of two isolated EPA, the superficial EPA originated from CFA and passed over the arch of the GSV, the deep EPA originated from the SFA and passed below the arch of the GSV. CFA=Common femoral artery, DEPA=Deep external pudendal artery, DFA=Deep femoral artery, FV=Femoral vein, GSV=Great saphenous vein, LASV=Lateral accessory saphenous vein, SEPA=Superficial external pudendal artery, SFA=Superficial femoral artery, SM=Sartorius muscle.

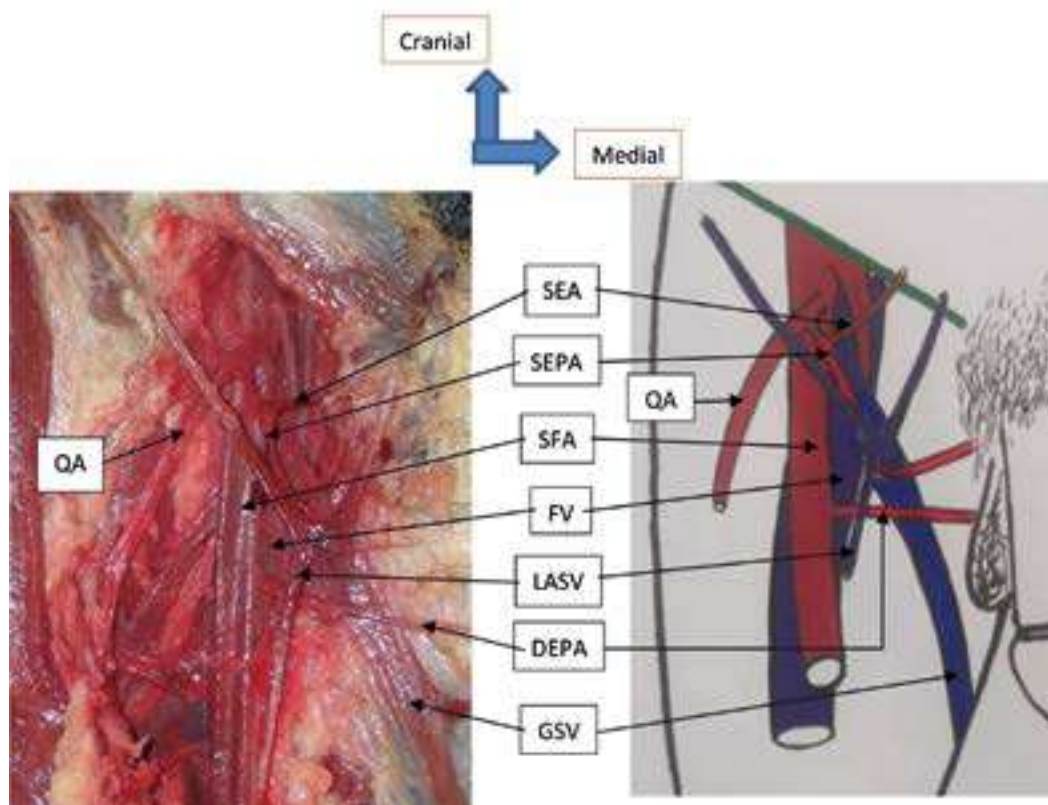


Fig. 5.- Two isolated EPA, the SEPA came from the QA through a common trunk with the SEA, the DEPA came from the SFA. Both EPA passed between the GSV in the back and the SVLA in the front. CFA=Common femoral artery, DEPA=Deep external pudendal artery, FV=Femoral vein, GSV=Great saphenous vein, LASV=Lateral accessory saphenous vein, QA=Quadricipital artery, SEA=Superficial epigastric artery, SEPA=Superficial external pudendal artery, SFA=Superficial femoral artery.

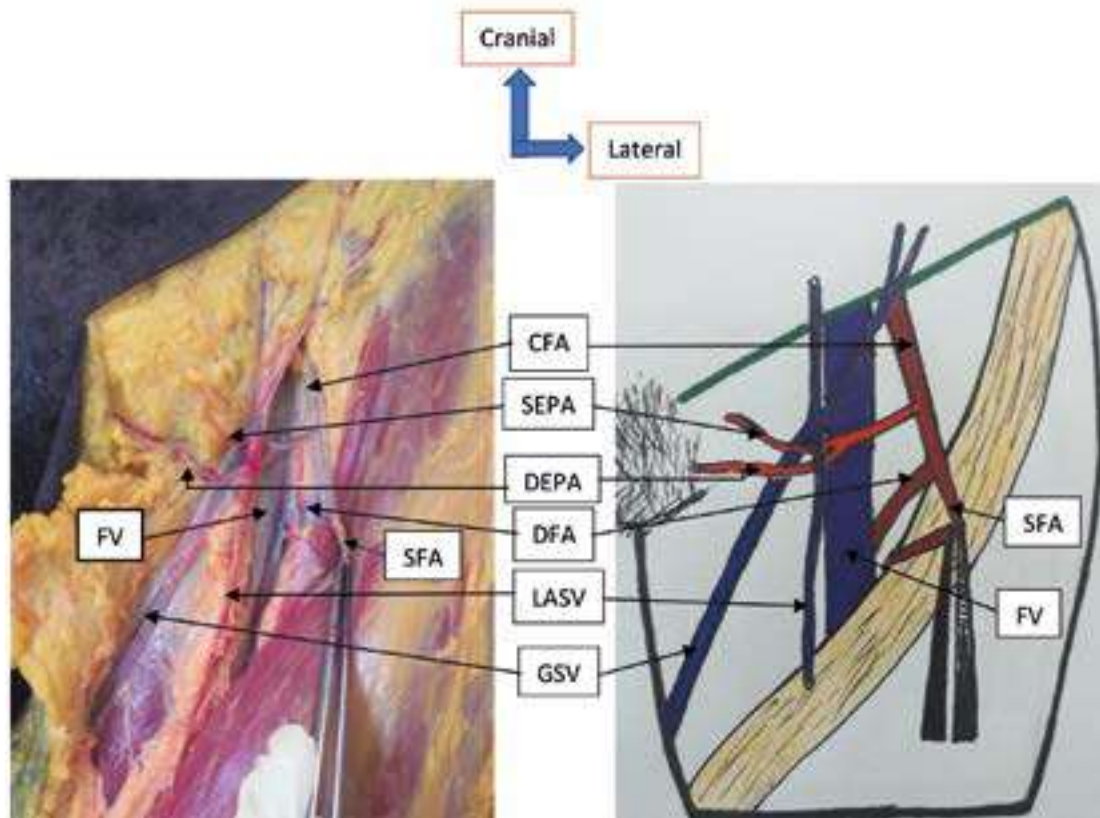


Fig. 6.- The superficial and deep EPA originated by a common trunk of the CFA. The common trunk split before reaching the arch of the GSV and both EPA passed between the GSV in the back and the SVLA in the front. CFA=Common femoral artery, DEPA=Deep external pudendal artery, DFA=Deep femoral artery, FV=Femoral vein, GSV=Great saphenous vein, LASV=Lateral accessory saphenous vein, SEPA=Superficial external pudendal artery, SFA=Superficial femoral artery.

In 7 cases (9.72%), there was a single EPA which pre-crossed the GSV passing behind the lateral accessory saphenous vein (Fig. 2). According to the side, this report was noted 4 times on the right and 3 times on the left; by sex, it was noted only in men.

In 11 cases (15.28%), the superficial EPA and the deep EPA originated in isolation, which the superficial EPA passing above the arch of the GSV, and the deep EPA passing below of the arch of the GSV (Fig. 4). Depending on the side, this arrangement was observed 5 times on the right and 6 times on the left; by sex, it was observed 9 times in men and 2 times in women.

In 6 cases (8.33%), the superficial EPA and the deep EPA originated by a common trunk that divided before reaching the arch of the GSV, then the superficial EPA passed over the arch of the GSV and the deep EPA passed below the arch of GVS. Depending on the side, this layout was noted twice right and 4 times left; by sex, it was noted 5 times in men and 1 time in women.

In 5 cases (6.94%), the two EPA (superficial and deep) originated in isolation and both passed below the arch of the GSV. This disposition was observed only in men, 3 times on the right and 2 times on the left.

In 3 cases, a common trunk passed below the arch of the GSV before dividing into superficial EPA and deep EPA. One of these 3 cases was observed on the right and the other 2 cases were observed on the left. According to sex, this disposition was observed 1 time in men and 2 times in women.

In 2 cases, the trunk common to both superficial and deep EPA passed behind the lateral accessory saphenous vein before dividing in front of the GSV. These 2 cases were observed in men, once on the right and on the left.

In 1 case, the common trunk of the two superficial and deep EPA divided before reaching the arch of the GSV, and the two superficial and deep EPA crossed the GSV by passing behind the lateral accessory saphenous vein (Fig. 6). This case was observed in a woman on the left side.

In 1 case, the superficial EPA and the deep EPA originated separately and both pre-crossed the GSV (Fig. 5). This case was observed in a man on the right.

In 1 case, the common trunk of the superficial and deep EPA divided before reaching the arch of the GSV, the superficial EPA pre-crossed the GSV passing behind the lateral accessory saphenous vein, and the deep EPA has passed behind from the GSV. This case was observed in a man on the left.

In 1 case, the GSV was duplicated and the single EPA passed between the 2 trunks. It passed behind the lateral trunk and in front of the medial trunk. This case was observed in a man on the right.

In the 2 cases where there were 3 EPA, the superficial passed over the arch of the GSV, the middle and the deep crossed the arch of the GSV after the division of their common trunk. One of these 2 cases was observed in a man on the right and the other case was observed in a woman on the left.

DISCUSSION

Number

In the present study, the EPA was visible in all cases. According to Hemmati et al. (2012), in their study of 228 patients who underwent surgery, the EPA was identified during all surgical explorations. Manerikar et al. (2015), in their study of 50 patients who underwent Trendelenburg surgery with GVS stripping, noted that the EPA was not seen in 2 patients (4%). According to Ramalingam and Rajeswari (2018), in a series of 50 cases, superficial EPA was not identified in 8 cases (16%). According to Preethiramy (2008), in 37 out of 50 cases (74%), the EPA was not seen at the saphenofemoral junction. According to Souroullas et al. (2016), in their study on the anatomy of the saphenofemoral junction in a consecutive series of 172 patients undergoing ligation of the unilateral primary saphenofemoral junction, EPA was identified in 150 cases (87.2%). La Falce et al. (2006), in their study, found the EPA in 46 out of 50 cases (92%).

In this study, the presence of a single EPA was the most common. It was noted in 40 cases (55.56%).

Castro et al. (1998) found in their study that the EPA was a single vessel in 55% of the cases. Henriet (1987) shows that, among 256 patients, 80% of women and 65% of men have a single APE. According to Gaye et al (2016), out of 22 dissected inguinal regions, in 15 cases (68.18%), there was only one EPA. In all of these studies, the presence of a single EPA was the most common, which confirms our results.

The presence of two EPA as noted in the anatomical works occupied the second position in this study. 30 cases (41.67%) were observed with a non-significant difference, since $P > 0.05$. Gaye et al (2016) also found it in second position, with 6 cases out of 22 with male predominance and on the right side. Henriet (1987) also finds this second position, but with a predominance of men and on the right side. According to Castro et al. (1998), the EPA was double in 30%, and with a common core in 15%.

The existence of three pudendal arteries is exceptionally reported in the literature (Gaye et al., 2016). In the present study, the presence of three APE was noted in 2 cases. Gaye et al. (2016) found, in their series, a common arterial trunk that trifurcates into three arterial branches, which they have named upper, middle and lower external pudendal arteries. This same observation is made by Henriet (1987) who, in addition, pointed out another rare provision namely three external pudendal arteries originating in isolation from the common femoral artery.

Origin

In the present study, in cases where there was only one EPA, it came from the CFA in 18 cases and from the SFA in 22 cases. Of the cases where there were two superficial and deep EPA, they were both from the CFA in 17 cases; in 7 cases, the superficial EPA came from the CFA and the deep EPA from the SFA; in 5 cases, the superficial EPA and deep APE both came from the SFA; in 1 case, the superficial APE came from the quadricipital artery and the deep APE from the SFA. Gaye et al. (2016) noted that, in their series, all the external pudendal arteries originate from the common femoral artery. Falce (2006) confirms this exclusive origin on the common femoral artery,

from a series of dissection of 50 inguino-femoral regions on anatomical subjects. An origin at the level of the deep femoral artery is described by 3 authors. Donnelly (2005) shows, out of a series of 2080 dissected inguinal regions, that 4.6% of external pudendal arteries have an origin on the deep femoral artery. Castro et al. (1998) noted in 1 in 20 dissections that the EPA originated from the deep femoral artery. In addition, Tanyeli (2006) describes this same origin on an isolated case of dissection. The origin of the APE of the superficial femoral artery was noted in 19 cases during a study of 20 dissections by Castro et al. (1998). Apart from this last study and ours, this origin of the APE has not been noted in English and French literature. In contrast, a superficial APE from the quadricipital artery as in this study has not been reported in the English and French literature.

Variations in the branching pattern of the femoral artery can be explained on the basis of abnormal development of the arterial network of the pelvic limb of the embryo (Çiftcioglu et al., 2009). The axial artery of the pelvic limb is derived from the fifth lumbar intersegmental artery. It is considered to be the branch of the internal iliac artery and extends over the face of the thigh. The femoral artery runs along the ventral surface of the thigh, opening a new canal to the pelvic limb. It arises from a capillary plexus that is connected proximally with the branches of the external iliac artery and distally with the axial artery (Standring et al., 2008). It is believed that the increased blood flow in these capillaries determines the final mature arterial pattern. Thus, the most suitable channels enlarge while others contract and disappear (Çiftcioglu et al., 2009; Prakash Kumari et al., 2010). Thus, the original variations of the EPA could be explained by the situation of the blood vessels going to the external genitalia in which the blood flow is increased.

Original mode

In the present study, in all cases where there was only one EPA, it originated in isolation. The existence of two EPA (superficial and deep) that are born separately was noted in the present study in 15 cases (20.83%). Gaye et al. (2016) found it in two patients. Henriët (1987) noted it in 15 out of

149 patients. On the other hand, La Falce (2006) noticed it a little more frequently, with 21 cases out of 46 external pudendal arteries found. The existence of two APE (superficial and deep) that arise through a common trunk was observed here in 13 cases (18.06%). La Falce (2006) found this configuration in 24% of his dissections. It was found in 25% of cases by Peera and Sugavasi (2013). The existence of two EPA, the superficial EPA of which originates through a common trunk with the inferior epigastric artery while the deep EPA is born separately, was observed in the present study in 2 cases. According to Nafees and Usmani (2018), in 2 cases out of 25 dissected lower limbs, the superficial EPA appeared as a common trunk with a superficial epigastric artery. This same configuration was noted by Myageri et al. (2018) in 5 out of 40 cases (12%), and by Taylor and Daniel (1975) in 3 out of 20 cases (15%). The existence of three APEs, of which the superficial EPA originates from a trunk with the superficial epigastric arteries and superficial iliac circumflex, or with the inferior epigastric artery, while the middle and deep PAE arise from a common trunk reported in the literature. Gaye et al. (2016) noted in 1 case an arterial trunk, which is divided into three upper, middle and lower EPA. The exceptional arrangement illustrated by three upper, middle and lower external pudendal arteries, which have separate origins on the common femoral artery, has been described in one patient by a single author (Henriët, 1987).

Reports of the external pudendal artery with the arch of the great saphenous vein

o In the present study, the most frequent report was the sub crossing of the arch of GSV by the single EPA. The latter passed behind the GSV and in front of the femoral vein. We noted it in 32 cases (44.44%). Gaye et al. (2016) found that the single EPA crosses the butt of the GSV in 8 out of 22 cases. This provision was noted by Henriët (1987) in 70.4% of the cases. According to Ramalengam and Rajeswari (2018), in their series of 50 dissections, in 26 cases (52%), the superficial EPA was found posterior to the great saphenous vein. Ruji (2016) in 72 of 80 cases, or 90% of the cases in his study, was able to clearly demonstrate the superficial

EPA between the GSV and the common femoral vein. Hemmathi et al. (2012) studied 228 varicose vein patients who underwent surgery. They noted that the EPA crossed behind the saphenofemoral junction in 60.5%. Manerikar et al. (2015) studied 50 patients who underwent Trendelenburg surgery with stripping of a large saphenous vein. They found that the superficial EPA crossed the saphenofemoral junction posteriorly in 28 (56%) patients. These different studies and ours have noted that the passage of the EPA below the arch of the GSV and behind the GSV is the most frequent report. Ndiaye (2006) finds, in his series, 50% of external pudendal arteries that under-intersect the arch of the great saphenous vein. This report exposes to lesions of the external pudendal artery, during the dissection of the proximal part of the trunk of the great saphenous vein. We can also confuse, at the time of ligation of the venous afferents of the arch of the great saphenous vein, the terminal part of the external pudendal artery and the external satellite pudendal vein (Gaye et al., 2016).

The existence of the two isolated EPA, whose superficial EPA passes over the arch of the GSV, and the deep EPA crosses the butt of the GSV, was the second most frequent report in the present study. This is the classic relationship of EPA with the arch of GSV noted in the anatomy books. We noted it in 11 cases (15.28%). This provision noted in 1 case by Gaye et al. (2016), in 8 cases out of 10 (80%) by Mostafa (2006).

In the present study, in 7 cases (9.72%), there was a single APE that pre-crossed the GSV passing behind the lateral accessory saphenous vein. Donnelly et al. (2005) describe an external pudendal artery which passes between a great saphenous vein and an accessory saphenous vein in 4.6% of his observations. Henriët (1987) describes an external pudendal artery that passes between the great saphenous vein and the vein of Jacomini. These situations increase the surgical difficulty, and at the same time the risk of injury to the external pudendal artery (Gaye et al., 2016).

In the present study, in 6 cases (8.33%), the superficial EPA and the deep EPA originated by a common trunk that divided before reaching the arch of the GSV, including the superficial EPA, which passed over the arch of the GSV, and the

deep EPA, which passed below the arch of the GSV. This provision was noted by Mostafa (2006) in 1 case.

The existence of two isolated EPA (superficial and deep) that both passed below the arch of the GSV was observed in 5 cases (6.94%) in the present study. Gaye et al. (2016) noted this provision in 1 case.

A common trunk of the two EPA (superficial and deep) which passes below the arch of the GSV before dividing was observed 3 times in the present study. Mostafa (2006), in his study, noted that in 1 case there was a single long external pudendal trunk that followed the same course of the deep external pudendal artery. It gave branches similar to the superficial external and deep external arteries.

In the present study, in 1 case, the common trunk of the superficial and deep EPA divided before reaching the arch of the GSV, the superficial EPA pre-crossed the GSV by passing behind the accessory lateral saphenous vein, and the deep EPA passed behind the GSV. Gaye et al. (2016) noted, in 1 case, the single trunk which, before reaching the arch, divides and surrounds it like forceps. This latter arrangement is described once by Ndiaye (2006).

In the present study, in 1 case, the GSV was duplicated and the single EPA passed between the 2 trunks. It passed behind the lateral trunk and in front of the medial trunk. According to Donnelly et al. (2005), in 4.6%, the EPA passed back to a large tributary or a trunk of the bifid GSV and in front of the second trunk, making identification of the second trunk particularly difficult. This last finding is similar to our case. Gaye et al. (2016) had found, in one patient, a GSV presenting a single trunk with a double stick throwing itself on the common femoral vein, and passage of a single EPA in this loop formed by the two sticks and the trunk of the GSV.

CONCLUSION

Most often, there is only one EPA. When there are two EPA, they can originate in isolation or through a common core. The EPA contracts variable and close relationships with the arch of the GSV. Since

lesions of the EPA can lead to impotence, these reports must be known by surgeons to avoid damaging the EPA during surgical treatment of varicose veins of the pelvic limb.

ACKNOWLEDGEMENTS

We thank Pr Mohamed Keïta for correcting the article and for his encouragement, Dr Mahamoud Cissé for doing statistical test of the article, and Pr Seydou Doumbia for his financial support to the Bamako anatomy laboratory.

REFERENCES

ABE ST, YAMAGUCHI Y, HATA K, YAMAGUCHI T (1992) Penile reconstruction with de-epithelized superficial external pudendal artery flap. *J Urol*, 147: 155-157.

BOUCHET A, CUILLERET J (1996) La région inguino-fémorale. In: Anatomie topographique descriptive et fonctionnelle. Tome 3b, Le membre inférieur. 3^{ème} édition. Paris: SIMEP.

CASTRO M, BRENDA E, MARQUES A, PEREIRA MD (1998) Anatomic study of the external pudendal vessels to the anterior scrotal region. *EJ Plastic Surg*, 21: 86-90.

ÇIFTCIOGLU E, KALE A, KOPUZ C, EDIZER M, AYDLN E, DEMIR MT (2009) Medial circumflex femoral artery with different origin and course: a case report and review of the literature. *Folia Morphol*, 68: 188-191.

DONNELLY M, TIERNEY S, FEELEY TM (2005) Anatomical variation at the sapheno-femoral junction. *Br J Surg*, 92: 322-325.

DROUPY S, BENOIT G, GIULIANO F, JARDIN A (1997) Penile arteries in humans: origin-distribution-variations. *Surg Radiol Anat*, 19: 161-167.

GAYE M, NDIAYE A, DIENG PA, NDIAYE A, BA PS, DIATTA S, CISS AG, NDIAGA NDOYE JM, DIOP M, NDIAYE A, NDIAYE M, DIA A (2016) Bases anatomiques des lésions de l'artère pudendale externe lors de la chirurgie des varices du membre pelvien. *Pan Afr Med J*, 24: 199.

GEORGE A, CUNHA GOMES D, THATTE RL (1986) Early division of pedicled flaps using a

simple devise: a new technique. *Br J Plastic Surg*, 44: 119-122.

HEMMATI H, BAGHI I, TALAEI ZADEH K, OKHOVATPOOR N, KAZEM NEJAD E (2012) Anatomical variations of the saphenofemoral junction in patients with varicose veins. *Acta Med Iran*, 50(8): 552-555.

HENRIET JP (1987) Saphenofemoral venous confluence and the external pudendal network: anatomical data and new statistics. *Phlébologie*, 40: 711-735.

LA FALCE OL, AMBROSIO JD, DE SOUZA RR (2006) The anatomy of the superficial external pudendal artery: a quantitative study. *CLINICS*, 61: 441-444.

MACCHI C, GIANNELLI F, CECCHI F, CORCOS L, REPICE F, CANTINI C, BRIZZI E (1996) Collateral circulation in occlusion of lower limb arteries: an anatomical study and statistical research in 35 old subjects. *Ital J Anat Embryol*, 101: 89-96.

MANERIKAR K, SINGH BAWA AP, PITHWA AK, SINGH G, SHROTRI H, GOOPTU S (2015) Risk factors and saphenofemoral junction in varicose veins. *Indian J Vasc Endovasc Surg*, 2: 134-138.

MAYER AR, RODRIGUEZ RL (1991) Vulvar reconstruction using a pedicle flap based on the superficial external pudendal artery. *Obstet Gynecol*, 78: 964-968.

MOSTAFA TM (2006) Anatomical study of the external pudendal arteries. *AAMJ*, 4: 177-187.

MYAGERI M, SURESH BB, RAMESH M (2016) A cadaveric study of superficial external pudendal artery in femoral triangle. *IJARS*, 7: AO31-AO34.

NAFEES H, USMANI DA (2018) Variations in the branching pattern of femoral artery: a cadaveric study. *Int J Med Res Prof*, 4: 266-269.

NDIAYE A, NDIAYE AB, NDOYE JM, DIARRA O, DIOP M, DIA A, NDIAYE M, SOW ML (2006) The arch of the great saphenous vein: anatomical bases for failures and recurrences after surgical treatment of varices in the pelvic limb, about 54 dissections. *Surg Radiol Anat*, 28: 18-24.

PEERA SA, SUGAVASI R (2013) Morphological study of branches of femoral artery in the femoral triangle-a human cadaveric study. *IJHSR*, 3: 14-19.

PRAKASH KUMARI J, BHARDWAJ AK, JOSE BA, YADAV SK, SINGH G (2010) Variations in the origins of the profunda femoris, medial and lateral femoral circumflex arteries: a cadaveric study in the Indian population. *Rom J Morphol Embryol*, 51:167-170.

PREETHI RAMYA T (2008) A study on the great saphenous vein including its surgical and radiological implications (Masters thesis). Madras Medical College, Chennai.

RAMALINGAM P, RAJEWARI K (2018) A study of relationship between great saphenous vein and superficial external pudendal artery and duplication of great saphenous vein in South Indian population. *IOSR-JDMS*, 17: 81-86.

RIJU R (2016) Sapheno-femoral junction anatomy and haemodynamics in Indian patients. *Amrita J Med*, 12: 16-22.

SOUROULLAS P, BARNES R, SMITH G, NANDHRA S, CARRADICE D, CHETTER I (2016) The classic saphenofemoral junction and its anatomical variations. *Phlebology: J Venous Dis*, 32: 172-178.

STANDRING S, BORLEY NR, COLLINS P, CROSSMAN AR, GATZOULIS MA, HEALY JC, et al. (Editors) (2008) Development of the pelvic girdle and lower limb. In: *Gray's Anatomy*, 40th ed. Churchill Livingstone, London, p 1463.

TANYELI E, YILDIRIM M, UZEL M, VURAL F (2006) Deep femoral artery with four variations: a case report. *Surg Radiol Anat*, 28: 211-213.

TAYLOR GI, DANIEL RK (1975) The anatomy of several free flap donor sites. *Plast Reconstr Surg*, 56: 243-253.

THATE RL, PATIL UA, DHAMI LD (1986) The combined use of the superficial external pudendal artery flap with a flap of the anterior rectus sheath for the simultaneous cover of dorsal and volar defects on the hand. *Br J Plast Surg*, 39: 321-326.

Evaluation of the therapeutic role of stem cells in experimental acetaminophen induced hepatotoxicity in adult male albino rat

Lamya A. Abd Elsalam^{1,2}, Shereen E. Tawfeek^{1,3}, Eman H. Nadwa^{4,5}, Bahaa Eldin A. Khaled^{1,6}

¹ Department of Anatomy, College of Medicines, Jouf University, Sakaka, Saudi Arabia

² Department of Anatomy and Embryology, Faculty of Medicine, Beni Suef University, Egypt

³ Human anatomy and Embryology Department, Faculty of Medicine, Zagazig University, Egypt

⁴ Department of Pharmacology and Therapeutics, College of Medicines, Jouf University, Saudi Arabia

⁵ Department of Medical Pharmacology, Faculty of Medicines, Cairo University, Egypt

⁶ Department of Anatomy and Embryology, Faculty of Medicine, Cairo University, Egypt

SUMMARY

Acetaminophen is a commonly used analgesic and antipyretic drug that could exert acute and chronic liver cell failure. Mesenchymal stem cell therapy offers advantages for tissue repair and regeneration in clinical research. To elucidate the therapeutic effect of stem cells on different doses of acetaminophen-induced hepatotoxicity in adult male albino rats, sixty adult male albino rats weighing 170-230 g were divided into six groups: Group I (Normal control) were injected intraperitoneally with isotonic saline three times over one week. Group II receive a single intravenous injection of MSC. Group III and IV: were injected intraperitoneally three times over one week by acetaminophen at a dose of 300 mg/kg (Group III) and 600 mg/kg (Group IV) respectively. Group V and VI were injected with acetaminophen 300 mg/kg (Group V) and 600 mg/kg (Group VI), followed in both groups by a single intravenous injection of MSC 24 hours after the last dose of acetaminophen. Blood samples were collected

from the tail vein of the rats for assessment of biochemical markers of liver, then they were anaesthetized and sacrificed. Liver homogenate was assessed for Malondialdehyde (MDA) and Super Oxide Dismutase (SOD). Liver specimens were subjected to histopathological examination and ultrastructural study. Statistical analysis was done for the results of hepatic biomarkers. Examination of specimens of group III and IV revealed disturbed hepatic architecture, nuclear and cytoplasmic degeneration and increased serum liver enzymes compared to the control group I. However, MSC markedly ameliorated these histological and laboratory alterations in both group V and VI. It could be concluded that stem cells had a beneficial role in treatment of hepatotoxicity exerted by acetaminophen administration in adult male albino rats.

Key words: Stem cells – Acetaminophen – Liver

Corresponding author:

Bahaa Eldin Ali Khaled. Department of Anatomy and Embryology, Faculty of Medicine, Cairo University, Egypt. Cell phone: +201060654118. E-mail: drbahaa10@hotmail.com / bamohamed@ju.edu.sa

Submitted: November 4, 2020. Accepted: December 11, 2020

INTRODUCTION

Acetaminophen is an over-the-counter (OTC), commonly consumed pain killer and antipyretic; however, its safety is not absolute. High doses can cause acute and chronic liver cell failure and is correlated with significant increase in liver enzymes (Jarsiah et al., 2017).

High doses of acetaminophen leads to saturation of pathways in the liver responsible for its conjugation, shunting its metabolism to cytochrome P450 (CYP450) enzyme that results in the formation of a toxic metabolite, N-acetyl-p-benzoquinone imine (NAPQI). NAPQI itself is detoxified by conjugation with glutathione, but in case of acetaminophen overdose hepatocellular supplies of glutathione become depleted; NAPQI therefore accumulates and induces an inflammatory cascade leading to cell necrosis and apoptosis through direct mitochondrial damage (Larson, 2007; Jaeschke, 2012).

N-acetylcysteine (precursor of glutathione) is the only therapeutic agent available for management of acetaminophen toxicity. The effectiveness of this antidote is time-related, in which it is only effective if given early in the course of toxicity. In cases of irreversible hepatic damage, liver transplantation is the last resort; however, this option is limited by availability of donors, costs, and complications of immunosuppression (Craig et al., 2012).

The value of mesenchymal stem cell (MSC) has been investigated in the field of tissue repair and regeneration. Potentially, MSC have the ability to replace injured tissues in the body, with minimal risk of adverse effects or rejection. Beside their ability to reside in injured organs, giving rise to subsequent generations with variable degrees of differentiation, MSC are postulated to convey immunomodulatory, anti-inflammatory and anti-fibrotic effects (Gurtner et al., 2007; Huang et al., 2016).

In treatment of acetaminophen toxicity, induction of liver regeneration by stem cell therapy is of potential value in improving outcomes (Bhushan et al., 2014). MSC convey hepatocyte-like markers, which make them a substantial alternative for liver transplantation (Scheers et al., 2011).

The aim of the present work is to evaluate the therapeutic effect of stem cells on different doses of acetaminophen-induced hepatotoxicity in adult male albino rats, and to assess the potential therapeutic role of MSC against that toxicity.

MATERIALS AND METHODS

Acetaminophen

It was supplied from Sigma Aldrich, dissolved in warm isotonic saline 0.9% and injected intraperitoneally (IP) to rats three times over one week at two different doses: 300 mg/kg (groups III and V) and 600 mg/kg (groups IV and VI) (Bhushan et al., 2014).

Bone marrow (BM)-derived mesenchymal stem cells (MSC)

MSC were obtained from the stem cell research unit at the Biochemistry Department of Kasr Alaini, Faculty of Medicine, Cairo University. Six-week-old male Sprague-Dawley rats were utilized to obtain the BM. Femora and tibiae of the animals were flushed with Dulbecco's modified Eagle's medium complemented by 10% fetal bovine serum. Afterwards, isolation of the nucleated cells and resuspension were carried out in complete culture medium complemented by 1% penicillin-streptomycin. Incubation of the cells was carried out at 37°C in 5% humidified CO₂ for 12–14 days as primary culture or upon formation of large colonies. When they developed (80–90% confluence), twice wash of the cultures was done using PBS then cells were trypsinized with 0.25% trypsin in 1 mmol/l EDTA for 5 min at 37°C. Resuspension of the cells was done in serum-supplemented medium and incubated in a culture flask, after centrifugation. The formed culture was named as first-passage culture (Alhadlaq and Mao, 2004; Raafat et al., 2015).

Characterization of BM-derived MSCs

At harvest time, identification of MSC was achieved by detection of their adhesiveness or their spindle shape. By flow cytometric evaluation, MSC express CD29, one of surface markers of rat's MSC (Payushina et al., 2006).

Labeling of stem cells with PKH26 dye

MSC were harvested during the 4th passage, and were labeled with PKH26 fluorescence linker dye (Sigma Aldrich, USA, Sigma brand, catalogue number: MINI 26), which was utilized for general cell-membrane labeling. It was used in the form of PKH26 dye stock solution (1 vial containing 0.1 ml, 1×10^{-3} M in ethanol) and diluent C (1 vial containing 10 ml), according to the manufacturer instructions for use. PKH26 is a red fluorochrome dye, which is stable and will divide equally when the cells divide. After staining with PKH dye, one can observe as many as eight divisions depending on how brightly the cells were stained initially and on the amount of surface area on the cells. Most commonly, 4-6 divisions can be visualized.

This dye was used in groups V and VI. The dose of MSC was 3×10^6 MSC in 0.5 ml phosphate buffer saline (PBS) (Kim et al., 2010), labeled with PKH26 dye, injected into the tail vein. Homing of the labelled cells in the liver was checked by fluorescent microscope (Sigma-Aldrich, Saint Louis, USA).

Animals and experimental design

Sixty adult male albino rats weighing 170-230 g were used in this study. They were obtained from the animal house, Faculty of Medicine, Cairo University. The experiment was carried out according to the standard guidelines of Institutional Animal Care and Use Committee and after Institutional Review Board approval. They were maintained under standard environmental and laboratory conditions with standard diet. The rats were divided equally into six groups, 10 rats each, as follows:

Group I (Control group): rats of this group were injected intraperitoneally three times over one week with one ml warm saline 0.9% (vehicle of acetaminophen). At day 7, they were injected with 0.5 ml of PBS (vehicle of MSC) intravenous, then they were sacrificed after one more week.

Group II (MSC treated group): rats of this group were injected intraperitoneally three times over one week with one ml warm saline 0.9% (vehicle of acetaminophen). At day 7, they received a

single intravenous dose of MSCs (3×10^6 cells in 0.5 ml PBS), then they were sacrificed after one more week.

Group III (Acetaminophen 300 mg/kg group): rats were injected with acetaminophen at a dose of 300mg/kg, then they were sacrificed after one more week.

Group IV (Acetaminophen 600 mg/kg group): rats were injected with acetaminophen at a dose of 600 mg/kg, then they were sacrificed after one more week.

Group V (Acetaminophen 300 mg/kg+MSC group): rats were injected with acetaminophen at a dose of 300 mg/kg followed by a single intravenous injection of MSC, as group II, at day 7, then they were sacrificed after one more week.

Group VI (Acetaminophen 600 mg/kg+MSC group): rats were injected with acetaminophen at a dose of 600 mg/kg followed by a single intravenous injection of MSC, as group II, at day 7, then they were sacrificed after one more week.

At the end of the experiment, blood samples were obtained for assessment of biochemical markers of liver from all groups, then the rats were anaesthetized and sacrificed. Liver specimens were collected for preparation of tissue homogenate to detect oxidant/antioxidant markers, for light and electron microscopic study to evaluate histological structure and for fluorescence microscopic study to detect homing of mesenchymal stem cells.

Serum preparation

By the end of the experiment, under isoflurane anesthesia, blood samples were collected, under complete aseptic conditions, from the rat retro-orbital venous plexus by means of micro-capillary glass tubes. Blood was allowed to coagulate at room temperature, and then samples were centrifuged at 4000 rpm for 20 min using a cooling centrifuge (Sigma 3-30 k, USA). The clear serum layer was separated and stored at -80°C for assessment of Serum aspartate aminotransferase [AST], alanine aminotransferase [ALT] (Reitman and Frankel, 1957) and Gamma glutamyl transferase [GGT] (Lowry et al., 1951).

Tissue homogenate preparation for oxidant/antioxidant markers

Homogenous preparation of tissue for oxidant / antioxidant markers. The portion of excised liver tissue was homogenized in a buffer of 50 mmol / l Tris-HCl (pH 7.4) and then centrifuged for 15 min at 10,000 g. Antioxidant status value at 4°C.

The resulting pellet was discarded and the supernatants were kept frozen immediately and then used for biochemical calculations. Determination of lipid peroxidation was done according to Ohkawa et al. (1979), as the formation of malondialdehyde (MDA) during an acid heating reaction. The activity of superoxide dismutase (SOD) was determined by measuring the inhibition of epinephrine autoxidation at pH 10.2 and 30°C, according to Misra and Fridovich (1972).

Histopathological assay

Rats of all groups were anesthetized with sodium thiopental 75 mg/kg (Gum and Cho, 2013). Liver specimens were carefully dissected, excised, prepared for histopathological examination and ultrastructural study.

Preparation of paraffin sections

Liver specimens were immediately fixed in 10% formalin solution in normal saline and embedded in paraffin. Blocks were prepared for sectioning at 4-5 microns. Sections of samples were collected on glass slides, deparaffinized, and stained by Hematoxylin and Eosin to show the general structure of the tissue, by Periodic Acid Schiff (PAS) to show the glycogen content and by Masson's trichrome to visualize the deposition of collagen fibers distribution (Bancroft and Gamble, 2008). Slides were examined by the light electric microscope (LEICA ICC50 W), Faculty of Agriculture, Cairo University.

Ultrastructure preparations (Hayat, 1986)

Fixation of liver specimens was carried out using 2.5% glutaraldehyde for 24-48 h, followed by washing in phosphate buffer (pH 7.2-7.4) three to four times for 20 min. The specimens were then post-fixed in a buffered solution of 1%

osmium tetroxide for 2 h, and after that washed in a similar buffer four times for 20 min each. Fixed specimens were dried out in increasing concentrations of ethyl alcohol (30%, half, 70%, 90%, and 100%), cleared in two changes of propylene oxide and inserted in Epon resin. The pitch squares underwent a process of trimming to get rid of the surplus tissue. Ultrathin sections (60-90 nm thick) and illustrative fields of semithin sections were chosen and were cut with a diamond knife using a Reichert OMVs ultra microtome, mounted on copper frameworks. These semithin sections were subjected to double staining with uranyl acetate and lead citrate (Weakley, 1981). The grids were examined and photographed using a transmission electron microscope (JEOL JEM-1200 EX II, Japan) operated at 60-70 kV, at (Electron Microscope Unit), pathology department, National Cancer Institute (NCI).

Statistical analysis

The collected data from liver biochemical markers were coded and analyzed by computer, using a data base software program. The collected data were organized, tabulated and statistically analyzed using SPSS software statistical computer package version 22 (SPSS Inc, USA). The mean and standard deviation were calculated. ANOVA (Analysis of variance) was used to test the difference of mean values of measured parameters among groups; multiple comparison between pairs of groups were performed using Tukey HSD (Post hoc range test). For interpretation of results, significance was adopted at $P \leq 0.05$, while P-values of <0.01 indicate highly significant results. All the results were expressed as mean \pm S.D.

RESULTS

Light microscopic results

Examination of rat liver specimens stained with haematoxylin and eosin of group I (Control group) and group II (MSC treated group) showed normal hepatic architecture; sections from these groups revealed mononucleated and binucleated hepatocytes radiating from the central vein, and hepatic sinusoids lined with flattened endothelial

cells. Kupffer cells could also be seen (Fig. 1A). The portal triad was seen formed of bile ductule lined with cuboidal or low columnar epithelium, a branch of the portal vein exhibiting a thin wall and wide lumen, as well as branches of the hepatic artery characterized by a thicker wall and narrower lumen (Fig. 1B).

The hepatic structure was moderately disturbed in group III (Acetaminophen 300 mg/kg group), where the central vein was engorged and dilated; the hepatic sinusoids also appeared engorged. Moreover, hepatocytes exhibited cytoplasmic vacuolation, pyknotic nuclei and karyolysis (Fig. 1C). Also, there was increase in Kupffer cells,

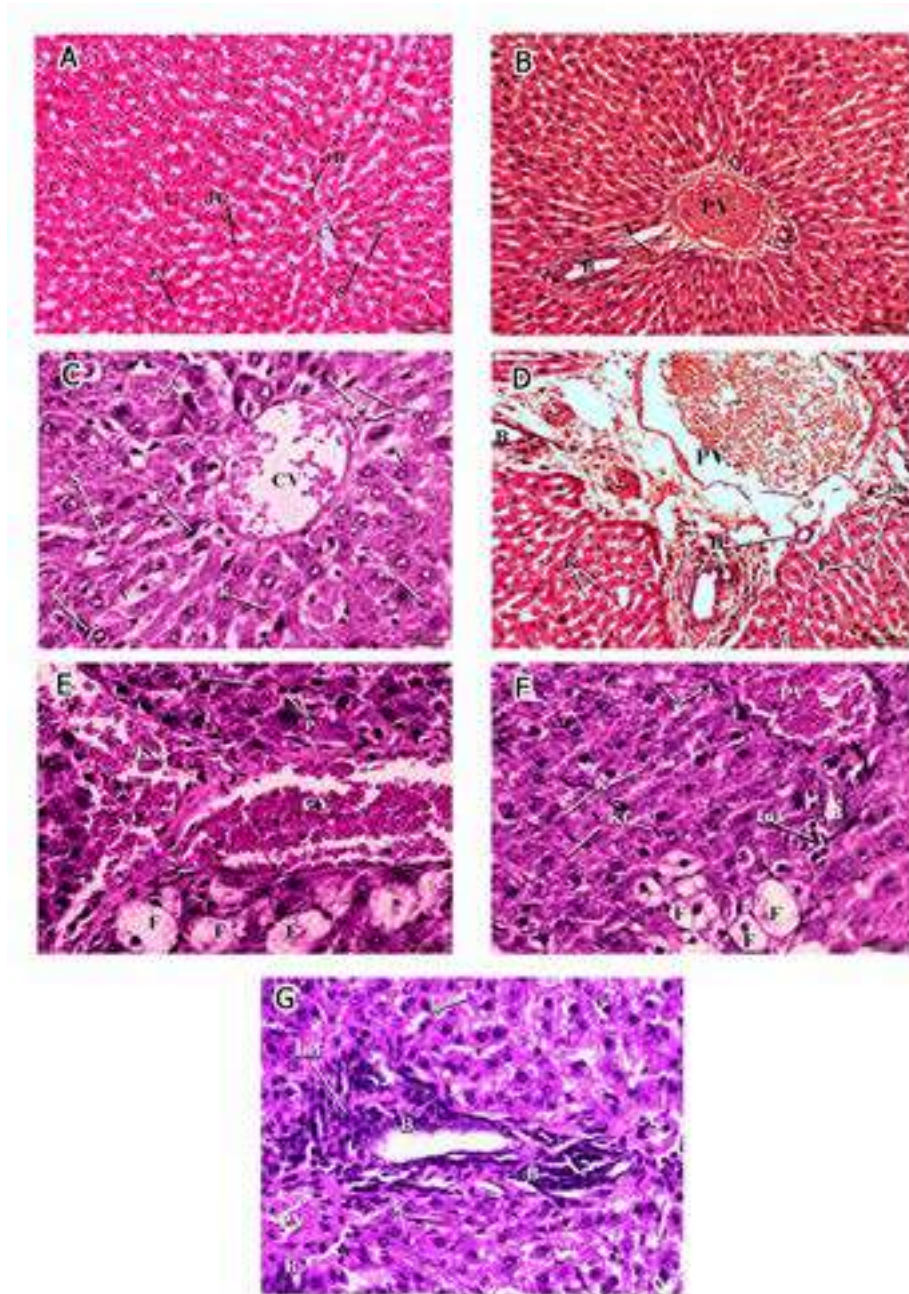


Fig. 1.- A, B Micrographs of group I (Normal control) and group II (MSC treated). **A-** normal hepatocytes (H1) radiating from the central vein (CV) and hepatic sinusoids (S) lined with flattened endothelial cells (E) and Von Kupffer cells (Kf). Binucleated hepatocytes are also seen (H2) (H&E, x100). **B-** the portal triad: bile ductule (B), portal vein (PV) and hepatic artery (A) (H & E, x400). **C, D:** Micrographs of group III. **C-** The central vein (CV) is engorged and dilated. Hepatic sinusoids (S) appeared engorged. Hepatocytes exhibit cytoplasmic vacuolation (V), pyknotic nuclei (P) and karyolysis (K). Increased Von Kupffer cells (Kf) could be observed. **D-** engorged portal vein (PV), proliferation of bile ductules (B) and thick hypertrophied hepatic artery (A). Hepatocytes exhibit cytoplasmic vacuolation (V), nuclear pyknosis (P) and karyolysis (K). Increased Von Kupffer cells (Kf) could be observed (H&E, x400). **E, F, G:** Micrographs of group IV. **E-** markedly congested central vein (CV). Most hepatocytes exhibit extensive fat degeneration (F), nuclear pyknosis (P) and karyolysis (K). Extravasated blood (Ext) could be seen (H&E, x400). **F-** markedly congested portal vein (PV). Most hepatocytes exhibit extensive fat degeneration (F), nuclear pyknosis (P) and karyolysis (K). Mononuclear cellular infiltration (Inf) around the bile ductule (B) could be observed. (H&E, x400). **G-** showing markedly hypertrophied portal vein (PV), hepatic artery (A), proliferation of bile ductules (B) surrounded by mononuclear cellular infiltration (Inf). Hepatocytes exhibit karyolitic nuclei (K) and cytoplasmic vacuolation (V) (H & E, x 400). Scale bars: A, C, E, F, G = 20 μ m.; B, D = 50 μ m.

engorged portal vein, proliferated bile ductules and thick hypertrophied hepatic artery (Fig. 1D). Examination of group IV (Acetaminophen 600 mg/kg group) exhibited marked disturbance of hepatic parenchymal architecture in the form of markedly congested central vein, extravasated blood (Fig. 1E), markedly congested or hypertrophied portal vein, thick hypertrophied hepatic artery and mononuclear cell infiltration around proliferated bile ductules (Figs. 1F, G). Moreover, most hepatocytes exhibited

extensive fat degeneration, nuclear pyknosis and karyolysis, and cytoplasmic vacuolation (Figs. 1E, F, G).

Examination of sections from group V (Acetaminophen 300 mg/kg+MSC group) showed more or less normal parenchymal architecture; most sinusoids and hepatocytes were radiating from the central vein, although few hepatocytes exhibited pyknotic and karyolytic nuclei. Mild increase of Kupffer cells could also be seen (Figs. 2A, B). Examination of portal area

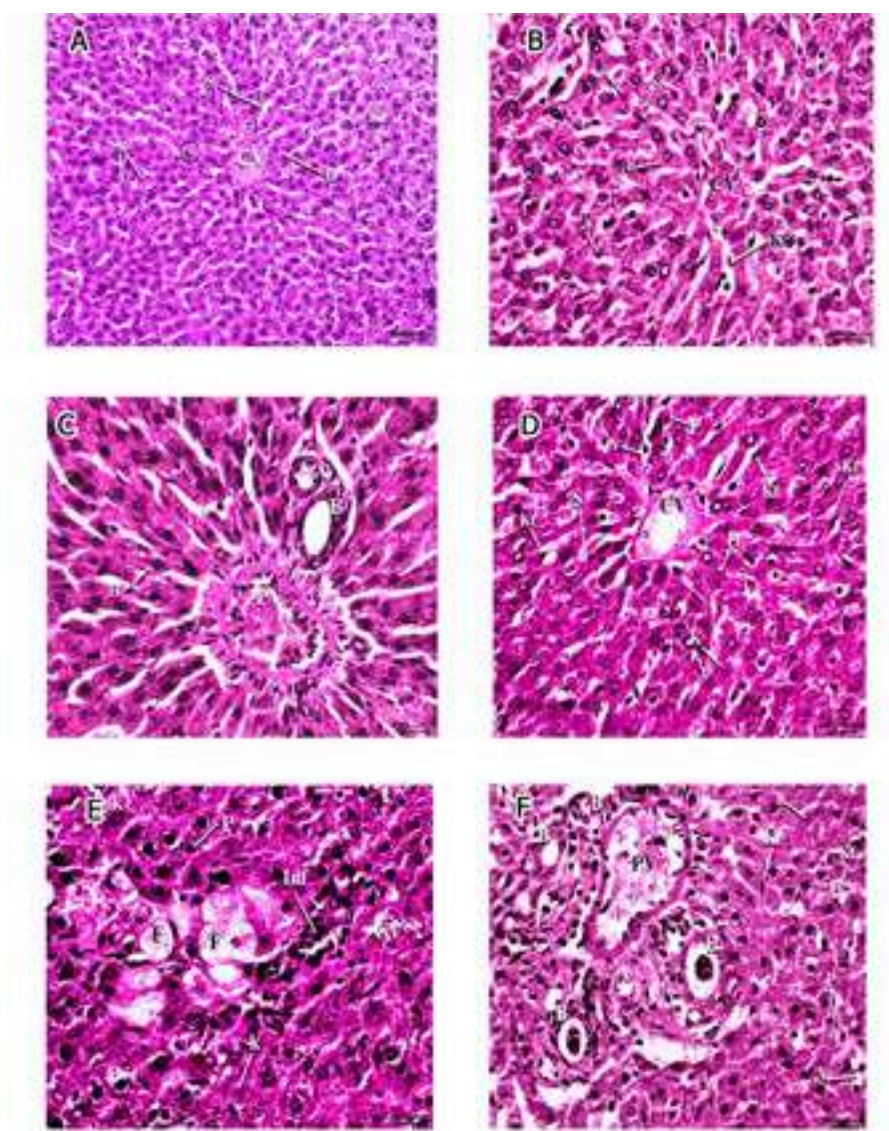


Fig. 2.- A, B, C: Micrographs of group V showing apparently normal parenchymal architecture. **A-** Most sinusoids (S) and hepatocytes (H) are apparently normal and radiating from the central vein (CV) although few hepatocytes exhibit pyknotic (Circle) and karyolytic nuclei (K). Mild increase in Von Kupffer cells could be seen (Kf) (H&E, x200). **B-** A higher magnification of the same group showing apparently normal sinusoids (S) and hepatocytes (H) normal and radiating from the central vein (CV) although few hepatocytes in the midzonal and peripheral areas of the lobule exhibit pyknotic (P) and karyolytic nuclei (K). Mild increase in Von Kupffer cells could be seen (Kf) (H&E, x400). **C-** apparently normal hepatocytes (H) around components of portal area; portal vein (PV), bile ductile (B) and hepatic artery (A) (H & E, x400). **D, E, F:** Micrographs of group VI. **D-** Most sinusoids (S) and hepatocytes (H) are apparently normal and radiating from the central vein (CV) although some hepatocytes exhibit cytoplasmic vacuolation (V), pyknotic (P) and karyolytic nuclei (K). Marked increase in Von Kupffer cells could be seen (Kf) (H&E, x400). **E-** markedly congested central vein (CV) surrounded by mononuclear cellular infiltration (Inf). Some hepatocytes exhibit extensive fat degeneration (F), nuclear pyknosis (P) and karyolysis (K) (H&E, x400). **F-** markedly hypertrophied portal vein (PV), hepatic artery (A) and marked proliferation of bile ductules (B). Hepatocytes exhibit karyolytic (K) and pyknotic (P) nuclei with cytoplasmic vacuolation (V). Marked increase of Von Kupffer cells could be seen (H&E, x400). Scale bars: A = 50 μ m.; B-F = 20 μ m.

revealed apparently normal hepatocytes around components of portal tract (Fig. 2C). While in group VI (Acetaminophen 600 mg/kg+MSC group) the cells showed mildly disturbed parenchymal architecture, most sinusoids and hepatocytes were apparently normal and radiating from the central vein, which appeared either normal (Fig. 2D) or markedly congested and surrounded by mononuclear cellular infiltration (Fig. 2E), markedly hypertrophied portal vein, hepatic artery and marked proliferation of bile ductules (Fig. 2F). Some hepatocytes exhibited extensive fat degeneration, cytoplasmic vacuolation,

pyknotic and karyolytic nuclei. Marked increase in Kupffer cells could also be seen (Figs. 2D, E, F).

In sections stained with PAS, the hepatocytes appeared to have a strong positive PAS reaction in the form of small red granules filling their cytoplasm, denoting considerable amount of glycogen in control group I and II (Fig. 3A) while these reactions gradually decrease in both group III and VI respectively, which showed moderate positive reaction in group III (Fig. 3B) and faint reaction in group IV (Fig. 3C). Group V restored the strong reaction again (Fig. 3D), while group VI exhibited a moderate one (Fig. 3E).

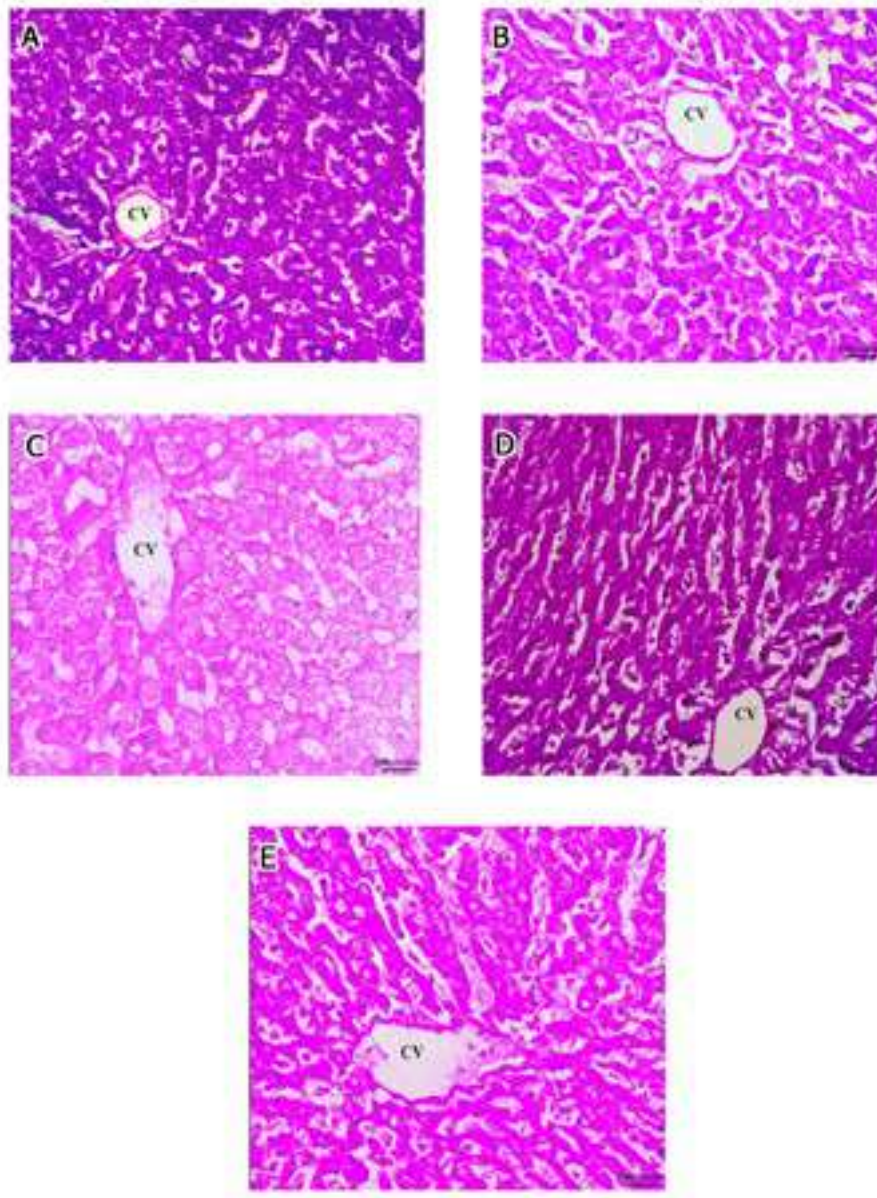


Fig. 3.- Micrographs showing the PAS reaction of the hepatocytic plates radiating from the central vein (CV). **A-** Micrograph of group I and II exhibiting a strong positive PAS reaction. **B-** Micrograph of group III exhibiting a moderate positive PAS reaction. **C-** Micrograph of group IV exhibiting a faint positive PAS reaction. **D-** Micrograph of group V exhibiting a strong positive PAS reaction. **E-** Micrograph of group VI exhibiting a moderate positive PAS reaction. (PAS, x400). Scale bars: A-E = 20 μ m.

Sections stained with Masson's trichrome demonstrated a thin layer of collagen fibers around the central vein and adjoining hepatic sinusoids, while there was a small amount of it surrounding the elements of the portal triad in control group I and group II (Figs. 4A, B). On the contrary, group III sections demonstrated moderate increase of these collagen depositions (Figs. 4C, D), and marked increase in group IV (Figs. 4E, F). Moreover, both groups V (Figs. 5A,

B) and VI (Figs. 5C, D) exhibited this noticeable collagen deposition.

Electron microscopic results

Electron microscopic examination of the control group I and MSC treated group II revealed normal structure of hepatocytes, where there was normal rough endoplasmic reticulum and spherical to ovoid mitochondria with intact cristae. The nucleus was surrounded by bilaminar envelope

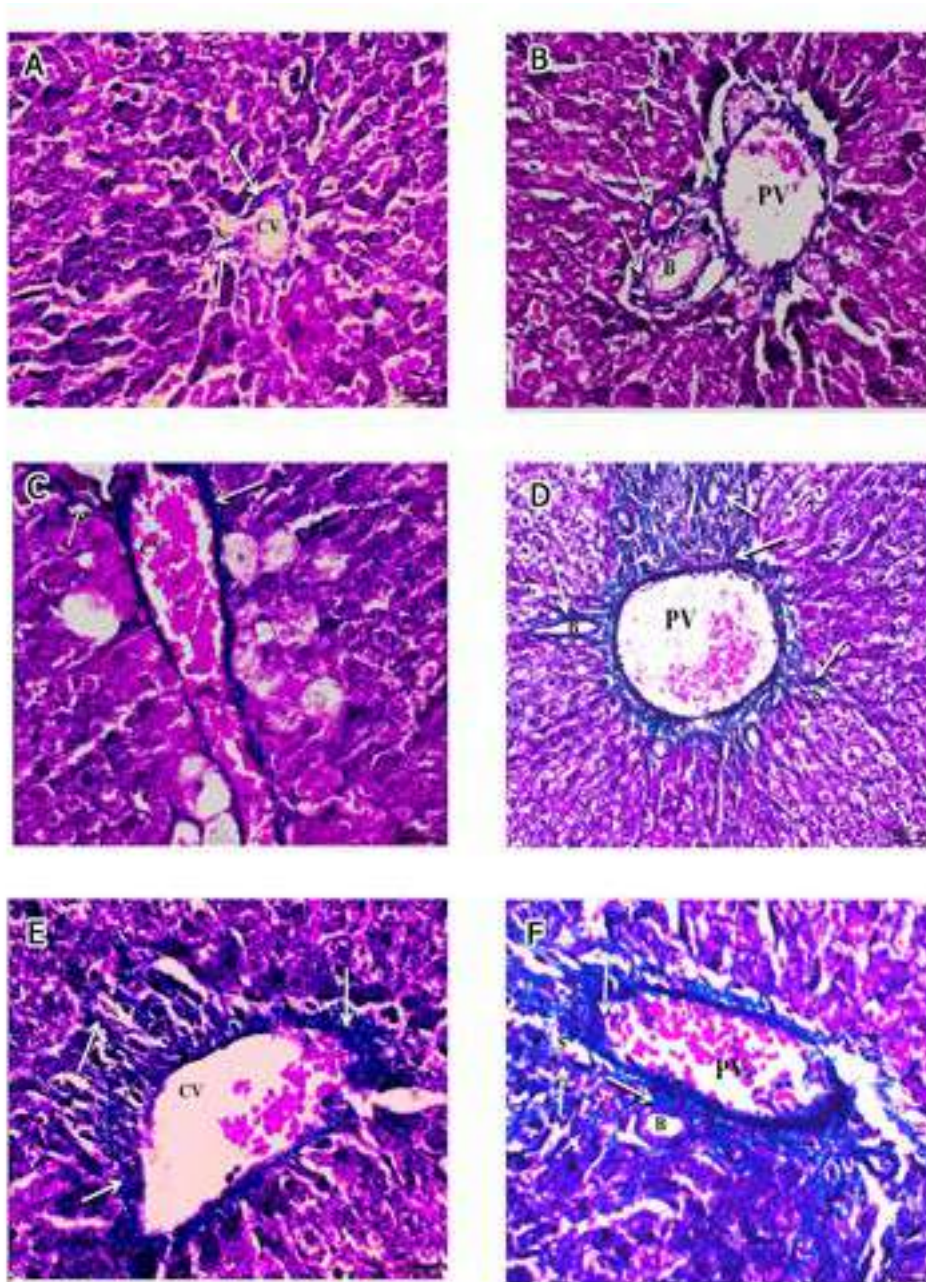


Fig. 4.- A, B of groups I and II. **A-** the normal distribution of collagen bundles (arrows) around the central vein (CV), hepatic sinusoids (S) and **B-** around the components of the portal triad: hepatic artery (A), bile ductile (B), portal vein (PV) and adjoining hepatic sinusoids (S). **C, D** of group III. **C-** moderate increase of collagen bundles (arrows) around the central vein (CV), hepatic sinusoids (S) and **D-** around the components of the portal triad: hepatic artery (A), bile ductile (B), portal vein (PV) and adjoining hepatic sinusoids (S). **E, F** of group IV. **E-** marked increase of collagen bundles (arrows) around the central vein (CV), hepatic sinusoids (S) and **F-** around the components of the portal triad: bile ductile (B), portal vein (PV) (Masson trichrome, x400). Scale bars: A, B, C, E, F = 20 μ m.; D = 50 μ m.

with nuclear pores, and displayed dispersed chromatin with a prominent nucleolus. Golgi apparatus could also be observed opposite nuclear pores (Fig. 6A). Examination of cells of group III revealed apparently normal nucleus with intact nuclear envelope, rough endoplasmic reticulum with maintained ribosomal surface and cytoplasmic rarefaction. Most of mitochondria were apparently normal, with intact cristae, and few of them were ballooned with absent cristae (Fig. 6B), while in group IV there was extensive damage of most of intracellular organelles with irregular

and extremely shrunken nuclei with clumped chromatin material, indented nuclear envelope, extensive cytoplasmic rarefaction, fragmented rough endoplasmic reticulum with lost ribosomal surface. Moreover, the mitochondria were mostly ballooned with absent cristae and disrupted membranes. Few mitochondria and rough endoplasmic reticulum were apparently normal (Figs. 6C, D), while in group V there was slight restoration of normal structure of the cells, which showed apparently normal nucleus, dispersed chromatin, prominent nucleoli, intact nuclear

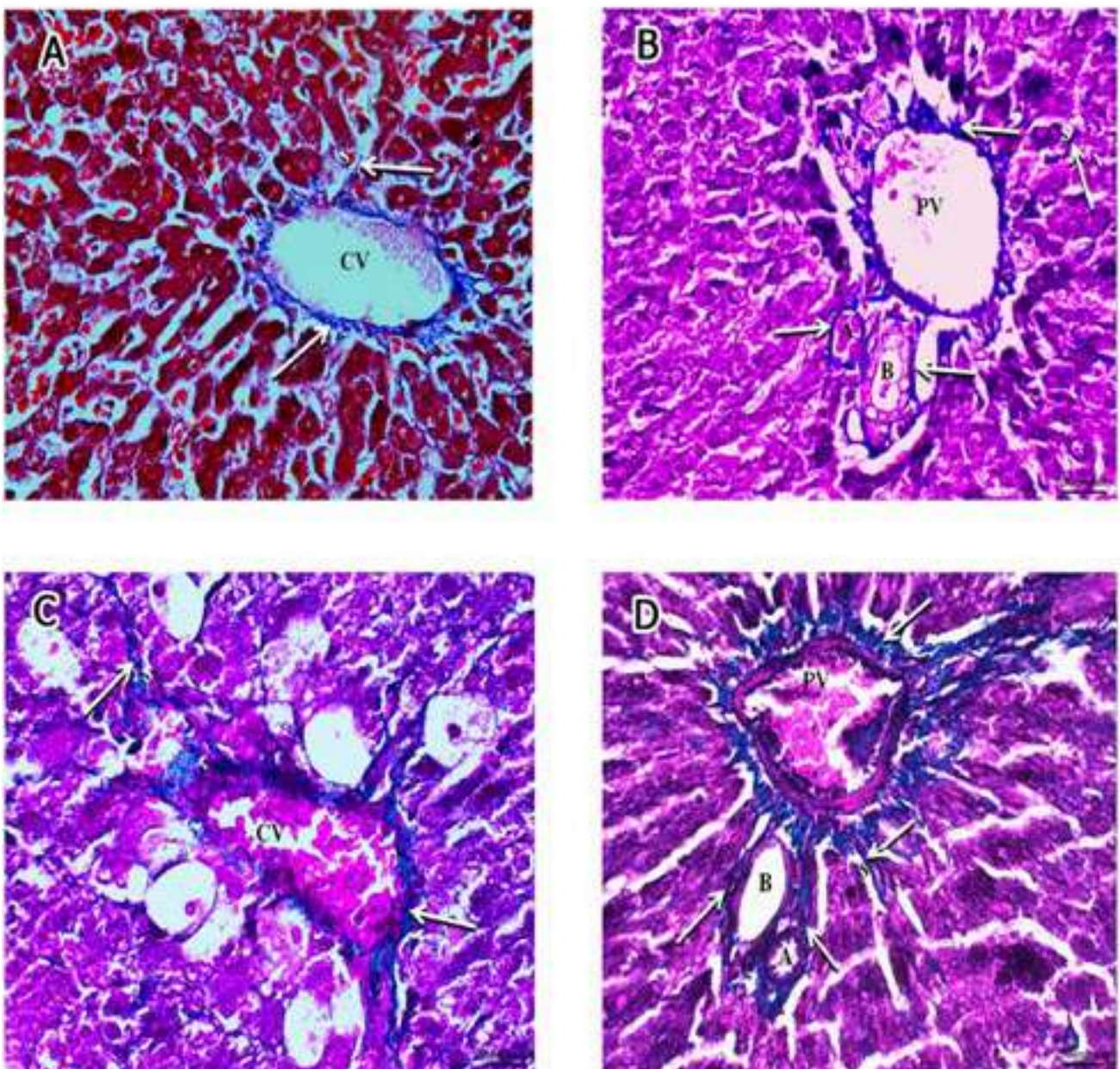


Fig. 5.- A, B of group V. A- almost normal distribution of collagen bundles (arrows) around the central vein (CV), hepatic sinusoids (S) and B- around the components of the portal triad: hepatic artery (A), bile ductile (B), portal vein (PV) and hepatic sinusoids (S). C, D of group VI. C- moderate increase of collagen bundles (arrows) around the central vein (CV), hepatic sinusoids (S) and D- around the components of the portal triad: hepatic artery (A), bile ductile (B), portal vein (PV); and adjoining hepatic sinusoids (S) (Masson trichrome, x400). Scale bars: A-D = 20 μ m.

envelope and Golgi apparatus opposite nuclear pores. Abundant mitochondria with normal cristal pattern were also detected with mild cytoplasmic rarefaction (Fig. 6E). Group VI also demonstrated mild return of the normal cellular structure,

where the nucleus appeared with fairly clumped chromatin material, prominent nucleolus and indented nuclear envelope, apparently normal rough endoplasmic reticulum with its ribosomal surface and few areas of cytoplasmic rarefaction.

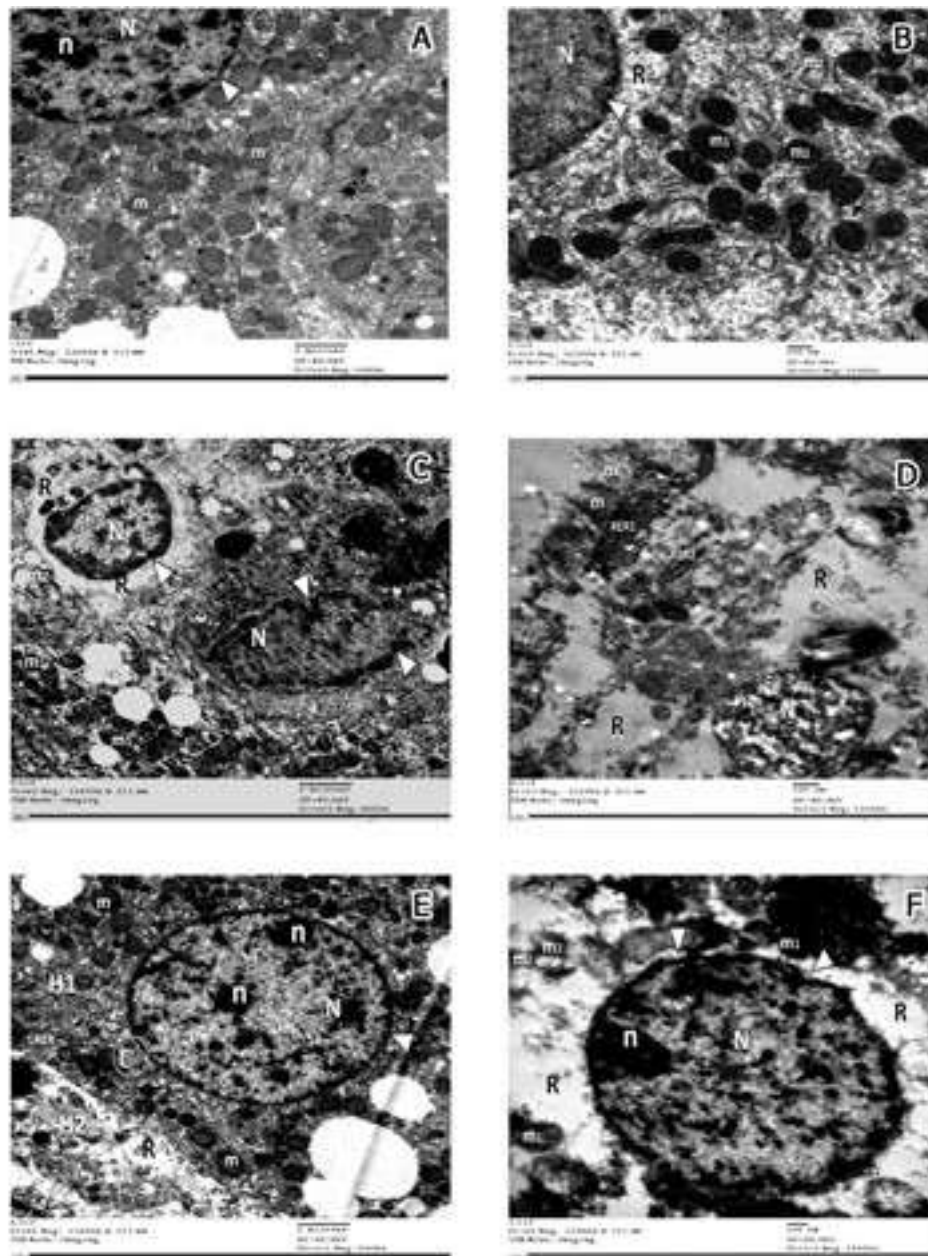


Fig. 6.- Electron micrographs of Group I and II (A) showing spherical to ovoid mitochondria (m) with intact cristae and rough endoplasmic reticulum (RER). The nucleus (N) is surrounded by bilaminar envelope with nuclear pores (arrowhead) and displays dispersed chromatin and an evident nucleolus(n). Golgi apparatus can be observed (circle) opposite nuclear pores (x6000). **B-** Group III displaying apparently normal nucleus(N) with intact nuclear envelop (arrowhead), rough endoplasmic reticulum (RER)with maintained ribosomal surface and cytoplasmic rarefaction (R). Most of mitochondria are apparently normal with intact cristae (m1) and few of them are ballooned with lost cristae (m2) (x12000). **C, D:** group IV, **C-** displaying irregular nuclei (N) with clumped chromatin material and indented nuclear envelope (arrowhead), extensive cytoplasmic rarefaction (R), degenerated rough endoplasmic reticulum with lost ribosomal surface (RER). The mitochondria are either apparently normal (m1) or ballooned with lost cristae (m2) (x6000); **D-** illustrating extremely shrunken nucleus with clumped chromatin material (N), extensive cytoplasmic rarefaction (R), ballooning of mitochondria with disrupted membranes (m). Rough endoplasmic reticulum is mostly fragmented (RER2) forming cisterns that lost their ribosomal surface and few are intact with normal ribosomal surface and parallel cisterns (RER1). x 12000). **E-** Group V demonstrating two hepatocytes; H1 showing: apparently normal nucleus with dispersed chromatin (N), prominent nucleoli (n) and an intact nuclear envelope (arrowhead), Golgi apparatus (circle) opposite nuclear pores. Abundant mitochondria (m) with normal cristal pattern, H2: displaying mild cytoplasmic rarefaction (R) (x6000). **F-** Group VI displaying a nucleus with fairly clumped chromatin material(N), prominent nucleolus (n) and indented nuclear envelope (arrowhead), apparently normal rough endoplasmic reticulum with its ribosomal surface (RER) and few areas of cytoplasmic rarefaction(R). Most of mitochondria (m1) appear normal and few of them are ballooned with damaged cristae and disrupted membranes (m2) (x10000). Scale bars: A, C, E = 2 µm; B, D, F = 500 nm.

Most of mitochondria appeared normal and few of them were ballooned with damaged cristae and disrupted membranes (Fig. 6F).

Labeling of stem cells with PKH26

In group V and VI, the MSCs labeled with PKH26 fluorescent dye were detected in the examined hepatic tissue, confirming homing of these cells into the liver (Fig. 7A, B).

Serum biochemical markers results

Serum liver biochemical markers (AST, ALT and GGT) showed statistically significant differences in group III, IV and VI compared to group I ($p < 0.0001$). There was a statistically significant difference between the group III and group IV. AST, ALT and GGT were significantly lower in group V compared to group III and in group VI

compared to group IV. Moreover, there was a statistically significant difference between the group V and group VI ($p = 0.004$). However, there was no statistically significant difference between the control and group V ($p = 0.657$) (Figs. 8A, B, C).

Liver oxidant/antioxidant markers results

Liver homogenate levels of MDA showed statistically significant difference in group III, IV and VI compared to group I ($p < 0.0001$). There was a statistically significant difference between the group III and group IV. MDA was significantly lower in group V compared to group III, and in group VI compared to group IV. Moreover, there was a statistically significant difference between the group V and group VI ($p = 0.004$). However, there was no statistically significant difference between the control and group V ($p = 0.842$) (Fig. 9A).

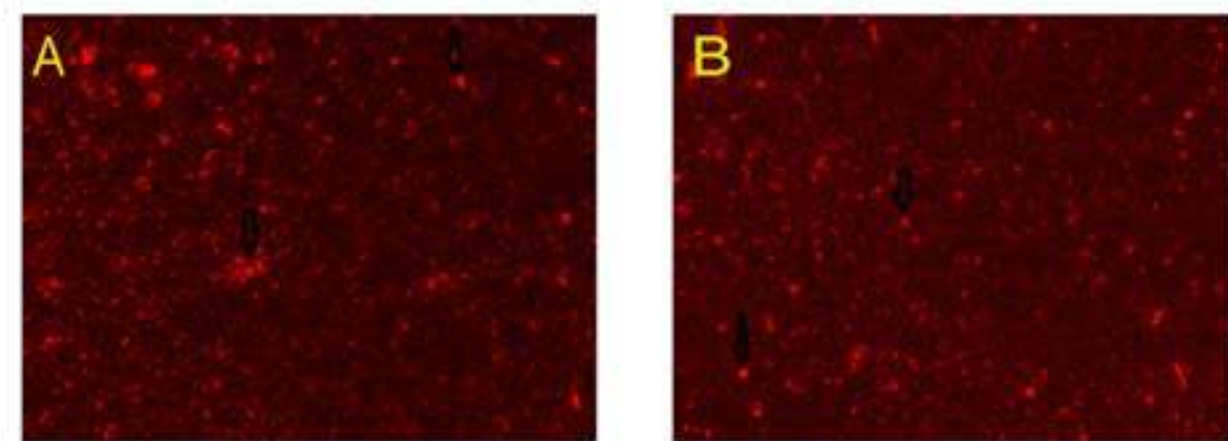


Fig. 7.- Micrographs of MSCs labelled with PKH26 fluorescent dye. A- Group V and B- Group VI. MSCs labelled with the PKH26 showed strong red auto fluorescence after transplantation into rats, confirming that these cells were seeded into the liver tissue.

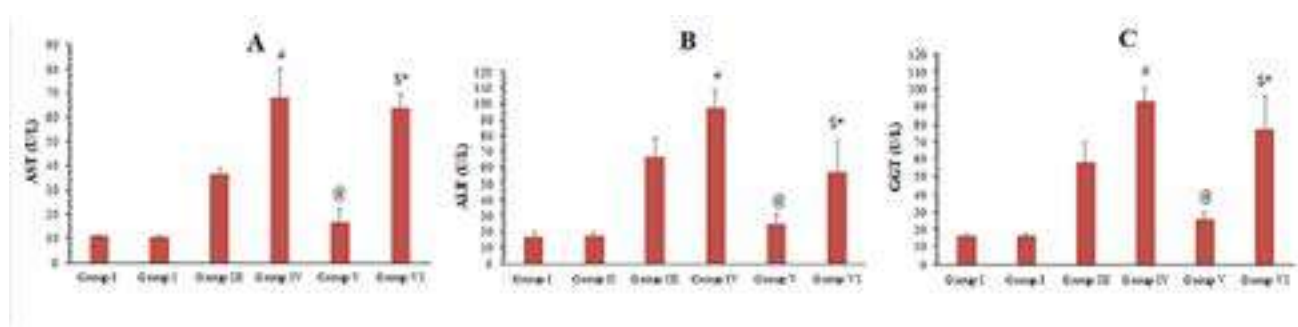


Fig. 8.- A- Mean values of AST obtained from the different groups of the examined animals. B- Mean values of ALT obtained from the different groups of the examined animals. C- Mean values of GGT obtained from the different groups of the examined animals. # significant from group III, @ significant from group III, \$ significant from group IV, * Significant from V.

Liver homogenate levels of SOD showed statistically significant difference in group III, IV and VI compared to group I ($p < 0.0001$). There was a statistically significant difference between the group III and group IV. SOD was significantly higher in group V compared to group III and in group VI compared to group IV. Moreover, there was a statistically significant difference between the group V and group VI ($p = 0.004$). However, there was no statistically significant difference between the control and group V ($p = 0.612$) (Fig. 9B).

pyknosis, karyolysis, depletion of glycogen content, cytoplasmic vacuolation and fatty degeneration. The biochemical study showed markedly elevated liver enzymes especially in high dose (600 mg/kg). The electron microscopic examination presented thick plasma membrane, cytoplasmic degeneration, rarefaction and fat degeneration, increased electron dense lysosomes, ballooning of mitochondria, fragmented rough endoplasmic reticulum and degenerated nucleus with clumped chromatin material. These results could be attributed to the increased oxidative stress

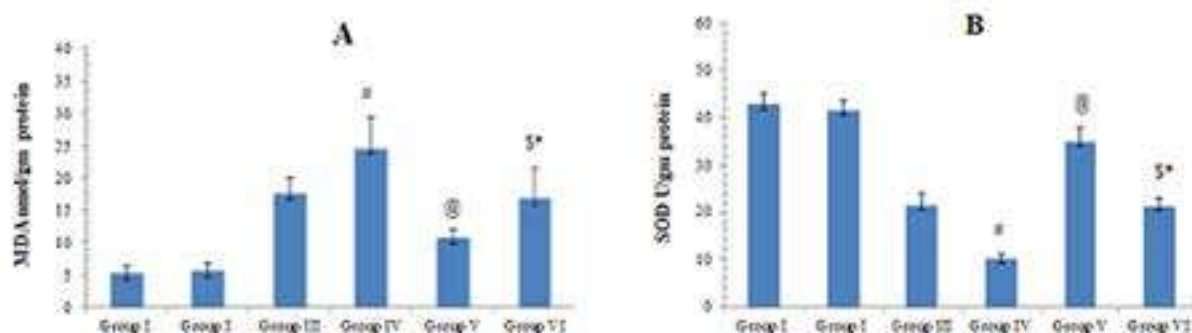


Fig. 9.- A- Mean values of MDA obtained from the different groups of the examined animals. B- Mean values of SOD obtained from the different groups of the examined animals. # significant from group III, @ significant from group III, \$ significant from group IV, * Significant from V.

DISCUSSION

Although acetaminophen is widely used for its analgesic and antipyretic actions, its overdose is also associated with hepatotoxicity (Wootton and Lee, 1990; Zimmerman and Maddrey, 1995; Lee, 2013). The present study demonstrated the effects of this toxicity, as well as the therapeutic values of MSCs to alleviate these effects.

In the present work, manifestations of the pathological impact of two different doses of acetaminophen on the rat liver were recorded in group III and group IV; 300 mg/kg and 600 mg/kg respectively, with marked histological and laboratory alterations in group IV. Light microscopic examination revealed disrupted hepatic parenchymal architecture, increased number of Kupffer cells, inflammatory cellular infiltration, dilatation and congestion of the central, portal veins and hepatic sinusoids, proliferated bile ductules, extravasated blood, hepatocytic degeneration in the form of nuclear

evidenced in groups III and IV by the significant increased level of MDA, indicating high level of the noxious reactive oxygen species (ROS), as well as the decreased level of the antioxidant enzyme SOD. These findings were in accordance with previous studies, which reported that large doses of acetaminophen lead to excessive formation of NAPQI, which triggers cell damage via an imbalance in oxidative stress involving high levels of ROS, such as hydroxyl radicals (OH), superoxide (O_2^-) and peroxy nitrite, with low levels of antioxidant enzymes, such as glutathione peroxidase and superoxide dismutase, eventually causing acute liver cell injury and cell death (Kay et al., 2011; McGill, 2012; Gum and Cho, 2013; Kane, 2018).

In the present work, mitochondrial and rough endoplasmic reticulum damage was evident in rats given acetaminophen alone (groups III and IV), which could be accredited to the imbalanced oxidative stress. This was in agreement with

Jaeschke et al., 2014 and Du et al., 2017), who attributed these findings to reactive oxygen species that directly injure the mitochondria, followed by disturbance of calcium homeostasis and protein synthesis with subsequent cell necrosis.

In the current study, acetaminophen administration was associated with marked increase in collagen fibers deposition. These findings were in agreement with Bai et al. (2017) and Alwahsh et al. (2019), who recorded hepatic fibrotic changes following repeated doses of acetaminophen. The mechanism of fibrosis was explained by Friedman (2008), who pointed out that the main cell responsible for fibrogenesis is the hepatic stellate cell which produces type I and type IV collagen. In case of injury, it undergoes activation, characterized by cellular proliferation with increased endoplasmic reticulum, increased contractility with prominent smooth muscle specific α -actin, increased secretion of cytokines and eventually fibrosis.

In the present work, groups III and IV also showed marked elevation in liver enzymes denoting marked liver cell damage, which could be also explained by ROS resulting from acetaminophen administration. Similar findings were found by Dart and Baily (2007), who mentioned that one gram of acetaminophen four times a day can cause elevation of liver enzymes three times the normal values. It was reported that administration of acetaminophen leads to marked increase in serum liver enzymes and decrease in serum albumin level with consequent liver cell failure.

Thuwaini et al. (2016) and Khorsandi et al. (2010) reported that acetaminophen leads to marked elevation of serum liver enzymes after one hour and three hours following administration, and added that evaluation of serum ALT in the early hours can be more helpful than AST level. Jarsiah et al. (2017) concluded that acetaminophen caused hepatic injury resulting from cell membrane and mitochondrial damage, and this was manifested by elevation of serum ALT and AST. Furthermore, GGT is released extensively from damaged hepatic cells to the blood stream, and hence it has a diagnostic value in hepatobiliary diseases. Such data were similar to the findings of the present research.

In the current study, MSC therapy markedly ameliorated the histological and biochemical alterations exerted by acetaminophen administration in groups V and VI, which could be attributed to the improvement of oxidative stress parameters in the form of significant decreased MDA and significant increased SOD levels in these groups. These findings were in accordance with Ayatollahi et al. (2014), who demonstrated the therapeutic role of MSC in case of hepatic injury caused by the oxidative stress of carbon tetrachloride. Moreover, Zeng et al. (2015) also reported the augmented therapeutic effect of MSC with intensified antioxidant power in the treatment of acute hepatic failure.

Previous studies (Huang et al., 2016; Wang et al., 2018) illustrated another mechanism underlying the therapeutic role of MSC in the form of the immunosuppression that downregulates proinflammatory cytokines (IL-1 α , IL-1 β) and upregulates anti-inflammatory cytokines (IL-6, IL-10). In addition, MSC improves liver function and increases expression of growth factors and cytokines that guide MSC home in the injured tissue, which promotes hepatic regeneration and restoration of normal liver functions. Moreover, MSC can differentiate into mature hepatocytes, with restoration of their structural and functional activity, regaining the normal hepatic parenchymal architecture. Vassilopoulos et al. (2003) and Milosavljevic et al. (2017) hypothesized that conversion of MSCs to hepatocytes may occur via cell fusion. Bystander effect is probably due to factors secreted by MSC that direct them to the site of injury, leading to increased mitotic activity of hepatocytes. The release of vascular endothelial growth factor from stem cells increasing the blood supply is another theory to explain the regeneration of injured liver cells and improvement in liver functions (Tang et al., 2006). Furthermore, MSC may act by overexpression of the Bcl-2 gene inhibiting apoptosis (Chen et al., 2001) or by suppression of interleukin-6 (IL-6) pathway inhibiting inflammation (Wang et al., 2006). Lastly, tissue-specific stem cells, such as oval cells in the liver may be stimulated by hepatic stellate cells enhancing the regeneration of the injured tissue (Austin and Lagasse, 2003).

In the current study, liver fibrosis was attenuated after administration of MSC. This could be explained by the theory that MSC express certain antifibrotic factors, such as matrix metalloproteinase 9 (MMP-9) and release some factors, such as soluble Kit- ligand related to their proliferation and differentiation (Kallis et al., 2007; Segovia-Silvestre et al., 2011). It was concluded that after 4 weeks of MSC transplantation, significant decrease of alpha smooth muscle specific α -actin occurred. Thus, transplanted MSC may inhibit activated stellate cells by them or guide them to apoptosis (Ezzat et al., 2012). Contradicting the observed data of the present study, Di Bonzo et al. (2008) and Yan et al. (2009) have demonstrated that MSC display a profibrogenic propensity. Indeed, intravenously infused umbilical cord MSC contributed to the myofibroblast population (smooth muscle specific α -actin and fibroblast secretory protein-1 positive cells) in liver injury.

MSC administration markedly decreased serum liver enzymes ALT, AST and GGT, which could be attributed to improved oxidative stress markers evidenced by significant increased SOD and significant decreased MDA levels. This was in accordance with Zhao et al. (2012), who mentioned that MSC injection causes marked decrease in serum levels of liver enzymes and serum bilirubin, and the results were better with early treatment due to restoration of normal cellular and functional pattern of hepatocytes as a result of MSC hepatic differentiation into hepatocytes. Kuo et al. (2008), Song et al. (2015) and Idriss et al. (2018) demonstrated that the effectiveness of stem cell therapy depends greatly on the route of transplantation. They revealed that intravenous MSC-derived hepatocyte transplantation in rescuing liver failure was superior to intrasplenic, intraperitoneal, or even intrahepatic transplantation.

Conclusion

The overdose of acetaminophen results in deleterious effects on the liver, which could be detected in the present work on the structure and biochemical aspects. MSC executed significant improvement of these harmful effects evidenced

by homing of MSC in liver and improvement at both structural and functional (confirmed by biochemical results of oxidative stress markers) levels.

REFERENCES

- ALHADLAQ A, MAO JJ (2014) Mesenchymal stem cells: isolation and therapeutics. *Stem Cells Dev*, 13: 436-448.
- ALWAHSH M, OTHMAN A, HAMADNEH L, TELFAH A, LAMBERT J, HIKMAT S, ALASSI A, MOHAMED F, HERGENRÖDER R, AL-QIRIML T, DOOLEY S, HAMMAD S (2019) Second exposure to acetaminophen overdose is associated with liver fibrosis in mice. *EXCLI J*, 18: 51-62.
- AUSTIN TW, LAGASSE E (2003) Hepatic regeneration from hematopoietic stem cells. *Mech Dev*, 120(1): 131-135.
- AYATOLLAHI M, HESAMI Z, JAMSHIDZADEH A, GRAMIZADEH B (2014) Antioxidant effects of bone marrow mesenchymal stem cell against carbon tetrachloride-induced oxidative damage in rat livers. *Int J Org Transplant Med*, 5(4): 166-173.
- BAI Q, YAN H, SHENG Y, JIN Y, SHI L, JI L, WANG Z (2017) Long-term acetaminophen treatment induced liver fibrosis in mice and the involvement of Egr-1. *Toxicology*, 382: 47-58.
- BANCROFT JD, GAMBLE M (2008) Connective tissue stains. In: Bancroft J (ed). *Theory and Practice of Histological Techniques*. Churchill-Livingston Elsevier, London, pp 135-160.
- BHUSHAN B, WALESKY C, MANLEY M, GALLAGHER T, BORUDE P, EDWARDS G, MONGA SP, APTE U (2014) Pro-regenerative signaling after acetaminophen-induced acute liver injury in mice identified using a novel incremental dose model. *Am J Pathol*, 184(11): 3013-3025.
- CHEN Z, CHUA CC, HO YS, HAMDY RC, CHUA BH (2001) Overexpression of Bcl-2 attenuates apoptosis and protects against myocardial I/R injury in transgenic mice. *Am J Physiol Heart Circ Physiol*, 280(5): H2313-H2320.
- CRAIG DG, BATES CM, DAVIDSON JS, MARTIN KG, HAYES PC, SIMPSON KJ (2012) Staggered overdose pattern and delay to hospital presentation

are associated with adverse outcomes following paracetamol-induced hepatotoxicity. *Br J Clin Pharmacol*, 73(2): 285-294.

DART RC, BAILEY E (2007) Does therapeutic use of acetaminophen cause acute liver failure? *Pharmacotherapy*, 27(9): 1219-1230.

DI BONZO LV, FERRERO I, CRAVANZOLA C, MARESCHI K, RUSTICHELL D, NOVO E, SANAVIO F, CANNITO S, ZAMARA E, BERTERO M, DAVIT A (2008) Human mesenchymal stem cells as a two-edged sword in hepatic regenerative medicine: engraftment and hepatocyte differentiation versus profibrogenic potential. *Gut*, 57(2): 223-231.

DU K, FARHOOD A, JAESCHKE H (2017) Mitochondria-targeted antioxidant Mito-Tempo protects against acetaminophen hepatotoxicity. *Arch Toxicol*, 91: 761-773.

EZZAT T, DHAR DK, MALAGO M, DAMINK SWO (2012) Dynamic tracking of stem cells in an acute liver failure model. *World J Gastroenterol*, 18(6): 507-516.

FRIEDMAN SL (2008) Mechanisms of hepatic fibrogenesis. *Gastroenterology*, 134(6): 1655-1669.

GUM SI, CHO MK (2013) Recent updates on acetaminophen hepatotoxicity the role of nrf2 in hepatoprotection. *Toxicol Res*, 29(3): 165-172.

GURTNER GC, CALLAGHAN MJ, LONGAKER MT (2007) Progress and potential for regenerative medicine. *Annu Rev Med*, 58: 299-312.

HAYAT A (1986) Principles of tissue preparation for electron microscopy. In: Hayat MA (ed). *Basic techniques for transmission electron microscopy*, 1st edn. Macmillan Press, New York, pp 22-46.

HUANG YJ, CHEN P, LEE CY, YANG SY, LIN MT, LEE HS, WU YM (2016) Protection against acetaminophen-induced acute liver failure by omentum adipose tissue derived stem cells through the mediation of Nrf2 and cytochrome P450 expression. *J Biomed Sci*, 23(1): 5.

IDRISS NK, SAYED HG, OSAMA A, SABRY D (2018) Treatment efficiency of different routes of bone marrow-derived mesenchymal stem cell injection in rat liver fibrosis model. *Cell Physiol Biochem*, 48(5): 2161-2171.

JAESCHKE H, MCGILL MR, RAMACHANDRAN A (2012) Oxidant stress, mitochondria, and cell death mechanisms in drug-induced liver injury: lessons learned from acetaminophen hepatotoxicity. *Drug Metab Rev*, 44(1): 88-106.

JAESCHKE H, XIE Y, MCGILL MR (2014) Acetaminophen-induced liver injury: from animal models to humans. *J Clin Transl Hepatol*, 2(3): 153-161.

JARSIAH P, NOSRATIA, ALIZADEH A, HASHEMI-SOTEH SMB (2017) Hepatotoxicity and ALT/AST enzymes activities change in therapeutic and toxic doses consumption of acetaminophen in rats. *International Biol Biomed J*, 3(3): 119-124.

KALLIS YN, ALISON MR, FORBES SJ (2007) Bone marrow stem cells and liver disease. *Gut*, 56(5): 716-724.

KANE AE, MITCHELL SJ, PAJKOS JM, MCKENZIE C, JONES B, COGGER V, COUTEUR DGL, CABOD R, HILMER SN (2018) Acetaminophen hepatotoxicity in mice: Effect of age, frailty and exposure type. *Exp Gerontol*, 73: 95-106.

KAY HY, KIM YW, RYU DH, SUNG SH, HWANG SJ, KIM SG (2011) Nrf2-mediated liver protection by sauchinone, an antioxidant lignan, from acetaminophen toxicity through the PKC δ -GSK3 β pathway. *Br J Pharmacol*, 163(8): 1653-1665.

KHORSANDI LS, JAVADNIA F, ORAZIZADEH M, ABDOLAHI M (2010) Effect of green tea (*Camellia sinensis* L.) extract on acetaminophen induced acute hepatotoxicity in mice. *Iranian J Med Arom Plants*, 26(1): 22-29.

KIM TH, KIM JK, SHIM W, KIM SY, PARK TJ, JUNG JY (2010) Tracking of transplanted mesenchymal stem cells labeled with fluorescent magnetic nanoparticle in liver cirrhosis rat model with 3-T MRI. *Magn Reson Imaging*, 28(7): 1004-1013.

KUO TK, HUNG SP, CHUANG CH, CHEN CT, SHIH YRV, FANG SCY, YANG VW, LEE OK (2008) Stem cell therapy for liver disease: parameters governing the success of using bone marrow mesenchymal stem cells. *Gastroenterology*, 134(7): 2111-2121.

LARSON AM (2007) Acetaminophen hepatotoxicity. *Clin Liver Dis*, 11(3): 525-548.

- LEE WM (2013) Drug-induced acute liver failure. *Clin Liver Dis*, 17(4): 575-586.
- LOWRY OH, ROSEBROUGH NJ, FARR AL, RANDALL RJ (1951) Protein measurement with the folin phenol reagent. *J Biol Chem*, 193: 265-275.
- MCGILL MR, WILLIAMS CD, XIE Y, RAMACHANDRAN A, JAESCHKE H (2012) Acetaminophen-induced liver injury in rats and mice: comparison of protein adducts, mitochondrial dysfunction, and oxidative stress in the mechanism of toxicity. *Toxicol Appl Pharmacol*, 264(3): 387-394.
- MILOSAVLJEVIC N, GAZDIC M, SIMOVIC MARKOVIC B, ARSENIJEVIC A, NURKOVIC J, DOLICANIN Z, DJONOV V, LUKIC ML, VOLAREVIC V (2017) Mesenchymal stem cells attenuate acute liver injury by altering ratio between interleukin 17 producing and regulatory natural killer T cells. *Liver Transplant*, 23(8): 1040-1050.
- MISRA HP, FRIDOVICH I (1972) The role of superoxide anion in the autoxidation of epinephrine and a simple assay for superoxide dismutase. *J Biol Chem*, 247(10): 3170-3175.
- OHKAWA H, OHISHI N, YAGI K (1979) Assay for lipid peroxides in animal tissues by thiobarbituric acid reaction. *Anal Biochem*, 95(2): 351-358.
- PAYUSHINA OV, DOMARATSKAYA EI, STAROSTIN VI (2006) Mesenchymal stem cells: sources, phenotype, and differentiation potential. *Biol Bull*, 33: 2-18.
- RAAFAT N, ABDEL AAL SM, ABDO FK, EL GHONAIMY NM (2015) Mesenchymal stem cells: in vivo therapeutic application ameliorates carbon tetrachloride induced liver fibrosis in rats. *Int J Biochem Cell Biol*, 68: 109-118.
- REITMAN S, FRANKEL S (1957) A colorimetric method for the determination of serum glutamic oxalacetic and glutamic pyruvic transaminases. *Am J Clin Pathol*, 28(1): 56-63.
- SCHEERS I, LOMBARD, NAJIMI M, SOKA EM (2011) Cell therapy for the treatment of metabolic liver disease: an update on the umbilical cord derived stem cells candidates. *Open Tissue Eng Regen Med J*, 4: 48-53.
- SEGOVIA-SILVESTRE T, REICHENBACH V, FERNÁNDEZ-VARGO G, VASSILIADIS E, BARASCUK N, MORALES-RUIZ M, KARSDAL MA, JIMÉNEZ W (2011) Circulating CO3-610, a degradation product of collagen III, closely reflects liver collagen and portal pressure in rats with fibrosis. *Fibrogenesis Tissue Repair*, 4(1): 19.
- SONG YM, LIAN CH, WU CS, JI A, XIANG JJ, WANG XY (2015) Effects of bone marrow derived mesenchymal stem cells transplanted via the portal vein or tail vein on liver injury in rats with liver cirrhosis. *Exp Therap Med*, 9(4): 1292-1298.
- TANG J, XIE Q, PAN G, WANG J, WANG M (2006) Mesenchymal stem cells participate in angiogenesis and improve heart function in rat model of myocardial ischemia with reperfusion. *Eur J Cardio-Thoracic Surg*, 30(2): 353-361.
- THUWAINI MM, KADHEM HS, HATEM HA (2016) Reducing the effects of paracetamol-induced hepatic damage in rat with fluvastatin drug. *Univ Thi-Qar J*, 11(4): 143-161.
- VASSILOPOULOS G, WANG PR, RUSSELL DW (2003) Transplanted bone marrow regenerates liver by cell fusion. *Nature*, 422(6934): 901.
- WANG M, TSAI BM, CRISOSTOMO PR, MELDRUM DR (2006) Pretreatment with adult progenitor cells improves recovery and decreases native myocardial proinflammatory signaling after ischemia. *Shock*, 25(5): 454-459.
- WANG YH, WU DB, CHEN B, CHEN EQ, TANG H (2018) Progress in mesenchymal stem cell-based therapy for acute liver failure. *Stem Cell Res Therapy*, 9(1): 1-9.
- WEAKLEY BS (1981) A beginner's handbook in biological transmission electron microscopy. Ed. Churchill Livingstone; 2nd ed.
- WOOTTON FT, LEE WM (1990) Acetaminophen hepatotoxicity in the alcoholic. *South Med J*, 83(9): 1047-1049.
- YAN Y, XU W, QIAN H, SI Y, ZHU W, CAO H, ZHOU H, MAO F (2009) Mesenchymal stem cells from human umbilical cords ameliorate mouse hepatic injury in vivo. *Liver Int*, 29(3): 356-365.
- ZENG W, XIAO J, ZHENG G, XING F, TIPOE G, WANG X, HE C, CHEN Z, LIU Y (2015) Antioxidant

treatment enhances human mesenchymal stem cell anti-stress ability and therapeutic efficacy in an acute liver failure model. *Sci Rep*, 5: 11100.

ZHAO W, LI JJ, CAO DY, LI, ZHANG LY, HE Y, YUE SQ, WANG DS, DOU KF (2012) Intravenous injection of mesenchymal stem cells is effective in treating liver fibrosis. *World J Gastroenterol*, 18(10): 1048-1058.

ZIMMERMAN HJ, MADDREY WC (1995) Acetaminophen (paracetamol) hepatotoxicity with regular intake of alcohol: analysis of instances of therapeutic misadventure. *Hepatology*, 22(3): 767-773.

The anatomic study of extracranial structures related to tuberculum pharyngeum

Nazli G. Ceri¹, Ayse G. Sahmelikoglu¹, Fulden Cantas², Gizem Sakalli¹

¹ Department of Anatomy, Faculty of Medicine, Aydin Adnan Menderes University, Aydin, Turkey

² Department of Biostatistics, Faculty of Medicine, Aydin Adnan Menderes University, Aydin, Turkey

SUMMARY

Knowledge of the anatomy of this region is extremely important in determining the surgical approach in craniovertebral junction pathologies and tumors. Therefore, the distance of the tuberculum pharyngeum (TP), which is located in the center of this region, to other close and significant anatomical structures is important. This study was conducted using a total of 64 craniums. The width of the pars basilaris at the level of the TP and the distance from the TP to anatomical formations such as opisthion, basion, protuberentia occipitalis externa, condylus occipitalis, canalis caroticus, processus styloideus, foramen stylomastoideum, processus mastoideus and ala vomeris were measured. The difference in measurements between sexes and sides were evaluated. The distances from the TP to opisthion, protuberentia occipitalis externa, condylus occipitalis, left canalis caroticus, processus styloideus, foramen stylomastoideum and processus mastoideus were statistically higher in males than in females. On the other hand, no significant difference was observed between the sexes in the width of the pars basilaris at the level of the TP and in the distance between the TP to the basion, right canalis caroticus and ala vomeris. There was no statistically significant difference between the distances from TP to

condylus occipitalis, canalis caroticus, processus styloideus, foramen stylomastoideum, processus mastoideus and ala vomeris in both sides and both sexes. In male and female anatomical structures, the pars basilaris ossis occipitalis placed between the vomer and foramen magnum are similar in size. Although the distance of TP to important structures was significantly higher in males than in females, it was observed that the distances of TP to the right and left anatomical structures were symmetrical in all craniums. We think that knowledge of the cranium base morphometry and its bilateral symmetry will guide the interventions to be made here by taking the opposite side as a model.

Key words: Anatomy – Clivus – Cranium – Morphometric – Tuberculum pharyngeum

INTRODUCTION

Tuberculum pharyngeum (TP), which gives attachment to the pharyngeal raphe, the highest attachment of the superior pharyngeal constrictor, is a small elevation found on the midline of the pars basilaris ossis occipitalis (the basilar part of the occipital bone) (Standring, 2016). On the extracranial surface, the pharyngeal tubercle is located in the midline around the junction of the

Corresponding author:

Nazli Gulriz Ceri, MD PhD. Department of Anatomy, Faculty of Medicine, Aydin Adnan Menderes University, 09100 Aydin, Turkey. Phone: +90 533 565 9868; Fax: +90 256 212 0146. E-mail: drnazligulrizceri@gmail.com. Orcid no: 0000-0001-5486-1824

Submitted: November 10, 2020. Accepted: December 14, 2020

middle and lower clivus. There may be a small bone rise between the TP and the anterior margin of the foramen magnum, and this structure is called the crista pharyngea, but it is a very rare occurrence (Hofmann and Prescher, 2012).

The base of the cranium provides the support and protection of vital organs such as the brain and cerebellum, as well as forming the transition point of important vascular and neural structures located between the cranium and the upper cervical region. (Sharma and Garud, 2011). Trauma-induced disorders, tumors, vascular system diseases and degenerative diseases are frequently seen at the craniocervical junction, and treatment for these lesions are usually surgical (Zhong et al., 2018; Patel et al., 2016). Surgical approaches such as transoral-transpharyngeal directly reach the ventral midline of the basis cranii externa, and at the same time prevent damage to some important anatomical structures such as the sixth through the twelfth cranial nerves, internal carotid artery, internal jugular vein, inferior petrosal sinus, and inferior petroclival vein located in this region. These approaches afford direct and relatively safe avenues with few vital neurovascular structures in the midline plane. In lesions that require a posterior approach, the distance between the TP and the surrounding structures is surgically important (Wang et al., 2016; Hitotsumatsu et al., 1999; Patel et al., 2016).

In this study, we measured the distance between the TP and other anatomical formations, so as to determine the surgical confidence interval and to prevent damage during the surgical treatment of lesions or tumors that will occur in this area. In addition to radiological studies in this area, measurements obtained from studies on dry bones will provide healthier results and guide the surgeons.

MATERIALS AND METHODS

This study was conducted using a total of 64 randomly selected adult craniums (22 female and 42 male) without any structural deformities obtained from the bone archive in the Department of Anatomy, Faculty of Medicine, Aydin Adnan Menderes University. Measurement of the closest

distance from the TP (Fig. 1, Table 1), as the main point of reference, to important structures were made with the help of an electronic clip. At the beginning of the study, 10 randomly selected craniums were independently evaluated by two observers. A day later, the same measurements were repeated and the intra-observation reliability was evaluated.

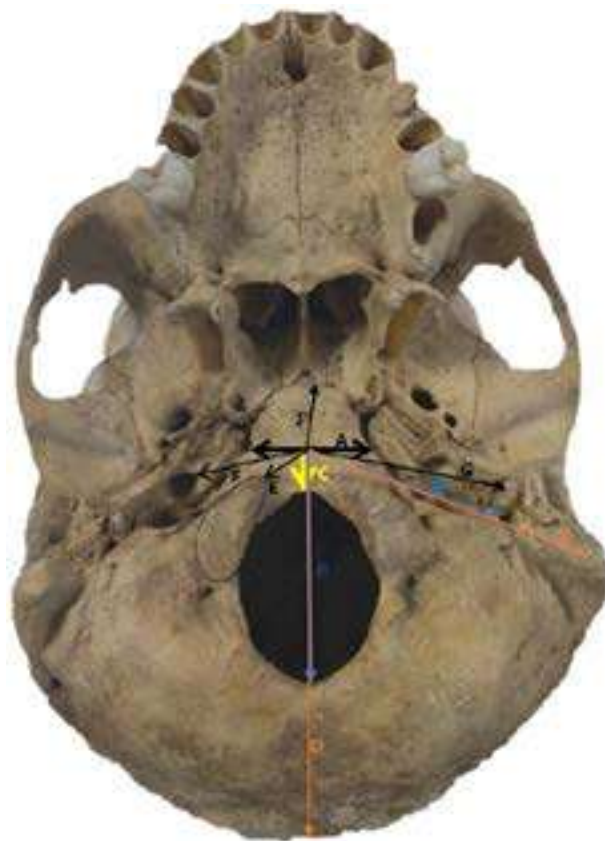


Fig. 1.- The location of the measurements in Table 1 in the basis cranii externa (Bone archive of Department of Anatomy).

Statistical analysis

Whether or not quantitative variables conform with normal distribution was examined using the Kolmogorov-Smirnov test. Groups were compared by using two-independent samples t- tests for normally distributed variables and Mann Whitney U test for variables that did not show normal distribution. Dependent variables with normal distribution were compared with paired t test, and non-normally distributed dependent variable were compared with Wilcoxon T test. Statistically, $p < 0.05$ values were considered significant.

Table 1. The closest measurements between tuberculum pharyngeum and anatomic structures.

Pars basilaris width at the level of tuberculum pharyngeum (TP-PB)	A
Distance between tuberculum pharyngeum and opisthion (TP-O)	B
Distance between tuberculum pharyngeum and basion (TP-B)	C
Distance between tuberculum pharyngeum and protuberentia occipitalis externa (TP-POE)	D
Distance between tuberculum pharyngeum and condylus occipitalis (TP-CO)	E
Distance between tuberculum pharyngeum and canalis caroticus (TP-CC)	F
Distance between tuberculum pharyngeum and processus styloideus (TP-PS)	G
Distance between tuberculum pharyngeum and foramen stylomastoideum (TP-FS)	H
Distance between tuberculum pharyngeum and processus mastoideus (TP-PM)	I
Distance between tuberculum pharyngeum and ala vomeris (TP-AV)	J

RESULTS

In the study, the distance of the TP to 9 important anatomical structures and the pars basilaris width were evaluated using 64 craniums of known sexes (Fig. 1, Table 1).

In Table 2, the distances from the TP to opisthion, protuberentia occipitalis externa, condylus occipitalis, left canalis caroticus, processus styloideus, foramen stylomastoideum and processus mastoideus were statistically higher in males than in females. On the other hand, no significant difference was observed between the sexes in the width of the pars basilaris at the level of the TP and in the distance between the TP to the basion, right canalis caroticus and ala vomeris.

In Tables 3 and 4, there was no statistically significant difference between the distances from TP to condylus occipitalis, canalis caroticus, processus styloideus, foramen stylomastoideum, processus mastoideus and ala vomeris in both sides and both sexes.

DISCUSSION

For surgeons and clinicians, the structures in the basis cranii externa are very important. There are also studies evaluating clivus and condylus occipitalis morphometrically (Kızıllanat et al.,

2006; Ozer et al., 2011; Ji et al., 2012). There are studies investigating the structure of basis cranii not only in the bone tissue in that region, but also in connective tissue and its properties related to membranous structures (Krmpotić-Nemanić et al., 2006; Aparna et al., 2019). As a matter of fact, even the distance of fossa navicularis, which is a rare variation on craniums, to TP has been measured (Cankal et al., 2004). TP is the central point of the nasopharynx and together with the anatomical structures adjacent to it, it is important in both breathing and swallowing (Krmpotić-Nemanić et al., 2006; Aparna et al., 2019). Despite the importance of the region, the insufficient number of studies led us to evaluate this area in morphometric detail.

In a study conducted in Croatia, Krmpotić-Nemanić et al. (2006) evaluated the distance of osseous epipharynx to anatomical formations in 60 basis cranii externa. Similar to our study, they measured the distance of the TP to ala vomeris, the basion, and the pars basilaris width at the level of the tuberculum pharyngeum. They did not observe any significant sex-related difference and reported the data only by age distribution. Likewise, we did not detect any significant difference between the sexes in these three parameters. In addition, they recorded the distance between the TP and the basion as 8.6 ± 2.0 mm, the width in the pars basilaris as 26.8 ± 5.5 mm and the distance between the ala vomeris as 17.27 ± 3.8 mm. In our study, the distance between the TP and the basion was 12.58 ± 1.40 mm in males and 11.97 ± 1.27 mm in females, the width of the pars basilaris was 24.92 ± 2.72 mm in male and 24.11 ± 2.72 mm for female and the distance from both sides of ala vomeris was 17.60 ± 2.17 mm for the right-side and 17.49 ± 2.15 mm on the left-side in males, and 18.50 ± 1.55 mm on the right-side and 18.50 ± 1.41 mm on the left-side in females. We thought that the reason for the difference in the values obtained might be due to the difference based on population and sex.

A study (Erdem et al., 2018) where twenty-six adult dry skulls were measured reported that the distance between TP and canalis caroticus was 26.7 ± 2.00 mm on the left-side and 27.5 ± 2.22 mm on the right-side, while the distance between

condylus occipitalis was 16.4 ± 1.59 mm on the left-side and 16.3 ± 1.79 mm on the right-side.

In our study, we determined that the distance between the TP and condylus occipitalis on the right-side was 16.76 ± 1.70 mm in males and 15.38 ± 1.65 mm in females, on the left-side was 16.97 ± 2.82 in males and 15.28 ± 1.40 mm in females; the distance between the TP and the canalis caroticus on the right-side was 31.80 ± 2.19 mm in males and 31.60 ± 2.79 mm in females, on the left was 31.81 ± 2.16 mm in males and 30.27 ± 1.44 mm in females. There is no significant difference between the sides in these studies. While they did not discriminate sex for these measurements in their studies, we found a significant difference between sexes.

In contrast to Zhong et al. (2018) who, without sex discrimination, found the distance between the TP and opisthion as 10.23 ± 0.55 mm in the measurements on the basis cranii externa made on CT, our study found that this distance was 46.34 ± 6.83 mm in males and 44.68 ± 2.85 mm in

females and that it was statistically significantly lower in females.

Ji et al. (2012) performed a radiological study on 40 craniums, and found that the distance to the anterior part of the condylus occipitalis was 15.65 ± 1.65 mm on the left-side and 15.60 ± 1.91 mm on the right-side and the distance of the TP to the canalis caroticus was 24.26 ± 2.05 mm on the left-side, 26.25 ± 2.26 mm on the right-side. In our study, we determined that the distance of the TP to the condylus occipitalis to the anterior part as 16.76 ± 1.70 mm on the right-side, 16.97 ± 2.82 mm on the left-side for males, 15.38 ± 1.65 mm on the right-side and 15.28 ± 1.40 mm on the left-side for females; the distance of the TP to the canalis caroticus was 31.80 ± 2.19 mm on the right-side and 31.81 ± 2.16 mm on the left-side for males, and 31.60 ± 2.79 mm on the right-side and 30.27 ± 1.44 mm in the left-side for females. Our study differs from those similar studies, as they did not separate the sexes of bones and there is difference in measurement methods used.

Table 2. Descriptive statistics of quantitative variables in male and female groups (mm).

Mm	Min.-Max.	Male	Female	Mean±SD	p
		Mean±SD	Min.-Max.		
TP-PB	17,89-33,21	24,92±2,72	20,79-29,91	24,11±2,72	0,306
TP-O	4,01-52,79	46,34±6,83	40,49-49,00	44,68±2,85	0,005
TP-B	9,09-17,12	12,58±1,40	10,22-15,25	11,97±1,27	0,125
TP-POE	57,31-98,13	87,57±6,88	59,77-93,61	81,57±8,88	0,008
TP-CO right	13,82-20,29	16,76±1,70	18,46-12,09	15,38±1,65	0,008
TP-CO left	13,33-31,82	16,97±2,82	11,78-17,19	15,28±1,40	0,003
TP-CC right	25,54-36,69	31,80±2,19	27,35-38,02	31,60±2,79	0,772
TP-CC left	27,09-36,67	31,81±2,16	27,35-33,02	30,27±1,44	0,013
TP-PS right	37,31-46,64	41,65±2,31	34,72-43,03	40,00±2,27	0,017
TP-PS left	36,05-49,00	41,63±2,50	34,77-45,37	39,97±3,03	0,041
TP-FS right	40,50-49,36	43,70±2,19	39,47-45,37	41,60±1,61	0,001
TP-FS left	37,26-49,77	43,41±2,40	39,23-46,57	41,46±2,09	0,005
TP-PM right	25,42-63,21	56,37 ±5,59	48,53-58,32	53,77±2,60	0,001
TP-PM left	53,20-63,55	57,45±2,39	50,48-58,25	53,78±2,07	0,001
TP-AV right	14,17-22,77	17,60±2,17	14,95-20,89	18,50±1,55	0,132
TP-AV left	13,59-22,08	17,49±2,15	16,59-20,78	18,50±1,41	0,086

TP-PB: Pars basilaris width at the level of tuberculum pharyngeum, TP-O: Distance between tuberculum pharyngeum and opisthion, TP-B: Distance between tuberculum pharyngeum and basion, TP- POE: Distance between tuberculum pharyngeum and protuberentia occipitalis externa, TP-CO: Distance between tuberculum pharyngeum and condylus occipitalis, TP-CC: Distance between tuberculum pharyngeum and canalis caroticus, TP-PS: Distance between tuberculum pharyngeum and processus styloideus, TP-FS: Distance between tuberculum pharyngeum and foramen stylomastoideum, TP-PM: Distance between tuberculum pharyngeum and processus mastoideus, TP-AV: Distance between tuberculum pharyngeum and ala vomeris.

Table 3. Descriptive statistics of the dependent measurements in the male group (mm).

	Male		
	Right (Mean±SD)	Left (Mean±SD)	p
TP-CO	16,76±1,70	16,97±2,82	0,596
TP-CC	31,80±2,19	31,81±2,16	0,859
TP-PS	41,65±2,31	41,63±2,50	0,924
TP-FS	43,70±2,19	43,41±2,40	0,361
TP-PM	56,37 ±5,59	57,45±2,39	0,245
TP-AV	17,60±2,17	17,49±2,15	0,545

TP-CO: Distance between tuberculum pharyngeum and condylus occipitalis, TP-CC: Distance between tuberculum pharyngeum and canalis caroticus, TP-PS: Distance between tuberculum pharyngeum and processus styloideus, TP-FS: Distance between tuberculum pharyngeum and foramen stylomastoideum, TP-PM: Distance between tuberculum pharyngeum and processus mastoideus, TP-AV: Distance between tuberculum pharyngeum and ala vomeris.

Table 4. Descriptive statistics of the dependent measurements in the female group (mm).

	Female		
	Right (Mean±SD)	Left (Mean±SD)	p
TP-CO	15,38±1,65	15,28±1,40	0,363
TP-CC	31,60±2,79	30,27±1,44	0,080
TP-PS	40,00±2,27	39,97±3,03	0,943
TP-FS	41,60±1,61	41,46±2,09	0,731
TP-PM	53,77±2,60	53,78±2,07	0,980
TP-AV	18,50±1,55	18,50±1,41	0,974

TP-CO: Distance between tuberculum pharyngeum and condylus occipitalis, TP-CC: Distance between tuberculum pharyngeum and canalis caroticus, TP-PS: Distance between tuberculum pharyngeum and processus styloideus, TP-FS: Distance between tuberculum pharyngeum and foramen stylomastoideum, TP-PM: Distance between tuberculum pharyngeum and processus mastoideus, TP-AV: Distance between tuberculum pharyngeum and ala vomeris.

In Turkey, Aktas et al. (2013)'s study on cadavers identified the distance between the pharyngeal tubercle with arteria carotis interna as 38.95±4.67 mm. Since we used dry craniums in our study, we measured the distance of the TP to the canalis caroticus. We determined this distance as 31.80±2.19 mm on the right-side and 31.81±2.16 mm on the left-side for male, 31.60±2.79 mm on the right-side and 30.27±1.44 mm on the left-side for females. We think that morphometric studies performed on soft tissues affect the measurement values.

Although there are many studies on facial asymmetry (Al-Rudainy et al., 2019; Taylor et al., 2014; Sasaki et al., 2020; Linden et al., 2018), studies evaluating neurocranial asymmetry are almost nonexistent. Tuberculum pharyngeum, which is located in the center of the region where surgical interventions are frequently performed is surrounded by structures that are

of vital importance. The fact that these important structures are at a similar distance on both sides of this point will increase the confidence interval of the interventions to be made by taking the opposite side as a reference.

CONCLUSION

The part of the occipital bone between the vomer and foramen magnum is similar in size in the male and female craniums. When the TP reference point was taken, it was seen that the distance to the anatomical structures was statistically longer in males, but it was symmetrical in all craniums. Knowing the distance of the tuberculum pharyngeum to many important anatomical structures will provide morphometric data for surgical interventions performed in this region. We think that morphometric studies of bone are anthropologically and surgically important.

REFERENCES

- AKTAS U, YILMAZLAR S, UGRAS N (2013) Anatomical restrictions in the transsphenoidal, transclival approach to the upper clival region: a cadaveric, anatomic study. *J Cranio-Maxillofacial Surg*, 41(6): 457-467.
- AL-RUDAINY D, JU X, MEHENDALE FV, AYOUB A (2019) Longitudinal 3D assessment of facial asymmetry in unilateral cleft lip and palate. *Cleft Palate-Craniofac J*, 56(4): 495-501.
- APARNA J, SANGEETHA S, PREMAVATHY D (2019) Anatomy and clinical significance of clivus and its neighboring structures. *Drug Invention Today*, 12(4): 774-776.
- CANKAL F, UGUR HC, TEKDEMIR I, ELHAN A, KARAHAN T, SEVIM A (2004) Fossa navicularis: anatomic variation at the skull base. *Clin Anat*, 17(2): 118-122.
- ERDEM H, KIZILKANAT ED, BOYAN N, SOAMES R, OGUZO (2018) Anatomy and clinical importance of the extracranial clivus and surrounding structures. *Int J Morphol*, 36(2): 557-562.
- HITOTSUMATSU T, MATSUSHIMA T, RHOTON JR AL (1999) Surgical anatomy of the midface and the midline skull base. *Operative Techniques in Neurosurgery*, 2(4): 160-180.
- HOFMANN E, PRESCHER A (2012) The Clivus. *Clin Neuroradiol*, 22(2): 123-139.
- JI W, WANG XY, XU HZ, YANG XD, CHI YL, YANG JS, YAN SF, ZHENG JW, CHEN ZX (2012) The anatomic study of clival screw fixation for the craniovertebral region. *Eur Spine J*, 21(8): 1483-1491.
- KIZILKANAT ED, BOYAN N, SOAMES R, OGUZ O (2006) Morphometry of the hypoglossal canal, occipital condyle, and foramen magnum. *Neurosurg Quart*, 16(3): 121-125.
- KRMPOTIĆ-NEMANIĆ J, VINTER I, EHRENFREUND T, MARUSIĆ A (2006) Age-related changes in the anatomical landmarks of the osseous epipharynx. *Ann Anat*, 188(5): 459-467.
- LINDEN OE, HE JK, MORRISON CS, SULLIVAN SR, TAYLOR HO (2018) The relationship between age and facial asymmetry. *Plastic Reconst Surg*, 142(5): 1145-1152.
- OZER MA, CELIK S, GOVSA F, ULUSOY MO (2011) Anatomical determination of a safe entry point for occipital condyle screw using three-dimensional landmarks. *Eur Spine J*, 20(9): 1510-1517.
- PATEL CR, FERNANDEZ-MIRANDA JC, WANG WH, WANG EW (2016) Skull base anatomy. *Otolaryngol Clin North Am*, 49: 9-20.
- SASAKI J, HASEGAWA S, YAMAMOTO S, WATANABE S, MIYACHI H, NAGAO T (2020) Relationship between facial asymmetry and positional plagiocephaly analyzed by three-dimensional computed tomography. *J Cranio-Maxillofacial Surg*, 48(3): 193-198.
- SHARMA NA, GARUD RS (2011) Foramina of the posterior cranial base: a study of adult Indian skulls. *Rev Arg Anat Clin*, 3: 89-98.
- STANDRING S (2016) Gray's anatomy: the anatomical basis of clinical practice. 41th edition. Elsevier Health Sciences.
- TAYLOR HO, MORRISON CS, LINDEN O, PHILLIPS B, CHANG J, BYRNE ME, FORREST CR (2014) Quantitative facial asymmetry: using three-dimensional photogrammetry to measure baseline facial surface symmetry. *J Craniofac Surg*, 25(1): 124-128.
- WANG AJ, ZAIDI HA, LAWS JR ED (2016) History of endonasal skull base surgery. *J Neurosurg Sci*, 60(4): 441-453.
- ZHONG S, REN J, ZHANG Y, LI W, LI H, SONG S, ZHAO G, CHENG Y (2018) Anatomic study of craniocervical junction and its surrounding structures in endoscopic transoral-transpharyngeal approach. *J Craniofac Surg*, 29(7): 1973-1977.

Rare variant of hepatic arterial supply: a cadaveric case report with a literature review

Domagoj Ivanković^{1*}, Andrea Blažević^{2*}, Dominik Vicković¹, Danko Mikulić³

¹ School of Medicine, University of Zagreb

² Department of Anatomy and Clinical Anatomy, School of Medicine, University of Zagreb

³ Division of Abdominal Surgery and Organ Transplantation, Department of Surgery, University Hospital Merkur, Zagreb

SUMMARY

The most common pattern of hepatic arterial anatomy includes the left and right hepatic artery, both branching from the proper hepatic artery. We present a case where an additional, accessory hepatic artery, originating from the gastroduodenal artery, was found during anatomical dissection. The described artery enters porta hepatis separately, not following the left or right hepatic artery, which may implicate that the accessory artery provides arterial supply for the region defined as segments IVa and IVb (according to Couinaud's liver segment classification). Such an extremely rare variation of liver vascularization is poorly described in the literature, and it is not included in any of the currently valid classifications. The accessory artery presented in our case could be significant in clinical settings due to its impact on the outcome of surgical procedures.

Key words: Hepatic artery – Hepatobiliary surgery – Accessory artery – Anatomical variation

INTRODUCTION

Hepatic arterial anatomy has been the subject of many studies in recent literature. According to the literature, the incidence of hepatic artery

anatomical variations ranges from 20 to 50% (Fonseca-Neto et al., 2017). Most typically, the common hepatic artery is a branch of the celiac trunk. After branching of the gastroduodenal artery, the common hepatic artery continues its course as the proper hepatic artery. Then it bifurcates into the left and right hepatic artery, which then enter the liver through the porta hepatis. Multiple possible variants were classified in 1966 by Michels. Michels and colleagues performed a study on 200 dissections and classified variants into ten categories (Michels, 1966). Later, Michels' classification was modified by Hiatt's classification, in which six categories were defined (Noussios et al., 2017). However, according to the available literature and in addition to our finding, there are some variations of hepatic arterial vascularization that still cannot be entirely classified. Being familiar with these is crucial in surgical procedures relating to hepatobiliary and pancreatic surgery. We report a variant that is not described by either Michels' or Hiatt's classification.

CASE REPORT

Here we present an anatomical variation of liver vascularization found during anatomical

Corresponding author:

Andrea Blažević. Department of Anatomy and Clinical Anatomy, School of Medicine, University of Zagreb, Šalata 11, 10 000 Zagreb, Croatia. E-mail: andrea.blazevic@mef.hr

* DI and AB contributed equally to this study.

Submitted: September 10, 2020. Accepted: November 8, 2020

dissection. The variation was recognized upon opening the abdominal cavity and while dissecting porta hepatis. We found the celiac trunk originating from the abdominal aorta and branching normally into splenic, left gastric and common hepatic artery. Then, after arising from the celiac trunk, the common hepatic artery gave origin to its branch, the gastroduodenal artery. After branching of the gastroduodenal artery, the common hepatic artery ran further as the proper hepatic artery and finally split into the left and right hepatic artery, providing standard vascularization pattern with cystic artery arising from the right hepatic artery in the cystohepatic triangle (Caloti). While the course of the gastroduodenal artery was followed, its additional branch was noticed. The artery was parallel to the proper hepatic artery, medial to the common hepatic duct, superficial to the right hepatic artery, and at the level of the left hepatic artery. The artery entered porta hepatis between

the right and left hepatic artery, just medial to the common hepatic duct. The accessory artery branched 6 mm after the gastroduodenal artery rose from the common hepatic artery. The length of the described accessory artery was 33 mm, with a diameter of 3.5 mm. The diameter of the left hepatic artery was approximately the same as the accessory artery (4 mm), while the diameter of the right hepatic artery was significantly larger (6 mm).

Considering the course of the accessory artery and the fact that it enters porta hepatis separately, not following the left or right hepatic artery, we can assume it provides arterial supply for the region defined as segments IVa and IVb (according to Couinaud's liver segment classification).

COMMENTS

In 1966, Nicholas A. Michels established the classification of variants of hepatic arterial supply

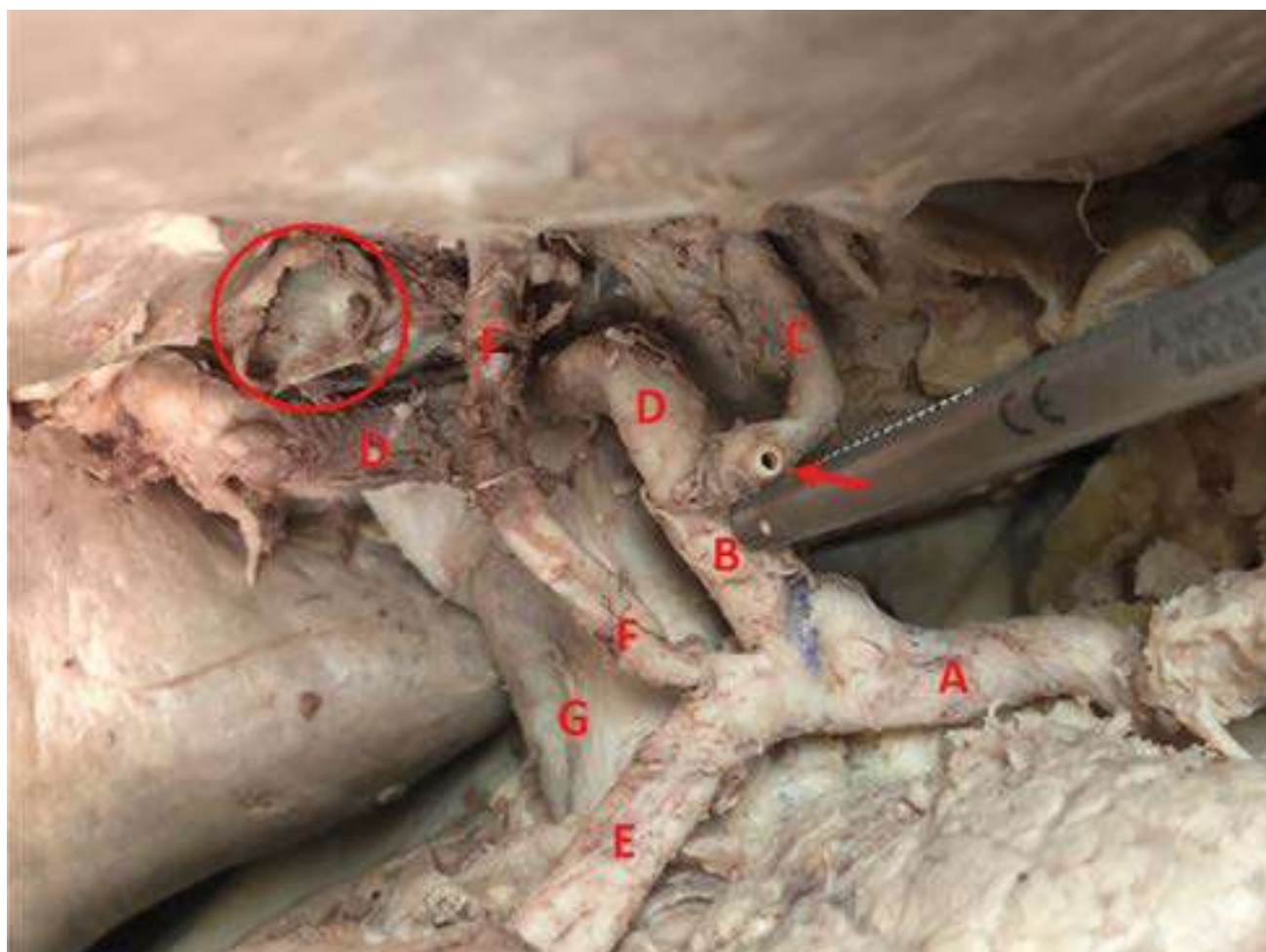


Fig. 1.- A – common hepatic artery; B - proper hepatic artery; C – left hepatic artery; D – right hepatic artery; E – gastroduodenal artery; F – accessory artery; G – portal vein; circle – common hepatic duct, cut; arrow – right gastric artery, cut.

dividing it into ten types (Michels, 1966). Type I (Normal anatomy), II (left hepatic artery branching from a left gastric artery), III (right hepatic artery branching from a superior mesenteric artery) and IV (right hepatic artery arising from the superior mesenteric artery associated with the left hepatic artery arising from the left gastric artery) are most frequently found, according to Michels' observations. Other variants of hepatic arterial supply, including the presence of accessory hepatic arteries or various combinations (type V – X) are less frequent (Fonseca-Neto et al., 2017). Later, in 1994, Jonathan R. Hiatt proposed another classification as an add-on to Michel's systematization. Hiatt reduced Michels' original ten groups to five most commonly found types, and introduced a sixth type of variation not previously described. In Hiatt's version, type 1 resembles a classic pattern, type 2 replaced or accessory left hepatic artery from the left gastric artery, and type 3 replaced or accessory right hepatic artery from the superior mesenteric artery. All the double replaced patterns are put together in the type 4 group. The common hepatic artery arising from the superior mesenteric artery is defined as type 5 or type 6 if branching directly from the abdominal aorta (Hiatt et al., 1994). The last case can also be considered as type 2b variation of celiac trunk vascularization according to Marco-Clement et al. (2016) classification. However, some reports demonstrate that not all variations are included in the existing classifications. One of the most substantial reports regarding hepatic artery variations performed by Gruttadauria et al. (2001) showed that more than 6% of variations are not covered by present systematization.

Gruttadauria et al. (2001) found, among other variations, replaced right hepatic artery originating from the renal artery, replaced right hepatic artery originating from the left gastric artery and the right hepatic artery from the gastroduodenal artery. Koops et al. (2004) in their study described a case of a replaced right hepatic artery branching directly from the abdominal aorta, whereas Löschner et al. (2015) reported an accessory right hepatic artery arising directly from the abdominal aorta. Winston et al. (2007) in his publication reported a case of the replaced

right hepatic artery from gastroduodenal artery, as well as a single case of the accessory artery for segment IV originating from the gastroduodenal artery, whereas Polguy et al. (2014) and Yamashita et al. (2015) described an accessory right hepatic artery arising from the gastroduodenal artery.

The embryological development of the liver might be a possible explanation for vascular variations of liver arterial supply. In early gestation life, the liver is supplied from three primary sources: the left hepatic artery from the left gastric artery, the middle hepatic artery, or common hepatic artery from the celiac trunk and the right hepatic artery from the superior mesenteric artery. During development, both right and left fetal hepatic artery should obliterate, leaving the whole liver vascularized by the middle hepatic artery (future common hepatic artery). In the case of partial or complete persistence of the fetal vascular pattern, anatomical variations may occur (Polguy et al., 2014; Noussios et al., 2017)

The clinical significance of accessory hepatic artery lies in surgical procedures involving the pancreatic head, bile duct, and liver. Pancreaticoduodenectomy (Whipple's procedure) is a surgical procedure indicated in tumors of the pancreatic head, ampulla, and distal bile duct. Sometimes it can be performed in duodenal resection and chronic pancreatitis (Karim et al., 2018). During pancreaticoduodenectomy, the gastroduodenal artery is ligated just distal to its take-off from the proper hepatic artery. In the case of an existing accessory hepatic artery arising from the gastroduodenal artery, ligating proximally to the branching of the accessory hepatic artery may result in necrosis of the liver or bile ducts. However, it should be kept in mind that in case of malignant neoplasm of the pancreatic head, due to the preservation of the accessory hepatic artery, complete cancer resection may be compromised (Madhu and Harish, 2013; Chawla et al., 2018). Additional care should be taken in case of hepatoduodenal ligament resection. In liver transplantation, knowing the exact arterial vascularization of the liver is crucial in preserving complete blood supply to the graft or both grafts in case of split liver transplantation (Madhu and Harish, 2013). Furthermore, knowing exact

vasculobiliary configuration in LDLT (living donor liver transplantation) is mandatory in order to prevent injuries and complications both in the liver graft and in the remaining donor liver (Kishi et al., 2010). Interestingly enough, Fouzas et al. (2019) reported in their study the increased incidence of early hepatic artery thrombosis in grafts with anatomic variations. Taking all of the stated into consideration, preoperative imaging of liver blood supply is mandatory in order to minimize complications during and after the operative procedure (Winston et al., 2007).

A limitation of our presumption is that we do not have any imaging or clinical proof of the significance of our accessory artery. Even though this finding may have a strong clinical impact, in order to determine its true relevance additional clinical test and research should be done.

Conclusion

Having in mind that numerous anatomical variations, not included in any of existing classifications, could be present, it is crucial to be familiar with those deviations while performing surgical procedures including hepatobiliary system, pancreas, and duodenum. The presented case of the accessory artery might be significant in clinical settings due to its impact on intra- and postoperative outcomes.

ACKNOWLEDGEMENTS

The authors would like to thank the body donor for his selfless gift for the benefit of science and medical education. We would also like to thank all the members of Department of Anatomy and Clinical Anatomy, School of Medicine, University of Zagreb and Division of Abdominal Surgery and Organ Transplantation, Department of Surgery, University Hospital Merkur, Zagreb for their kind cooperation and help. The authors thank Krunoslav Užarević, PhD, Ruđer Bošković Institute, Zagreb and Mia Vrbanac Užarević for their comments and suggestions.

REFERENCES

CHAWLA A, ROSENTHAL MH, CLANCY TE (2018) Implications of the replaced right hepatic

artery originating from the gastroduodenal artery in the setting of a pancreatic head mass. *Clin Imag*, 52: 189-192.

FONSECA-NETO OCL da, DE SOUZA LIMA HC, RABELO P, VIEIRA DE MELO PS, AMORIM AG, MOURA LACERDA C (2017) Anatomic variations of hepatic artery: a study in 479 liver transplantations. *Arq Bras Cir Dig*, 30(1): 35-37.

FOUZAS I, PAPANIKOLAOU C, KATSANOS G, ANTONIADIS N, SALVERIDIS N, KARAKASI K, VASILEIADOU S, FOUZA A, MOULOU DI E, IMVRIOS G, PAPANIKOLAOU V (2019) Hepatic artery anatomic variations and reconstruction in liver grafts procured in Greece: the effect on hepatic artery thrombosis. *Transplant Proc*, 51(2): 416-420.

GRUTTADAURIA S, FOGLIENI CS, DORIA C, LUCA A, LAURO A, MARINO IR (2001) The hepatic artery in liver transplantation and surgery: Vascular anomalies in 701 cases. *Clin Transplant*, 15(5): 359-363.

HIATT JR, GABBAY J, BUSUTTIL RW (1994) Surgical anatomy of the hepatic arteries in 1000 cases. *Ann Surg*, 220(1): 50-52.

KARIM SAM, ABDULLA KS, ABDULKARIM QH, RAHIM FH (2018) The outcomes and complications of pancreaticoduodenectomy (Whipple procedure): Cross sectional study. *Int J Surg*, 52: 383-387.

KISHI Y, IMAMURA H, SUGAWARA Y, SANO K, KANEKO J, KOKUDO N, MAKUUCHI M (2010) Evaluation of donor vasculobiliary anatomic variations in liver graft procurements. *Surgery*, 147(1): 30-39.

KOOPS A, WOJCIECHOWSKI B, BROERING DC, ADAM G, KRUPSKI-BERDIEN G (2004) Anatomic variations of the hepatic arteries in 604 selective celiac and superior mesenteric angiographies. *Surg Radiol Anat*, 26(3): 239-244.

LÖSCHNER C, NAGEL SN, KAUSCHE S, TEICHGRÄBER U (2015) Hepatic arterial supply in 1297 CT-angiographies. *RoFo (Fortschritte auf dem Gebiet der Röntgenstrahlen und der Nuklearmedizin)*, 187(4): 276-282.

MADHU YC, HARISH K (2013) Accessory right hepatic artery and its implications for a surgeon. *Ind J Surg*, 75(1 suppl.): 492-494.

MARCO-CLEMENT I, MARTINEZ-BARCO A, AHUMADA N, SIMON C, VALDERRAMA JM, SANUDO J, ARRAZOLA J (2016) Anatomical variations of the celiac trunk: cadaveric and radiological study. *Surg Radiol Anat*, 38(4): 501-510.

MICHELS, NA (1966) Newer anatomy of the liver and its variant blood supply and collateral circulation. *Am J Surg*, 112(3): 337-347.

NOUSSIOS G, DIMITRIOU I, CHATZIS I, KATSOURAKIS A (2017) The main anatomic variations of the hepatic artery and their importance in surgical practice: review of the literature. *J Clin Med Res*, 9(4): 248-252.

POLGUJ M, PODGÓRSKI M, HOGENDORF P, TOPOL M (2014) Variations of the hepatobiliary vasculature including coexistence of accessory right hepatic artery with unusually arising double cystic arteries: Case report and literature review. *Anat Sci Int*, 89(3): 195-198.

WINSTON CB, LEE NA, JARNAGIN WR, TEITCHER J, DEMATTEO RP, FONG Y, BLUMGART LH (2007) CT angiography for delineation of celiac and superior mesenteric artery variants in patients undergoing hepatobiliary and pancreatic surgery. *Am J Roentgenol*, 189(1): W13-9.

YAMASHITA K, HASHIMOTO D, ITOYAMA R, OKABE H, CHIKAMOTO A, BEPPU T, BABA H (2015) Accessory right hepatic artery branched from gastroduodenal artery. *Surg Case Rep*, 1: 90.

In regard to “Unusual case of absence of suprascapular notch and foramen”

Azzat Al-Redouan, David Kachlik

Department of Anatomy, Second Faculty of Medicine, Charles University, Prague, Czech Republic

SUMMARY

We read the case report by Hegazy AA, Hegazy MA (2020), “Unusual case of absence of suprascapular notch and foramen” *Eur J Anat*, 24 (4): 269-272, addressing an unusual case of absence of suprascapular notch and foramen, with interest. However, we would like to point out that this case is rather a discrete type of suprascapular notch (SSN), and it is not a rare case.

Key words: Suprascapular notch – Scapula – Variant – Types

Dear Editor,

We read the case report by Hegazy and Hegazy (2020), addressing an unusual case of absence of suprascapular notch and foramen, with interest. However, we would like to point out that this case is rather a discrete type of suprascapular notch (SSN), and it is not a rare case.

The suprascapular notch (SSN) is a notch presented as an indentation between two peaks where the suprascapular ligament attaches. The enclosing superior transverse scapular ligament (STSL), or its ossification forming a foramen, is a crucial component of the SSN anatomical definition (Rengachary et al., 1979; Duparc et al 2010; Polguy et al., 2011; Polguy et al., 2013; Kannan et al., 2014; Kumar et al., 2014; Al-

Redouan et al., 2020). Even though evaluating the STSL on dry bones has its limitation, its two sites of attachments are observable and palpable on dry bones. A total absence of a SSN will entitle a non-existing ligament, and its attachment site can be evaluated on dry bone in close approximation of the site of omohyoid muscle attachment. This will constitute the SSN's medial peak, while the SSN lateral peak is a part of the base of the coracoid process.

In 1942, Hrdlicka introduced five types of the SSN based on subjective observation of its shape, Type-I being the discrete form, and reported its prevalence to be 5.5% in a sample of 2722 scapulae (Hrdicka, 1942). In 1979, Rengachary et al. introduced an adopted six-type SSN classification based on its shape, Type-I having an absent notch and being defined by its wide depression, and it was found in 8% of 211 SSN samples (Rengachary et al., 1979). Additional studies used Rengachary's classification and reported 12.4% (Albino et al., 2013) and 20% (Kannan et al., 2014) of the aforementioned SSN type in their samples. Another study applied a modified Rengachary's classification and reported within the same category of SSN type to be 3.43% (Agrawal et al., 2001).

In 2011, Polguy et al. introduced a modified parametric form of SSN classification, in which Type-V donates the discrete type of SSN, and was found to be 11.6% in their dry-bone specimens

Corresponding author:

Azzat Al-Redouan, MD. Second Faculty of Medicine, Charles University, Department of Anatomy, V Uvalu 84, 150 06 Prague, Czech Republic.
E-mail: azzat.al-redouan@ifmotol.cuni.cz.

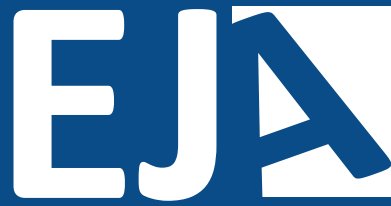
Submitted: November 21, 2020. **Accepted:** November 28, 2020

collection (Polguy et al., 2011), and in 12.9% of CT-evaluated specimens (Polguy et al., 2013). Additional studies have reported this discrete type of SSN in 32.4% (Kumar et al., 2014) and 21.3% (Al-Redouan et al., 2020), respectively.

To our knowledge, we would place the reported SSN by (Hegazy and Hegazy, 2020) to be Type-I, according to the old classification introduced by Hrdicka (Hrdicka, 1942) and adopted by Rengachary et al. (Rengachary et al., 1979), based solely on the shape appearance of the SSN, as well as to be Type-V according to the more recent classification introduced by Polguy et al. (Polguy et al., 2011), based on its appearance as a discrete notch, and its upper width versus depth parameters need to be measured to assess their ratio.

REFERENCES

- AGRAWAL D, SINGH B, DIXIT SG, GHATAK S, BHARADWAJ N, GUPTA R, AGRAWAL GA, NAYYAR AK (2001) Morphometry and variations of the human suprascapular notch. *Morphologie*, 99(327): 132-140.
- ALBINO P, CARBONE S, CANDELA V, ARCERI V, VESTRI AR, GUMINA S (2013) Morphometry of the suprascapular notch: correlation with scapular dimensions and clinical relevance. *BMC Musculoskelet Disord*, 14: 172-181.
- AL-REDOUAN A, HUDAK R, NANKA O, KACHLIK D (2020) The morphological stenosis pattern of the suprascapular notch is revealed yielding higher incidence in the discrete type and elucidating the inevitability of osteoplasty in horizontally oriented stenosis. *Knee Surg Sports Traumatol Arthrosc*, [doi: 10.1007/s00167-020-06168-1. Online ahead of print Jul 25].
- DUPARC F, COQUEREL D, OZEEL J, NOYON M, GEROMETTA A, MICHOT C (2010) Anatomical basis of the suprascapular nerve entrapment, and clinical relevance of the supraspinatus fascia. *Surg Radiol Anat*, 32(3): 277-284.
- HEGAZY AA, HEGAZY MA (2020) Unusual case of absence of suprascapular notch and foramen. *Eur J Anat*, 24(4): 269-272.
- HRDICKA A (1942) The scapula: visual observations. *Am J Phys Antropol*, 29: 73-94.
- KANNAN U, KANNAN NS, ANBALAGAN J, RAO S (2014) Morphometric study of suprascapular notch in Indian dry scapulae with specific reference to the incidence of completely ossified superior transverse scapular ligament. *J Clin Diagn Res*, 8(3): 7-10.
- KUMAR A, SHARMA A, SINGH P (2014) Anatomical study of the suprascapular notch: quantitative analysis and clinical considerations for suprascapular nerve entrapment. *Singap Med J*, 55(1): 41-44.
- POLGUJ M, JĘDRZEJEWSKI K, PODGÓRSKI M, TOPOL M (2011) Morphometric study of the suprascapular notch: proposal of classification. *Surg Radiol Anat*, 33(9): 781-787.
- POLGUJ M, SIBIŃSKI M, GRZEGORZEWSKI A, GRZELAK P, MAJOS A, TOPOL M (2013) Variation in morphology of suprascapular notch as a factor of suprascapular nerve entrapment. *Int Orthop*, 37(11): 2185-2192.
- RENGACHARY SS, BURR D, LUCAS S, HASSANEIN KM, MOHN MP, ATZKE H (1979) Suprascapular entrapment neuropathy: a clinical, anatomical, and comparative study. *Neurosurgery*, 5(4): 447-451.



European Journal of Anatomy